AFWAL-TR-82-2115

AIRCRAFT FUEL TANK INERTING SYSTEM

Richard L. Johnson
Joseph B. Gillerman
AiResearch Manufacturing Company
A Division of The Garrett Corporation
2525 West 190th Street
Torrance California 90509

JULY 1983

Final Report for Period 8 May 1978 — 30 JULY 1983

Approved for Public Release; Distribution Unlimited

Aero Propulsion Laboratory
Air Force Wright Aeronautical Laboratories
Air Force Systems Command
Wright-Patterson Air Force Base 45433

NOTICE

When Government drawings, specifications, or other data are used for any purpose other than in connection with a definitely related Government procurement operation, the United States Government thereby incurs no responsibility nor any obligation, whatsoever; and the fact that the government may have formulated, furnished, or in any way supplied the said drawings, specifications, or other data, is not to be regarded by implication or otherwise as in any manner licensing the holder to any other person or corporation, or conveying any rights or permission to manufacture, use, or sell any patented invention that may in any way be related thereto.

This report has been reviewed by the Office of Public Affairs (ASD/PA) and is releasable to the National Technical Information Service (NTIS). At NTIS, it will be available to the general public, including foreign nations.

This technical report has been reviewed and is approved for publication.

Gregory W. Gandee
GREGORY W. GANDEE, Project Engineer
Fire Protection Branch
Fuels and Lubrication Division

Robert G. Clodfelter
ROBERT G. CLODFELTER, Chief
Fire Protection Branch
Fuels and Lubrication Division

FOR THE COMMANDER

Robert D. Sherrill
ROBERT D. SHERRILL, Chief
Fuels and Lubrication Division
Aero Propulsion Laboratory

If your address has changed, if you wish to be removed from our mailing list, or if the addressee is no longer employed by your organization, please notify AFWAL/POSH, WPAFB, OH 45433 to help us maintain a current mailing list.

Copies of this report should not be returned unless return is required by security considerations, contractual obligations, or notice on a specific document.

Unclassified

SECURITY CLASSIFICATION OF THIS PAGE (When Data Entered)

REPORT DOCUMENTATION PAGE		READ INSTRUCTIONS BEFORE COMPLETING FORM
1. REPORT NUMBER AFWAL-TR-82-2115	2. GOVT ACCESSION NO. ADA141863	3. RECIPIENT'S CATALOG NUMBER
4. TITLE (and Subtitle) AIRCRAFT FUEL TANK INERTING SYSTEM		5. TYPE OF REPORT & PERIOD COVERED Final Report 8 May 1978 - 30 July 1983
		6. PERFORMING ORG. REPORT NUMBER 81-18143
7. AUTHOR(s) Richard L. Johnson Joseph B. Gillerman		8. CONTRACT OR GRANT NUMBER(s) F33615-77-C-2023
9. PERFORMING ORGANIZATION NAME AND ADDRESS AiResearch Manufacturing Company 2525 W. 190th Street Torrance, California 90509		10. PROGRAM ELEMENT, PROJECT, TASK AREA & WORK UNIT NUMBERS P.E. 63246F Project 2348 01 01
11. CONTROLLING OFFICE NAME AND ADDRESS Aero Propulsion Laboratory (AFWAL/POSH) AF Wright Aeronautical Laboratories (AFSC) Wright-Patterson AFB, OH 45433		12. REPORT DATE July 1983 13. NUMBER OF PAGES 253
14. MONITORING AGENCY NAME & ADDRESS(if different from Controlling Office)		15. SECURITY CLASS (of this report) Unclassified 15a. DECLASSIFICATION/DOWNGRADING SCHEDULE

16. DISTRIBUTION STATEMENT (of this Report)

Approved for public release; distribution unlimited

17. DISTRIBUTION STATEMENT (of the abstract entered in Block 20, if different from Report)

18. SUPPLEMENTARY NOTES

19. KEY WORDS (Continue on reverse side if necessary and identify by block number)

Nitrogen-Enriched Air
In-Flight Inert Gas Generation
Permeable Membrane
Oxygen-Nitrogen Separation
Fuel Tank Inerting
On-Board Inert Gas Generation
OBIGGS
Fuel System Protection
Inerting

20. ABSTRACT (Continue on reverse side if necessary and identify by block number)

The program successfully demonstrated the feasibility of using permeable-membrane, hollow fibers to generate an inert gas to protect the aircraft fuel system against fire and explosion induced by natural sources or combat. The initial contract requirements included a flight demonstration of an onboard inert gas generator system (OBIGGS) using an Air Force KC-135A aircraft. The design of an inert gas ge tor (IGG) is highly dependent on the flight profile, engine characteristics, . fuel system designs. Mission analysis translated

DD FORM 1 JAN 73 1473 EDITION OF 1 NOV 65 IS OBSOLETE

Unclassified

SECURITY CLASSIFICATION OF THIS PAGE (When Data Entered)

20. Abstract (continued)

these parameters into an 8 lb/min inert gas generator that produced less than 9-percent oxygen. A life-cycle cost (LCC) analysis compared the state-of-the-art liquid nitrogen (LN_2) system utilized on the C-5A aircraft against the IGG system designed for the KC-135A. Results showed the IGG system reduced LCC by 60 percent. Further, the IGG system eliminates the logistic constraints imposed by the use of LN_2, thus allowing unrestricted deployment of the aircraft.

A second LCC analysis was conducted in which the permeable-membrane system was compared against the blue foam design used on the C-130 aircraft. The LCC analysis shows a great advantage for OBIGGS over blue foam. Net operation and maintainance saving amount to $75.934/flight hour. With such a large savings, complete payback for OBIGGS design, development and initial hardware costs will be attained in 3.5 years. Yearly savings thereafter will be $28.9 million. Thus the total 20-year life savings for OBIGGS over blue foam amounts to $471.2 million. This study does not address the replacement of materials lost in electrostatically induced fuel tank fires for systems that use blue foam.

During the program, funding cuts eliminated the flight test demonstration. The IGG delivered to the Air Force consisted of the Air Separation Module (ASM) and associated controls. This system will undergo extensive ground simulation of the flight conditions to verify system performance.

The externally pressurized polymethylene hollow fiber bundles are expected to exceed the 20-year life expectancy of the aircraft. Maintenance requirements would be minimal, and would primarily entail periodic replacement of the water/particulate filter. The OBIGGS for the KC-135A aircraft would weigh approximately 850 lb, compared to an LN_2 system of 1660 lb. The delivered unit met the goals of processing engine bleed air into an oxygen-depleted product that contained less than 9-percent oxygen. A flight test demonstration is required to transfer this technology to fixed-wing aircraft such as the C-5B and C-130.

SUMMARY

The concept of an onboard inert gas generator system (OBIGGS) that processes engine bleed air into an oxygen-depleted product has been successfully demonstrated. The inert gas, consisting of 91 to 95 percent nitrogen, in turn keeps the fuel tank ullage inert, and thus eliminates the threat of fire or explosion due to combat-induced damage or natural ignition sources such as lightning. This inert gas generator (IGG) is based on the permeable-membrane approach and represents the culmination of approximately 10 years of research.

The performance of the OBIGGS system overcomes many of the concerns and logistic problems associated with the state-of-the-art liquid nitrogen system of the C-5A aircraft. A life-cycle cost analysis indicates the IGG will cost 60 percent less than the LN_2 system. In an LN_2 system the primary factor affecting the cost is the need to replenish the LN_2 after every two flights. The OBIGGS, a self-contained independent system, provides the logistic independency required to meet the requirements of various Air Force operational scenarios.

The initial program included a flight test demonstration of the IGG on the available Air Force-designated flight test aircraft, a KC-135A. The mission profile, engine characteristics, and fuel system must be considered to establish the required inert gas flow for any system. These factors must be assigned an appropriate system penalty normally associated with weight, bleed air, or fuel usage. A change in any factor can change flow requirements. Analysis of the existing KC-135A aircraft established an inert gas requirement of 8 lb/min containing less than 9-percent oxygen. Note that current technology for the IGG applies only to cargo aircraft; application of this technology to fighter aircraft would require integration of the inert requirements into the basic fuel system design so that the fuel tanks would operate at higher pressures.

The inert gas generator (IGG) air separation module (ASM) utilizes permeable membranes to separate the oxygen from the engine bleed air source. These permeable membranes were developed by Dow Chemical under Air Force sponsorship. The permeable membranes consist of a bundle of hollow fibers with a diameter of 40 microns and a 6-micron wall thickness. The structure of the polymethylpentene material permits the oxygen to permeate through the wall and leave a nitrogen-enriched stream.

During the program both internally pressurized and externally pressurized modules were analyzed. Experience gained during the program and in Dow's commercial applications of this technology to inerting of flammable chemical storage tanks resulted in the decision to use the externally pressurized modules. Analysis of permeable membrane characteristics established an optimum envelope which consisted of an inlet pressure of 85 psia and an operating temperature of 75°F. The air separation module (ASM) will have a life expectancy in excess of the 20-year life of the aircraft. The only maintenance required would be the periodic replacement of the filter that removes excess water and particulate contaminants. Other equipment for conditioning of the air is of the standard ECS type; this equipment has high reliability.

Significant redirection of the program was required due to budget reductions. In lieu of flight testing, the basic portion of the IGG system--the ASM, and associated controls--is being subjected to extensive ground testing at WPAFB. The test capabilities at WPAFB provide a high degree of flight simulation, including operation of the ASM at the simulated altitudes, using the signals generated by the appropriate fuel system climb/dive valves. The inert product will be monitored and distributed to a fuel tank, which also operates at the appropriate simulated altitude. Results of this testing will be the subject of a future Air Force report.

In addition to the KC-135 evaluation, cost of ownership for the C-130 aircraft also was evaluated. This study on the permeable membrane OBIGGS was compared against the existing blue foam. The life-cycle cost analysis performed for the C-130 aircraft indicates a significant reduction $75.934/flight hour in operation and maintenance costs for the permeable membrane OBIGGS. The primary factors affecting the higher cost of blue foam are: (1) its extensive on-aircraft scheduled maintenance, and (2) its system weight, which is more than twice that of the permeable-membrane OBIGGS. With the large savings in operation and maintainance, the LCC analysis shows payoff for OBIGGS in 3.5 years; this includes initial hardware costs plus design and development costs. Operation and maintainance savings amount to $28.9 million per year; this figure is based upon 564 flight hours per year per aircraft, for a fleet of 674 aircraft. The 20-year LCC savings accrued by using the OBIGGS will be $471.9 million.

The final configuration improved upon the design goals of less than 9 percent O_2 at 8 lb/min and 5 percent O_2 at 3 lb/min. However, other considerations resulted in the decision to produce only half-size test units. The projected weight of a production unit for the KC-135A was 853 lb, compared to an LN_2 system weight of 1660 lb.

The potential benefits from reduced weight, reduced life-cycle costs, and logistics independency should be pursued in a follow-on flight test program, which would provide for technology transfer to aircraft such as the C-5B, C-17, or C-130.

During the program many documents were generated. Table 1 summarizes these documents.

LIST OF DOCUMENTS PREPARED IN SUPPORT OF THE USAF-AFAPL FUEL TANK INERTING SYSTEM FOR THE AIRCRAFT UNDER CONTRACT F33615-77-C-2023

	Report No.	Date	Title	Abstract
1.	78-14914, Rev. 2	June 22, 1982	Statement of Work Flight Test Gas Monitoring System Fuel Tank Inerting System for Aircraft	This statement covers the development program for a flight test gas monitoring system and the required support for an advanced development program to develop an onboard, self-contained inert gas generator system for the protection of aircraft fuel tanks from explosions induced by either natural or hostile environment ignition sources.
2.	78-14917, Rev. 2	June 22, 1982	Statement of Work Hollow Fiber Membrane Module Fuel Tank Inerting System for Aircraft	This statement of work covers the development program for hollow fiber permeable membrane modules for an advanced development program to develop an onboard, self-contained, inert gas generator system for the protection of aircraft fuel tanks from explosions induced by either natural or hostile environment ignition sources. The system shall be proven suitable for application to operational aircraft by extensive ground and flight testing.
3.	78-15110, Rev. 1	October 26, 1979	Contract Work Breakdown Structure Fuel Tank Inerting System for Aircraft	This report contains a contract work breakdown structure for an aircraft fuel tank inerting system as prepared for the Air Force Systems Command.
4.	78-15119	(published monthly)	Monthly R&D Status Report Fuel Tank Inerting System for Aircraft	This report summarized the program activity during each monthly reporting period of 50-month program to design, build, and test an onboard inert gas generator-type fuel tank inerting system.
5.	78-15133(47)	(published monthly)	Program Schedule Fuel Tank Inerting System for Aircraft	This report presents the current program schedule.
6.	78-15295	August 30, 1978	Management Information System Description Fuel Tank Inerting System for Aircraft	This system provides the information and management framework required to establish and maintain effective program management, as prepared for the U.S. Air Force.
7.	78-15415, Rev. 1	April 19, 1979	Fuel Tank Inerting System for Aircraft Task 1-1, Inerting System Comparison for KC-135A Tanker Aircraft	This document provides a summary of the conceptual design studies conducted for the KC-135A aircraft. The purpose of the studies was establish tradeoff comparison information for liquid nitrogen and permeable membrane inerting techniques for the aircraft wing fuel tanks only.
8.	78-15416	November 14, 1978	Fuel Tank Inerting System for Aircraft Task 1-1, Inerting System Comparison for YC-14 AMST.	This report describes the results of a comparison of inerting systems for the YC-14 AMST aircraft.

LIST OF DOCUMENTS (continued)

	Report No.	Date	Title	Abstract
9.	78-15464, Rev. 1	March 5, 1979	System Requirement Model Specification Fuel Tank Inerting System for Aircraft	This specification establishes the performance and design requirements for a permeable membrane onboard, self-contained inert gas generator system to provide sufficient inert gas to reduce the oxygen concentration in the fuel tank ullage below explosive levels.
10.	78-15526	October 30, 1978	Capabilities Summary KC-135 Tanker Mission Management System (Exploratory Development Area PMRN-79-74)	This report summarizes the experience and capabilities of AiResearch engineering as they pertain to the development of systems for flight management.
11.	79-15673	January 22, 1979	Fuel Tank Inerting System for Aircraft Preliminary Interface Data U.S. Air Force	Data is presented to provide information to Boeing to initiate Modification Planning, Task 1-2. Utilizing this data, Boeing will prepare Part 1, Class II modification documentation for the KC-135 appropriate for flight test evaluation by the 4950th Test Wing at Wright-Patterson Air Force Base.
12.	79-15740	February 5, 1979	Fuel Tank Inerting for Aircraft Task 1-4, Flight Test Planning Failure Modes and Effect Analysis for KC-135A	This report describes the results of Task 1-4, Flight Test Planning, Failure Modes, and Effect Analysis, for the KC-135A aircraft.
13.	79-15910	April 12, 1979	Fuel Tank Inerting System for Aircraft Preliminary Hazard Analysis for KC-135 Fuel Tanker Aircraft System	This report contains the results and conclusions from the preliminary hazard analysis for the AiResearch fuel inerting system to be used on the KC-135 aircraft. The objective of the analysis was to evaluate the proposed design o identify inherent design and and procedural hazards, and to establish special procedures an, precautions.
14.	79-15992, Rev. 2	August 22, 1980	Fuel Tank Inerting System for Aircraft Task 2-1, System Design Research Development Test Plan	This document describes the research and development tests to be performed by AiResearch on a fuel tank inerting system for the KC-135A aircraft. The plan defines the analytical test approaches and test plans required for Phase 2, Test Hardware Development.
15.	79-16069	June 19, 1979	Statement of Work Air Separation Module	This statement of work covers air separation module (ASM) for aircraft inerting and oxygen generator for aircrew breathing applications.
16.	79-16070	June 19, 1979	Acceptance Test Requirements Air Separation Module AiResearch PN 2202303	This report presents a description of the acceptance test procedure to be performed on AiResearch PN 2202303 Air Separation Module (ASM) prior to shipment.
17.	79-16127	July 2, 1979	Technical Proposal for KC-135 Mission Management System	This report describes the proposed KC-135 tanker Mission Management System (MMS).

LIST OF DOCUMENTS (continued)

Report No.	Date	Title	Abstract
18. 80-16754	February 11, 1980	Critical Item Produce Specification For a Hollow Fiber Membrane Assembly	This specification establishes the performance, design, test manufacture, and acceptance requirements for a hollow fiber membrane assembly suitable for implementation into a system for inerting a KC-135 aircraft. The system will be used for aircraft fuel tank inerting or appropriate ground test simulation. This specification describes the requirements for a single hollow fiber membrane assembly.
19. 80-16804	April 29, 1980	Statement of Work Development of Improved Polymehtylpentene Hollow Fibers for Aircraft Fuel Tank Inerting System Air Separation Modules.	This statement of work covers the development program to be implemented for improving of polymethylpentene hollow fibers for use in air separation modules for aircraft fuel tank inerting systems.
Report No.	Date	Title	Abstract
20. 80-16953, Rev. 2	November 24, 1980	System Description for Aircraft Fuel Tank Inerting U.S. Air Force	This report describes the aircraft fuel tank inerting system to be used for tests to be conducted at the U.S. Air Force Aero Propulsion Laboratory Test Facility.
21. 80-16993, Rev. 1	July 30, 1980	Fuel Tank Inerting for Aircraft, Test Instrumentation For Phase 2 Research and Development Testing	This report describes test instrumentation to be used for Phase 2 research and development testing of aircraft fuel tank inerting.
22. 80-17000	March 27, 1980	Fuel Tank Inerting System for Aircraft Study on Operations of FTIS at Laboratory Ambient Conditions	This report contains results of a study of the operation of the fuel tank inerting system for aircraft at laboratory ambient conditions.
23. 80-17162	November 24, 1980	Description of Components Used in Aircraft Fuel Tank Inerting System	This report presents a detailed description of the components used in the aircraft fuel tank inerting system described in AiResearch Report 80-16953.
24. 80-17213	August 26, 1980	Fuel Tank Inerting System for Aircraft, Subsystem Hazard Analyses for KC-135 Tanker Aircraft	This report contains the results of the subsystem hazard analysis performed on the fuel tank inerting system (PN 2202750).

PREFACE

This final report describes an effort conducted by AiResearch Manufacturing Company, Torrance CA, for the Aero Propulsion Laboratory, Air Force Wright Aeronautical Laboratories, Air Force Systems Command, Wright-Patterson AFB, Ohio. This work was accomplished under Contract F33615-77-C-2023, PE 63246F, Project 2348, Task 01, and Work Unit 01. The Air Force project engineers were R.G. Clodfelter and G.W. Gandee.

The principal investigators for the AiResearch Manufacturing Company were Mr. Richard L. Johnson and Mr. Joseph B. Gillerman, under the direction of Mr. Scott A. Manatt of the Environmental and Energy Systems Department. Also contributing to this program were Mr. Myron A. Quan, in analysis; Mr. Samuel M. Railing, in design; Mr. Perry Bond and Mr. Michael Robinson, in testing; and Mr. Gordon Deckman and Mr. Robert A. Goodsell, in the reduction and organization of data for this report. All work reported was performed at AiResearch facilities in Torrance, California, with the exception of auxiliary studies and manufacture of permeable membrane modules, which were subcontracted as follows: Boeing Aerospace Company, Wichita, Ka., for flight test planning and airframe support; Falcon Research and Developoment, Denver, Co., for flight-test gas monitoring; and Dow Chemical USA for the manufacture of permeable membrane modules. The principal contributor at Dow Chamical Research Center, Walnut Creek, Ca, was Mr. Tim Revak.

CONTENTS

Section		Page
	REPORT DOCUMENT PAGE	i
	SUMMARY	iii
	LIST OF DOCUMENTS	v
	PREFACE	viii
	CONTENTS	ix
	LIST OF TABLES	xii
	LIST OF ILLUSTRATIONS	xiv
	LIST OF ABBREVIATIONS AND SYMBOLS	xvi
1	INTRODUCTION	1
	Scope	1
	Background	1
	Initial Program Breakdown	1
	Restructured Program	2
	Work Completed	2
	Program Management	4
	Major Subcontractors	4
2	INERT GAS GENERATION SYSTEM CONCEPTUAL DESIGN	7
	System Considerations	7
	Design Mission Profile	8
	Inerting Requirements	8
	Membrane Air Separation Module Design	13
	ASM Air Supply System	26
	Emergency Descent Provisions	36
	Prime System Candidate Comparison	37
	Design Philosophy	39
	Handling of Dissolved Air Released from Fuel	41
3	LIQUID NITROGEN SYSTEM CONCEPTUAL DESIGN	47
	System Considerations	47
	Design Mission Profile	47
	System Description	50
	System Weight	50
	Logistics	52
	Flexibility	52
	Hardware	52

CONTENTS (Continued)

Section		Page
4	COST-OF-OWNERSHIP COMPARISON FOR KC-135 AIRCRAFT	55
	Assumptions	55
	Reliability	55
	Life Cycle Costs	57
	Initial Costs	57
	Maintenance Costs	57
	Operating Costs	59
5	FLIGHT TEST PLANNING	65
	Gas Monitoring System	65
	Aircraft Modifications	70
6	SYSTEM DESIGN	85
	Performance Analysis	85
	Description of Laboratory Test System	88
	Temperature Control System Description	93
	Flight Profile Operation	95
	Instrumentation	98
	Package Assembly	98
7	HARDWARE FABRICATION AND TESTING	101
	General	101
	Air Separation Modules	101
8	AIR SEPARATION MODULE SUPPLEMENTAL DEVELOPMENT	129
	Phase 1 Efforts	129
	Phase 2 Efforts	129
9	CONCLUSIONS AND RECOMMENDATIONS	131
	Conclusions	131
	Recommendations	131
Appendix		
A	DOW CHEMICAL COMPANY REPORT, DATED MARCH, 1979	133
B	DOW CHEMICAL COMPANY REPORT, DATED JUNE 8, 1981	171
C	COST-OF-OWNERSHIP COMPARISON FOR C-130 AIRCRAFT	235

TABLES

Table		Page
2-1	Preliminary IGG System Analysis for ASM Without Wash Flow --Unpressurized Fuel Tank	12
2-2	Characteristics of Halon Inertent System for KC-135A Emergency Descent	36
2-3	Comparison of IGG System Candidates for KC-135A Sea Level Descent Operation, 103°F Day with 154 gr/lb Humidity	37
3-1	KC-135A Mission Data	49
4-1	Estimated Component Mean-Time-Between-Failures (MTBF)	56
4-2	Cost Assumptions	58
4-3	Maintenance Cost of Ownership Elements	59
4-4	Estimated Energies Used During Typical System Operation	60
4-5	Cost of Operation	61
4-6	Cost-of-Ownership Summary	63/64
5-1	Bleed Air Source Options for the FTIS	74
6-1	Comparison of Hot Day Performance for Aircraft and Laboratory Test Conditions	86
6-2	Comparison of Standard Day Performance for Aircraft and Laboratory Test Configurations	87
6-3	Fuel Tank Inerting System Components	91
6-4	FTIS Instrumentation Description	100
7-1	BMF-1 Through BMF-7 Module Fabrication Characteristics	104
7-2	Shell Flow-ΔP Values for BMF-1 Through BMF-7 (cfm/psid)	104
7-3	Air Separation Performance of Modules BMF-1 Through -7	106
7-4	Design Conditions for BMF Modules	107
7-5	Design Module Performance as a Function of Average Shell Pressure (Computer Isolation)	107

TABLES (Continued)

Table		Page
7-6	Fiber Gas Separation and Hoop Strength Study	108
7-7	Air Separation Module (ASM) Design Characteristics at 8.85 lb/min Design Point	110
7-8	LMF-1 Through LMF-5 Module Fabrication Characteristics	116
7-9	Air Separation Performance of Modules LMF-1 Through LMF-5	116
7-10	IGG Performance	125

ILLUSTRATIONS

Figure		Page
2-1	KC-135A Tanker Design Mission	9
2-2	KC-135A Fuel Tank Locations and Fuel Tank Inerting and Scrub System Lines	10
2-3	KC-135A Rates of Descent	11
2-4	ASM System Performance at 0.4 psid Tank Ullage Pressure	14
2-5	ASM System Performance at 1.0 psid Tank Ullage Pressure	15
2-6	ASM System Performance at 2.0 psid Tank Ullage Pressure	16
2-7	Hollow-Fiber Permeable Membrane Air Separation Module	19
2-8	Air Separation Module Low Side Pressure Loss as a Function of Packing Factor	22
2-9	Effect of Pressure and Temperature on Internally Pressurized Fiber Life	22
2-10	Effect of ASM Feed Pressure on Life and Weight of Internally Pressurized Fibers	23
2-11	Effect of ASM Feed Temperature on Life and Weight of Internally Pressurized Fibers	24
2-12	Required Fiber Bundle Size for KC-135A Aircraft	25
2-13	Concept I - Each Fiber Bundle Individually Packaged in a Pressure Vessel	27
2-14	Concept II - Waste Flow has Common Pressure Vessels	28
2-15	Concept III - All Flows Have Common Pressure Vessels	29
2-16	Basic Schematic Options, Inert Gas Generation System	30
2-17	Combination High/Low Stage Bleed IGG System	31
2-18	Non-Integrated Inert Gas Generation System	32
2-19	Integrated Inert Gas Generation System	33
2-20	Duct Size and Velocity	35
2-21	Typical Inert Gas Generation System	38

ILLUSTRATIONS (Continued)

Figure		Page
2-22	Cargo Compartment Dimensions	40
2-23	Typical Air Content of JP4 Aviation Gas Turbine Fuel	42
2-24	Inert Gas Oxygen Concentration vs Variation of Flow-rate From Design Value	43
2-25	Purge Gas Requirements to Control the Release of Dissolved Air From Fuel During Climb	44
3-1	Simplified Schematic of LN_2 Storage and Conditioning System	48
3-2	KC-135A Pressurization and Scrubbing System Schematic Diagram	51
3-3	Logistics of LN_2 Supply	53/54
5-1	Preliminary Arrangement Fuel Tank Gas Measuring System (FTGMS)	67
5-2	Fuel Inerting High-Spool Independent Air Source Concept	71
5-3	KC-135A Inert Gas System Conceptual Design	72
5-4	Fuel Tank Inerting System Schematic	81
6-1	Vacuum Requirements	89
6-2	Estimated Cooling Air Pressure Drop of Ram Air Heat Exchanger	89
6-3	Fuel Tank Inerting System Schematic	90
6-4	FTIS Electrical Schematic	92
6-5	Schematic Diagram, Dewpoint/Anti-Ice Control Valve	94
6-6	Schematic Diagram, Temperature Control Valve	95
6-7	Descent Switch and Valve Operation	96
6-8	FTIS Schematic Showing Test Instrumentation	99
7-1	Hollow Fiber Membrane Bundle	102
7-2	Air Separation Module	103
7-3	Cross-Sectional View of ASM with Externally Pressurized Membranes	112

ILLUSTRATIONS (Continued)

Figure		Page
7-4	Inertant Flow as a Function of Oxygen Content and Feed Air Pressure	113
7-5	Fiber Life of Externally Pressurized Membrane ASM as a Function of Fiber Pressure and Temperature	114
7-6	Side View of IGG Showing Instrumentation Test Ports	117
7-7	View of IGG Showing Control Box and Auxiliary Hardware Connector	118
7-8	View of IGG Showing Exhaust Parts and Inert Gas Outlet Port	119
7-9	View of IGG System Test Setup	121
7-10	View of IGG Test Setup and Control Panel	122
7-11	IGG System Test Setup Schematic	123
7-12	View of IGG Auxiliary Hardware	126
7-13	Schematic of Hardware Provided for IGG Laboratory Testing at WPAFB	127/128

ABBREVIATIONS

ACM	Air cycle machine
AGE	Aerospace ground equipment
ALL	Airforce laser laboratory
ASD	Aircraft Systems Division (USAF)
ASM	Air separation module
ATC	(Trade Name)
ATGA	ATC gas analyzer
BMF	Dow model designation
C/D	Climb/dive
CG	Center of gravity
CRT	Cathode ray tube
ECS	Environmental control system
EMC	Electromagnetic compatibility
FH	Flight hour
FMEA	Failure mode and effects analysis
FTGMS	Fuel tank gas measuring system
FTIS	Fuel tank inerting system
GFE	Government-furnished equipment
GUARD	Garrett unified automated reliability data
IGG	Inert gas generator
LCC	Life-cycle cost
LMF	Dow model designation
L_{HP}	Life at high pressure
L_{LP}	Life at low pressure
L_U	Useful life
MTBF	Mean time between failures
OBIGSS	Onboard inert gas generator system
PHA	Preliminary hazard analysis
PMP	Polymethylpentene
PSI	Pounds per square inch
R&D	Research and development
SAFTE	Simulated aircraft fuel tank program
SHX	Secondary heat exchanger
SO	Shutoff
SOV	Shutoff valve

SECTION 1

INTRODUCTION

SCOPE

This report describes the work performed by the AiResearch Manufacturing Company, Torrance, California, a division of The Garrett Corporation, to produce an advanced development fuel tank inerting system (FTIS) for aircraft. The work was performed under U.S. Air Force Contract F33615-77-C-2023.

BACKGROUND

Studies and tests showed that the most practical and economical fuel tank inerting concept is a permeable membrane system capable of effectively reducing the oxygen content of the supply air to the fuel tank ullage. The decision was reached to develop such a system for demonstration purposes in a KC-135A tanker aircraft. The system employs high pressure air from the engine and conditions it to a pressure and temperature suitable for use at the inlet of an air separation module (ASM). The ASM incorporates a permeable membrane made of polymethylpentene (PMP) hollow fibers, which allow preferential passage of oxygen over nitrogen through the membrane. The resulting nitrogen-rich inertant is used to pressurize the fuel tank ullage space.

INITIAL PROGRAM BREAKDOWN

The program was initially divided into three phases, covering the following tasks:

Phase 1 - System Tradeoffs/Requirements

- Task 1-1: Inerting System Comparison
- Task 1-2: Supplemental Investigation
- Task 1-3: Flight Test Gas Monitoring System
- Task 1-4: Flight Test Planning
- Task 1-5: Phase 1 Airframe Support
- Task 1-6: Phase 1 Program Management

Phase 2 - Test Hardware Development

- Task 2-1: System Design
- Task 2-2: System Fabrication
- Task 2-3: System test
- Task 2-4: Test Plan Preparation
- Task 2-5: Phase 2 Airframe Support
- Task 2-6: Phase 2 Program Management

Phase 3 - Installation and Aircraft Tests

Task 3-1: Aircraft Modification
Task 3-2: Ground Checks
Task 3-3: Flight Test Program
Task 3-4: Data Evaluation/Analysis
Task 3-5: Phase 3 Airframe Support
Task 3-6: Phase 3 Program Management

RESTRUCTURED PROGRAM

Phase 1 was started in May, 1978, and progressed according with the program plan. In August, 1979, near the completion of Phase 1, the Air Force redirected the program as a cost saving measure. Phase 2 was restructured to delete all tasks connected with flight testing. Phase 3 was eliminated. The remaining Phase 2 tasks then consisted of:

Task 2-1: System Design
Task 2-2: Supplemental Investigations
Task 2-3: System Fabrication
Task 2-4: System Test
Task 2-6: Program Management

In January 1981, the scope of the program was further reduced as a result of Air Force budgetary considerations. All work related to hardware fabrication was stopped except for system components that were almost completed. The hardware to be shipped was limited to those components necessary to conduct laboratory testing of the inert gas generation assembly at WPAFB.

WORK COMPLETED

A brief description of the work completed in Phases 1 and 2 follows:

Inerting System Comparison (Task 1-1)

The objective of this task was to conduct a tradeoff analysis between a permeable membrane inert gas generator (IGG) and a state-of-the-art, liquid nitrogen (LN_2) inerting system. After an analysis of available Air Force test aircraft, the KC-135 was chosen for the tradeoffs. The permeable membrane IGG has more advantages and is more cost-effective for the KC-135A aircraft. This is mainly due to the high cost of operation and maintenance of the LN_2 system. The life cycle cost analysis indicates IGG cost of ownership is significantly less than LN_2. The primary factor affecting cost is the need to replenish LN_2 after every two flights.

Supplemental Investigation (Task 1-2)

Dow Chemical conducted studies to improve the properties and methods of manufacture of the permeable membrane air separation modules. These studies included various methods of cross-linking to add strength and stability to the fibers and methods of manufacturing that would result in the optimum fiber size with minimum fiber breakage. The studies were continued into Phase 2 of the restructured program.

Flight Test Gas Monitoring (Task 1-3)

Falcon Research and Development Company studied design approaches for a flight test gas monitoring system based on the use of government-furnished Analog Technology Corporation Model 2001 Gas Monitor.

The core of the sample transport subsystem was being designed by Falcon with an emphasis on components already proven on the Simulated Aircraft Fuel Tank (SAFTE) program of the Air Force. Sample line switching was to be performed by a Scanivalve with two banks of twelve channels each. Both banks were fixed in relation to each other and driven on a common shaft by a stepper solenoid. One bank was termed "primary", and was dedicated to tank sample lines with ports in the top of the tanks. The "secondary" bank was allocated to any excess of sampling points high in the tanks, and to any that might be immersed in fuel for a relatively longer period of mission time.

Scanivalve position indicator lights were provided on a panel in front of the operator. During normal tank readings, the Scanivalve controller automatically steps through the sampling positions at a rate manually input into the controller. The operator could override this operation at any time, and could manually select a fixed port or manually advance sampling positions. The manual modes could be used by the in-flight operator between periods of relatively rapid data collection for all tank sample lines available. The operator could select backpurge of one or both banks. If one bank was in backpurge, automatic sequencing of the other bank could still be accomplished.

Flight Test Planning (Task 1-4)

Flight test planning required coordination between the USAF 4950 Test Wing, AiResearch, and Boeing. In performing this task, significant interface responsibilities were defined; the KC-135A tanker aircraft was designated as the test bed; and mission management plans, especially with respect to flight safety and interfaces with other systems, were reviewed.

Airframe Support (Task 1-5)

Airframe modification requirements were coordinated with Boeing Aerospace, the airframe manufacturer.

System Design (Task 2-1)

The design was based on a fuel tank inerting system to be used for ground tests in accordance with the Phase 2 restructured program.

Supplemental Investingation (Task 2-2)

This was a continuation of Task 1-2 and consisted of studies and tests by Dow Chemical to seek ways of upgrading the properties of the hollow fiber membrane with respect to permeability, cross-linking, annealing, and orientation.

During this program, a number of areas were explored and evaluated: fiber size optimization, fiber lifetime variations with stress and temperature, fiber

crosslinking to increase mechanical strength, module performance simulation, characterization of actual module operating performance, and module fabrication techniques. From data gathered on 6-in.-dia. devices, design equations were obtained for predicting performance in devices of larger diameters. Details of these investigations are presented in Appendix A.

System Fabrication (Task 2-3)

The initial plan was to fabricate a complete ground test system in Phase 2. This system fabrication was then limited to those components considered essential for the ground evaluation of the IGG. Test system fabrication was limited to those components essential for testing the inert gas generator.

System Test (Task 2-4)

At the time of the stop order, the design of the test system setup was completed and its fabrication had been initiated. The only additional activity in this task was the final checkout and performance verification of the air separation module (ASM) planned for delivery to the Air Force at the completion of the program.

PROGRAM MANAGEMENT

AiResearch was responsible for the overall design and integration of the fuel tank inerting system. Included in the responsibility was overseeing subcontracting efforts with respect to air separation module development, aircraft modification requirements, inflight monitoring system design, and flight test planning. Mechanical and performance interfaces for the inerting system, the test aircraft and the supporting equipment were identified and potential problems resolved. Close liaison was established early in the program between AiResearch, the major subcontractors, and cognizant Air Force personnel. AiResearch also performed system analyses and designed, developed, and fabricated ground test hardware.

One of the major efforts in the program was the detail design of the inert gas generation subsystem package. The subsystem, assembled into a high-density arrangement characteristic of aircraft environmental systems, required the accurate establishment of all mechanical interface data for its components and for the test aircraft. In addition, its design provided for the dynamic environments associated with aircraft performance and inerting requirements. As the design of the flight subsystem and component packages proceeded, it was necessary to iterate their external interfaces with the resultant effects on the aircraft modification.

MAJOR SUBCONTRACTORS

The following major subcontractors assisted AiResearch in the development of the fuel tank inerting system and its originally planned flight test program.

Dow Chemical Company

In Phase 1, Dow studied ways of improving the properties and methods of manufacturing the polymethylpentene hollow-fiber membranes used in the air separation modules. These studies included investigations into cross-linking methods to increase the fiber strength and into manufacturing methods to produce an optimum size for minimum breakage. The Dow studies were continued into Phase 2. In this phase, ways were also sought to upgrade the fiber properties with respect to permeability, annealing, and orientation. Extensive testing was performed in conjunction with the Phase 2 studies.

Boeing Aerospace Company

In Phase 1, Boeing conducted studies to ensure that the aircraft operational factors, such as airframe modification requirements and flight test planning, were properly addressed. In addition, Boeing coordinated mission management plans with the Air Force 4950 Test Wing and AiResearch in regard to flight safety and interfaces with other systems. In the restructuring of Phase 2, all flight test planning and airframe support activities were deleted from the program.

Falcon Research and Development

In Phase 1, Falcon was selected to develop an onboard integrated gas monitoring system that would be compatible with the KC-135A test program. The system was designed to operate in conjunction with a government-furnished mass spectrometer. All Falcon activities were halted when the flight test portion of the program was eliminated.

SECTION 2

INERT GAS GENERATION SYSTEM CONCEPTUAL DESIGN

SYSTEM CONSIDERATIONS

As part of Task 1-1, Inerting System Comparison, a conceptual design study for an inerting system based on the use of permeable membranes as an onboard inert gas generation source was performed.

Major differences in requirements dictated the designs for the permeable membrane inert gas generation (IGG) system and the LN_2 system. While the LN_2 system is overall integrated inert gas quantity sensitive (and potentially limited by detail single and multi-mission planning), the IGG system is sized primarily by inert gas flow rate requirements. The selection of missions maximizing the instantaneous flow rates selected for analysis provide assurance that the IGG system will exhibit a flexibility enabling the generation of sufficient inert gas to prevent its becoming a consideration in mission planning.

The baseline design aircraft, the KC-135A, possesses fuel tank pressure limitations dictated by considerations not associated with the IGG system. Sensitivity analysis has indicated that pressurized fuel tank considerations, taken into account at the time of initial airframe design, can be expected to further improve the favorable weight advantage of the IGG system by additional utilization of the accumulator potential of the fuel ullage space to reduce instantaneous inert gas flow requirements. Operating the fuel tank at increased pressure reduces the required inert gas flow as follows:

Tank Ullage Pressure (psid)	Inert Gas Flow (lb/min)
0.0	14.55
0.4	12.45
1.0	10.65
2.0	8.85

The increased fuel tank pressure differential allows greater aircraft altitude variation while maintaining inert gas conditions within the fuel tank ullage space. The increased pressure differential also allows use of a smaller and lighter OBIGGS.

Computer performance prediction data show that the maximum required inertant flow is reduced when ullage design operating pressure is increased. The data show that at 2.0 psid, the maximum inert flow is reduced to 8.85 lb/min at a maximum ullage oxygen concentration of 9 percent. By utilizing this higher ullage pressure, the ASM size is reduced, as is bleed flow.

The conceptual design and supporting studies for the IGG system applicable to the KC-135A tanker aircraft included the following topics. Each of these is discussed in subsequent paragraphs.

(1) Design Mission Profile

(2) Inerting Requirements

(3) Membrane Air Separation Module (ASM)

(4) ASM Air Supply System

(5) Emergency Descent Provisions

(6) Prime System Candidate Comparison

(7) Design Philosophy

(8) Handling of Dissolved Air Released From Fuel

DESIGN MISSION PROFILE

The KC-135A IGG system was designed to the mission profile shown in Figure 2-1. Selected design data corresponding to the numbered points shown on the profile diagram are presented in the associated table.

Figure 2-2 shows the location of the fuel tanks in the KC-135A aircraft and a sketch of the fuel tank inerting and scrub system. The IGG system design does not include inerting of the body tanks. Only the ullage volumes of the center wing, No. 1, 2, 3 and 4 main, and the No. 1 and 4 reserve tanks are included.

Figure 2-3 shows the descent rates for the KC-135A aircraft. As indicated, the gear down, flaps up, no air brakes, descent curve was used for the IGG system design. A separate Halon system could be used to maintain a non-explosive ullage mixture during emergency descent.

INERTING REQUIREMENTS

The inert gas flow rate requirement is the highest during descent, when the fuel tank ullage pressure has to be increased to keep pace with the increasing ambient air pressure. Table 2-1 presents the preliminary results of an analysis of the KC-135A design mission. The tabulated data is based on a scrubbing system, which is operated on the ground and during climb out and cruise.

As can be seen from Table 2-1, the sea-level descent on the final leg of the mission requires the largest membrane surface area to obtain the required inert gas product. This identifies the IGG system design point. The following table defines the design point conditions and requirements for the KC-135A IGG system:

POINT	ALTITUDE (FEET)	MACH NUMBER	FUEL FLOW (LB/HR)	ULLAGE (GALLONS)	MISSION TIME (HRS)	H.S. BLEED PRESS. (PSIA)	H.S. BLEED TEMP. (^{O}F)
1	0	0.423	28,930	1,806	0.05	149.8	725
2	15,000	0.555	22,090	2,575	0.22	108.2	685
3	33,000	0.780	13,140	3,652	0.62	72.8	656
4	31,000	0.680	11,660	5,036	1.37	68.4	622
5	30,000	0.682	9,570	9,012	1.95	61.7	583
6	45,500	0.780	7,320	13,552	3.11	39.5	616
7	46,000	0.780	4,880	14,168	3.64	40.8	641
8	30,000	0.670	7,840	14,236	3.71	54.4	649
9	30,000	0.695	6,000	14,782	4.21	61.1	582
10	15,000	0.515	5,420	14,936	4.29	70.4	561
11	2,500	0.221	7,700	15,398	4.54	111.9	642
12	27,000	0.650	5,720	16,168	4.83	61.5	572
13	15,000	0.515	5,420	16,322	4.95	70.4	560
14	0	0.378	16,970	16,476	5.10	121.2	658

S 31909 A

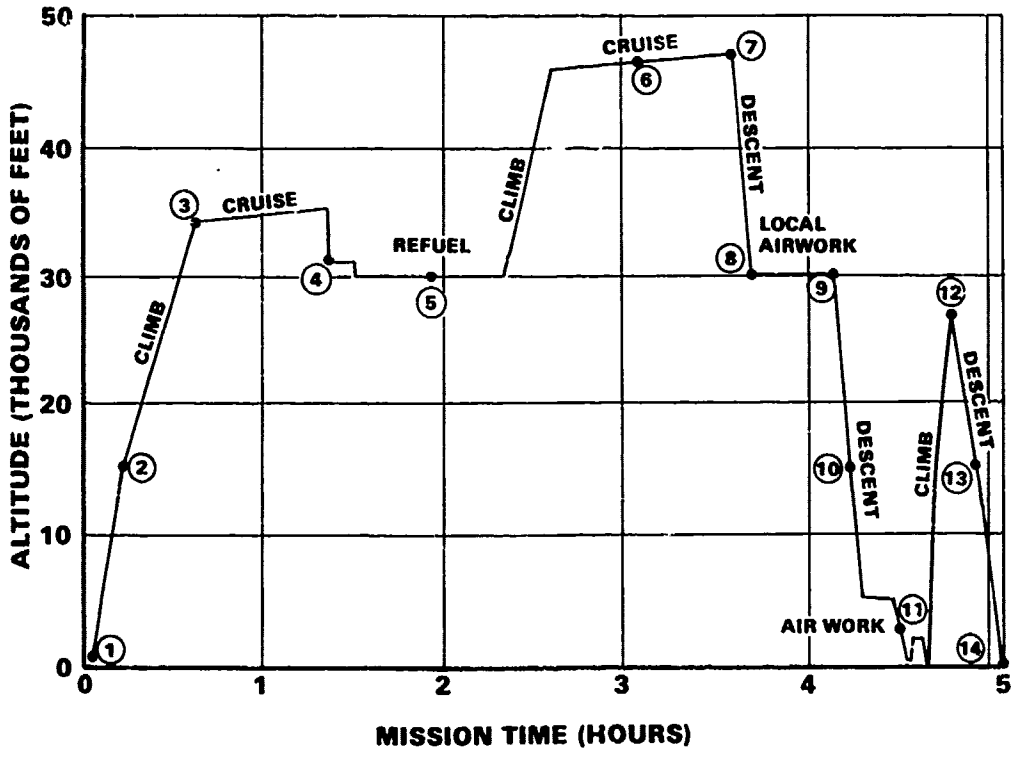

Figure 2-1. KC-135A Tanker Design Mission

S 32003 A

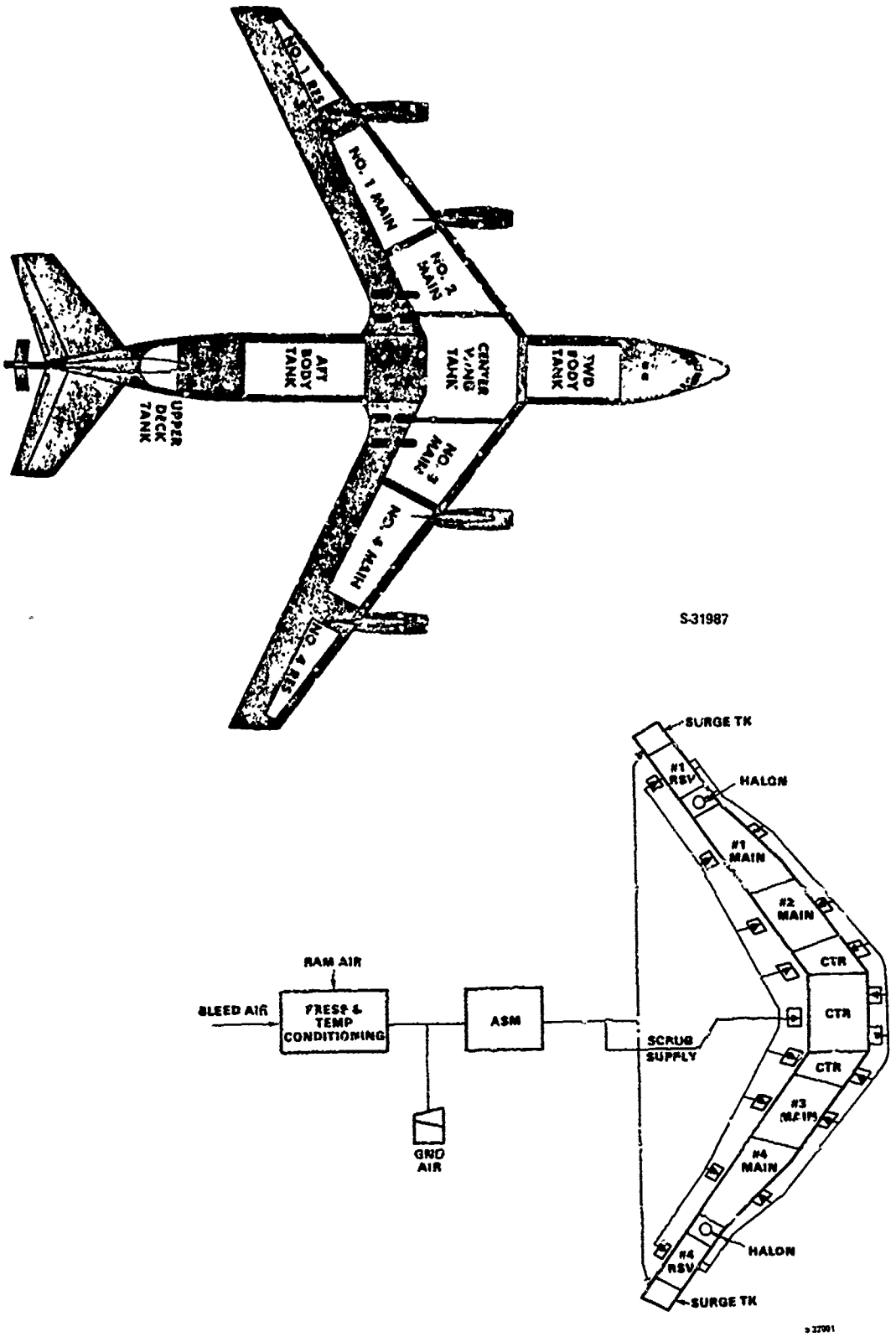

Figure 2-2. KC-135A Fuel Tank Locations and Fuel Tank Inerting and Scrub System Lines

NOTES:

1. **ALL DESCENTS ARE AT GROSS WEIGHT = 125,000 LB**
2. **ENROUTE & GEAR DOWN DESCENTS ARE FROM KC-135A FLIGHT MANUAL PERFORMANCE APPENDIX TWO ENGINES AT IDLE THRUST, TWO AT POWER REQUIRED FOR AIR CONDITIONING**
3. **EMERGENCY DESCENT IS BASED ON FLIGHT MANUAL PROCEDURE USING CLEAN AIRPLANE PLACARD AIRSPEED AS SHOWN AND ALL ENGINES AT IDLE THRUST**

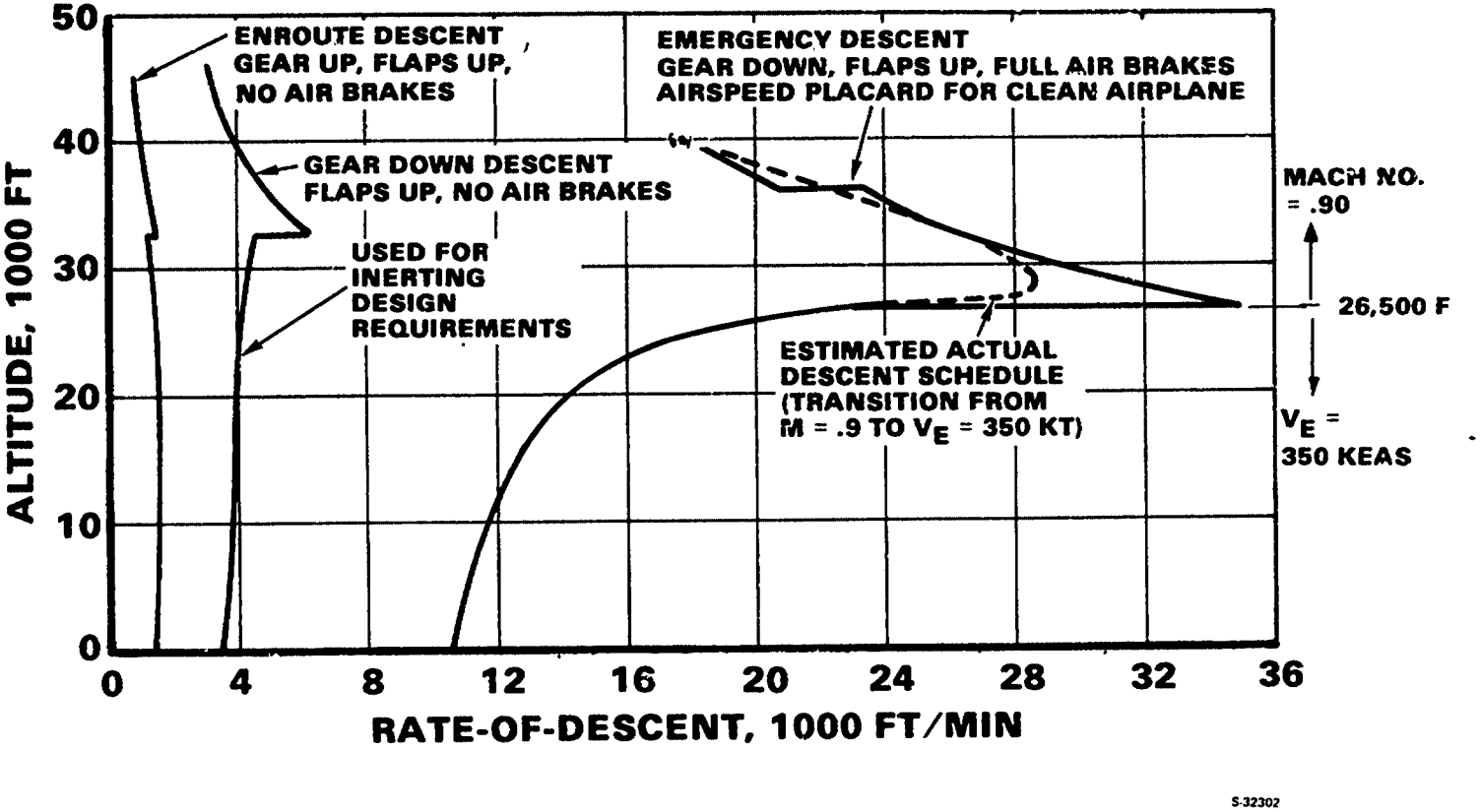

Figure 2-3. KC-135A Rates of Descent

TABLE 2-1

PRELIMINARY IGG SYSTEM ANALYSIS FOR ASM WITHOUT WASH FLOW --
UNPRESSURIZED FUEL TANK

	HIGH ALTITUDE DESCENT			DESCENT TO LOW ALTITUDE			FINAL LEG DESCENT		
AIRCRAFT OPERATION									
ALTITUDE, FT	46,000	32,500	30,000	30,000	15,000	5,000	27,000	15,000	0
RATE OF DESCENT, FT/MIN	2,800	6,000	4,000	4,000	3,800	3,500	4,100	3,800	3,600
HIGH STAGE BLEED PRESSURE, PSIA	33.8	41.0	44.1	48.4	57.2	84.3	51.0	57.2	90.7
AMBIENT PRESSURE, PSIA	2.04	3.89	4.36	4.36	8.29	12.23	4.39	8.29	14.70
ASM REQUIREMENTS									
PRODUCT OXYGEN CONCENTRATION, VOLUME % MAXIMUM	9	9	9	9	9	9	9	9	9
INLET PRESSURE, PSIA (100 PSID)	104.1	105.8	106.2	106.2	109.7	113.1	106.7	109.7	113.1
INLET TEMPERATURE, °F	75	75	75	75	75	75	75	75	75
INERT GAS PRODUCT FLOW RATE, LB/MIN	2.13	7.75	5.95	6.15	9.49	13.09	7.06	10.37	14.55
RESULTS									
COMPRESSOR PRESSURE RATIO	3.42	2.87	2.67	2.67	2.08	1.49	2.33	2.13	1.30
ASM FEED AIR FLOW RATE, LB/MIN	4.1	14.7	11.3	11.7	18.0	25.5	13.4	19.7	28.1
MEMBRANE SURFACE AREA REQ'D, SQ. FT.	24,800	88,700	67,800	70,100	105,000	148,000	105,000	114,000	198,000

S-31905

Aircraft Conditions	Bleed Air Conditions		
Landing at end of descent	Engine Stage	Pressure (psia)	Temperature (°F)
Gear down, flaps up, no airbrakes	High	96.7	565
Sea level, 0.378 Mach flight	Low	34.5	298
3600 ft/min rate of descent	Ambient Conditions		
16,683 gallons ullage	14.70 psia, 103°F		
43 gpm fuel flow	154 grains of water/lb of dry air		

Inerting Requirements

9 vol. % O_2, balance inert

System Performance Analysis

The system performance analysis computer program was updated to (1) include the revised ASM performance program which refined the "leakage and block" characteristics and (2) provide ullage concentration outputs as a function of the mission profile. Computer generated system performance plots are presented in Figures 2-4, 2-5, and 2-6, which demonstrate the reduction of the maximum required inertant flow with increased ullage design operating pressures. The data shows that for the same ASM configuration, the maximum inertant flow of 12.45 lb/min at a tank ullage pressure of 0.4 psid is reduced to 10.65 lb/min at 1.0 psid and to 8.85 lb/min at 2.0 psid, while maintaining a maximum ullage oxygen concentration of 9 percent. By utilizing the higher ullage pressure, the ASM size can be reduced while maintaining the higher inertant flow rate. Conversely, for a constant ASM size the required inertant flow rate can be reduced, permitting a reduction of bleed air usage.

MEMBRANE AIR SEPARATION MODULE DESIGN

The air separation module (ASM) consists of one or more cylindrical bundles of membrane fibers. These fibers are hollow tubes in which the feed air flows in one end and the product inert gas flows out the other end. In this configuration, the waste flow permeating through the membrane walls flows from the inside to the outside of the hollow fibers. It is then collected and dumped overboard. Near the end of the program, it was found necessary because of module fabrication problems to design a smaller size (9 in.) ASM, utilizing an "outside-in" flow configuration for the waste flow permeating through the hollow-fiber membrane walls. This design is discussed in Section 7, Hardware Fabrication.

Separation Principle

The separation of mixed gases into enriched streams involves the use of a polymeric membrane surface. A gas mixture, under pressure, is introduced to one side of this membrane material. Because of differing membrane permeation rates

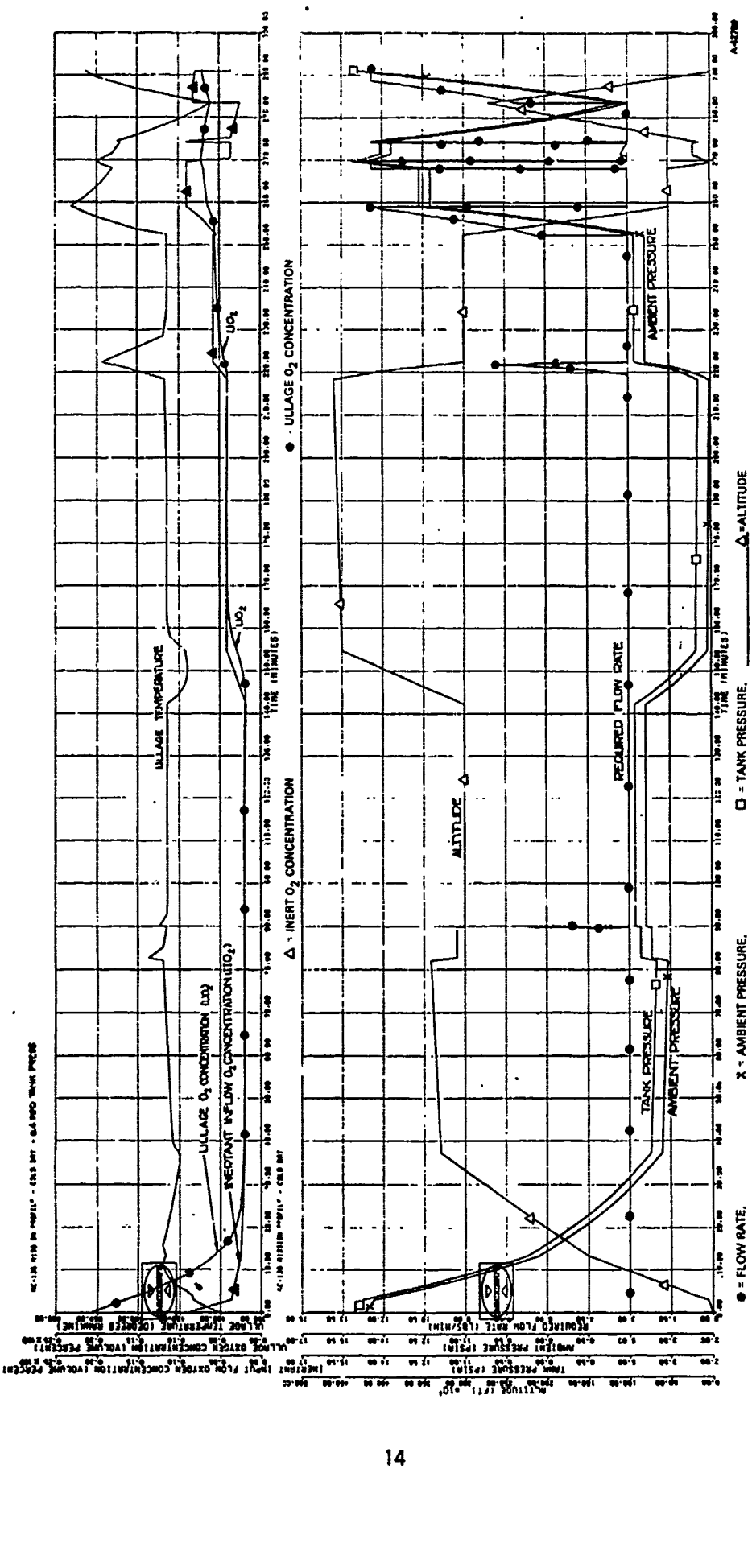

Figure 2-4. ASM System Performance at 0.4 psid Tank Ullage Pressure

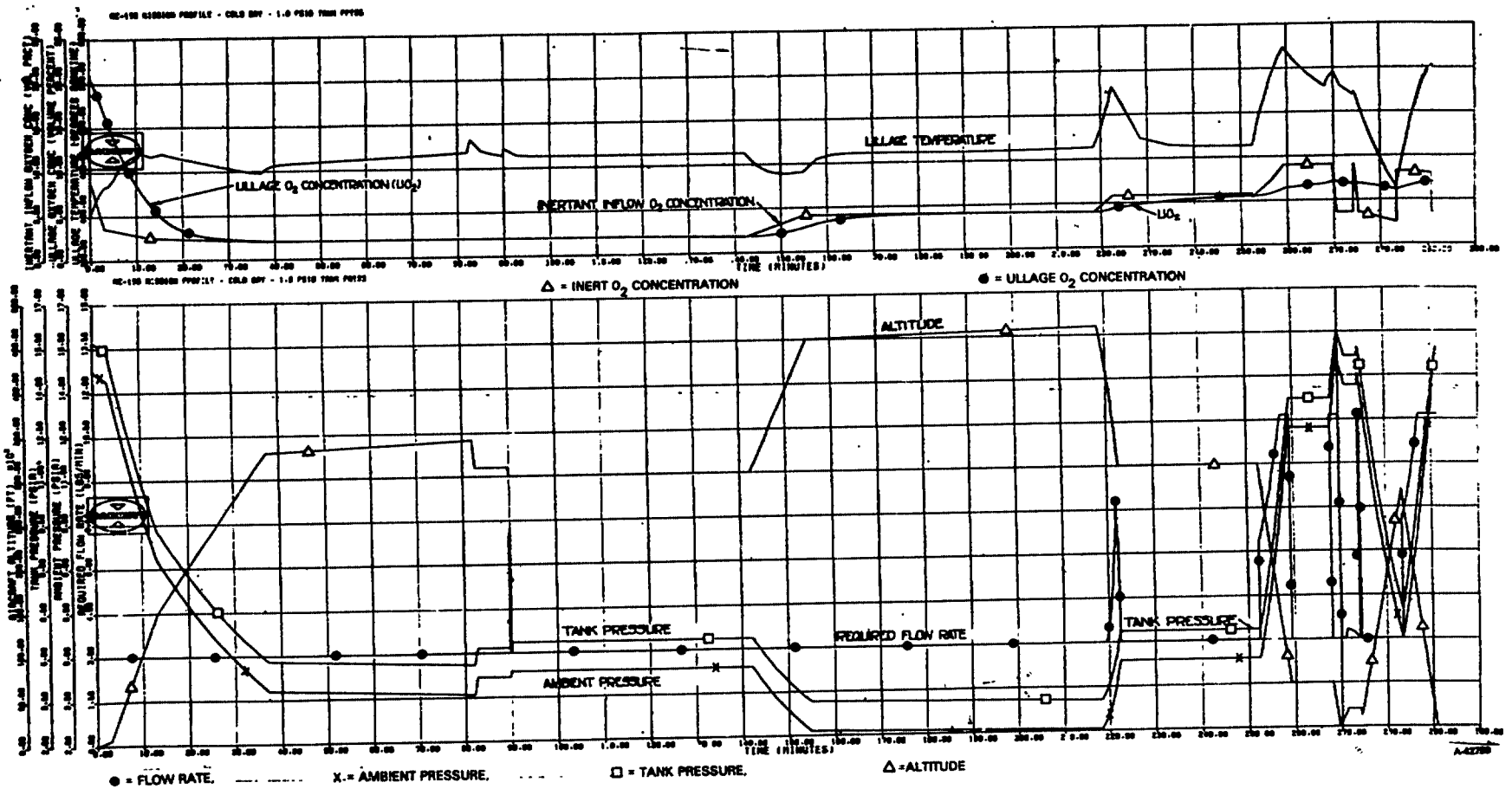

Figure 2-5. ASM System Performance at 1.0 psid Tank Ullage Pressure

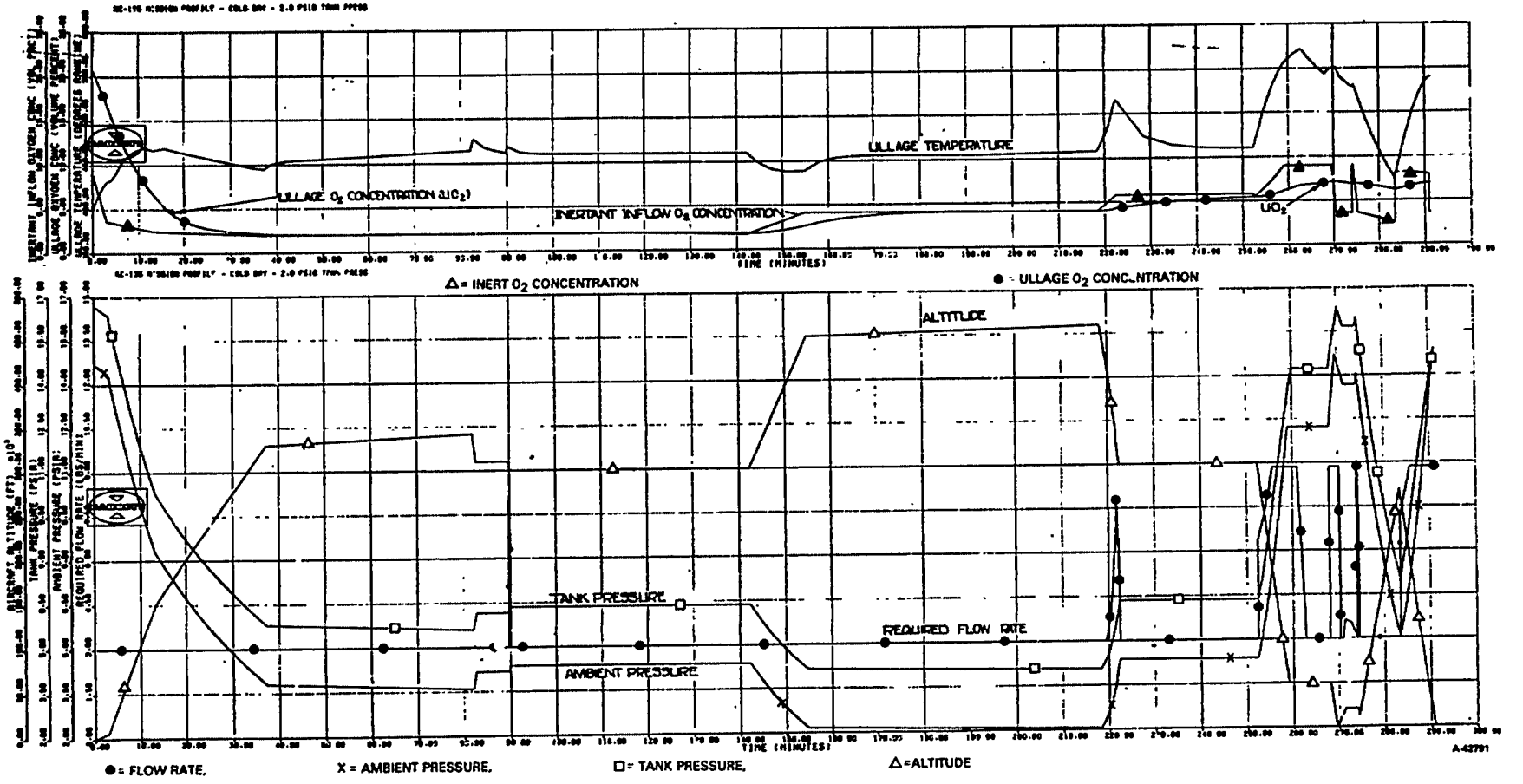

Figure 2-6. ASM System Performance at 2.0 psid Tank Ullage Pressure

for the various gases in the mixture, the high-pressure gas becomes depleted of the components with the highest permeability, thereby becoming enriched in low-permeability gases, while the permeant is enriched in concentration of the high-permeability gases. Air approaches a binary mixture of oxygen and nitrogen, of which the oxygen (the more permeable gas) is approximately 21 percent.

Membrane mass transfer may be conveniently analyzed by using the activated diffusion model. That is, the gases transfer through the membrane walls first by dissolving into the polymer surface, then by concentration gradient-driven diffusion through the polymer, and finally by evolution at the opposite surface. The combination of these processes constitutes permeable gas transfer. Although gas diffusion is only a part of the transfer mechanism, it usually is rate-controlling, allowing the surface concentration of dissolved gas to be in near equilibrium concentration with free-stream-gas partial pressures in accordance with Henry's Law.

The baic relationship to describe mass transfer across a permeable membrane boundary may be described by the following equation.

$$Q_i = \frac{TP_i \; A \; \Delta P_i}{th} \qquad (2\text{-}1)$$

where: Q = mass transfer rate through the membrane

A = surface area of membrane normal to permeate flow

ΔP = free stream partial pressure difference (driving force)

th = material thickness

TP = permeability coefficient

subscript i = i^{th} gas

This equation relates mass transfer rate to the partial pressure difference (the driving potential) in a manner similar to Fourier's relationship for heat transfer rate as a function of temperature difference as the driving potential. In Equation 2-1, the proportionality constant is called the permeability coefficient. This coefficient is ideally a function only of the polymeric membrane material and of the gas being transferred at a given temperature.

Hollow-Fiber Configuration

Though gas permeation through thin films of solid materials has long been recognized, and though data have been collected to show that certain gases permeate through a given material more readily than other gases, actual practical applications have been limited. With few notable exceptions, gas enrichment by the use of permeable membranes has remained a laboratory curiosity. The major drawback limiting the application of membrane separation has been the problems encountered in scaling small laboratory test apparatus to useful separation rates.

The permeability of even the most permeable of materials is low when evaluated in terms of apparatus requirements for even modest separation rates. The low permeabilities require large surface areas of extremely thin membranes. Total surface area requirement has been provided by manifolding the sheets to achieve the required surface area in a compact package geometry. This presents two severe problems: (1) flat sheets of a thin material cannot support much pressure differential, and (2) a means to manifold alternate passages is required. Several approaches to increase the structural load bearing capability of flat membranes have been tried. In general, the favored approach has been to provide a second material for strength. This usually takes the form of a matrix material as a porous backing plate or as a fabric material that has been impregnated with the membrane polymer to form small flat-plate surfaces between fabric fibers. In either case, care must be taken to provide sufficient separation of alternate plates to allow the required flow. While these techniques significantly increase the load-bearing capabilities of the membrane surface, they tend to increase greatly the volume required to contain the required active surface area, which further complicates the manifolding difficulties.

The second problem, that of manifolding the sheets to interconnect alternate passages, has been troublesome. The difficulty here lies in the fact that not all edges are to be connected but rather adjacent passages must be separately manifolded to form alternate high- and low-pressure passages, each separated by the thin film membrane.

The development of small hollow fibers has provided a practical breakthrough in solving the structural difficulties associated with flat plates. Since hollow fibers form their own pressure vessels, no additional backing material or structural support is required. A high-pressure gas stream introduced into (or around) the hollow fibers can be supported by the proper polymeric material selection and design to limit the resultant stress to acceptable levels. The selection of a relatively high-strength material enables self-supporting tube wall thickness to be relatively thin for small tube sizes under hoop stress. In addition, the absence of the requirement for a structural backing material allows the package size to be reasonably small.

The problem of joining alternate flat plates, which is encountered when using thin films, is reduced to manifolding tubes when hollow-fiber permeable membranes are considered. This is accomplished by winding the tubes around a core as in filament winding processes. Winding results in a continuous fiber that is further processed by forming a bonding agent as a tube-sheet about each end of the unit. By machining the end of the tube-sheet, the loops at the ends of the fibers are severed, thereby opening the tubes at the ends to form manifolded parallel tubes whose structure resembles a tube-and-shell heat exchanger as shown in Figure 2-7.

Equation 2-1 permits the mass transfer rates to be calculated for a given gas through a permeable membrane barrier if the geometry of the membrane, the local partial pressure of the gas on either side of the barrier, and the permeability coefficient of the gas membrane system are known. Equation 2-1 applies to both internally and externally pressurized module designs. The geometry (surface area and material thickness) can be measured; thus, the analytical prediction of mass transfer rates depends on the control of the

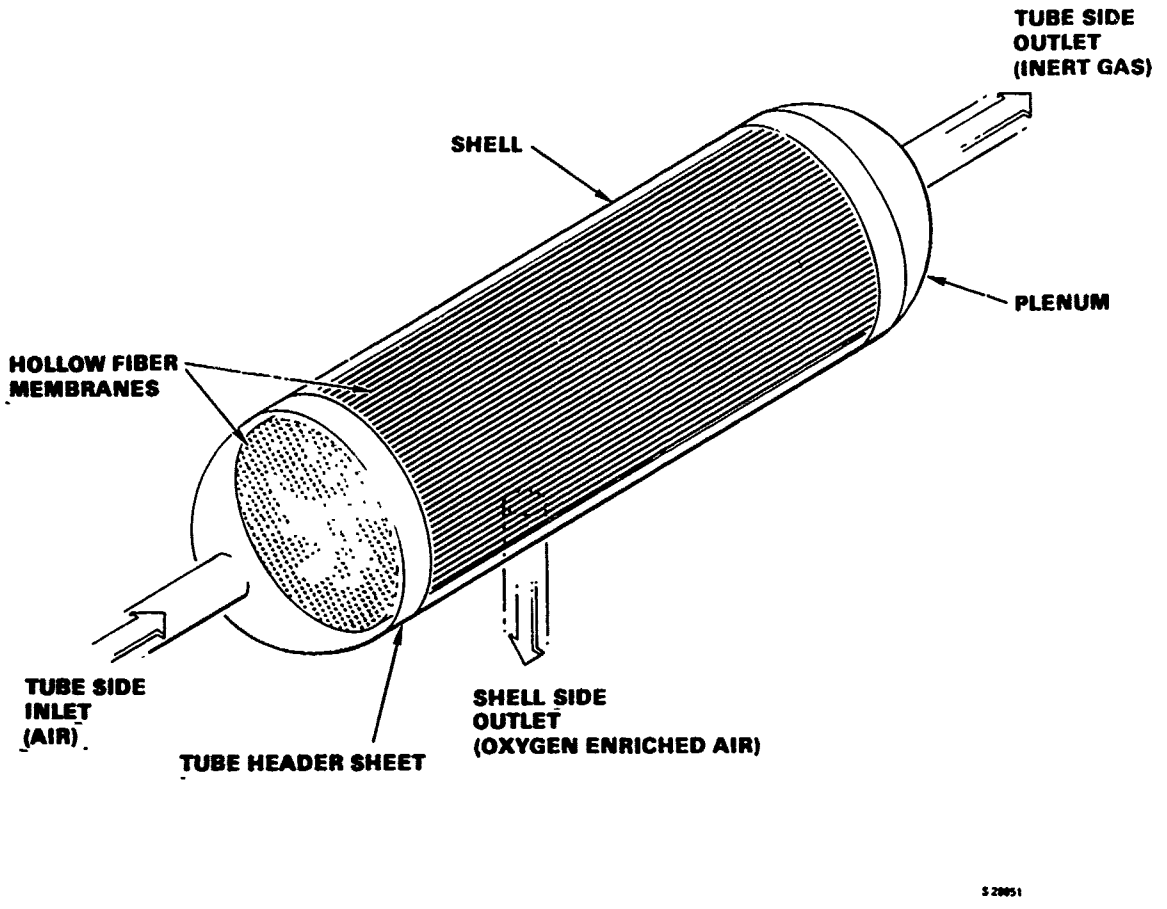

Figure 2-7. Hollow-Fiber Permeable Membrane Air Separation Module

permeability coefficients and the partial pressure of the gas on each side of the membrane barrier. For hollow-fiber geometry, the surface area normal to net gas transfer is a function of radius, the surface area is based on log-mean surface area, and the material thickness is the difference in radial dimension.

The general form of the mass transfer equation, as shown in Equation 2-1, can be written for an oxygen/nitrogen two-gas system as:

$$\dot{Q}_O = \frac{TP_O A \, \Delta P_O}{\Delta X} \qquad (2\text{-}2)$$

and

$$\dot{Q}_N = \frac{TP_N A \, \Delta P_N}{\Delta X} \qquad (2\text{-}3)$$

where the subscripts O and N denote oxygen and nitrogen, respectively.

At the limiting concentration, as discussed above:

$$\frac{\dot{Q}_O}{Q_N} \alpha \frac{Conc_O}{Conc_N} \alpha \frac{P_O}{P_N} \qquad (2\text{-}4)$$

where P_O and P_N are the tube side oxygen and nitrogen partial pressures, respectively. If the oxygen concentration of the remaining gas sample is denoted by the symbol c, where:

$$c = \frac{P_O}{P_O + P_N} \qquad (2\text{-}5)$$

and the ratio of the permeability coefficients for oxygen and nitrogen defined by the symbol TP_r where:

$$TP_r = \frac{TP_O}{TP_N} \qquad (2\text{-}6)$$

an expression for the limiting value of c may be derived. By substituting the definitions of total pressures as the sum of partial pressures, and the tube partial pressures as a sum of the permeant side partial pressure plus the driving force partial pressure for each gas, the following relationship is found to exist as the theoretical minimum oxygen concentration.

$$\frac{P}{P'} = \frac{\left[c' \frac{1-c}{c} TP_r - (1-c')\right]}{c\left[\frac{1-c}{c} TP_r + 1\right] - 1} \qquad (2\text{-}7)$$

where P = tube side total pressure

P' = shell side total pressure

c' = shell side oxygen concentration

The solution of expression (2-7) for c, the tube side limiting oxygen concentration, results in a quadradic equation. The meaningful root may be expressed as follows:

$$c = \frac{-Y - \sqrt{Y^2 - 4XZ}}{2X} \qquad (2\text{-}8)$$

where: $X = P\,(TP_r - 1)$

$Z = c' TP_r\, P'$

$Y = (c' - 1)\, P' - X - Z$

Wash vs. Non-Wash Configurations

The fiber bundle will have gas enriched in oxygen on the outside of the fiber tubes. When this gas consists of the permeant flow only, it contains approximately 36 percent oxygen. This high oxygen content decreases the driving potential of oxygen partial pressure across the membrane. Diluting the permeant gas with normal air can reduce the oxygen concentration greatly, thus resulting in a potentially smaller membrane area. The diluting flow is termed "wash" air.

A problem associated with the use of wash flow is the pressure drop it produces. This results in a higher pressure level outside the fiber tubes, which reduces the pressure ratio across the tubes and, in turn, decreases the driving potential for permeating flow through the membrane.

Figure 2-8 shows the pressure drop outside the fibers as a function of packing factor and diameter ratio. Due to the large increase in pressure drop associated with the use of wash flow, it was concluded that the wash flow would not be used during the conceptual design phase.

Effect of Pressure and Temperature on Fiber Life

Figure 2-9 shows projections of the life of the membrane fibers as a function of the pressure differential across the tubes (inside minus outside) and the fiber temperature. As can be seen, the life is very sensitive to both parameters. As a result, only the aircraft operating time during which the fibers are exposed to maximum pressure and temperature will significantly affect the life.

Based upon the availability of pressurized air in the KC-135 aircraft, a conceptual design point of 75°F for fiber operating temperature would be optimum. This temperature was selected because 75°F is the best performance and life condition when a nominal feed pressure of 85 psig is available. Studies of fiber performance and life are presented in Appendixes A and B.

Arbitrarily assuming the ASM should be designed for 1000 missions and that 0.85 hour of each mission is at the maximum (design) pressure condition, the design useful life becomes 850 hours. From Figure 2-9, this can be seen to correspond to a pressure differential of approximately 100 psi at 75°F.

Figure 2-10 shows the life and fiber weight of the KC-135A ASM as a function of feed pressure at 75°F. Figure 2-11 shows similar curves where life and fiber weight vary with temperature as the feed pressure is constant at 115.5 psia and the outlet waste pressure at 15.5 psia.

ASM Packaging Alternatives

Figure 2-12 presents the size of the fiber bundles as a function of the number of bundles used for a conceptual ASM design. It was anticipated that fiber bundle diameters slightly in excess of 13 inches could be manufactured for the demonstration units, although information now available indicates that an 8-inch diameter is the maximum econimical size. See Section 7

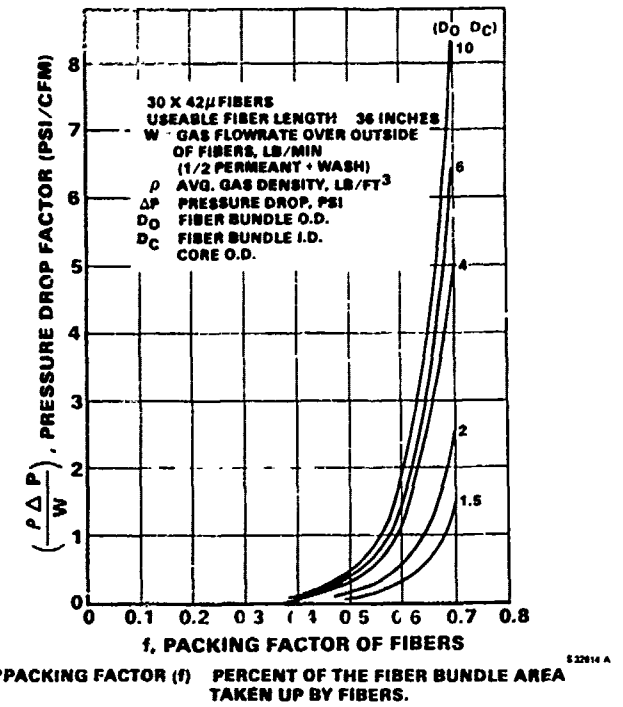

*PACKING FACTOR (f) PERCENT OF THE FIBER BUNDLE AREA TAKEN UP BY FIBERS.

Figure 2-8. Air Separation Module Low Side Pressure Loss as a Function of Packing Factor

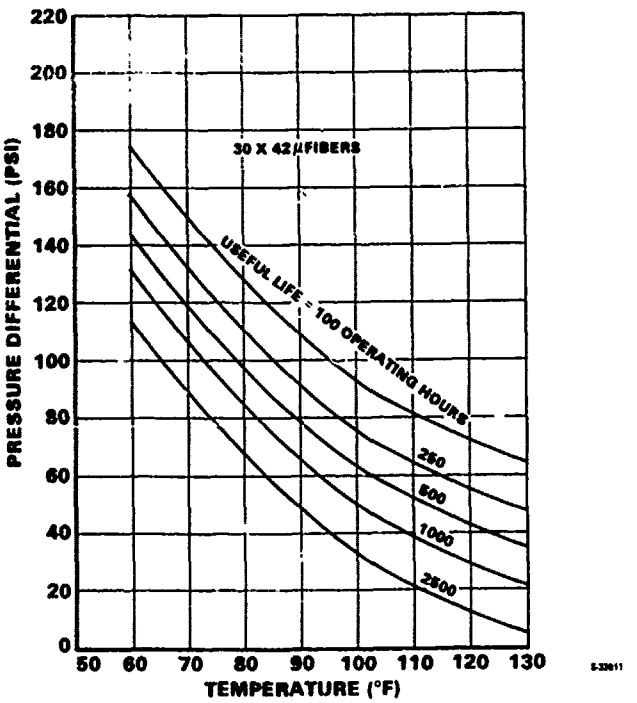

Figure 2-9. Effect of Pressure and Temperature on Internally Pressurized Fiber Life

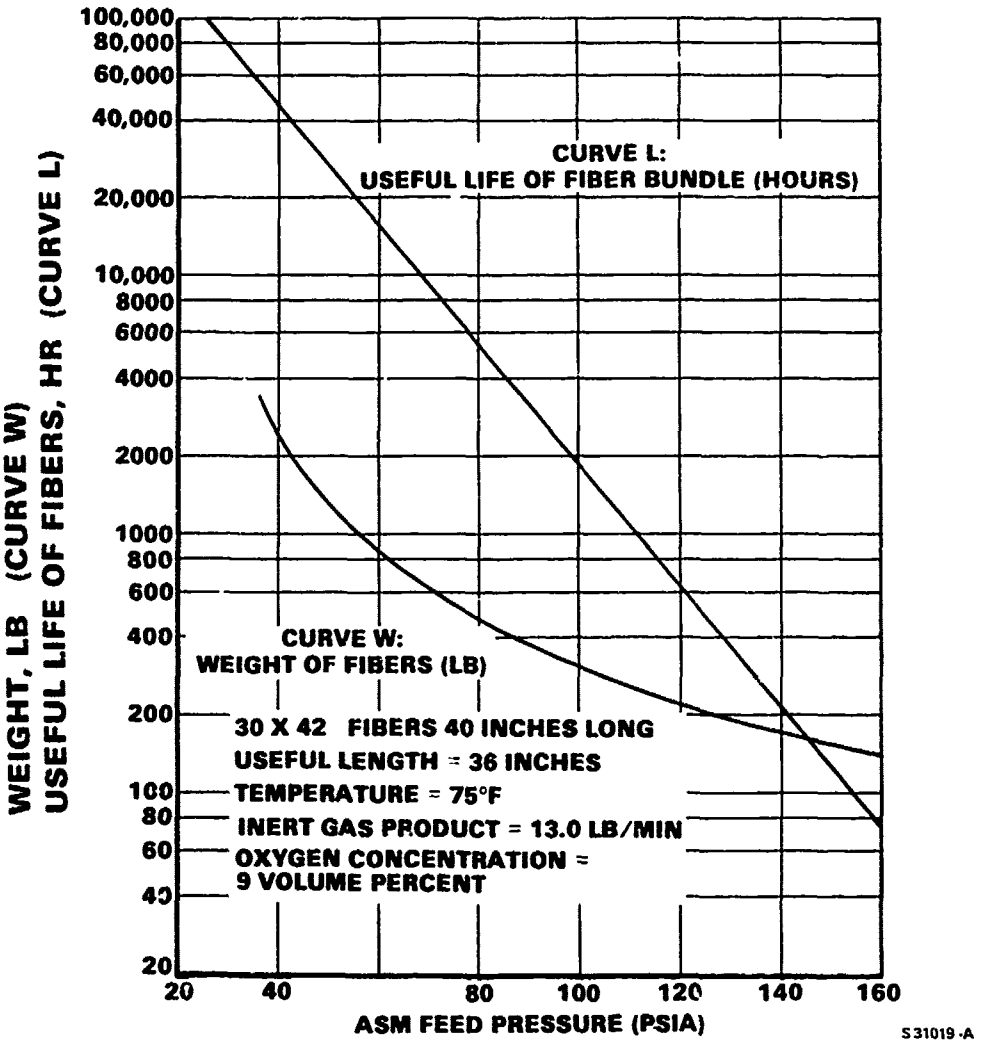

Figure 2-10. Effect of ASM Feed Pressure on Life and Weight of Internally Pressurized Fibers

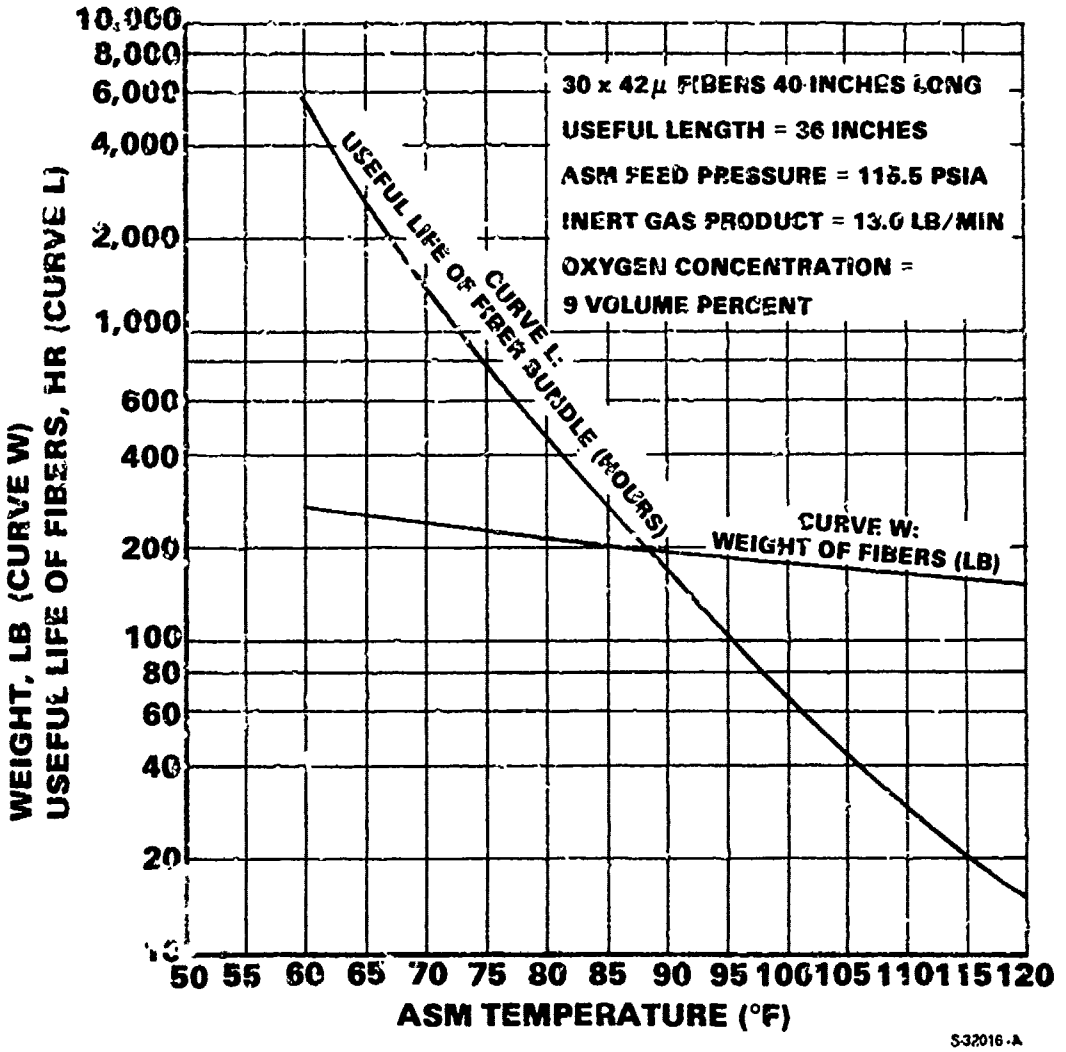

Figure 2-11. Effect of ASM Feed Temperature on Life and Weight of Internally Pressurized Fibers

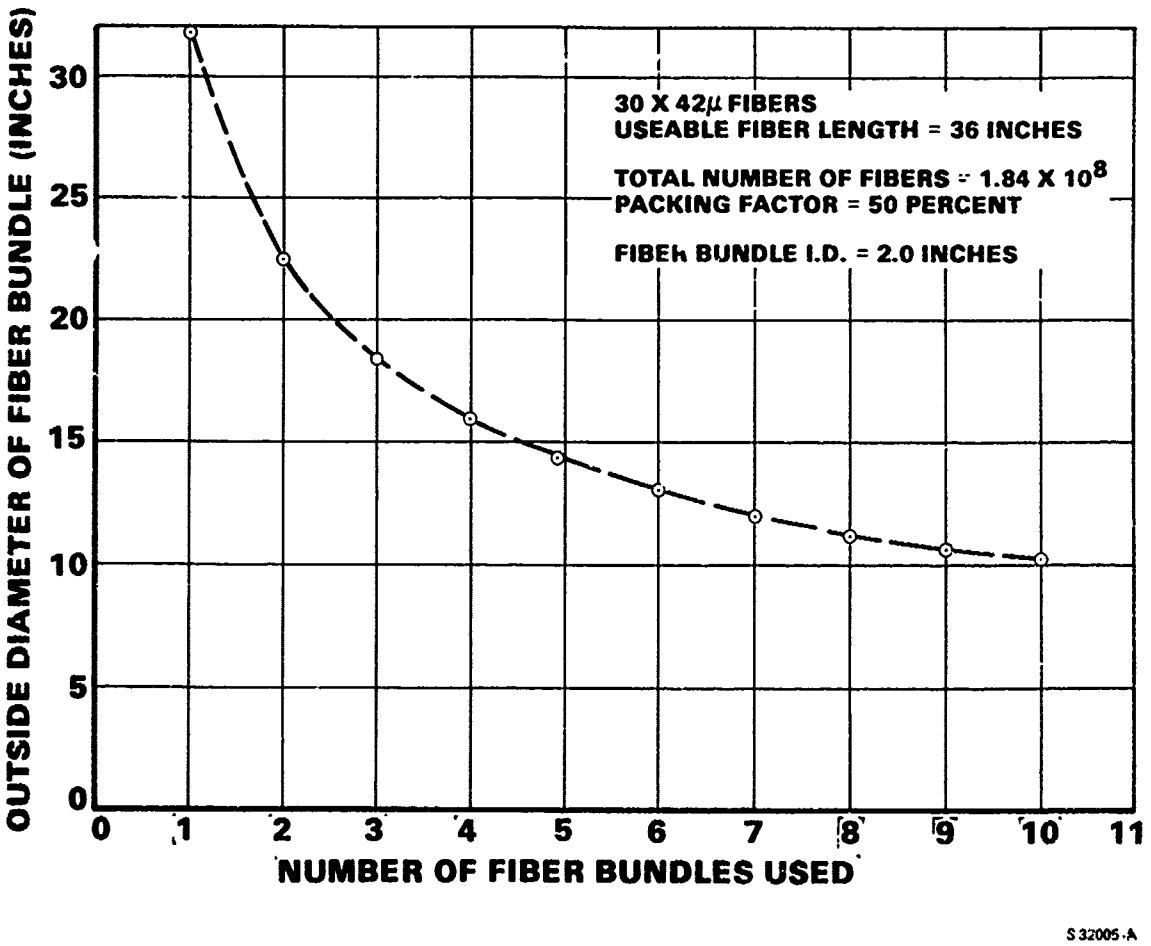

Figure 2-12. Required Fiber Bundle Size for KC-135A Aircraft

for details. The primary packaging alternatives for an ASM consisting of multiple cylindrical bundles of membrane fibers are as follows:

Manifolding Alternatives

Concept I - Individual pressure vessels and external manifolding of all flows

Concept II - Common manifold of one flow in a single pressure vessel and external manifolding of the other two flows

Concept III - Common internal manifold of each flow in a single pressure vessel

End Cap Alternatives	End Cap Retention Alternatives
a. Flat plate	a. Bolted flange
b. Hemispherical	b. V-band

Figures 2-13 through 2-15 are cross-sectional drawings of typical ASM fiber bundle packages that illustrate the above manifold alternatives.

ASM AIR SUPPLY SYSTEM

The basic ASM air supply system options are shown schematically in Figure 2-16. Engine bleed air provides the source of high pressure feed flow to the ASM. A number of heat sink candidates and ASM wash flow sources are listed in this figure.

The high-stage bleed air pressure is generally not at a pressure sufficiently high to minimize the ASM size and weight. Therefore, it is compressed by a turbocompressor to provide the desired pressure level. To reduce the compressor power requirement, the inlet bleed air is cooled prior to compression. It is cooled again and temperature controlled prior to entering the ASM. The cold air leaving the turbine portion of the turbocompressor is used as the heat sink to provide the desired feed air temperature (approximately 70°to 80°F).

The air used to drive the turbine can be taken from any point in the schematic diagram of Figure 2-16 or can be low-stage bleed air. However, a thermodynamic balance cannot always be obtained by taking air from any point. For example, using high- or low-stage bleed air directly will not allow the turbine discharge air to be under 75°F.

Figures 2-17 through 2-19 present the three most promising schematic arrangements. Figure 2-18 uses low-stage bleed air to drive the turbine, Figure 2-18 uses high-stage bleed air tapped from between the two heat exchangers downstream of the compressor outlet, and Figure 2-19 uses the product inert gas (which is still at high pressure).

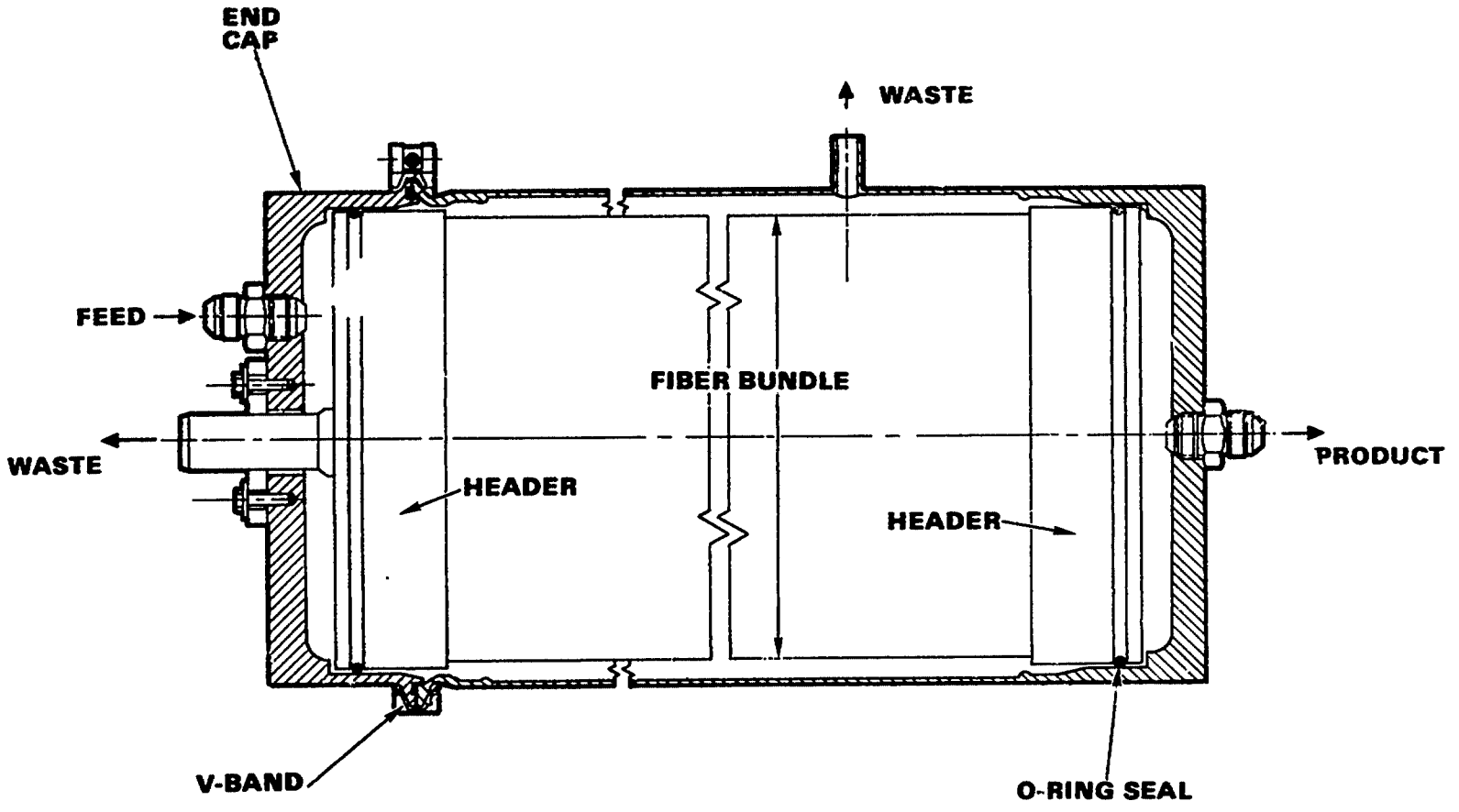

Figure 2-13. Concept I - Each Fiber Bundle Individually Packaged in a Pressure Vessel

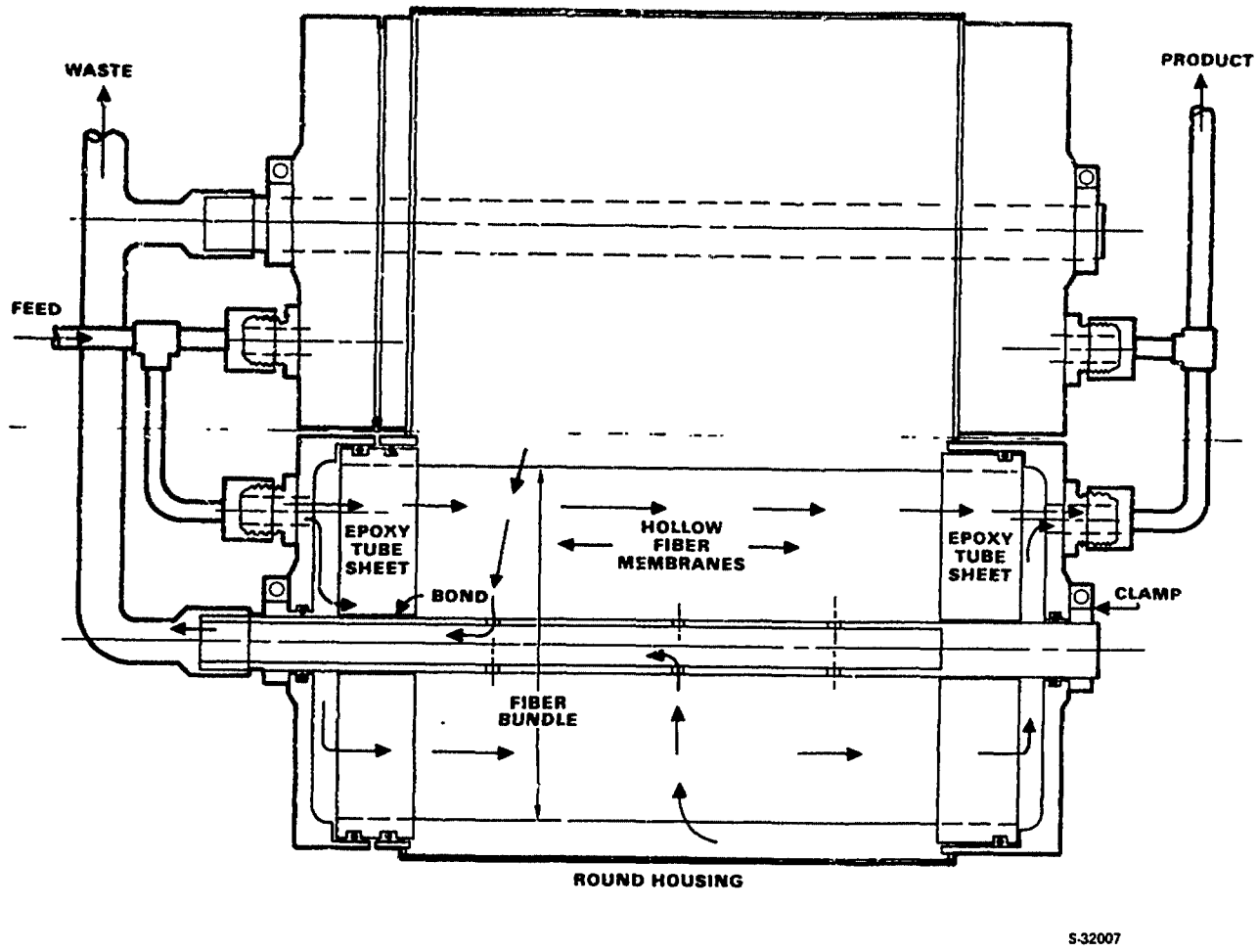

Figure 2-14. Concept II - Waste Flow Has a Common Pressure Vessel

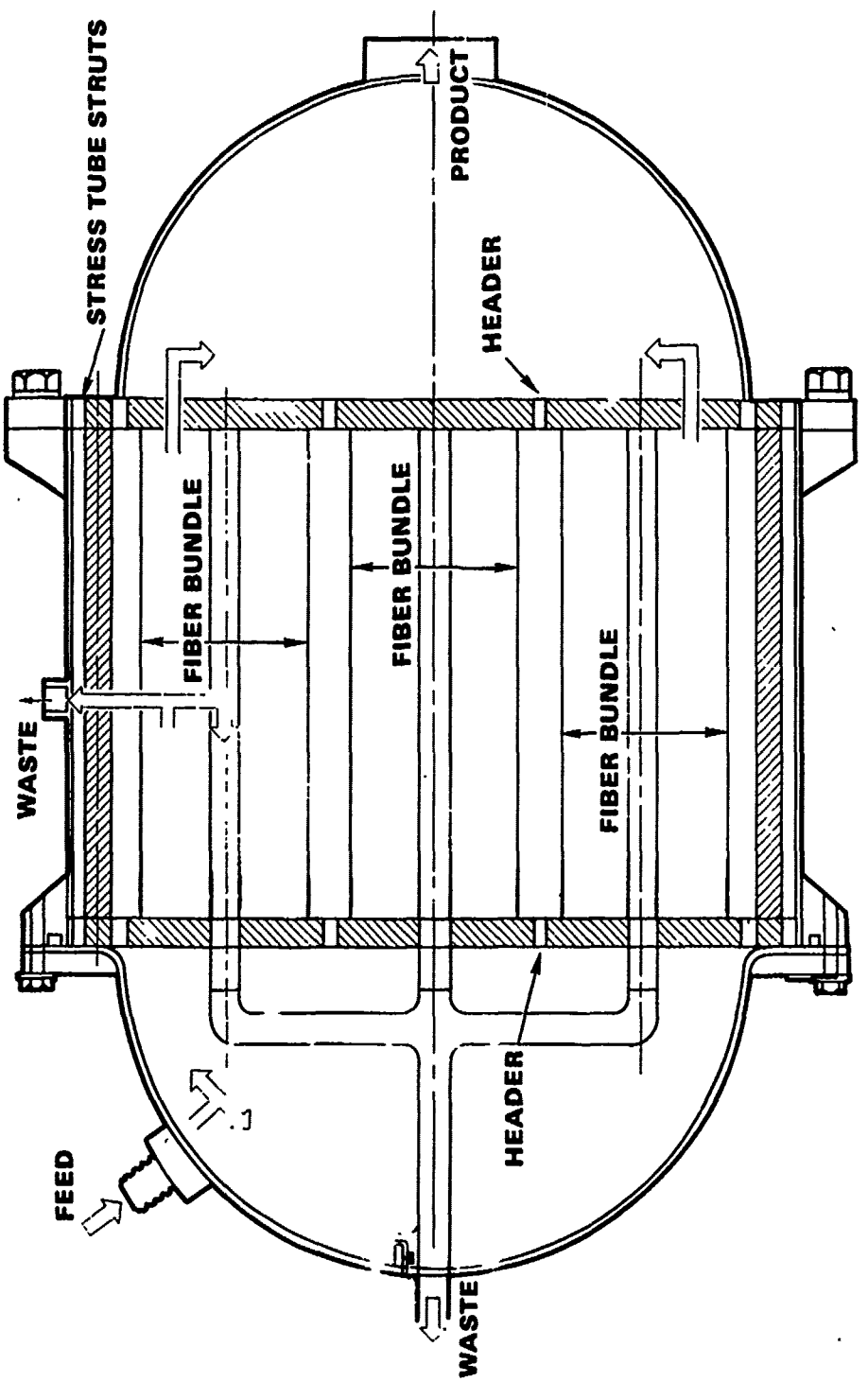

Figure 2-15. Concept III - All Flows Have Common Pressure Vessel

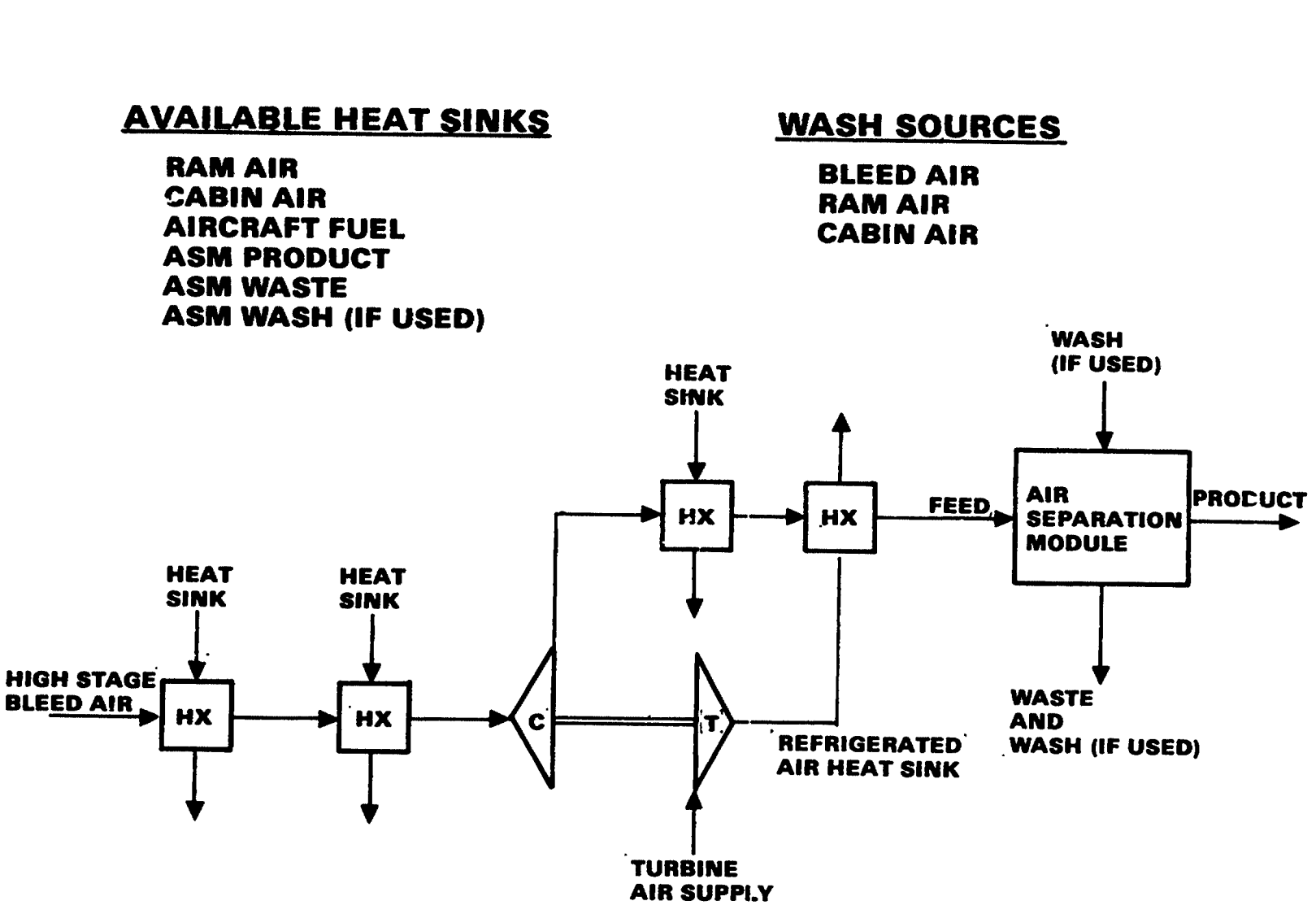

Figure 2-16. Basic Schematic Options
Inert Gas Generation System

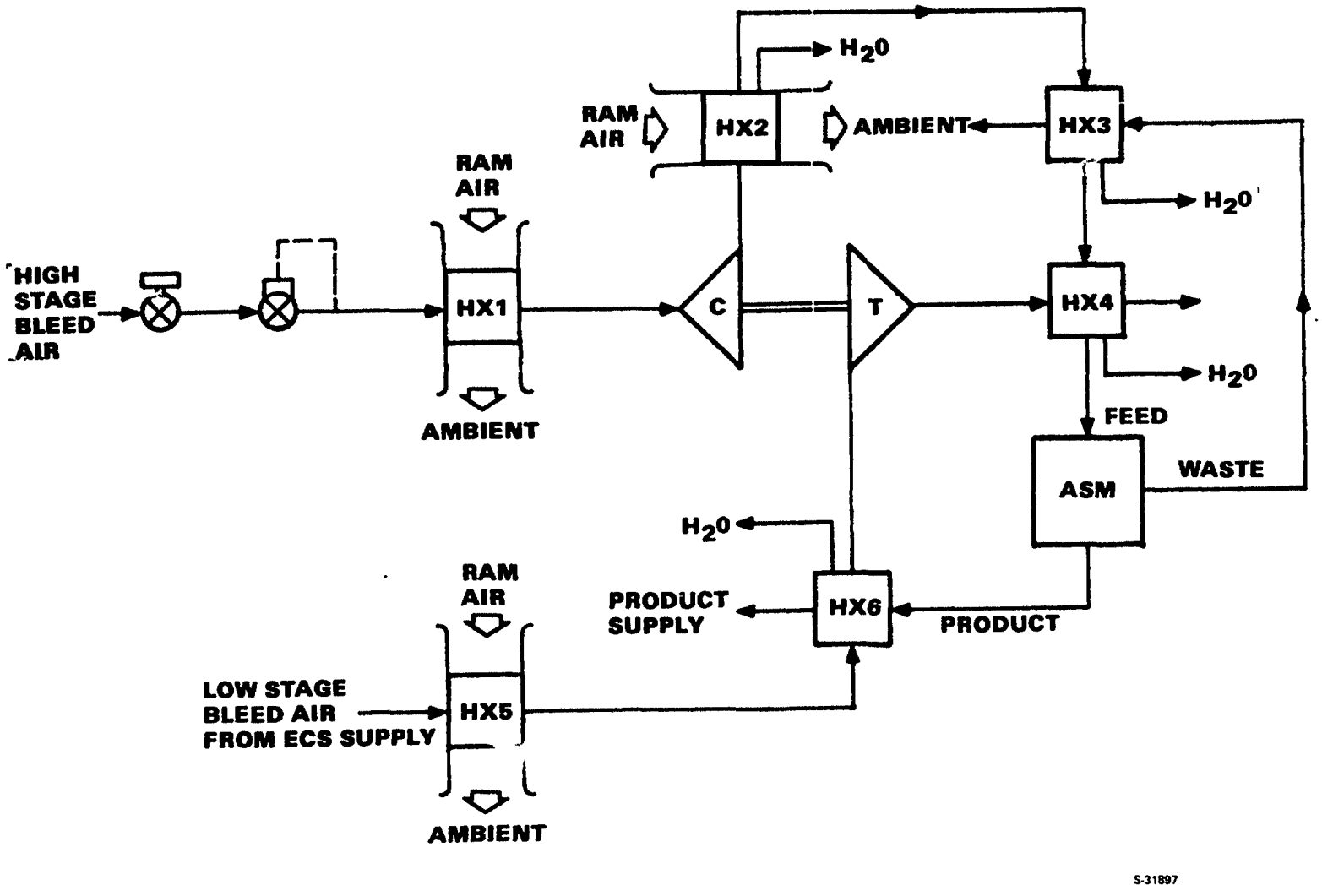

Figure 2-17. Combination High/Low Stage Bleed IGG System

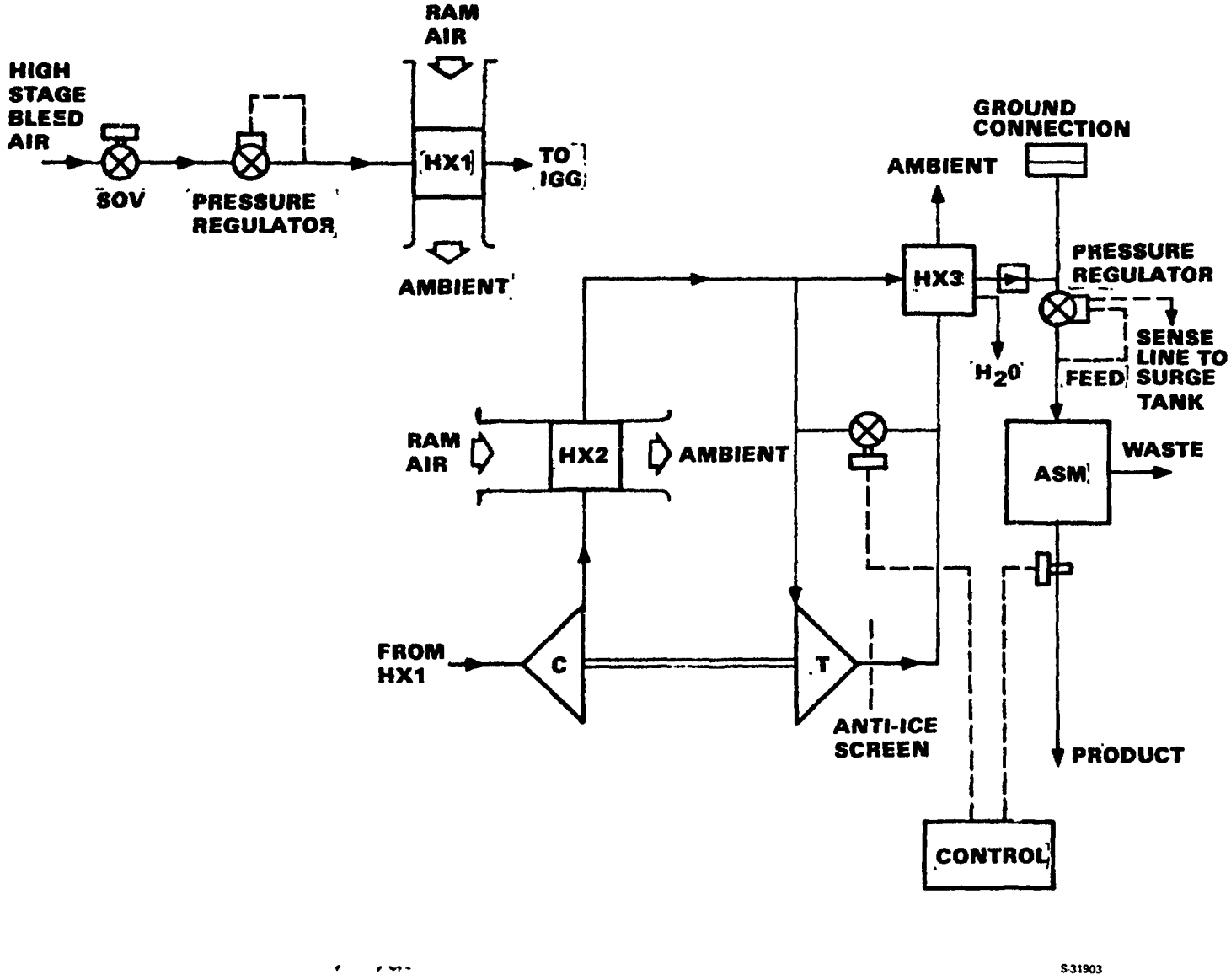

Figure 2-18. Non-Integrated Inert Gas Generation System

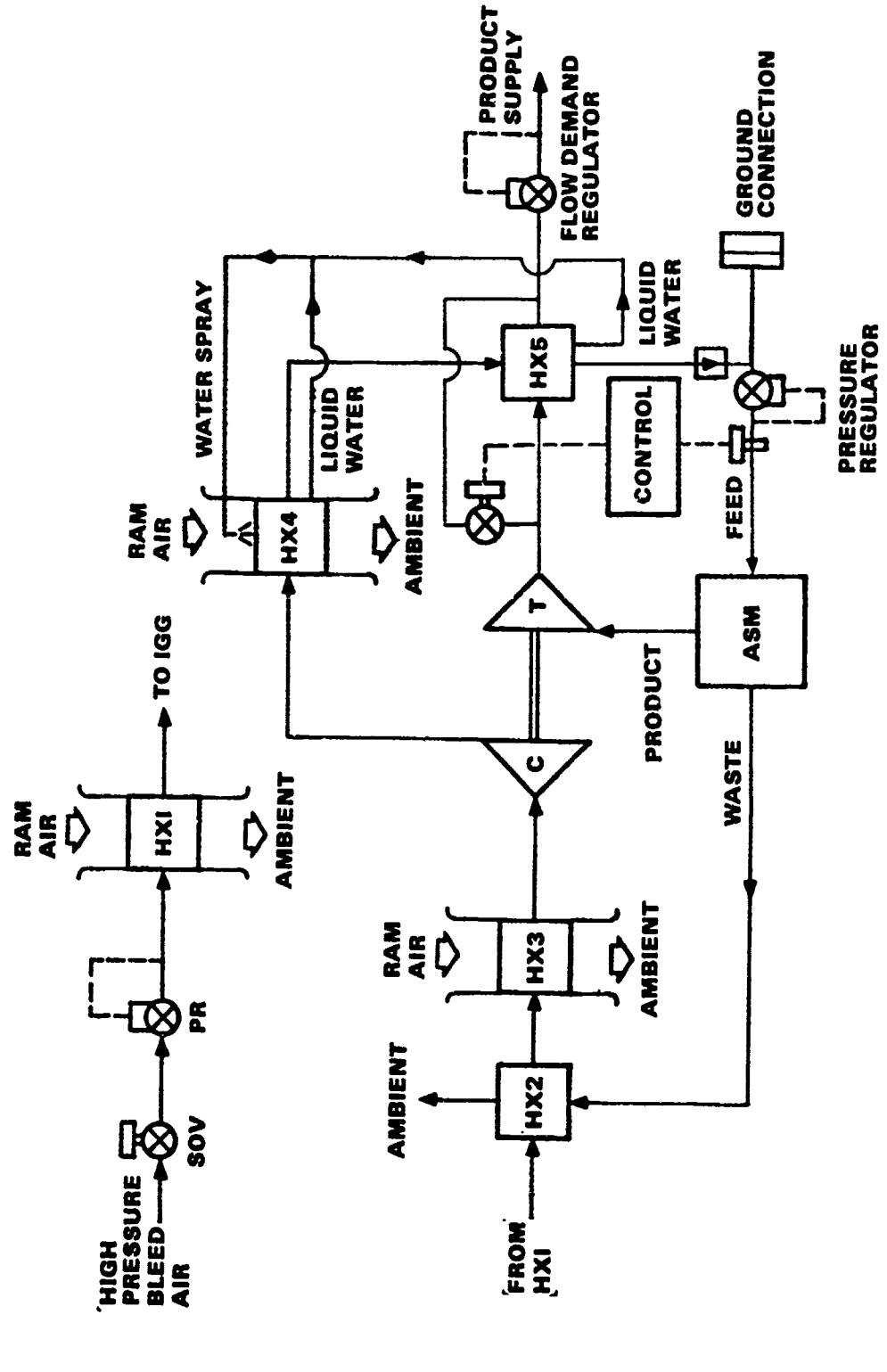

S31898

Figure 2-19. Integrated Inert Gas Generation System

The combination high/low-stage bleed inert gas generation (IGG) system shown in Figure 2-17 is very marginal in performance. Every available heat sink must be utilized to provide the desired 75°F ASM supply air temperature. In addition, the heat exchangers require high effectiveness, making them large in size.

The system shown in Figure 2-18 is basically a bootstrap-type, air-cycle, air-conditioning system, with the ASM feed air supply being tapped from the turbine inlet. This system arrangement requires the fewest number of heat exchangers and provides the required performance. It has the advantage of flexibility in that it can easily accommodate changes in ASM requirements. However, it does require more high-stage bleed air. This system is termed "non-integrated" because it is essentially independent of the ASM and can be developed using a simulated ASM. The other two candidates do not have this ability.

The system shown in Figure 2-19 is termed the "integrated" system because it uses the ASM product to drive the turbine, thus tying ASM performance to the performance of the air supply system. The integrated system, however, provides the least penalty to the aircraft. It is the lightest and uses the least bleed air and ram air. These advantages are provided at the expense of complexity and cost. Development of this system requires more detailed ASM operating experience than currently exists, since any change in ASM requirements or performance will necessitate changes in the air supply portion of the IGG system.

Figure 2-20 shows duct diameter and velocity head as a function of Mach number and pressure for the inert gas product flow rate. For the non-integrated system approach, the product gas pressure is about 98 psia. At Mach 0.15, the resultant velocity head is 1.5 psi. The corresponding duct diameter is about 0.7 inch. When the flow splits into two ducts to supply the wing tanks, the required duct size drops to 0.5-inch diameter.

The integrated system has a much lower product inert gas supply pressure, about 24 psia. At Mach 0.15, the velocity head is 0.4 psi and the required duct diameter is about 1.4 inches for the full flow. This reduces to 1.0 inch for the split flow to the wings.

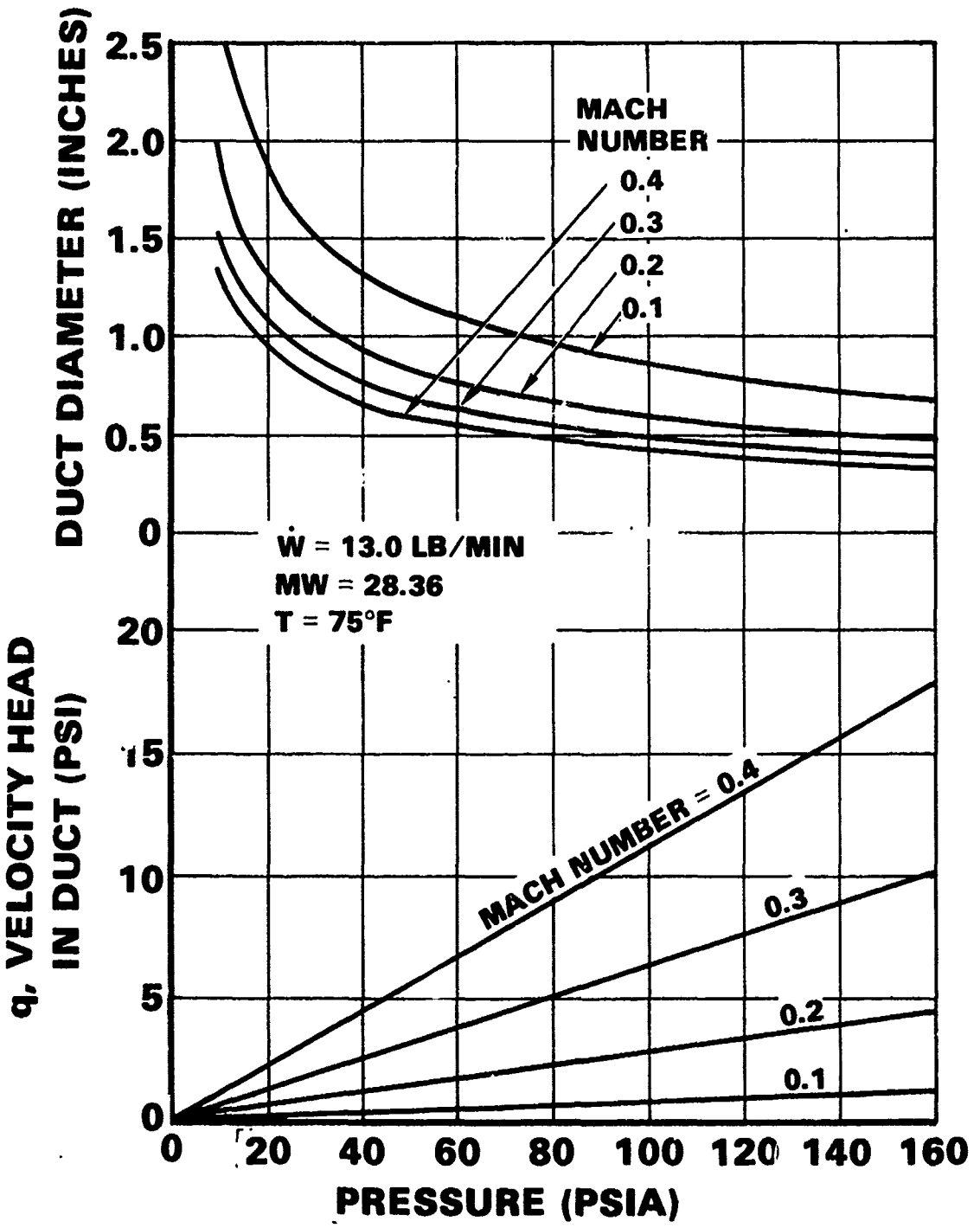

S-32012

Figure 2-20. Duct Size and Velocity Head

EMERGENCY DESCENT PROVISIONS

The IGG system described herein uses Halon 1301 fire extinguishing agent to augment the inert gas supply generated onboard the KC-135A aircraft. This results in an IGG system size considerably smaller than if the system were designed to meet the rare emergency descent conditions with inert gas generated onboard the aircraft.

Table 2-2 lists the characteristics of the Halon emergency extinguishing system during emergency descent flow augmentation using Halon 1301 fire extinguishing agent (CF_3Br). This system can be initiated by an electrical signal from the cockpit at the pilot's discretion.

TABLE 2-2

CHARACTERISTICS OF HALON INERTANT SYSTEM
FOR KC-135A EMERGENCY DESCENT

Halon Supply Requirements

- Total ullage for emergency descent at end of mission = 2203 cu ft
- 8 vol. percent of Halon required to inert tanks = 176 cu ft
- Halon density at 430°R and 14.7 psia = 0.487 lb/cu ft
- Halon required = 86 lb or 43 lb/side

Halon Tank Requirements

- 14.5 in. dia. welded steel sphere
- Volume = 1596 cu in.
- Capacity = 45 lb Halon
- Fill density = 48.7 lb/cu ft
- Pressurized expulsion = 360 psi
- Total filled weight = 65 lb
- Electrical operation by pilot on emergency descent

PRIME SYSTEM CANDIDATE COMPARISON

Table 2-3 presents a comparison of the three prime IGG system candidates. The bleed air and ram air requirements at the sea level descent design point (8.85 lb/min) and the fixed system weights are shown. As can be seen, the integrated system is the lightest and uses the least bleed air and ram air.

TABLE 2-3

COMPARISON OF IGG SYSTEM CANDIDATES FOR
KC-135A SEA LEVEL DESCENT OPERATION
103°F DAY WITH 154 GR/LB HUMIDITY

	Non-Integrated System	Integrated System	Combination High/Low Bleed System
High stage bleed airflow at design point, lb/min	48	26	26
Low stage bleed airflow at design point, lb/min	0	0	24
Ram airflow at design point, lb/min	135	55	180
Inert gas generation system equipment weight, lb			
Air supply and conditioning	87	73	148
Air separation module	475	475	475
Valves and controls	35	35	35
Ducting and plumbing*	170	130	195
Emergency Halon system	140	140	140
Total weight, lb	907	853	993

It should be noted that the air separation module dominates the weight, being approximately half of the total system weight.

Figure 2-21 depicts the inert gas generation system packaging concept that could be used for the flight demonstration unit. It is mounted on a pallet for ease of installation in the KC-135A cargo compartment. As can be seen, the air

*The integrated system is lowest in weight. It has the least ram airflow and therefore needs the smallest diameter ram air ducting.

NOTE: DIMENSIONS ARE IN INCHES

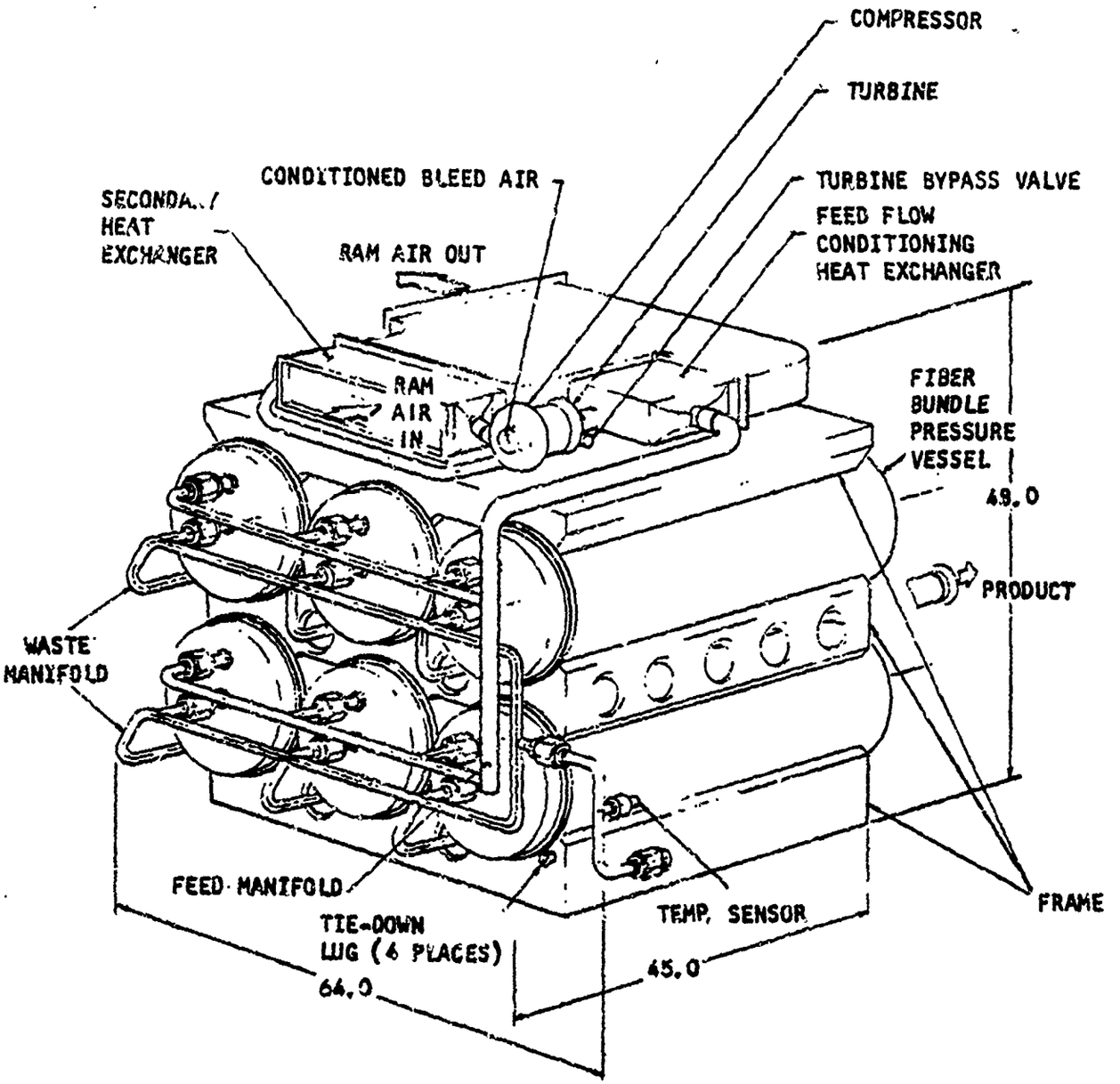

Figure 2-21. Typical Inert Gas Generation System

supply system components make up a small portion of the system volume. Figure 2-22 shows that there is ample room in the KC-135A cargo compartment to place the IGG system flight demonstration unit.

DESIGN PHILOSOPHY

Demonstration Unit

The IGG system for flight demonstration of the membrane air separation module was designed to meet the basic objective of the demonstration, which was to establish the performance capability of the membrane approach to aircraft fuel tank inerting and conform to the considerations listed below (in descending order of importance):

1. Demonstrate membrane ASM performance capability.
2. Limit development to membrane ASM.
    a. Provide independent air supply.
    b. Minimize interfaces.
3. Keep hardware cost down.
    a. Use boilerplate ASM.
    b. Use existing heat exchangers, valves, and turbocompressors.
    c. Combine precooler and primary heat exchangers.
4. Package for easy installation.
    a. Pallet in cargo compartment.
5. Minimize aircraft penalties for:
    a. Fixed weight
    b. Bleed and ram air
    c. Electric and hydraulic power

The conclusion to be derived from these considerations is that the non-integrated version of the IGG system configuration should be used for flight demonstration.

Production Units

Future production IGG systems should be designed for larger quantity fabrication methods, using the following considerations:

1. Provide required performance.

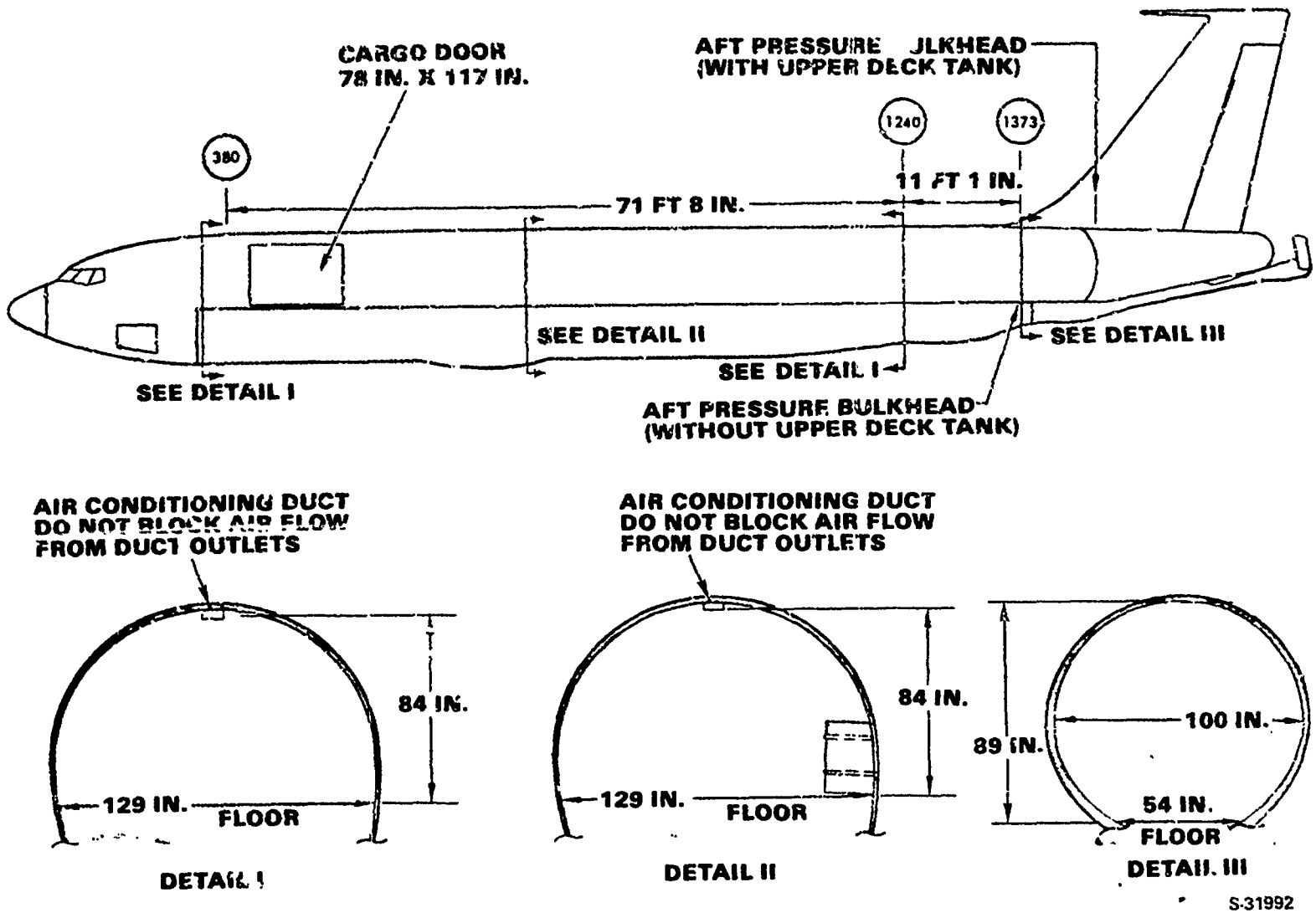

Figure 2-22. Cargo Compartment Dimensions

2. Minimize aircraft penalties.

3. Minimize cost of ownership.

The conclusion to be drawn here is that the integrated IGG system concept should be pursued for production units.

HANDLING OF DISSOLVED AIR RELEASED FROM FUEL

The various atmospheric gases are soluble in hydrocarbon fuels to varying degrees. The total dissolved gas is shown in Figure 2-23 for JP-4 aircraft fuel in contact with air at various temperatures and pressures. Because oxygen is more soluble than nitrogen, this dissolved gas is enriched in oxygen over the gas in the vapor phase. For 21 percent oxygen in the vapor phase, the dissolved gas is 30 percent oxygen. For 6 percent in the vapor, the dissolved gas would be 9.2 percent oxygen. As the fuel tank pressure is decreased with increasing aircraft altitude, these dissolved gases will be partially or completely released. The composition of the gas released will depend on the precise manner of this release. If the dissolved gases remain in equilibrium with the tank pressure, the gases will be gradually released as the aircraft climbs. If the fuel becomes supersaturated, there will be a sudden release of all the gas above the equilibrium value when the fuel is disturbed.

Three basic ways can be used to handle the dissolved air in the fuel to assure an inert atmosphere in the ullage space. They are:

1. Scrub fuel during fueling operation and maintain an inert blanket.

2. Scrub fuel continuously during climb.

3. Scrub fuel intermittently during climb.

Of course, combinations of these methods can also be used.

If it were possible to equilibrate the fuel on the ground with gas containing less than 6 percent oxygen, the dissolved oxygen would not be a potential hazard. This could be done by storing the fuel under an inert gas blanket or by sparging either during the fueling operation or in the fuel tanks of the aircraft. If the aircraft must operate with fuel which has dissolved gases, a purge flow must be provided during climb to dilute the gas being released by the fuel.

As an example, if the purge flow is 3 lb/min or 33.8 percent of design flow from Figure 2-24, the resulting purge gas oxygen content will be 3 percent.

NOTE: Figure 2-24 is based upon an IGG producing inert gas with 9.0 percent oxygen concentration at a flow of 8.87 lb/min.

From Figure 2-25, 3-percent purge gas relates to 0.005 lb of gas per gallon of fuel; thus 3 lb/min purge flow will inert 600 gal/min of fuel. Based upon an estimated initial fuel load of 16,200 gal, the 3 lb/min purge would take only 27 min to inert fuel ullage to 3 percent oxygen concentration. This

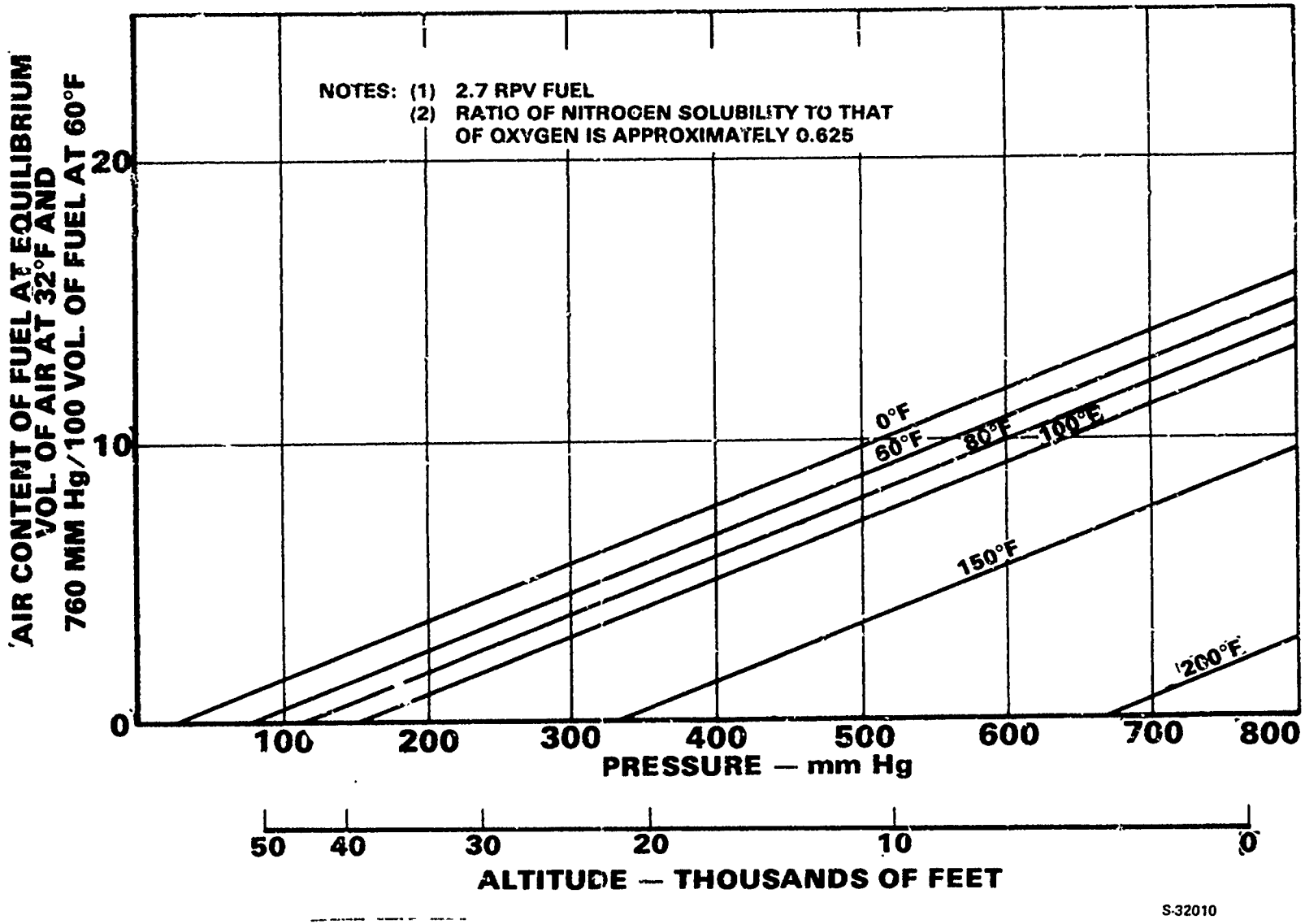

Figure 2-23. Typical Air Content of JP4 Aviation Gas Turbine Fuel

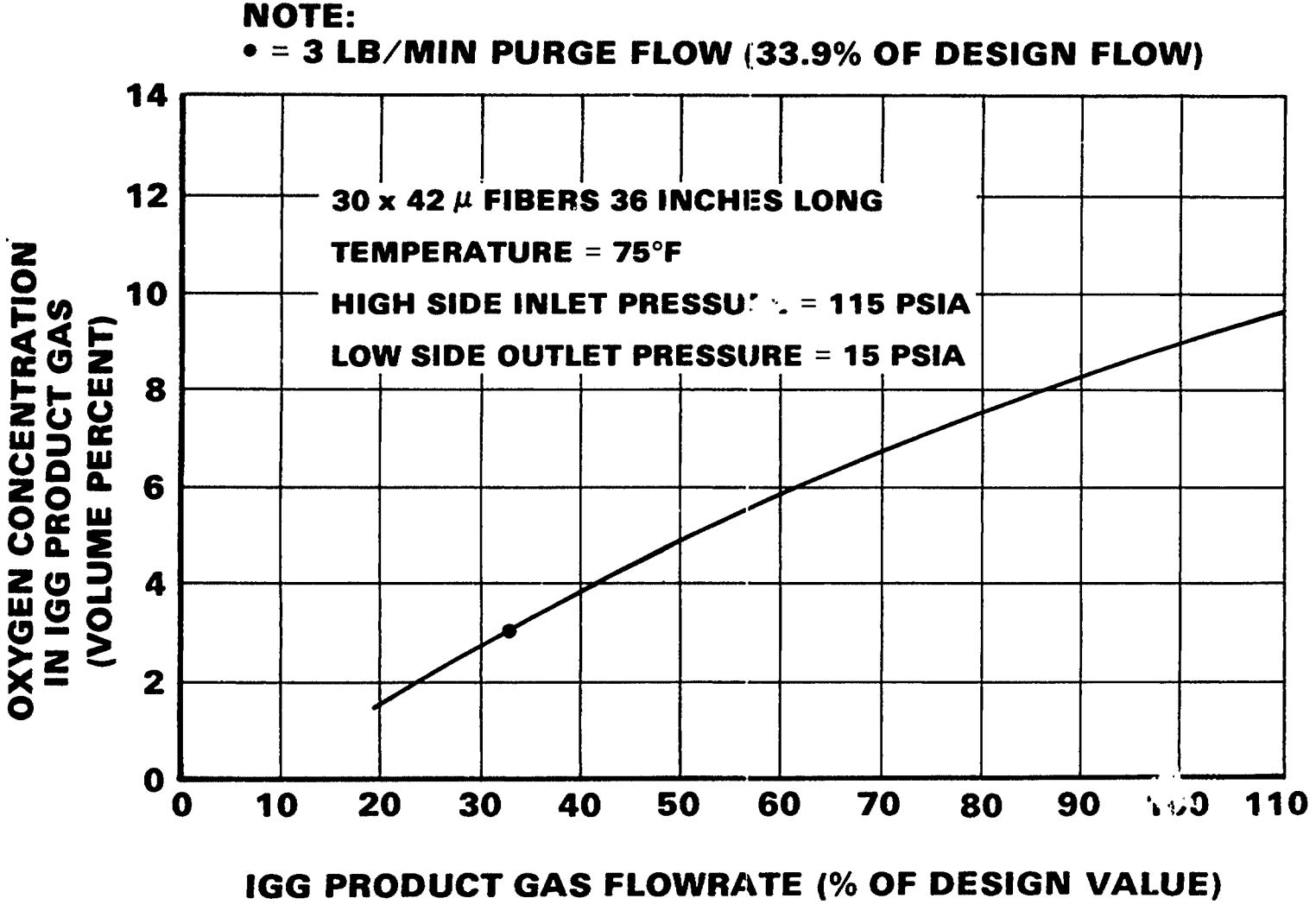

Figure 2-24. Inert Gas Oxygen Concentration vs Variation of Flowrate From Design Value

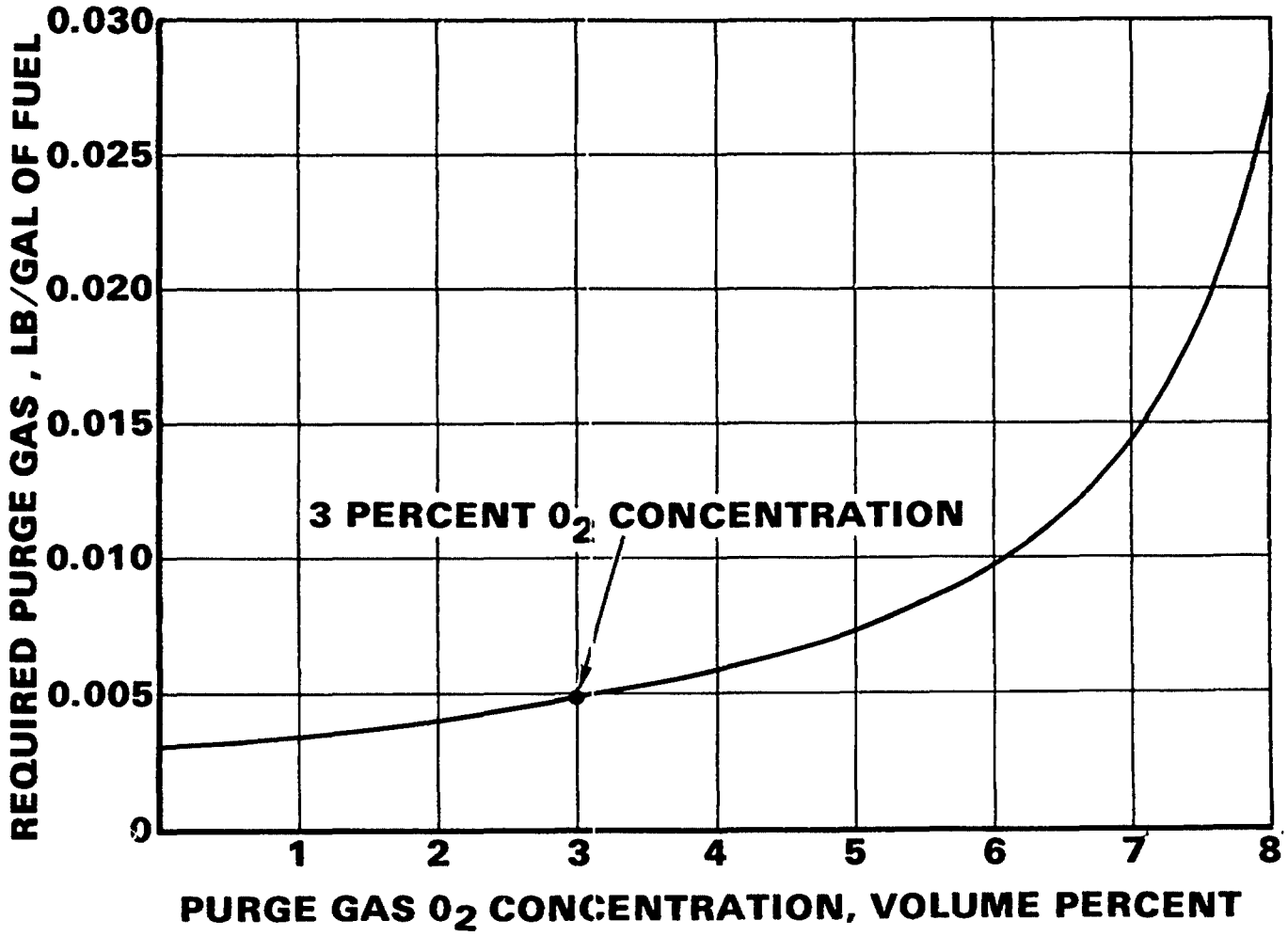

Figure 2-25. Purge Gas Requirements to Control the Release Of Dissolved Air From Fuel During Climb

time will be reduced during climb and cruise as a function of fuel use. During initial climb and cruise, the fuel is reduced to 14,354 gal, as shown by the first 3 points of Figure 2-1. During this initial 37.2 min, the average amount of fuel in the tanks would be 15,277 gal, reducing the inerting time to 25.46 min.

For the fuel load at takeoff, a constant purge gas flow through the fuel into the tanks of 3 lb/min is more than adequate to scrub the dissolved oxygen from the fuel and maintain an inert atmosphere in the ullage space.

SECTION 3

LIQUID NITROGEN SYSTEM CONCEPTUAL DESIGN

SYSTEM CONSIDERATIONS

To compare the IGG and LN_2 inerting systems, a conceptual design for a system based on the use of stored LN_2, similar to the state-of-the-art C-5A system, was developed.

Figure 3-1 shows a simplified schematic of a liquified gas storage and conditioning system. The liquified gas (LN_2) has a fluid temperature of -320°F at NBP; therefore, it is necessary to store it in an evacuated insulated dewar to maintain the fluid in a liquid phase. Since the storage dewar is not a thermally perfect insulator, heat leaks into the dewar cause vaporization of the LN_2. This "standby" loss must be considered in the quantity of fluid to be stored so that the minimum quantity to fulfill the mission requirement is available after the standby losses have been incurred.

To conduct the most effective trade-off comparison, it was determined to utilize the state-of-the-art LN_2 inerting system concept used for the C-5A aircraft, since it is an operational system. In this manner, actual data on the LN_2 system can be utilized as the basis for the KC-135A design.

DESIGN MISSION PROFILE

The C-5A system requirements specify that the LN_2 system shall provide enough gas to maintain the inerted tanks for two maximum range, maximum altitude missions and, in addition, have a 48-hour ground time reserve (stand-by losses). The KC-135A model mission profile consists of two tanker missions and a 48-hour ground time. A single-mission profile for the KC-135A was presented in Figure 2-1. Table 3-1 presents the data used to define the mission profile presented in Figure 2-1.

An analysis of the mission profile for a KC-135A aircraft wing tank with a 16,476 gal ullage was conducted by individual segments to determine the quantity of LN_2 required to maintain the pressurized ullage volumes. A summary of the LN_2 weight requirements follows:

Scrub flow (1)	35 lb
Fuel depletion	120 lb
Descent pressurization	588 lb
48-hour standby loss (2)	77 lb
Total	820 lb of LN_2

(1) Based on C-5A data of 50 lb of LN_2 for 49,000 gallons of fuel

(2) Based on C-5A data of 25 lb of LN_2 for 24 hr per dewar. The KC-135 dewar has an estimated 77 percent of C-5A surface area; therefore standby loss would be 19.25 lb of LN_2 for 24 hr per dewar.

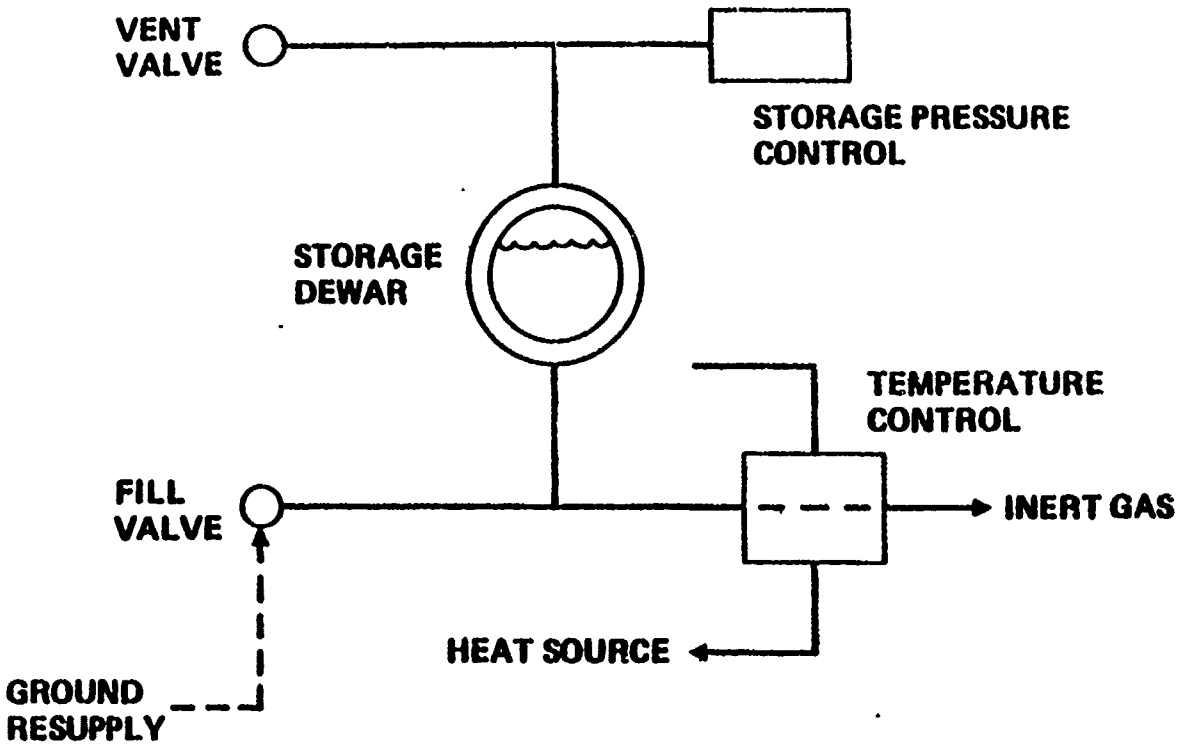

Figure 3-1. Simplified Schematic of LN_2 Storage and Conditioning System

TABLE 3-1

KC-135A MISSION DATA
(Excerpted from Boeing Data Document D180-24758-1, Rev. B, Page 2-3)

Mission Flight Condition (4) No.	Description	Gross Weight 1000 lb	Altitude ft	Mach No.	Thrust Per Eng. F_{μ} (lb)	Total Fuel Flow (lb/hr)	Mission Time (4) (hrs)	Descent Rate (3) (ft/min)
1	Start climb	260	0	0.423	7740 (1)	28930	0.05	
2	Climb	255	15000	0.555	5950 (1)	22090 B	0.22	
3	Start cruise	248	33000	0.780	3510	13140	0.62	
4	Start orbit	239	31000	0.680	3220	11660	1.37	
5	Refuel	189	30000	0.682	2640	9570	1.95	
6	Cruise	137	45500	0.780	1940	7320	3.11	
7	Start descent	133	46000	0.780	580/2080 (2)	4880	3.64	2800
8	Start local airwork	133	30000	0.670	2135	7840	3.71	
9	Start descent	129	30000	0.695	360/2850 (2)	6000	4.21	4000
10	Descent	128	15000	0.515	220/1980 (2)	5420	4.29	3600
11	Airwork	125	2500	0.221	1836	7700	4.54	
12	Start descent	120	27000	0.650	340/2450 (2)	5720	4.83	4100
13	Descent	119	15000	0.515	220/1980 (2)	5420	4.95	3950
14	End descent	118	0	0.378	4450	16970	5.10	

Notes: (1) Normal rated thrust

(2) Outboard engines at idle, inboard engines at thrust for cabin air

(3) Gear down descent rate from flight manual

(4) Flight conditions based on 5.1 hr tanker mission

SYSTEM DESCRIPTION

The LN_2 inerting system for the KC-135A is essentially a scaled-down version of the system used on the C-5A, with the following differences:

a. Dewars are smaller, since the quantity of stored fluid required is less.

b. Valves and plumbing associated with the fire system are deleted.

c. Scrub and distribution systems are reduced to be compatible with the KC-135A wing tanks.

Figure 3-2 presents the C-5A schematic, as modified to the specific configuration of the KC-135A tanker.

SYSTEM WEIGHT

The C-5A LN_2 system dry weight (as described in Parker-Hannifin Report S171-4-0105, dated March 24, 1974) is 2104 lb, exclusive of cargo firefighting equipment. Each dewar weighs 607.5 lb, and heat exchangers, valves, controls and plumbing comprise the remainder of the weight.

If the same ratio of pounds of LN_2 per pound of dewar is applied to the KC-135A dewars, the resultant weight is $\frac{607.5}{750} \times 405 = 328$ lb.

A reduction in weight resulting from the reduced scrub plumbing for the KC-135A is 10 lb.

The weight summary (in pounds) of both systems is as follows:

	C-5A	K-C135A
Dewars	1215	660
Heat exchangers	415	*
Remainder (service panel, valves, controls, plumbing)	474	190
Dry weight	2104	850
Inerting LN_2	1200	820
Service weight	3304	1670

*Heat exchangers not required for this design

Note: The IGG weight is only 853 lb, as shown in Table 2-3.

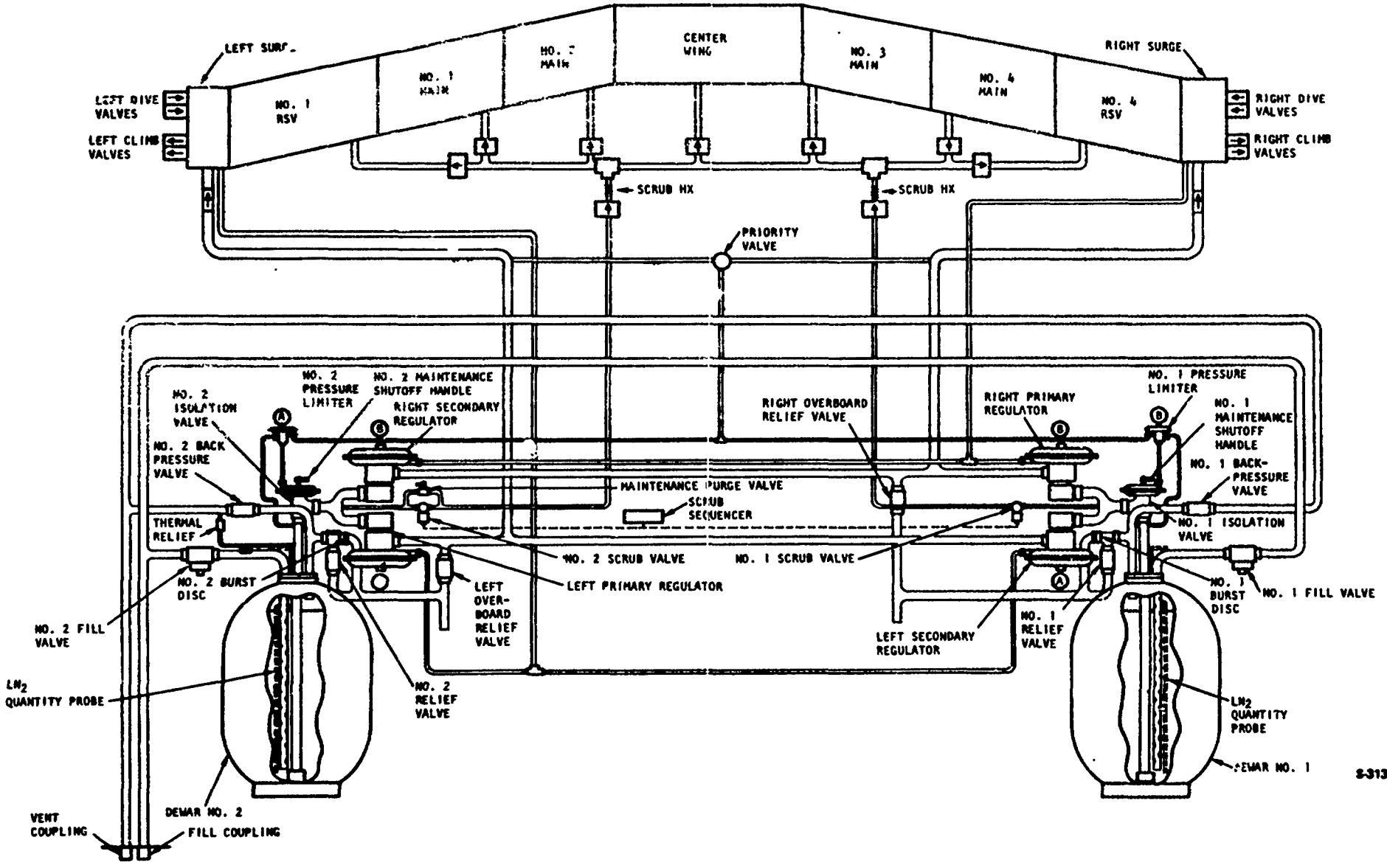

Figure 3-2. KC-135A Pressurization and Scrubbing System Schematic Diagram

These system weights reflect certain guidelines that must be maintained to fulfill the requirement of maintaining the tanks inerted for the full missior. The 853-lb OBIGGS has a favorable weight advantage over the LN_2 system; OBIGGS weight is shown in Table 2-3.

LOGISTICS

A guaranteed supply of LN_2 must be available at all sites where the aircraft is expected to land and lay over in excess of 24 hours. Figure 3-3 presents the logistics of LN_2 supply. For specific military installations, it may be possible to load the service carts directly at the distillation plant. As a general rule, however, losses are incurred both in servicing and standby for the cycle shown in Figure 3-3 and must be considered in the total quantity of LN_2 used.

The supply and storage cycle shown in Figure 3-3 is a typical cycle, from manufacture to aircraft installation. During this cycle LN_2 losses will occur. Typically, transfer losses range from 10 to 20 percent when the tank being filled is at cryogenic temperature. At higher temperatures the losses can be up to 150 percent of the tank being filled. Typical storage and transportation losses are less than 1 percent per day. Due to these losses a quantity of LN_2 five times greater than the aircraft requirement must be manufactured to complete a given cycle.

"Top off" servicing of the aircraft dewars must be performed once the stand-by time has exceeded the allotted 24 hours. Although the C-5A and the KC-135A aircraft normally operate in and out of established installations that have provisions for LN_2 servicing, other aircraft (such as the C-130 or C-17) may operate out of forward bases where LN_2 may not be available.

FLEXIBILITY

After completion of the second mission profile, it is presently not possible to land at an alternate field and maintain the inerting system. Layover between missions while refueling must be limited to 24 hours if LN_2 servicing is not available.

HARDWARE

Heat leak into the LN_2 dewars is the critical parameter to insure meeting the mission profile requirements. A minor degradation of the vacuum in the dewar will provide higher heat leakage and higher losses both in the standby and flight modes, which may result in premature depletion of the onboard supply of inert gas to provide the required protection. As can be seen, the LN_2 storage system is a simple straight-forward approach to providing a stored inertant for fuel tank inerting. The system is quantity sensitive and does not allow much latitude for deviation from the design missions. In aircraft such as the C-5A, where it is known that the destination installation does not have LN_2 servicing, a full serviced LN_2 cart can be carried within the aircraft to perform the reservicing required, although a reduced payload capability will be incurred.

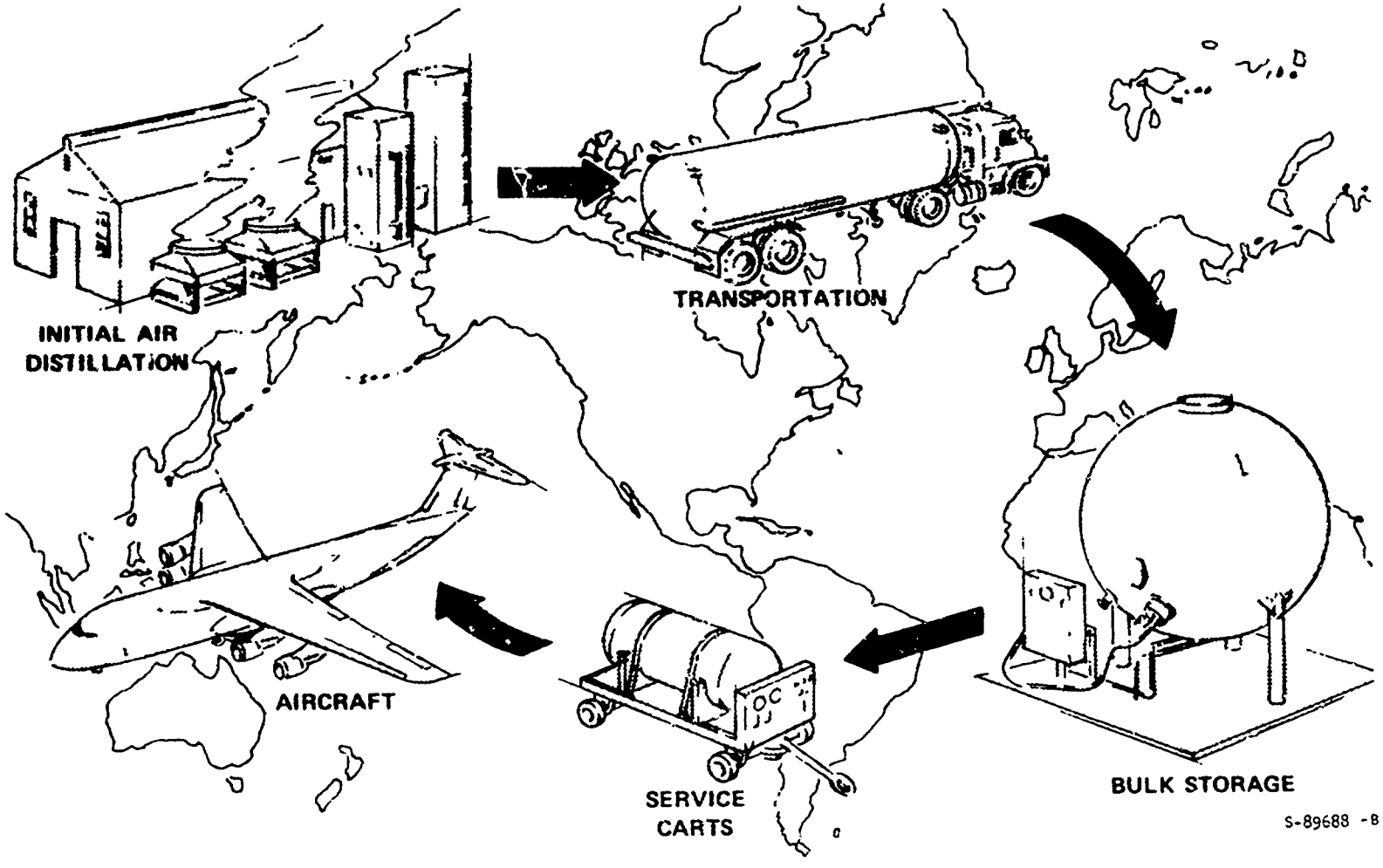

Figure 3-3. Logistics of LN_2 Supply

SECTION 4

COST-OF-OWNERSHIP COMPARISON FOR KC-135 AIRCRAFT

ASSUMPTIONS

A comparative analysis of cost-of-ownership for the KC-135 fleet was performed for the integrated, permeable membrane, inert gas generator (IGG) and the liquid nitrogen (LN_2) fuel tank inerting systems. The analysis pertained to the wing tanks only; the fuselage fuel tanks were not considered. Included in this analysis were initial cost, aircraft maintenance cost, and operating cost. (Operating costs do not include the required portable ground service or storage units.) All LN_2 was assumed to be purchased from commercial sources with leased on-base storage facilities. The cost of transportation and leasing of the on-base storage facilities was assumed to be a part of the $0.038/lb cost of LN_2; the 1983 price of LN_2 is $2.77 per 1000 cu ft at normal pressure and temperature (NPT).

RELIABILITY

A reliability analysis is an important consideration in system design. In addition to providing a comparative measure of the meantime-between-failures (MTBF) for various systems, the reliability analysis is the starting point for estimating maintainability costs. The integrated IGG system design shown in Figure 2-17 consists of a number of individual components of the type in use in aircraft pneumatic systems. The membrane air separator was integrated into a system using components of established performance. The left half of Table 4-1 presents an estimate of the MTBF for each IGG system component. The estimated MTBF values are representative of established values for generic components of the same type for similar applications. Where available, data shown in Table 4-1 were taken from field experience for components used on DC-9, DC-10, B-747, and other commercial aircraft. These data from aircraft operators are summarized in the AiResearch GUARD (Garrett Unified Automated Reliability Data) System report, which is updated monthly, and in other field data sources. MTBF estimates for the membrane modules and filter consider the effect of scheduled replacement frequency.

The data of Table 4-1 compare well with data for air-cycle environmental control systems (ECS), which are in use in most military and commercial aircraft.

The baseline LN_2 system design shown in Figure 3-2 consists of individual components of the type in use in the C-5A LN_2 fuel tank inerting system. The right half of Table 4-1 presents an estimate of the MTBF for each LN_2 system component. The estimated MTBF values are representative of established values for generic components of the same type for similar applications. The MTBF values were derived from data supplied in the AIA Fuels Safety Subcommittee analysis report for a DC-9 LN_2 fuel tank inerting system.

TABLE 4-1

ESTIMATED COMPONENT MEAN-TIME-BETWEEN-FAILURES (MTBF)

IGG System			LN_2 System		
Item Description	Qty. Per Aircraft	MTBF Hrs X 1000 Oper. Hrs	Item Description	Qty. Per Aircraft	MTBF Hrs X 1000 Oper. Hrs
Primary Climb & Dive Valve*	2	90	Ground Service Valve	1	30
Secondary Climb & Dive Valve*	2	80	Installation Packaging	1	500
Scrub Check Valve*	9	80	Primary Climb & Dive Valve*	2	80
Scrub Solenoid Valve	2	80	Secondary Climb & Dive Valve*	2	80
Air Shut Off Valve	1	40	Scrub Check Valve*	9	80
Air Regulator	1	40	Primary Check Valve	2	80
Precooler (HX-1)	1	100	LN_2 Dewar	2	100
Waste Heat Recovery (HX-2)	1	100	LN_2 Quantity Probe/Sig Cond.	2	25
Primary HX (HX-3)	1	100	LN_2 Fill Valve	2	40
Turbocompressor	1	30	LN_2 Fill Coupling	1	50
Secondary HX (HX-4)	1	100	Back Pressure Valve	2	40
Regenerator (HX-5)	1	100	Vent Coupling	1	50
Water Extractor	2	1000	Relief Valve	4	40
Pressure Regulator	1	40	Burst Disk	2	700
Filter	1	100	Isolation Valve	2	40
ASM Assembly Package	1	500	Primary Regulator	2	40
Membrane - Element	6	100	Secondary Regulator	2	40
Flow Demand Regulator	2	40	Scrub Valve	2	40
Temp Sensor/Controller	1	40	Scrub Sequencer	1	15
Temperature Control Valve	1	40	Pressure Limiter	2	40
Air Check Valve	1	80	Thermal Relief	2	40
Halon Storage Bottle	2	40	Priority Valve	1	40
Halon Discharge Valve	2	80	Manifold Dewar	2	40
Halon Check Valve	10	80	System Installation Hardware	1	500
Ground Air Connector	1	50			

*Common Hardware

LIFE CYCLE COSTS

Cost of ownership is an important consideration in the selection of any airborne system. Not only the initial acquisition costs, but also the cost of operating and maintaining the system over its entire life cycle, must be considered. In the more sophisticated forms of financial analysis, the relationship between capital expenditure and calendar time has become increasingly important in making decisions. If system life cycle costs are evaluated in available, more sophisticated use of the data may be feasible and applied, as appropriate, by the user. Accordingly, only absolute cost values are presented here. All estimated costs are in 1983 dollars.

INITIAL COSTS

The inital cost is the price of a shipset of hardware at the time of acquisition of the system. An analysis of the cost of a shipset of hardware for the applicable system was prepared. The analysis was based on a preliminary design of the hardware components shown and verified by cost comparisons made against historical data for other airborne systems, with appropriate substitution in hardware content. This study was based on a lot release of 683 shipsets (615 aircraft population plus 68 spares). The initial costs included flight system hardware, aircraft installation, and portable ground service units, and was based on 1978 data. Fiber spinning, a significant fraction of the IGG cost, is subject to downward revision as production capacity and production rates are increased.

MAINTENANCE COSTS

Maintenance costs are those costs of ownership that are due to system replacement and repair needs. Numerous cost-related assumptions were required to establish maintenance cost estimates. Where background data were available, historical information was used in determining the maintenance cost assumptions.

The maintenance cost assumptions are summarized in Table 4-2, and elements pertinent to the maintenance support costs are summarized in Table 4-3. Cost elements attributable to performance of maintenance are comparable to those presently being demonstrated on similar pneumatic systems in military aircraft service. The estimated maintenance cost per flight hour over the life of the system (in 1983 dollars) is the result of a preliminary quantitative maintainability analysis to evaluate scheduled on-aircraft preventive maintenance, on-aircraft corrective maintenance, and shop-level maintenance actions. The cost estimate is the result of a study in which each system component has been evaluated in terms of the task frequency (resulting from the reliability analysis of Table 4-1), task definition, maintenance crew size requirements, maintenance man-hours per task, and (ultimately) maintenance man-hours per flight hour. Labor costs were then evaluated by applying the proper labor rate.

An examination of the costs in Table 4-3 shows the on-aircraft scheduled maintenance spares costs to be of little significance in maintenance cost evaluations. The cost is low largely as a result of the extended life of the hollow fiber permeable membranes, based on the design operating life of 1000 hr at maximum stress conditions. System operation will result in peak design pressures only during the segment when high fuel ullage gas purge rates are required.

TABLE 4-2

COST ASSUMPTIONS

ASM operating stress rates, hr/fh	0.131
Total ac population	615
Typical wing size, squadrons	2
Typical squadron size, ac	18
Average annual total population fh	242,310
Average annual fh/ac	394
Average mission length, fh	5.1
Average missions/yr/ac	77
Average missions/yr/squadron	1386
Total squadrons	34
Aircraft on 24-hr standby/squadron	2
Average recharge of LN_2/day/standby/ac	1
Average recharge of LN_2/yr/ac	41
Average missions/yr/wing	2772
Average landings/yr/ac	77
Average ASM operating stress hr/yr/ac	50
Spare system sets/squadron	2
System design life, yr	20
Age design life, yr	20
Average labor rate, $/hr	33.40
Average ground service units/wing	4
Fuel cost, $/lb	0.1526
LN_2 cost, $/lb	0.038
Average aircraft/ground service unit	9

ac = aircraft
fh = flight hour

TABLE 4-3

MAINTENANCE COST OF OWNERSHIP ELEMENTS

	Cost per Flight-Hour	
	IGG System	LN_2 System
On-aircraft scheduled maintenance man-hour cost per flight hr (mmh/fh x 33.40)	$0.0002078	--
On-aircraft scheduled maintenance cost per flight hour	$0.00040	--
On-aircraft corrective maintenance labor cost per flight hr (mmh/oh x 2 x 33.40)	$0.04233	$0.05190
Shop repair labor cost (mmh/oh x 2 x 33.40)	$0.1392	$0.13074
Shop repair material cost per flight hr ($/fh x 2)	$0.2058	$0.92283
Total	0.38794	1.10547

Calculations based on the mission profile of Figure 2-1 represent 0.131 hr/fh of stress out of the 5.1-hr design mission profile. Accordingly, applying this ratio to the annual aircraft flight utilization assumption of Table 4-2, the fibers can be expected to be pressurized to stress limits for only about 50 hr/yr, yielding a 20-yr expected membrane useful life.

OPERATING COSTS

Based on design analysis, the average aircraft energies used by the system for various flight segments can be determined for the typical flight profile shown in Figure 2-1. Since the operation of the systems require energies that vary significantly for various flight segments, Table 4-4 shows separate energy requirements for pre- and post-flight ground operation, and for the climb, cruise, and descent flight segments. These energy requirements represent relatively small increases in airflow and electrical power requirements for the baseline design aircraft, and are not expected to increase the requirement beyond aircraft capacities.

Aircraft penalties for the KC-135A installed system energy (and weight) are shown in Table 4-5. These penalty factors, considered for the estimated system requirements (Table 4-4), result in an estimate of the aircraft fuel consumption rate associated with the use of these energies. Application of the appropriate aircraft fuel costs then provides a measure of operating cost associated with the system's use of energies, and with its installed weight.

TABLE 4-4

ESTIMATED ENERGIES USED DURING TYPICAL SYSTEM OPERATION

Mission Segment	Time Duration, hours	IGG Airflow Requirements		Fuel Penalty, lb fuel/mission segment	
		Ram Air, lb/min	Bleed Air, lb/min	Ram Air Fuel Penalty Factor 0.4918 $\frac{\text{lb fuel/hr}}{\text{lb air/min}}$	Bleed Air Fuel Penalty Factor 1.8441 $\frac{\text{lb fuel/hr}}{\text{lb air/min}}$
Ground	0.09	0	17.64	0	2.928
	0.56	49.3	17.64	13.578	18.217
Climb (1.11)	0.29	79.24	17.64	11.301	9.434
	0.26	45.16	17.64	5.775	8.458
	0.50	48.23	17.64	11.859	16.265
Cruise (3.23)	2.32	50.64	17.64	57.779	75.469
	0.41	30.78	17.64	6.206	13.337
	0.07	44.49	25.8	1.532	3.330
Descent (0.67)	0.33	73.24	25.8	11.886	15.700
	0.27	70.0	25.8	9.295	12.846
Total mission time, hr	5.1				
Fuel penalty, lb/mission				129.211	175.984
Fuel penalty, lb/flight hr				25.3355	34.5066
Cost penalty, $/flight hr*				$ 3.866	$ 5.2656

*Assume 1983 fuel cost of $1.00/gallon ($0.1526/lb)

Aircraft fuel costs have increased substantially in recent years and are subject to further fluctuations in the future. For this study in 1983, a cost for JP-4 fuel of $1.00/gal ($0.1526/lb) was assumed. To evaluate the operating cost at a future time, a higher fuel cost assumption may be more appropriate. Fuel use and associated costs for 1983 are shown in Table 4-5. As can be seen, the costs are predominantly due to bleed air and system weight.

TABLE 4-5

COST OF OPERATION

Expendable	IGG System		LN_2 System	
	Expendable Weight, lb/FH	Expendable Cost, $/FH	Expendable Weight, lb/FH	Expendable Cost, $/FH
LN_2 at $0.038 $/lb*	-0-	-0-	647.29	12.29851
Fuel at $0.1526 $/lb				
Bleed air 1.3441 $\frac{\text{lb fuel/hr}}{\text{lb air/min}}$	34.5066	5.2656	-0-	-0-
Ram air 0.4918 $\frac{\text{lb fuel/hr}}{\text{lb air/min}}$	25.3355	3.866	-0-	-0-
Penalty				
Weight 0.0369 $\frac{\text{lb fuel/hr}}{\text{lb installed weight}}$	32.5458	4.9664	61.623	9.4037
Power 0.0005 $\frac{\text{lb fuel/hr}}{\text{watt}}$	0.100	0.01526	0.100	0.01526
Total		14.11326		21.71747

*Usage based upon ratio with C-5A using actual data.

Actual data from the user was employed to estimate the LN_2 requirements. The basis of this determination was a letter from Lt. Col. R. M. Horton, Chief, Energy Management Division Directorate of Supply, dated November 16, 1978.

The cost and amount of LN_2 purchased for C-5A inerting systems in 1978 was 22,453 tons at $68.00 per ton ($1,526,804); LN_2 cost per lb was $0.034. For the C-5A three-month sample period (July, August, and September of 1978), 11,707 flight hours (FH) were logged; projected out to a year, this comes to 46,828 FH for all C-5A aircraft using LN_2 inerting systems. As noted above, the C-5A total LN_2 usage for 1978 was 22,453 tons (44,906,000 lb). By simple calculation, the C-5A LN_2 usage associated with fuel tank inerting was 958.95 lb/FH, using a storage tank LN_2 weight ratio of 0.675 (C-5A=1200 lb vs KC-135=810 lb). The projected KC-135 LN_2 usage is 647.29 lb/FH. Assuming operations improved between 1978 and 1983, the usage was reduced to 50 percent of 1978 value. This results in a projected usage of 323.645 lb/FH. Based on 1983 LN_2 cost of $0.038/lb above, the KC-135 LN_2 system would experience an expendable cost of $12.29851/FH, as shown in Table 4-5.

Summary

Cost of ownership in 1983 dollars of the two fuel tank inerting systems is summarized in Table 4-6. The major cost element in the IGG system is the initial cost ($230K) per aircraft. Operation and maintenance are of minor significance ($111K) or about 32 percent of the total 20-yr life expectancy cost of $342K. For the LN_2 system, operation and maintenance is about 37 percent ($180K) of the total 20-yr cost ($478K), including initial cost. Projected to the entire fleet of 615 aircraft, the IGG system costs are $42.5 million less than the LN_2 system costs of $110.8 million. This figure includes an estimated 50-percent reduction in operation and maintenance costs of the LN_2 system due to the learning curve.

TABLE 4-6

COST-OF-OWNERSHIP SUMMARY

Cost Element	IGG System Cost, $	LN_2 System Cost, $
Flight system	80,000	78,000
Installation	150,000	120,000
AGE	500	4,166
Initial cost total $/aircraft	230,500	202,166
Maintenance, $/FH/aircraft	0.38794	1.10547
Operation, $/FH/aircraft	14.11326	21.71747
Total maintenance and operating costs, $/FH/aircraft	14.5012	22.87217
Yearly cost at 394 FH/yr, $/aircraft	5,561	9,012
20-year cost, $/aircraft	111,200	180,240
Yearly 615-aircraft cost	3,419,780	5,542,160
20-year cost for 615 aircraft	68,395,630	110,843,170
Net savings for IGG system	42,447,540	-0-

SECTION 5

FLIGHT TEST PLANNING

GAS MONITORING SYSTEM

General

Task 1-3 covered all efforts related to the development of a gas monitoring system to be used in the flight test program to measure the oxygen concentrations in the fuel tank ullage and the inert gas generator output. The subcontractor responsible for this task was Falcon Research and Development of Denver, Colorado. A government-furnished mass spectrometer, Analog Technology Corporation Model 2001, was selected to monitor the gas composition in flight.

Sample Transport Subsystem

The core of the sample transport subsystem was being designed by Falcon with an emphasis on components already proven on the Simulated Aircraft Fuel Tank (SAFTE) program of the Air Force. Sample line switching was to be performed by a Scanivalve with two banks of twelve channels each. Both banks were fixed in relation to each other and driven on a common shaft by a stepper solenoid. One bank was termed "primary", and was dedicated to tank sample lines with ports in the top of the tanks. The "secondary" bank was allocated to any excess of sampling points high in the tanks, and to any that might be immersed in fuel for a relatively longer period of mission time.

For simplicity, backpurging with heated nitrogen gas would be performed on each bank individually, or both at once. Providing individual sample line selection for backflushing was deemed too complex and expensive for the limited benefit derived.

The IGG output gas sample was supplied to the primary bank and the IGG input gas sample was provided to the secondary bank. In this manner, simultaneous backpurging could be accomplished on all tank sampling lines, while data could be obtained in real time using the analyzer on the input and output of the IGG. No nitrogen backflushing was deemed advisable for the IGG lines, and check valves were considered to prevent backflow.

Scanivalve position indicator lights were provided on a panel in front of the operator. During normal tank readings, the Scanivalve controller automatically steps through the sampling positions at a rate manually input into the controller. The operator could override this operation at any time, and manually select a fixed port or manually advance. The manual modes could be used by the in-flight operator between periods of relatively rapid data collection for all tank sample lines available. The operator could select backpurge of either or both banks. If one bank was in backpurge, automatic sequencing of the other bank could still be accomplished. It was determined that a relatively constant analyzer flowby pressure (2 to 3 torr) should be maintained. A suitable regulator was procured for the SAFTE system, and was being specified for this system. Brassboard testing indicated that real time accurate data should be displayed

by the analyzer in both the SAFTE and IGG applications with this regulation. Flowby pressure was a critical parameter that was to be displayed and recorded.

Options were considered for interfacing the core of the sample transport subsystem with the lines routed through the aircraft. An attractive approach was the one similar to the installation on the C-135 aircraft using the mass spectrometer installation for LN_2 inerting. The lines could be routed from the rack to an open position in the cargo floor, exposing the subfloor, which is the pressure-tight partition. A removable panel could be replaced with an identical one having the necessary through-bulkhead fittings for all sample transport lines. Each line could have an individual manual shutoff valve for secure closure of these lines without their removal. In addition, a fail-closed solenoid-operated valve was also recommended for each line for remote closure of any and all lines, particularly in an emergency shutdown mode.

Preliminary Design of Fuel Tank Gas Measuring System (FTGMS)

The preliminary arrangement of the FTGMS is shown on Figure 5-1. The fundamental arrangement of the racks in relation to the table was based upon Falcon's discussion with Mr. Stanford of ASD flight test. The displays/controls of most immediate concern were directly in front of the crew member responsible for the FTGMS. Secondary control apparatus, such as circuit breakers and startup/shutdown controls, were located in the rack immediately next to the operator's table. It appeared that there was space in the rack for GFE data recorders. It was recommended that the power conversion equipment be located a significant distance away from this area to minimize the chance of interference with the analyzer. It was understood that this should cause no problem, since self-contained power conversion equipment was available GFE and could be mounted well away from the operator's area, well to the rear in the cargo compartment.

The surge tank is shown, but could be eliminated since anticipated fluctuations in sample transport subsystem had not materialized in brassboard testing.

Cooling and shock mounting of the GFE analyzer/control module on the operator's table is not shown, but is definitely required. A small fan had proven sufficient for operating the SAFTE analyzer computer at room temperature (air-conditioned to 70°-75°F). It was estimated that this will suffice for aircraft cargo compartment temperatures to about 80°F. If operation of the analyzer above 80°F temperature is required, a source of cool air is deemed necessary. The ALL C-135 analyzer was provided with a dedicated air conditioning unit. The computer could malfunction at elevated temperatures, but permanent damage had not resulted with localized air temperatures in excess of 95°F.

Figure 5-1 also shows the conceptual design similar to the prior mass spectrometer application to the C-135 for inerted tank tests. A cargo floor section was removed. In this region, a pressure-tight panel in the "sub-floor was modified for the tank sampling lines. The manual shutoff valves and fail-closed solenoid valves were located in series in each line in a separate vertical cabinet. Either or both of these valves could be mounted upon the sub-floor panel if the panel is sufficiently large.

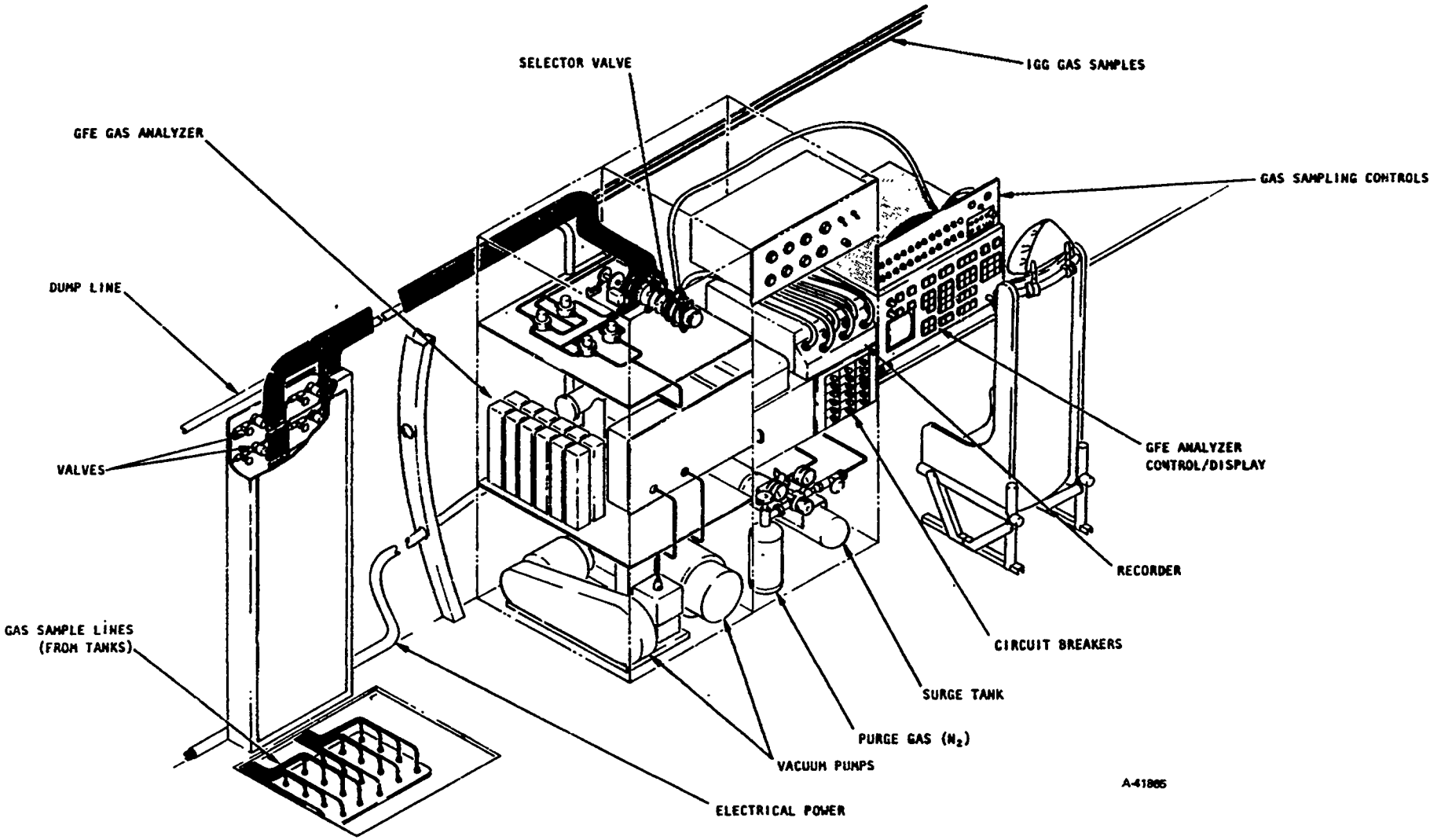

Figure 5-1. Preliminary Arrangement Fuel Tank Gas Measuring System (FTGMS)

Further knowledge on the GFE analyzer permitted a sampling cycle and crew procedure to be defined. The operator could ascertain that the selector valve was in the initial sampling position, and then start the auto-analysis mode of the analyzer. When the analyzer finished the analysis of the first sample, it would shift into the record mode and dump the data into the digital tape recorder. This "record" signal would also be provided to an interfacing board, which commands the selector valve to advance to the next port position and establish "good" sample flow, while the analyzer's data is being transferred to the recorder. This process could be repeated until the operator manually terminates the sequence. The selector valve could then progress from ports 1 through 24, and then revert back to port 1 for another cycle.

An analog signal was provided through a wafer switch on the selector valve shaft, modified ("stepped") by a cam to differentiate between the "primary" and the "secondary" banks. This signal could be digitized and also recorded with the analyzer output data. This plus a trace gas would give a highly reliable means of assuring that the analysis data were being provided to the correct port.

The fastest sampling rate would be about 2 seconds per port, giving a minimum time for analyzing all 24 channels (maximum) of 48 seconds. The data transfer could be accommodated with a dedicated digital recorder with a minimum rate of 7,000 bits/second. There was some question as to the handling of data other than that of the analyzer and the selector valve on one digital recorder. First, it was preferable that the other data such as temperatures and pressures, be digitized. Secondly, some interfacing should be provided which gives the analyzer priority for data recording. When the recorder/selector valve was not transmitting data, the other channels could be periodically sampled.

Eight runs of computer program CRITOR were made to support the design of the sample transport lines. A 100-micron diameter orifice was finally selected, giving a tank sampling (bleed) rate of 75 ml/min per sampling line at standard conditions in the tank ullage. A line ID of 0.093 in. was selected to produce a sample transport time over 80 feet of line of 13 seconds. For a 100-foot line, the transport time would be 15 seconds. These times avoid excessive in-line diffusion.

This system provided for choked flow at the inlet orifice from 2.5 psia to 14.7 psia. The pressure just downstream from the choked flow orifice was calculated as 65 torr for 14.7 psia in the tank, and 19 torr for 2.5 psia in the tank. For the entire range, the absolute pressure flowing by the analyzer could be maintained at 7 $\pm$1 torr by the downstream regulator.

Calculations were performed on the adiabatic expansion of sample gas from the tank ullage to just downstream from the inlet orifice. For example, to expand from 70°F and 14.7 psia to 65 torr, the calculated final temperature assuming adabiatic expansion is -197°F. Brassboard testing at this temperature showed no problem since the heat available in the fittings prevents condensation at concentrations as high as 10 volume percent of JP-4S.

However, at an assumed temperature of -70°F for ullage and line temperatures, and vapors liberated from liquid fuel at 70°F, in-line condensation is virtually assured. Further calculations were performed in this temperature

range. Based on the above, heating with a backpurging gas (nitrogen) would not be sufficient, either at a low flow rate dumping into the tank (75 ml/min per sample line), or at a high flow rate (500 ml/min) being externally dumped or recirculated. However, flow with heated nitrogen at 200° to 250°F was still a valuable feature for backpurging lines which could have been contaminated with liquid fuel or condensate.

Application of GFE Analyzer

It was concluded from brassboard testing that the analyzer's computer was not sufficiently documented and reliable to operate on the data before it was provided to the recorder. The only prudent course was to record peak data in its most basic form, which did not involve any modification by the computer. This was the auto analysis mode, with data provided to the recorder in RS-232C format from display number 11. The data could be reduced off-line after the flight.

This approach required some manual data recording by the operator from the CRT both before and after the flight. As a minimum, the background gas concentrations in the analyzer and a full spectrum scan (AMU 1 to 200) should be performed on the fuel tank vapors before and after the flight, for evaluating and averaging any changes in the analyzer chamber gases or the aircraft fuel.

However, the recommended approach to use of the analyzer was to bypass the computer to the maximum degree. This limited concern mainly to the operation of the mass spectrometer portion.

Detailed data on the application of the ATC gas analyzer (ATGA) in the Airborne Laser Laboratory was received by Falcon in January, 1979. This provided invaluable insight on modifications potentially necessary to ATGA S/N 2 for use in IGG flight tests. A common calibration standard was established to permit direct application of gas calibration data between the IGG and SAFTE.

Falcon participated in a coordination meeting at Wright Patterson AFB on March 27, 1979. As a result of discussions during this meeting with respect to the conflicting references to MIL-STD-882 vs. MIL-STD-882A, the Air Force determined that MIL-STD-882A would be the controlling document. Falcon was directed to revise the FTGMS preliminary hazard analysis (PHA) in accordance with MIL-STD-882A. (The PHA was submitted as AiResearch Report 79-15910, dated April 12, 1979.) At this same meeting, Falcon was directed to investigate the compatibility of the GFE analyzer dedicated to the FTIS program, ATGA Model 2001, S/N 2, with the 4950th Test Wing data handling and storage equipment. This was to include a telemetry link to the ground station for diagnosis of inflight performance.

On March 30, 1979, a meeting was held at the 4950th Test Wing with Falcon on the telemetry station that would be used. Particularly attractive was the evident capability to program a dedicated computer to convert, among other things, raw peak data from the in-flight analyzer to gas concentrations to obtain real-time readout for diagnostic purposes. The CRT evidently had the capability to duplicate the CRT display of the ATGA, plus simultaneously display results of calculations performed on these data by the ground computer. Radio

communication directly between the in-flight operator and ground monitor was available. There was also the capability for tape storage and hard copy output. As a result, the following items were resolved at the meeting:

1. The 4950th Test Wing was to assume responsibility for EMC requirements with respect to AF test bed electrical power and FTGMS equipment. No EMC testing was planned for the electrical components, such as solenoid valves and pressure thermal switches which form part of the FTIS. Operation of the installed system during the Phase III ground testing was to validate EMC compatibility.

2. Falcon was to investigate the compatibility of the GFE analyzer with the 4950th data handling and storage equipment. This was to include a telemetry link to the ground station.

3. The 4950th Test Wing was to assume responsibility for the test bed electrical power supplies, interfaces, and load analysis with the FTGMS, except for the design and installation of the probe heaters and fuel tank instrumentation.

Fuel Tank Gas Monitoring System (FTGMS) Design and Installation

Boeing Drawing SK 3-71830-79-10 (Installation of FTGMS) was reviewed in March, 1979. Additional installation concepts for the probes were described. A potential moisture freezing problem in the relief valve and bypass tube portion of the probe (as pointed out by Falcon) needed investigation for safety and this was to be done by Boeing. The electrical system interface and installation responsibility between Boeing, the 4950th Test Wing, and the Falcon equipment needed to be established.

AIRCRAFT MODIFICATIONS

General

The planned flight test aircraft was to be a KC-135A aircraft supported by the 4950th Wing at Wright-Patterson Air Force Base, Ohio. The flight test planning task involved the planning, design, and review process to be directed by AFSCR 80-33 and coordinated with the 4950th Test Wing. Preliminary work on this task was started in November, 1978, to ascertain which portions of Part I, Class II modification documentation could be submitted for Air Force review to expedite flight test planning.

Problem areas encountered in the initial phases of this task were related primarily to the fuel tank inerting system (FTIS) bleed air supply. Independent air source concepts are shown in Figure 5-2.

AiResearch prepared a failure modes and effects analysis for Boeing use in their preparation of the preliminary hazards list for Part 1 of the modification documentation. As a result of this analysis, additional controls were incorporated to protect the system from specific failure modes. The schematic of the KC-135A fuel tank inert gas system conceptual design is presented in Figure 5-3.

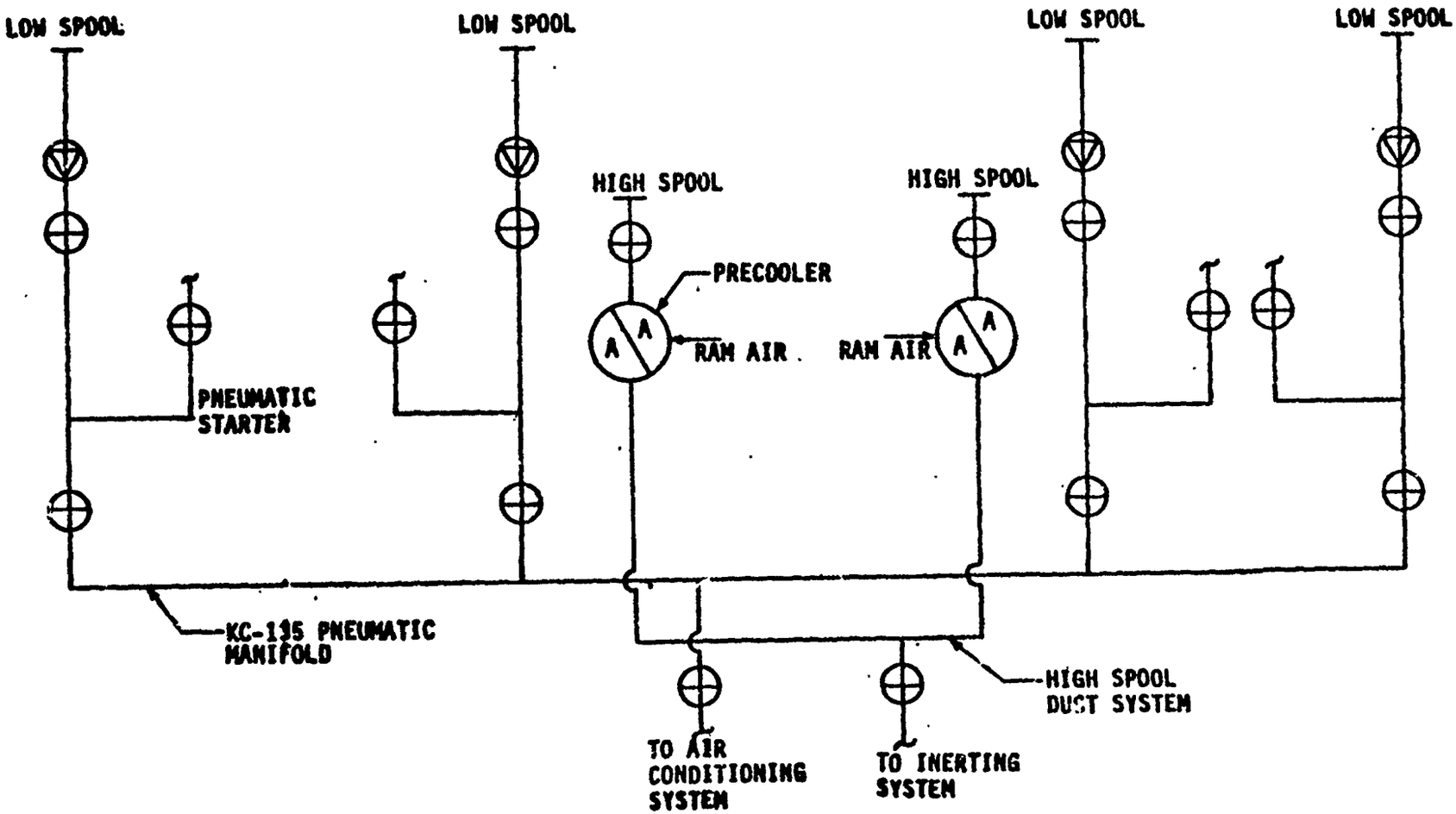

Figure 5-2. Fuel Inerting High-Spool Independent Air Source Concept

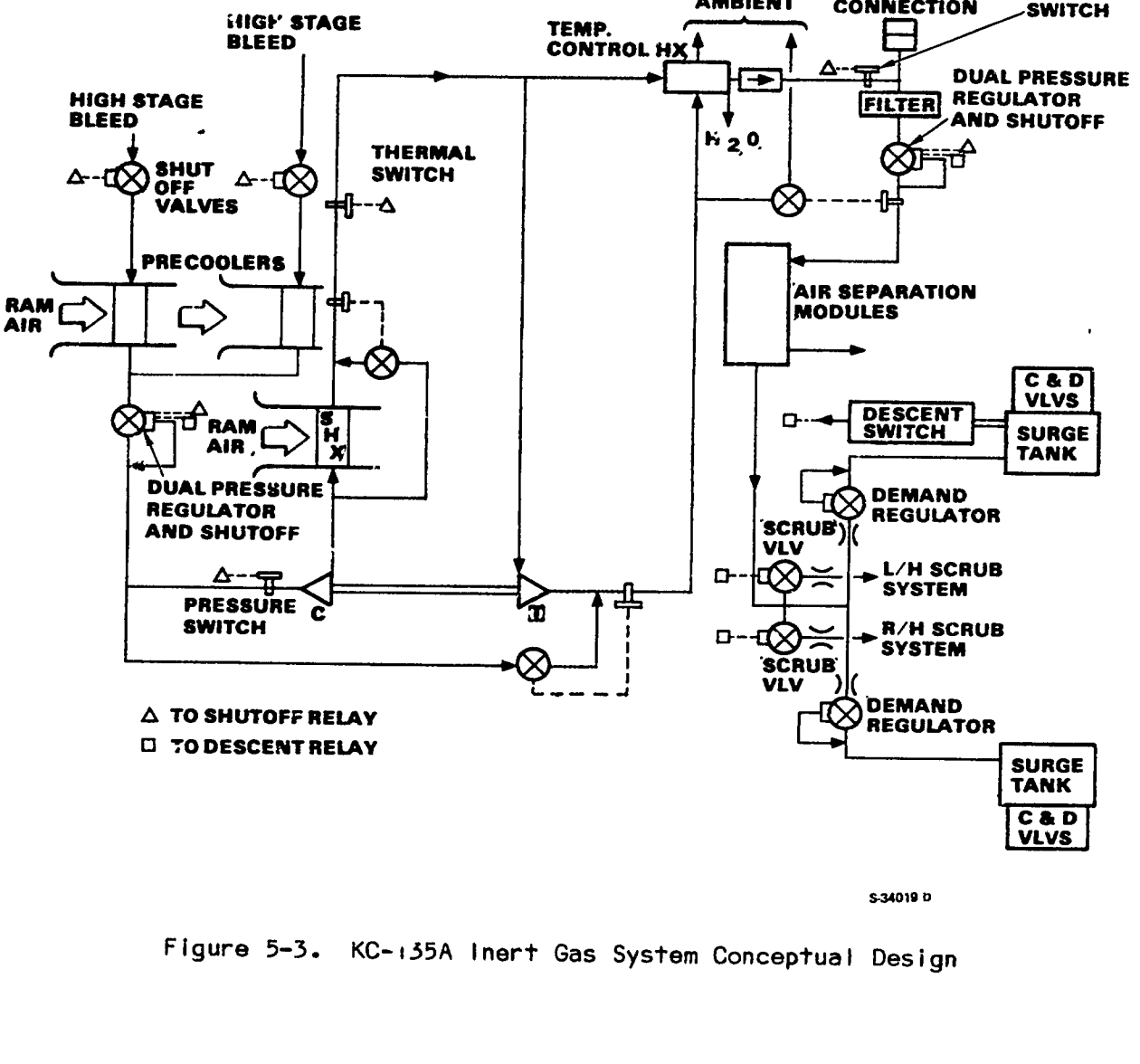

Figure 5-3. KC-135A Inert Gas System Conceptual Design

Coordination Meeting Decisions

1. Flight Test Planning Coordination Meeting

A flight test planning coordination meeting for the FTIS was held at Boeing-Wichita on February 15, 1979. The major topic was the viability of the six optional air source concepts discussed in Table 5-1.

2. Technical Coordination Meeting

A technical coordination meeting was conducted at Boeing-Wichita on March 15, 1979. The following summarizes the significant results of the meeting.

(a) Air Source Configuration and Design--The need for an ejector for ground static operation of the precooler was discussed. The present KC-135A operating procedure requires bleed air to be switched off during takeoff. Hence, it was decided that the precooler installation should not be designed for ground static operation due to (a) bleed air cutoff and (b) space and bleed air source problems for the ejector. Ground operation of the IGG will be from air supplied by suitable ground carts instead of the engine bleed air source.

(b) Vent System and C/D Valve--Boeing provided a preliminary vent system analysis and the climb/dive (C/D) valve performance characteristics that would be required. Final requirements for the C/D valves were to be provided by Boeing. Several C/D valve redundancy concepts were discussed. Three options were:

(1) Provide a large enough valve effective area for both the primary and secondary portions of a valve similar to the DC-9 valve.

(2) Add a Carter valve (similar to the 727) on the bottom surface of the outboard surge tank.

(3) Place two Carter valves in parallel in a bifurcated S-duct.

(c) IGG System--Boeing described the proposed installation concept for fuel tank inerting, including bleed air routing, inert gas distribution system, gas sampling distribution, and general space allocation in the cargo compartment for the IGG and FTGMS pallets.

A new fuel pump would be needed in each of the outboard reserve tanks for providing motive flow to the scrubbers. AiResearch was to investigate the fuel tank area coverage provided by each nozzle during scrubbing of fuel with inert gas.

Halon bottles would be installed in the cargo compartment due to limited space and access hole size in the dry bay area of the wing. Halon was to be introduced into the surge tank for distribution into the ullage of other tanks for emergency descent. Halon was to be distributed by separate dedicated tubing instead of combined Halon/N_2

TABLE 5-1

BLEED AIR SOURCE OPTIONS FOR THE FTIS

Air Source Concept	Description	Modification Status/ Feasibility
1	Existing low-spool bleed system	Minimum modification costs but not feasible for inerting due to low pressures
2	Independent high-spool bleed air system precooled at single inboard engine (without disturbing existing water injection and quickstart system)	Not feasible due to insufficient duct envelope (3-in. duct)
3	Same as Concept 2 except bleed air from both inboard engines	Not feasible due to insufficient duct envelope
4	Mixed low-spool/high-spool with ejector pump using existing low-spool duct system. Mode of operation: boosted low-spool during climb/ cruise; direct high-spool during descent	Feasible to install; pressure at cruise lower than high-spool. High pressure air is available during descent. May require larger inerting system to meet cruise requirements.
5	Independent high-spool system on a single inboard engine with the following deactivations: • Remove water injection system ducting from inboard engine/wing • Remove "quickstart" starter • Install precooler in fuel heater space • Install pneumatic start on inboard engine	Feasibility questionable due to small water lines (1-1/4 in.) in leading edge (costly modification)
6	Same as Concept 5 with high-spool installation on both inboard engines	Feasible installation, but modification will be costly

tubing. Halon compatibility with air-frame materials and with the engine needed investigation.

Boeing provided ram air supply pressure and temperature data. This data was based on flush scoops and recovery factors of 60 percent for fuselage side scoops and 70 percent for strut scoops.

(d) FTGMS Design and Installation--The Boeing installation drawing was reviewed. Additional installation concepts for the probes were described. A potential moisture freezing problem in the relief valve and bypass tube portion of the probe (as pointed out by Falcon) needed investigation for safety. The electrical system interface and installation responsibility between Boeing, the 4950th Test Wing, and the Falcon equipment needed to be established. The present length limit for the gas sampling probe inside the fuel tank (36 inches) may be met in some of the tanks.

(e) Safety and Hazard Analysis--Boeing provided a preliminary draft of a system safety program plan based on MIL-STD-882A.

(f) D1-E-31158/M Status Review--The scope, responsibility, and adequacy of available data for paragraph numbers 1.1.1 through 1.1.14 of D1-E-31158/M were discussed.

3. Testing Coordination Meeting

A testing coordination meeting was held at Boeing-Wichita on April 17 and 18, 1979. A synopsis of some of the items reviewed is presented below.

(a) Overview of Airplane Modification--The overall scope of the Part 1 modification plan was presented. The scope included definition of the various subsystems which are being developed by AiResearch, Falcon, and Boeing. The Part 1 plan was to be developed for the designated EC-135N test airplane, Serial Number 60-372.

(b) System Installation--Major points concerning the installation of the inert gas generation system for the test airplane were:

1. All wing fuel tanks inerted--reserves, mains, and center wing

2. Removals--water injection system and engine quick start

3. Cargo compartment equipment installation--air separation module (ASM), scrub valves, ram air, and exhaust

4. Wing-mounted equipment--inert gas distribution plumbing, demand regulators, scrub ejectors, fuel supply, nozzles, climb/dive valves, engine bleed air ducting, descent switch, and reserve tank overflow line

5. Cockpit mounted equipment--controls and displays

It was determined that the system needed a safety switch to prevent inadvertent bleed air operation during ground operation and an over-temperature switch to prevent excessive hot air in the nacelle strut or wing in the event of a duct rupture.

The exhaust duct installation on the cargo deck was also reviewed. It was decided that a common exhaust duct from the IGG pallet and FTGMS pallet would be acceptable if there was no safety problem. AiResearch indicated that the maximum oxygen concentration in the ASM exhaust would be approximately 35 percent by volume, but very close to ambient concentration in the total mixed ram air, turbine air, and ASM exhaust.

The structural installation concept was reviewed. It was estimated that about 40 penetrations would have to be made through the structure for routing of plumbing.

The 28-vdc interface on the IGG was to be a Boeing responsibility. During Phase 2, Boeing would determine the exact installation.

(c) Halon System Installation--The Halon system was to be installed with one 105-lb storage container in the cargo compartment. Halon was to be injected into the wing surge tank by distribution lines passing through the wing tanks to the surge tanks. The cockpit control and display was to incorporate a guarded switch for Halon actuation.

(d) FTGMS System--The FTGMS pallet was to be located in the cargo compartment. Gas sampling probes were to be installed in each wing tank. Ullage pressure pickups were to be placed in all wing tanks, but ullage and fuel temperature pickups were to be located in the left wing tanks only. Controls the displays were to be integral with the FTGMS.

An additional safety analysis was indicated to deal with sample line configuration and heaters. Also, a recommendation regarding exhausting the FTGMS into the FTIS exhaust was to be developed by Boeing-Wichita.

(e) System Safety--This presentation showed a preliminary safety organization for the program.

(f) Structural Integrity--The structural integrity requirements in terms of loads, static strength, durability, damage tolerance, vibration, sonic fatigue, and flutter were discussed.

(g) Acoustic, Vibration and Sonic Fatigue Analysis--Analyses were to be conducted to determine if the FTIS installation would result in any objectionable or excessive vibration of airplane components or create noise fields that will impede crew performance or induce sonic fatigue failures during the life of the test program.

(h) Flutter Analysis--An analysis was to be conducted to determine if the FTIS installation would impact current aeroelastic stability of the test airplane.

(i) Vent System Analysis--The vent system requirements, criteria, and design were presented. The center tank was shown to be critical in every condition except the case of one vent blocked. In this case, Tanks 2 and 3 were critical. It was decided that the design criteria for system sizing should be the emergency descent curve with gear down placard, flaps up, and full air brakes.

(j) Test Outline to Verify Ram Air Exhausts--Data shown indicated that no test is required. The drag increase due to the FTIS was calculated to be 0.8 percent.

(k) Mass Properties Analysis--A representative weight and balance summary was shown with a plot of gross weight vs. CG. This analysis was made with the most adverse location of the FTIS cabin elements. No problems were indicated with weight and balance.

(l) Power Analysis - Engine Performance--The FTIS was to have an independent dedicated high pressure bleed system using 16th stage bleed air from Engines 2 and 3. Therefore, the FTIS operation was not expected to influence the ECS or anti-icing systems on the airplane. Since FTIS operation influences engine operation, however, the FTIS was to be shut off during ground engine operation and takeoff to avoid any impact on takeoff performance.

The estimated FTIS bleed flow does not exceed the allowable flow at any point in the design mission.

Electrical loads were estimated to be as follows:

IGG power required	15 amps, 28 vdc
FTGMS power required:	
Probe heaters (3.9 kva)	34 amps, 115 vac
Frequency converter (3.5 kva)	20 amps, 30-400 Hz
Miscellaneous controls and lights	(negligible)

(m) Operating Restrictions--The restrictions to be applied to the test aircraft because of the FTIS were the following:

1. The FTIS cannot be operated from engine bleed air during ground operation or takeoff.

2. The maximum descent rate is limited to that obtained with the gear-down placard speed and with the spoilers deployed.

All other limitations and restrictions caused on the 60-372 airplane because of "droop snoot" nose configuration will apply.

(n) Performance, Stability and Control--Performance analysis results were presented. Stability and control for the EC-135N aircraft with the FTIS and instrumentation installed was unchanged from the basic configuration.

(o) Demodification Plan--Objectives of the demodification plan were as follows:

1. Operation and maintenance of the airplane after demodification will be possible without any changes to the existing airplane manuals.

2. The structural configuration after demodification will exhibit a service life commensurate with the T.O. 1C-1-989 life extension structural modification (ECP 405).

4. Documentation Review Meeting

The review of the documentation presented for the Part 1 modification plan, system safety program plan, preliminary hazard analysis, and R&D test plan was conducted at WPAFB on May 31, 1979.

Highlights of the review discussions are presented below:

(a) Climb and Dive Valve Installation--Boeing reported a potential problem area which was uncovered subsequent to the submittal of the data. The M-1 and J-4 flux gate compass sensors are located in close proximity to the installed location of the climb and dive valves. Any magnetic materials within three feet of these sensors may affect the normal functioning of the navigation system. During the discussion it was pointed out that the LN_2 inerting program on a C-135N was conducted with climb and dive valves and pressure switches installed in the same area without any apparent effect on the compasses. The 4950th Test Wing was to determine if any compass/navigation problems were encountered. Boeing reported that the "Winglet Program" is encountering the same potential problem and data should be available on the effect of magnetic material installed in close proximity to the compass sensors.

(b) FTGMS Vent Line--It was pointed out that the overboard vent line for the FTGMS discharges above the wing and could dump fuel on the wing during static ground operation. AiResearch/Boeing was to investigate this condition.

(c) FTIS Controls and Displays--The control and display panel for the FTIS was to be located in the cockpit. It was pointed out that test system controls and displays are usually located at the flight test engineer's location with all systems controlled by the test bed

master power switch, which is located in the cockpit. The 4950th Wing was to investigate and specify the desired location for the FTIS control and display panel.

(d) Climb and Dive Valves Manual Override--The proposed climb and dive valves were to be normally closed valves, which are operated by differential pressure to provide fuel tank pressure control for both the ascent and descent flight conditions. When the system was operational, a solenoid-operated manual override was to be provided. When the system was non-operational, there was no manual override available. ASD engineering recommended that a means to physically maintain the valves in an open position be provided by installation of a device similar to that utilized in the earlier LN_2 inerting program conducted on the EC-135N.

(e) Halon System Failure Mode--It was pointed out by ASD that the PHA did not include the possible hazard of excessive Halon concentrations. All agreed that leakage flow would not be a problem, but a supply line failure in the cargo compartment simultaneous with initiation of Halon flow could introduce the total quantity of Halon into the cargo compartment. AiResearch was to analyze this condition.

(f) FTGMS Sample Lines--A discussion of a potential water trap and subsequent freezing in the gas sample line penetration at the fuel tanks was resolved when Falcon stated that a redesign by Boeing to eliminate the water trap was acceptable. This redesign was to be accomplished in the Phase 2 detail design effort.

(g) Aircraft Weight and Balance--It was pointed out by the 4950th Test Wing that the 103,600-lb aircraft weight includes the flight test instrumentation for the weight and balance data.

The 4950th was to provide the fuel management sequence to be used in determining the effect of the modification upon the center of gravity limits.

The 4950th stated that they calculated a maximum gross weight takeoff limitation of 186,000 lb for a 90°F ambient day due to the removal of the water injection systems. It was concludad that by proper fuel management and selective test scheduling, the program would not be affected.

(h) EMC--A discussion of the proposed approach for testing at the aircraft level for electromagnetic compatibility of the equipment was left unresolved. It was pointed out by AiResearch that much of the equipment used may be commercial equipment and may not meet requirements of MIL-STD-461A. Therefore, component testing would not be cost effective. Testing of the complete installed configuration on the aircraft would provide the best method of EMC evaluation and treatment of specific problems that may be indicated.

(i) Emergency Descent Profile--After discussions on the revised emergency descent profile, Boeing was requested to review the profile to determine the impact of using the existing profile down to 20,000 feet and a revised profile for the remainder of the descent.

(j) Phase 2 Detail Design--The 4950th was to provide AiResearch with a list of preferred material standards for utilization by Boeing in the detail design for the aircraft modification program.

Failure Modes and Effects Analysis (FMEA)

1. Objective and Results

The objective of the FMEA was to identify FTIS failure modes and their effects on the fuel system in the KC-135 aircraft in order to generate the preliminary hazards list for the Part 1 Modification Plan. These failure modes were classified per MIL-STD-882A, which evaluated the hazard classification in terms of the effect of the failure on safety of flight. Special attention was focused on single point failures which would adversely affect fuel system function and, therefore, flight safety. The FMEA was submitted as AiResearch Report 79-15740, Rev. 1, dated April 6, 1979.

No single point failures in the fuel inerting system were found which would cause overpressurization or underpressurization of the fuel tanks, or cessation of fuel flow. The worst case single point failure within the fuel inerting system would cause loss of fuel inerting capability with no other effect on fuel system performance.

Since the system employs pressurized air at elevated temperatures, it was recommended that Boeing evaluate adjacent or interfacing equipment of the KC-135 to ensure compatibility.

No Class I or II hazards were found. The failures in the fuel tank inerting system were identified as Class IV hazards per MIL-STD-882A.

2. FTIS Configuration

The air for the fuel tank inerting system is supplied from engine high stage bleed air as shown in Figure 5-4. The air enters the system through the shutoff valve, which is a solenoid-type pilot-operated pneumatic valve. The air exiting the shutoff valve enters a plate-fin-type air-to-air heat exchanger with the cold side supplied by ram air. Air exiting the precooler is then regulated by the bleed air dual pressure regulator and shutoff valve, which has high and low pressure settings. The air enters the turbocompressor, where it is compressed. The compressor exit air is ducted through a secondary heat exchanger to remove the heat of compression from the air. The airflow then splits to (1) power the turbine and (2) supply air to the ASM. Both the secondary and temperature control heat exchangers are air-to-air units. The cooling medium for the secondary heat exchanger is ram air. The cooling medium for the temperature control heat exchanger is turbine discharge air.

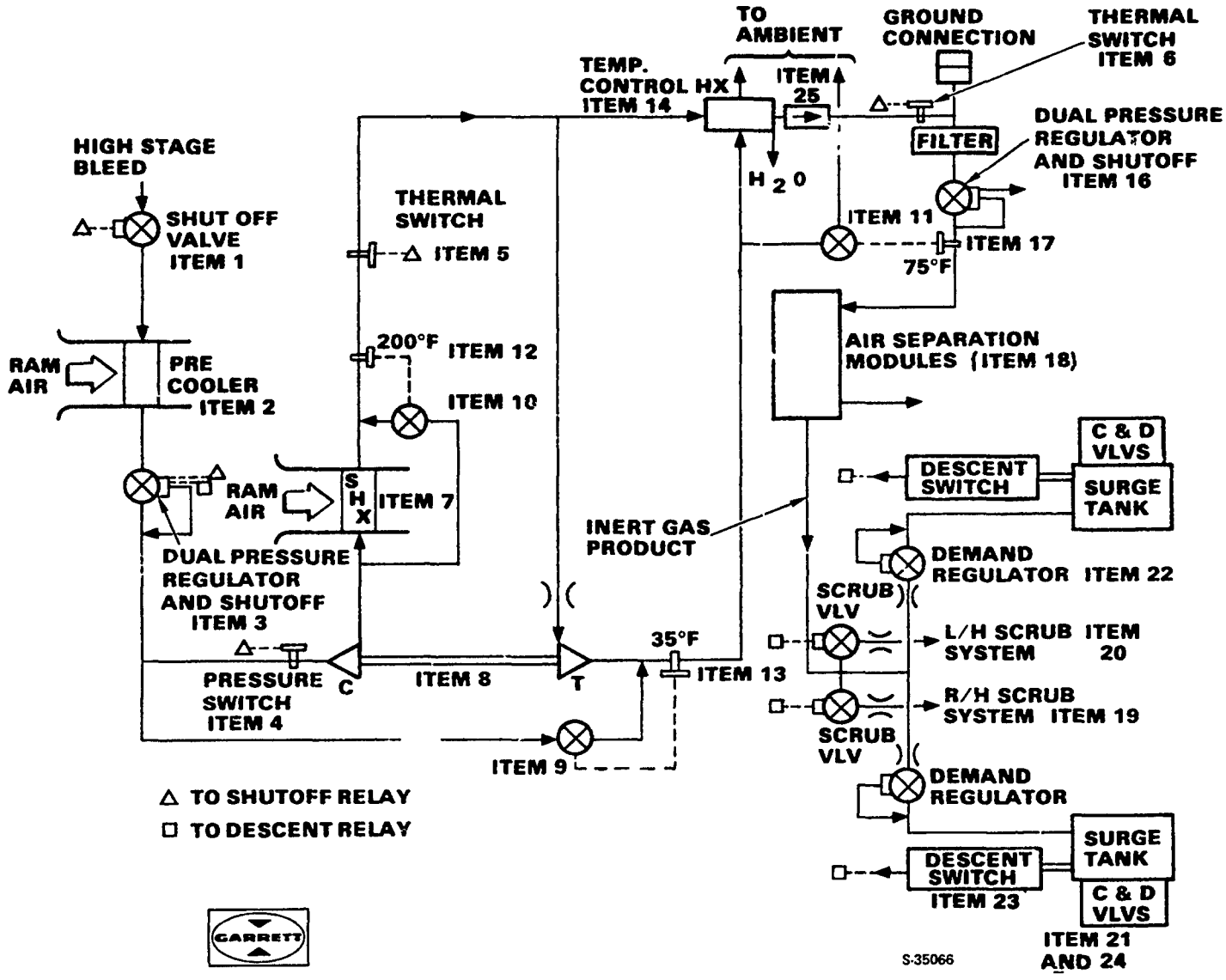

Figure 5-4. Fuel Tank Inerting System Schematic

There are two add-heat valves in the system, which supply additional heat to the air stream in two locations. One valve adds heat to the turbine discharge air if the temperature is 35°F or less; the other adds heat downstream at the secondary heat exchanger if the air temperature is 200°F or less. The temperature of the air entering the air separation module is closely monitored since the optimum production of the fuel inertant and life of the fibers on the ASM are a function of temperature. Ideally, the air entering the ASM should be 70° to 80°F. The devices monitoring system air temperatures and pressure are thermostats, thermoswitches, and pressure switches and regulators.

The air enters the air separation module after passing through a filter and a pressure regulator. The air is fed to the ASM at a rate of 30 lb/min at 115.5 psia and 75°F as a maximum condition. The fibers are permeable, hollow membranes; the oxygen-rich gas mixture flows to the outside and is dumped overboard. The nitrogen-rich gas mixture passes into the aircraft scrub system, where it is bubbled through the fuel tanks, absorbing the oxygen in the tanks at a fixed flow rate. It is also supplied to each of the demand regulators to maintain a given tank pressure with respect to ambient.

Because the membranes of the ASM are life sensitive to pressure and temperature, two thermoswitches and one pressure switch were added to the system. Signals from these switches will cause the bleed air pressure regulator to close in the event of a system failure resulting in overtemperature or overpressure upstream of the ASM.

The descent switches energize both the bleed air pressure regulator, item 3, and the ASM pressure regulator, item 16, to the high mode to ensure maximum flow to the system. Simultaneously, the descent switch de-energizes the scrub solenoids to preclude the introduction of higher oxygen concentrations, up to 9 percent, into the fuel.

The dive valves vent the fuel tank to allow a constant tank pressure. Air is vented into the fuel tank on dive if inertant flow is too low. The climb valve also acts to provide a constant fuel tank pressure. Inertant is vented from the tank if the tank-to-ambient P is exceeded. These valves are redundant, one being in each wing. Wing vent systems are interconnected, and each valve is designed for the total system flow capacity.

Airframe Support

The purpose of Task 1-5 was to ensure that all aircraft operational factors were addressed. This task was performed by the Boeing Aerospace Company, who were also involved in all other Phase 1 tasks that related in any way to test aircraft modifications and safety analyses.

Data requested from Boeing concerned the mission profiles for the KC-135A and YC-14 aircraft. The supporting data received from Boeing included aerodynamic propulsion, fuel system, aircraft configuration, and pneumatic data for the YC-14 and KC-135A aircraft. Data for the KC-135A were included earlier with the discussion of Task 1-1. The majority of the Boeing airframe support task was integrated with Task 1-4, Flight Test Planning.

Several meetings were held with Boeing, Seattle and Wichita, and AiResearch personnel in attendance to discuss the flight planning and aircraft support efforts. The following items were discussed or resolved at these meetings:

(a) A high pressure bleed air system was selected for the fuel tank inerting system. The selected concept, shown previously in Figure 5-4, provided a dedicated bleed air source for inerting package use only. Boeing considered several air source concepts in arriving at the selected system. The dedicated high spool bleed air system was selected primarily because:

1. The relatively small bleed duct sizes (1.5-in. dia.) will fit within the ducting envelope provided by deleting the water injection tubes from the engine wing leading edge.

2. The bleed air subsystem control was simpler than other concepts considered.

3. A dedicated air source concept eliminated problems in other pneumatic systems which could make flight test evaluation of the inerting system difficult.

(b) The C-5A climb/dive valves were too large to fit within the wing tip "S" duct, and will not be considered further. Candidate valves left to be considered were the DC-9, C-135, and 727 valves. The climb/dive valves were required to be redundant on each side of the aircraft.

(c) The modification requirements to install the Falcon gas sampling system were provided to Boeing. The plan was to install the sampling probes in the integral tanks only to preclude penetration of the bladder cells.

(d) A fuel scrub concept was proposed utilizing the Parker method, which uses motive fuel flow from the aircraft boost pumps to drive scrub ejectors. The scrub ejectors were to be installed in the integral portions of the tanks with a manifold concept which supplies nitrogen-scrubbed fuel to compartments and tanks remote from the boost pumps.

A fuel tank vent system analysis was made to determine the allowable pressure drop across the climb/dive valves.

Boeing studies indicated that Halon was compatible with the KC-135A fuel system, but may cause severe corrosion problems with engine combustors and exhaust areas.

SECTION 6

SYSTEM DESIGN

PERFORMANCE ANALYSIS

The detail design of the fuel tank inerting system was started in January, 1980, and was based on the restructured program in which the system was to be ground tested at Wright-Patterson Air Force Base rather than flight tested in a KC-135A aircraft. To design the system, a performance analysis was conducted to determine the impact on the operation of the fuel tank inerting system by changing some of the operating conditions to be compatible with the existing facility capability. Two specific areas were addressed: (1) system operation with the ACM turbine discharge exhausting to the laboratory ambient environment rather than to the proper simulated altitude and (2) definition of the required ram airflow at laboratory ambient conditions for supplying cooling air to the secondary heat exchanger.

Turbine Ambient Exhaust

Analysis of the system was conducted to determine the changes in performance as a result of discharging the turbine to laboratory ambient pressure. The increased back pressure on the turbine reduces the power developed by the turbine, thereby reducing the pressure rise developed by the compressor. The reduced compressor discharge pressure decreases the air separation module (ASM) differential pressure across the membranes, resulting in an increase of the oxygen concentration in the inertant flow.

A second effect of the turbine discharging to the laboratory ambient pressure is to increase the turbine discharge temperature. For most of the cases, the increased temperature can be accommodated by the system. However, for Conditions 6 and 7 the turbine exhaust temperature increases to 95°F, which is unacceptable since the 75°F inlet to the ASM is exceeded. The turbine discharge temperature was reduced to an acceptable level by increasing the bleed pressure by 4 psi in both cases. Tables 6-1 and 6-2 present the results of the analysis for both hot day and standard day conditions under aircraft design operation and laboratory operation. With the exception of Conditions 6 and 7, the bleed flow decreased as a result of the decrease in compressor discharge pressure, and the inertant oxygen concentration increased. For Conditions 6 and 7, the bleed flow remained essentially the same with the increased bleed pressure, while the oxygen concentration decreased slightly as a result of an increase in ASM supply pressure.

Secondary Heat Exchanger Cooling Airflow

Sea level cooling airflow requirements are also shown in Tables 6-1 and 6-2. The analysis assumed the use of laboratory air at 70°F and 70 percent relative humidity (77 gr/lb). The maximum flow required is 77.2 lb/min at standard day Condition 1. Homologues of ram air heat exchanger performance have been computed where possible; however, many aircraft design conditions result in bleed side outlet temperatures below 70°F. These low temperatures are not

TABLE 6-1

COMPARISON OF HOT DAY PERFORMANCE FOR AIRCRAFT AND LABORATORY TEST CONDITIONS

	AIRCRAFT CONFIGURATION									LABORATORY TEST CONFIGURATION							
	Bleed Pres, psia	Bleed Flow lb/min	Ram Air Flow, lb/min	Ram Air Inlet Temp, °F	SHX Bleed Out Temp, °F	Supply Pres, psia	Module Flow lb/min	Inert Flow, lb/min	Inert Conc, %	Bleed Pres, psia	Bleed Flow lb/min	Ram Air Flow lb/min	Ram Air Inlet Temp, °F	SHX Bleed Out Temp, °F	Supply Pres, psia	Module Flow, lb/min	Inert Flow, lb/min	Inert Conc, %
1	149.8	52.8	88.2	123	148	87.3	12.8	3.0	5.5	149.8	52.8	47.5	70	148	87.3	12.8	3.0	5.5
2	108.2	55.4	73.2	76	104	80.9	12.7	3.0	4.1	108.2	45.6	63.2	70	89	74.8	11.8	3.0	4.6
3	72.8	46.0	52.0	31	62	72.0	12.0	3.0	3.3	72.8	40.2	75.0	70	77	65.2	11.0	3.0	4.0
4	68.4	47.2	44.9	26	72	73.1	12.1	3.0	3.4	68.4	40.6	75.0	70	77	65.9	11.1	3.0	4.1
5	61.7	47.8	48.4	30	72	73.8	12.2	3.0	3.4	61.7	40.8	75.0	70	77	66.3	11.1	3.0	4.1
6	39.5	33.0	22.7	9	76	51.8	9.3	3.0	5.1	44.0	32.7	75.0	70	73	52.8	9.4	3.0	4.8
7	40.8	33.2	20.9	9	120	52.2	9.4	3.0	5.0	45.0	33.1	75.0	70	74	53.2	9.6	3.0	4.8
8	54.4	49.2	46.9	28	72	71.1	15.0	6.1	7.1	54.4	44.2	75.0	70	79	66.7	14.3	6.1	7.8
9	61.1	55.0	49.5	32	90	81.6	16.6	6.1	5.9	61.1	51.4	75.0	70	88	78.2	16.1	6.1	6.2
10	70.4	67.3	63.3	72	135	92.5	19.9	8.3	7.8	70.4	60.9	63.2	70	118	90.5	19.6	8.3	8.0
11	111.9	68.8	62.7	110	247	101.0	20.4	8.3	8.4	111.9	68.2	52.5	70	235	101.0	20.4	8.3	8.4
12	61.5	56.8	51.7	38	96	82.1	17.5	6.9	6.7	61.5	52.3	75.0	70	89	78.4	16.9	6.9	7.2
13	70.4	67.4	64.0	72	133	92.5	19.9	8.3	7.8	70.4	60.9	60.0	70	124	90.4	19.6	8.3	8.0
14	121.2	69.0	65.9	119	247	102.3	20.4	8.3	8.6	121.2	69.1	53.3	70	248	102.3	20.4	8.3	8.6

TABLE 6-2

COMPARISON OF STANDARD DAY PERFORMANCE FOR AIRCRAFT AND LABORATORY TEST CONFIGURATIONS

	AIRCRAFT CONFIGURATION									LABORATORY TEST CONFIGURATION								
	Bleed Pres, psia	Bleed Flow lb/min	Ram Air Flow, lb/min	Ram Air Inlet Temp, °F	SHX Bleed Out Temp, °F	Supply Pres, psia	Module Flow lb/min	Inert Flow, lb/min	Inert Conc, %	Bleed Pres, psia	Bleed Flow lb/min	Ram Air Flow lb/min	Ram Air Inlet Temp, °F	SHX Bleed Out Temp, °F	Supply Pres, psia	Module Flow, lb/min	Inert Flow, lb/min	Inert Conc, %
1	167.8	53.8	92.8	78	95	87.3	12.7	3.0	5.5	167.8	53.2	77.2	70	95	87.3	12.7	3.0	5.5
2	121.6	54.7	77.1	35	56	80.9	12.7	3.0	4.1	121.6	45.7	75.0	70	83	75.0	11.9	3.0	4.7
3	72.8	46.1	54.9	-9	14	72.0	12.0	3.0	3.4	72.8	40.2	75.0	70	77	65.1	11.0	3.0	4.0
4	68.3	47.3	48.2	-13	21	73.2	12.1	3.0	3.4	68.3	40.6	75.0	70	77	65.8	11.1	3.0	4.1
5	61.1	47.9	51.1	-9	22	73.8	12.2	3.0	3.4	61.1	40.8	75.0	70	77	66.2	11.1	3.0	4.1
6	39.5	34.3	25.2	-22	28	53.9	9.6	3.0	4.8	44.0	34.1	75.0	70	73	54.9	9.7	3.0	4.6
7	41.0	33.8	22.8	-22	45	54.8	9.8	3.0	4.6	45.0	34.8	75.0	70	73	55.9	9.9	3.0	6.9
8	54.5	52.0	49.2	-10	30	75 5	16.0	6.3	6.8	54.5	46.4	75.0	70	81	69.9	15.0	6.3	7.5
9	61.1	56.6	52.5	-8	39	84.3	17.2	6.2	5.7	61.1	53.1	75.0	70	90	80.6	16.6	6.3	6.1
10	70.3	69.9	66.6	31	87	95.9	20.7	8.5	7.5	70.3	64.6	75.0	70	108	93.8	20.4	8.5	7.8
11	111.9	77.3	67.2	66	151	101.0	20.6	8.5	8.5	111.9	75.0	68.0	70	148	101.0	20.6	8.5	8.5
12	61.8	58.7	54.6	-1	47	85.3	18.0	7.0	6.4	61.8	54.0	75.0	70	91	81.0	17.4	7.0	7.0
13	70.5	69.9	66.6	31	87	95.9	20.6	8.5	7.5	70.5	64.7	75.0	70	108	94.0	20.4	8.5	7.8
14	121.2	75.0	70.8	74	154	102.3	20.6	8.5	8.8	121.2	75.0	68.8	70	154	102.3	20.6	8.5	8.8

critical to system operation since the heat exchanger bypass valve controls the turbine inlet temperature to 250°F. System performance can thus be simulated adequately with the ram flow fixed as shown in the tables while still exercising the controls.

An alternative to conditioning the laboratory supply air to 70°F is to modulate the ram airflow, irrespective of ambient temperature, to obtain the secondary heat exchanger bleed air outlet temperature that is listed in the laboratory test portion of the tables. This approach will entail additional time required to set each condition, as well as the additional flow required with an increase in cooling air supply temperature. This, in turn, will require more capacity, both flow and pressure rise, from the laboratory supply.

Figure 6-1 shows the vacuum requirements for system operation. The majority of the exhaust flow from the FTIS emanates from the turbine discharge of the ACM. Figure 6-2 shows the estimated cooling air pressure duct of the ram air heat exchanger.

DESCRIPTION OF LABORATORY TEST SYSTEM

A schematic of the fuel tank inerting system is presented in Figure 6-3 and Table 6-3 and the electrical schematic is shown in Figure 6-4. These figures show the fuel tank inerting system as originally planned to be tested at the Aero Propulsion Laboratory facility. In Figure 6-3, the surge tanks simulate the ullage volume and the Item 8 C & D valves simulate the climb and dive valves. A detailed description of the FTIS components was presented in AiResearch Report 80-17162, dated November 24, 1980.

Facility air, which is preconditioned to a specific temperature and pressure to simulate a KC-135A precooler outlet bleed condition, enters the system through the facility bleed air shutoff valve, which is a normally-closed solenoid operated valve. From the shutoff valve, the bleed air flows through the bleed air dual pressure regulator and shutoff valve, Item 3-1. This valve has a high- and low-pressure regulation setting, controlled by the descent switch, Item 8. The descent switch senses the differential pressure between the surge tank and ambient. As the ambient pressure increases during descent, the switch energizes the descent relay, which changes the Item 3-1 regulator to the high pressure setting. Additional changes resulting from operation of the descent switch are described later.

The bleed air next enters the compressor end of the air-cycle machine (ACM), Item 3-2, where the pressure is boosted to a level useful for permeable membrane application. The accompanying heat of compression is rejected to ram air in the secondary heat exchanger (SHX), Item 3-3. The air leaving the secondary heat exchanger is controlled to 250°F by the SHX bypass valve, Item 3-4, which bypasses compressor discharge air around the heat exchanger. A portion of the high pressure 250°F air is ducted to the Item 4-1 air separation modules (ASM), while the remaining flow goes to the turbine, which drives the compressor. A dewpoint control maintains the turbine exhaust temperature at 0°F or the dewpoint (whichever is higher) by bypassing hot compressor inlet air to the turbine discharge. This prevents the buildup of ice in the turbine or in the heat exchanger downstream.

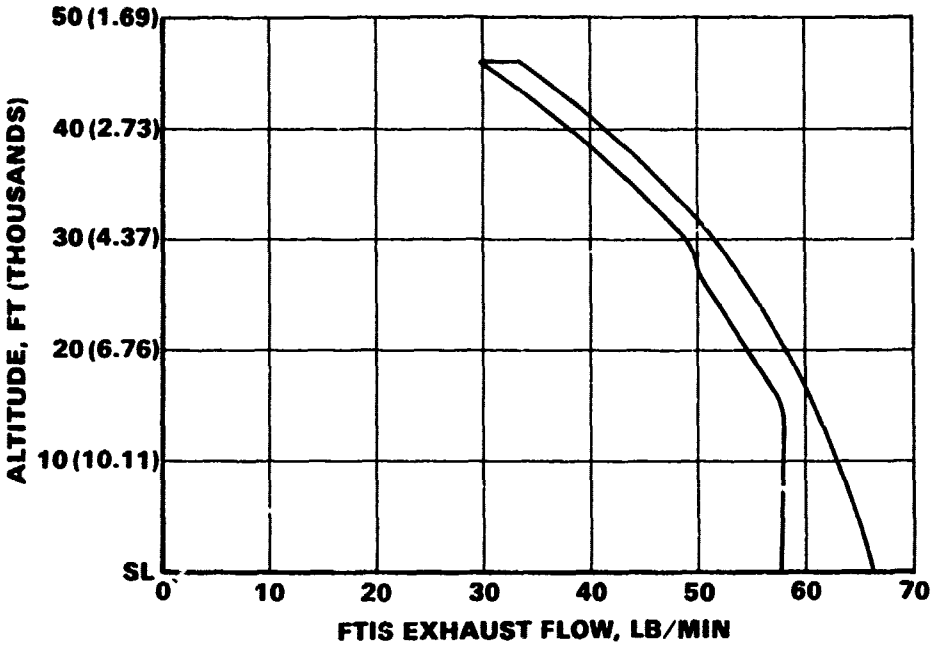

Figure 6-1. Vacuum Requirements

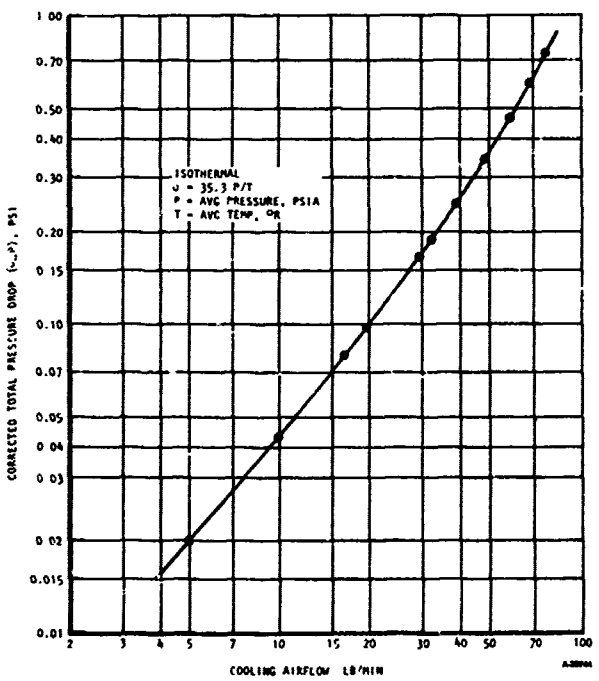

Figure 6-2. Estimated Cooling Air Pressure Drop of Ram Air Heat Exchanger

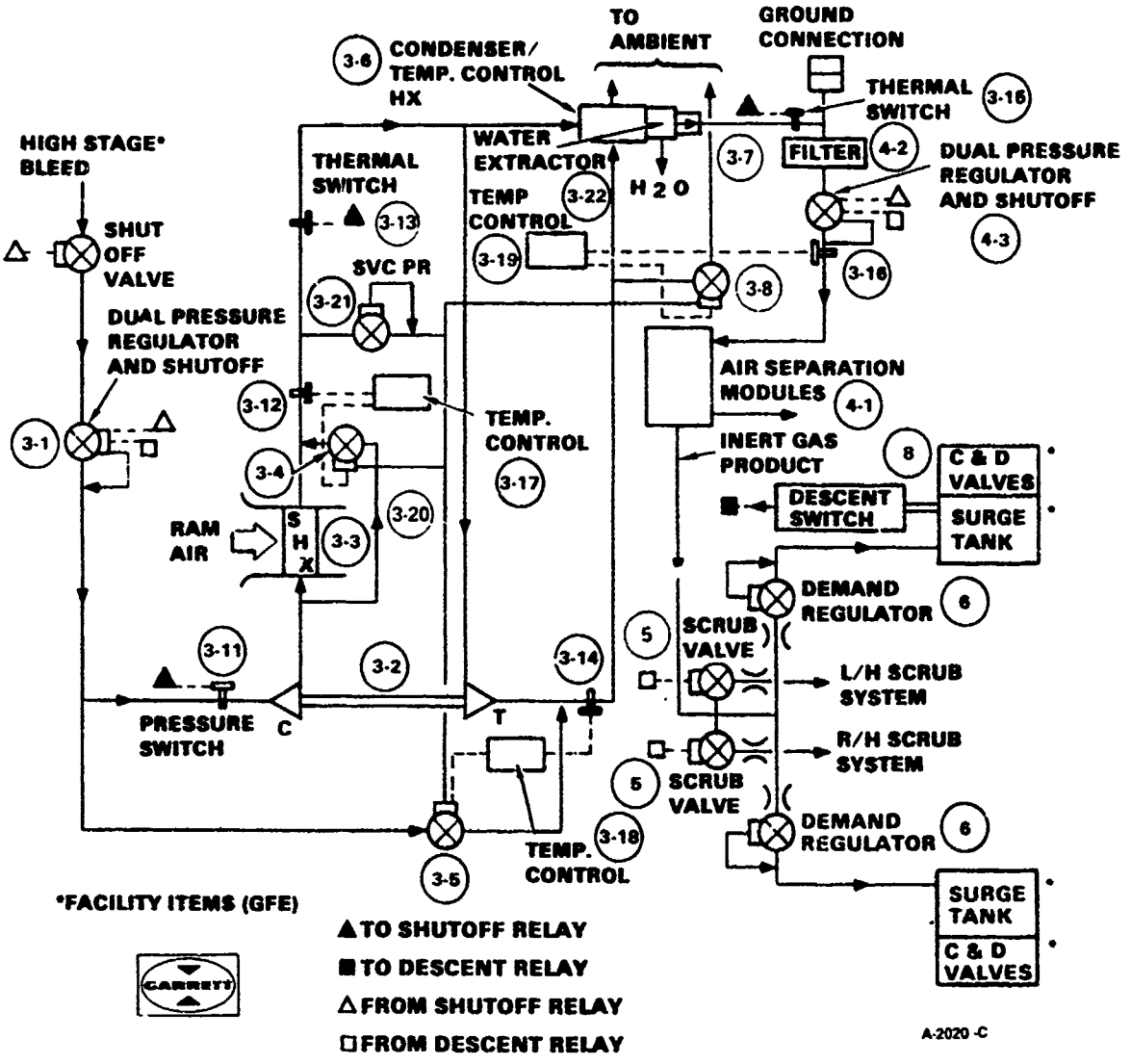

Figure 6-3. Fuel ..k Inerting System Schematic

TABLE 6-3

FUEL TANK INERTING SYSTEM COMPONENTS
PN 2202750-1-1

Item	Description	Part Number	Qty Req'd.
3	Bleed Air Conditioner Assembly	2202753-1	1
3-1	Dual Press Regulator	3214348-1	1
3-2	Air Cycle Machine (ACM)	581890-3-1	1
3-3	Secondary Heat Exchanger (SHX)	194468	1
3-4	SHX Bypass Valve	979420-1	1
3-5	Anti-Ice Valve	979448-1	1
3-6	Condenser/Thermal Control HX	194466	1
3-7	Check Valve	123504-2	1
3-8	Temp. Control Valve	979446	1
3-11	Pressure Switch (100 psig)	642001-1	1
3-12	Temp. Sensor (250°F)	624178-1	1
3-13	Thermal Switch (300°F)	641138-2	1
3-14	Temp. Sensor (0°F)	624178-1	1
3-15	Thermal Switch (100°F)	641138-1	1
3-16	Temp. Sensor (75°F)	624178-1	1
3-17	Temp. Controller (250°F)	624176-1	1
3-18	Temp. Controller (0°F)	624176-2	1
3-19	Temp. Controller (75°F)	624176-3	1
3-21	Reference Pressure Regulator	3214066-1	1
3-22	Water Extractor	194476	1
4	Inert Gas Generator Assembly	2202752-1	1
4-1	Air Separation Module	2202469-1	5
4-2	Filter	2202477	1
4-3	Dual Pressure regulator	3214350-1	1
5	Scrub Solenoid Valve	2202573	2
6	ΔP Demand Regulator (2 psid)	3214352-1	2
8	ΔP Descent Switch	2202574	1

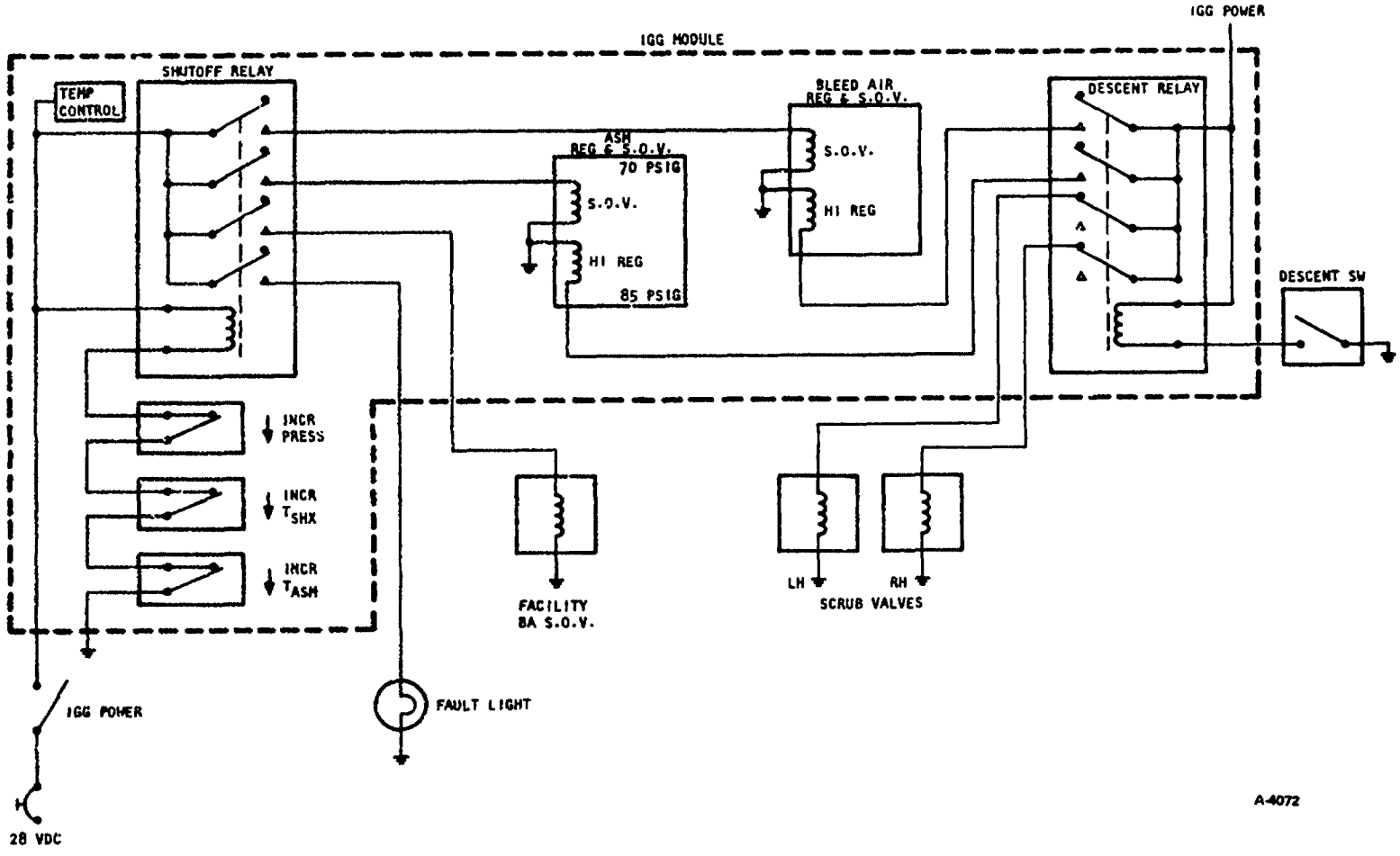

Figure 6-4. FTIS Electrical Schematic

The Item 3-5 valve, shown schematically in Figure 6-5, includes a pressure differential override servo. This servo provides anti-ice control operation as a function of pressure drop across the cold air side of the Item 3-6 heat exchanger. This mode of operation is in addition to the low limit temperature control function, which maintains the 0°F turbine discharge temperature. Temperature control system operation is described later.

In the event the differential pressure across the cold side of the heat exchanger rises above 2.5 psi, the differential pressure override servo provides pressure to the opening side of the actuator diaphragm. The resulting pressure differential across the valve actuator modulates the valve toward the open position to provide hot air.

The ASM inlet conditions are controlled and monitored to insure optimum performance and module life. Turbine discharge air is used to reduce the temperature of the air from the secondary heat exchanger into the Item 3-6 temperature control heat exchanger to a temperature of 75°F; any of the turbine air in excess of that required to maintain the 75°F temperature is routed directly overboard. The water condensed in the heat exchanger is removed by the Item 3-22 extractor. A filter, Item 4-2, and a second dual pressure regulator and shutoff valve, Item 4-3, just upstream of the module provide further conditioning of the inlet air. The Item 3-10 regulator is also controlled by the descent relay. Two thermoswitches, Items 3-13 and 3-15, and a pressure switch, Item 3-11, have been included in the system for failure modes as defined by the FMEA. These switches are normally closed and will open on increasing temperature or pressure, above their setpoints. Opening of any switch will de-energize the shutoff relay, which removes power from the Item 3-1 and 4-3 dual regulators and the facility C&D valves. A fault light on the control panel will also be activated.

The air separation module, containing millions of hollow polymethylpentene fibers, employs a continuous process in which pressurized air is exposed to the large surface area of the polymeric membrane material. Oxygen permeates the walls of the fibers preferentially, leaving a nitrogen-rich mixture. This inert product is directed to the fuel tanks via the aircraft scrub system, Item 5, and/or the demand regulators, Item 6. The demand regulators will allow inflow when the fuel tank pressure is less than 2 psig. The low pressure (permeant) side of the membrane is connected to a vacuum source for altitude simulation. The descent switch, Item 8, energizes the coil of the descent relay, which in turn energizes both the IGG and bleed air pressure regulators to the high mode setting to accommodate the higher inerting demand associated with descent and also de-energizes the scrub solenoids. This precludes the introduction of higher oxygen concentrates (up to 9 percent) into the fuel via the scrub solenoids during high flow (9 percent O_2) conditions.

TEMPERATURE CONTROL SYSTEM DESCRIPTION

Three separate and independent electropneumatic temperature control systems are provided to condition the bleed air for all of the segments of the KC-135A mission profile.

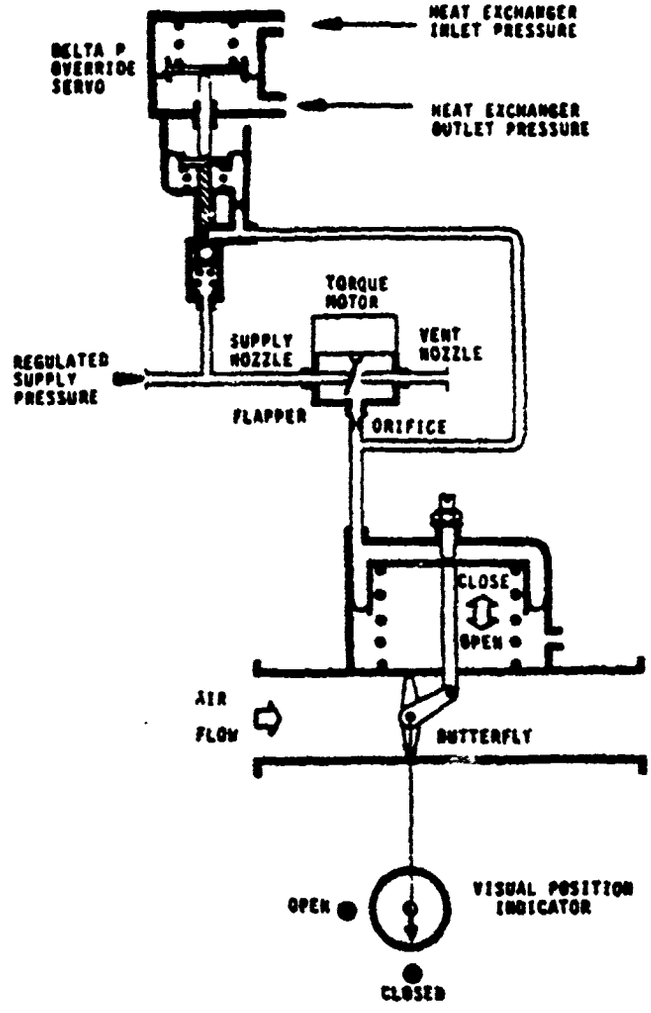

Figure 6-5. Schematic Diagram, Dewpoint/Anti-Ice Control Valve

The following description applies to all of the systems for electropneumatic operation. Refer to Figure 6-6 schematic for the temperature control valve.

The temperature control valve is a spoon butterfly type, with an electropneumatic control. The valve modulates in response to pressure from the torque motor, which operates in response to electrical signals from the temperature controller/sensor. The torque motor receives its supply pressure from the Item 3-21 service pressure regulator.

Application of current from the temperature controller, which provides a current signal (in response to the sensed temperature) to the torque motor, moves the flapper valve away from the inlet nozzle, increasing the pressure on the opening side of the valve actuator diaphragm. The resulting pressure differential across the valve actuator modulates the butterfly toward the open position, allowing more air to flow through the valve.

Shutoff operation is accomplished by reducing the electrical current to the torque motor below a specific minimum. This action positions the valve flapper to seal off supply pressure and simultaneously vents the opening chamber of the valve actuator to ambient. The valve butterfly then is moved to the closed position by the actuator closing spring.

FLIGHT PROFILE OPERATION

General

The sequence of control actions that occur during a typical mission cycle includes startup, climb, altitude cruise, descent, final approach and landing. Fuel tank pressurization is controlled by a subsystem consisting of the descent switch and relay, demand regulators, scrub valves, and climb and dive valves.

Startup

While the aircraft is on the ground with the engines running, the tanks are unpressurized. The state of the controls is as shown in the electrical schematic, Figure 6-4. When power to the inerting system is switched on, the bleed air shutoff valve and the air separation module (ASM) shutoff valve are energized open. Since the tanks are initially unpressurized, the demand regulators go full open and the descent switch closes, energizing the descent relay. The bleed air and ASM regulators are switched to the high settings and the scrub valves are switched off. Oxygen depleted air produced by the air separation modules flows to the tanks through the demand regulators.

The operation of the descent switch is shown in Figure 6-7. When the increasing tank pressure builds to 1.8 psig (nominal), the descent switch opens, placing the regulators on the low settings and activating the scrub system. The demand regulators close when tank pressure reaches 2.0 psig. The inert gas flow is now controlled by the scrub valve flow limiting orifices, which are sized to flow a maximum of 1.5 lb/min each at sea level. Tank pressure continues to rise. At 2.1 psig, the climb valves crack to prevent overpressurization.

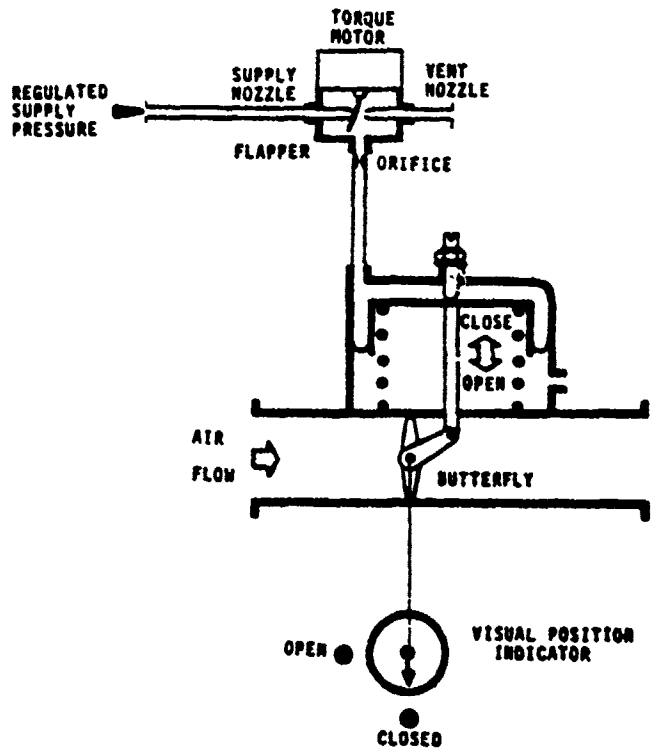

Figure 6-6. Schematic Diagram, Temperature Control Valve

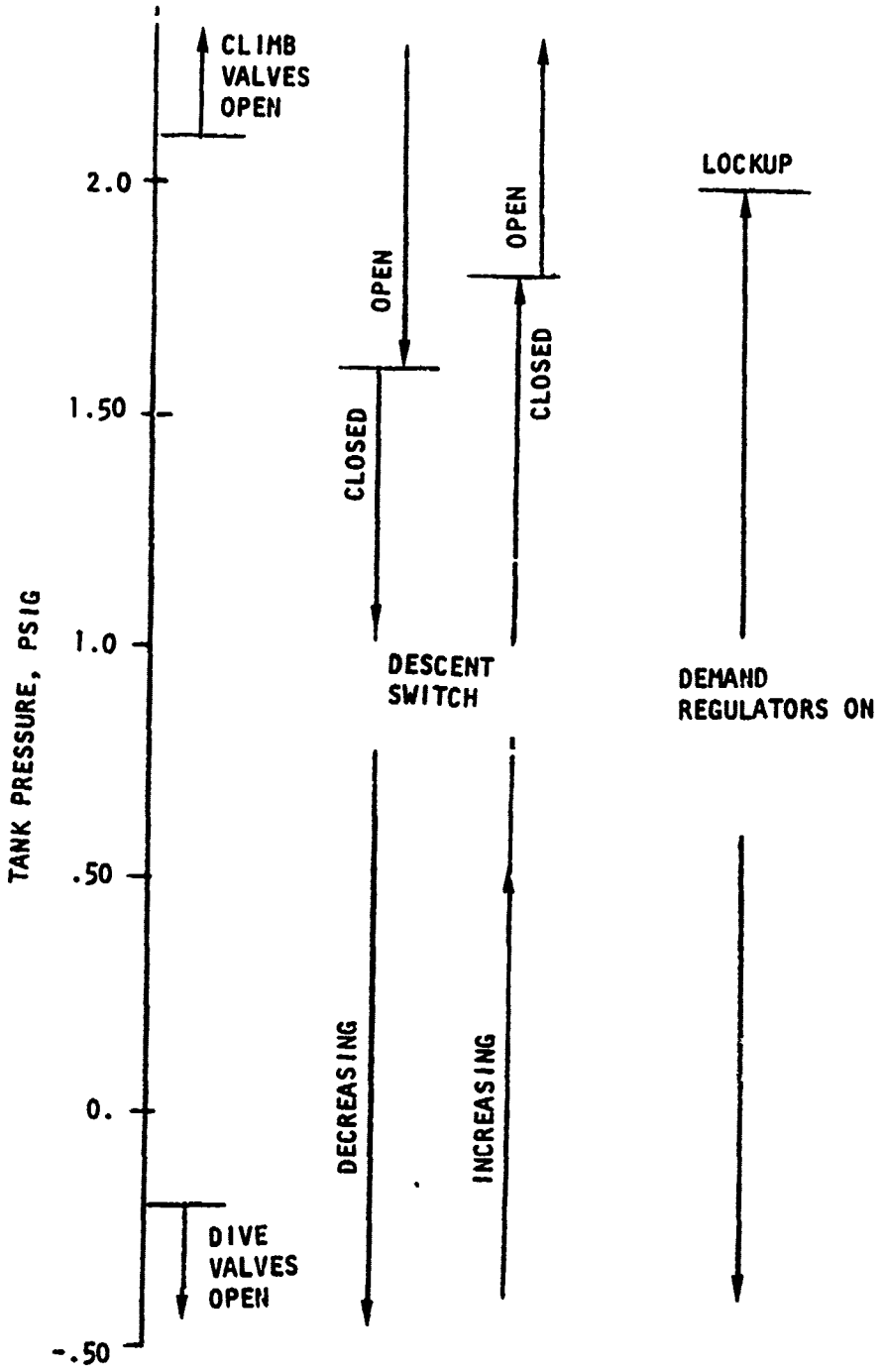

Figure 6-7. Descent Switch and Valve Operation

Climb

The aircraft takes off and climbs. Atmospheric pressure descreases with increasing altitude. The climb valves must outflow more to relieve the tank differential pressure which builds up due to both decreasing atmospheric pressure and inertant inflow through the scrub valves.

The actual flow required for pressurization is very low during ascent; however, the scrub flow must be maintained for another purpose. Air that dissolves in the fuel at sea level atmospheric pressure tends to come out of solution as the absolute pressure in the tank decreases during climb. The scrubbing process is designed to absorb oxygen from the fuel in a controlled fashion such that the oxygen concentration of the gas coming out of the fuel is always at a safe level.

As the aircraft climbs, the descent switch is open, the bleed air and ASM regulators remain at the low setting, and the scrub valves remain open. The demand regulators are locked up closed above 2 psig tank pressure, and the (climb) relief valves are relieving to maintain tank pressure at 2.3 psig.

Altitude Cruise

As the aircraft levels off and cruises at some high altitude, the scrub valves remain open but the inert scrub flow is less, due to the reduced available engine bleed pressure. At this point, however, the fuel has been sufficiently scrubbed, and this reduced inert gas flow is more than sufficient to make up for fuel usage and to maintain pressurization. The climb valves are metering to maintain tank pressure at 2.3 psig.

Descent

During descent, atmospheric pressure increases and the inert gas flow required for pressurization is highest. Depending on the rate of descent, tank ullage, and fuel flow rate, the inert scrub flow rate may become insufficient to maintain tank pressure at 2.3 psig. The relief valves close as the tank pressure decreases below 2.1 psig.

The inert supply flow is increased in several steps to accommodate the higher demand as controlled by the tank-to-ambient differential pressure. The demand regulators, which control tank pressure to 2.0 psig, will modulate when the tank pressure decays below this level. The descent switch, which is designed to detect sustained changes in aircraft altitude, energizes the descent relay when the tank pressure falls below 1.6 psig (see Figure 6-7). As observed from the electrical schematic, Figure 6-5, the descent relay switches the bleed air and ASM regulators to the high flow settings, and shuts down the scrub systems. The scrub flow is turned off during descent to preclude the introduction of high relative oxygen concentration air into the fuel, where oxygen might be redissolved.

The orifices of the demand regulators limit the supply flow to 5.5 lb/min each to prevent overpressurization of the tank during failure modes. The flow is sufficient to allow the ullage pressure to decay to near ambient at the end of the final descent of the design mission without the inflow of ambient air.

In the event of a failure in the supply system, the dive valves are set to crack at -0.2 psig to prevent excessive negative gage pressures within the tank.

Final Approach and Landing

As the aircraft levels off at low altitude and the aircraft ambient pressure stabilizes, tank pressurization starts to recover. The demand regulators are full open and the bleed air and ASM regulators are at the high setting. The sequence of events which occur as pressure builds during the final approach until the aircraft lands is similar to that described for startup.

INSTRUMENTATION

Location of instrumentation originally planned for testing at AiResearch is shown on Figure 6-8. Each parameter is coded P, T, W, or ΔP. These coded instrumentation points are listed in Table 6-4, which defines the parameter and location. All thermocouples within the FTIS were to be considered part of the system and intended for shipment with the FTIS. Instrumentation identified with an asterisk (*) in Figure 6-8 is considered laboratory equipment, and as such would not be part of the FTIS. Pressure sensor ports would be supplied in applicable locations within the FTIS package, although pressure transducers would not be included.

PACKAGE ASSEMBLY

The FTIS package assembly was reconfigured into two major subassemblies. The primary subassembly, the IGG system, which forms the base of the package, consists of the five air separation modules (ASM's) with the downstream interface at the discharge of the ASM's. The upstream interface commences at the water extractor discharge with those downstream components.

The other subassembly contains all bleed air conditioning hardware commencing with the dual pressure regulator and shutoff valve and terminating at the water extractor discharge. This method of packaging allows minimum changes for interfacing the bleed air conditioning and inert gas supply and control subsystems with the molecular sieve inert gas generation system.

The system design task was completed in July of 1980 and assembly, subassemblies and component outline drawings were transmitted to the Air Force.

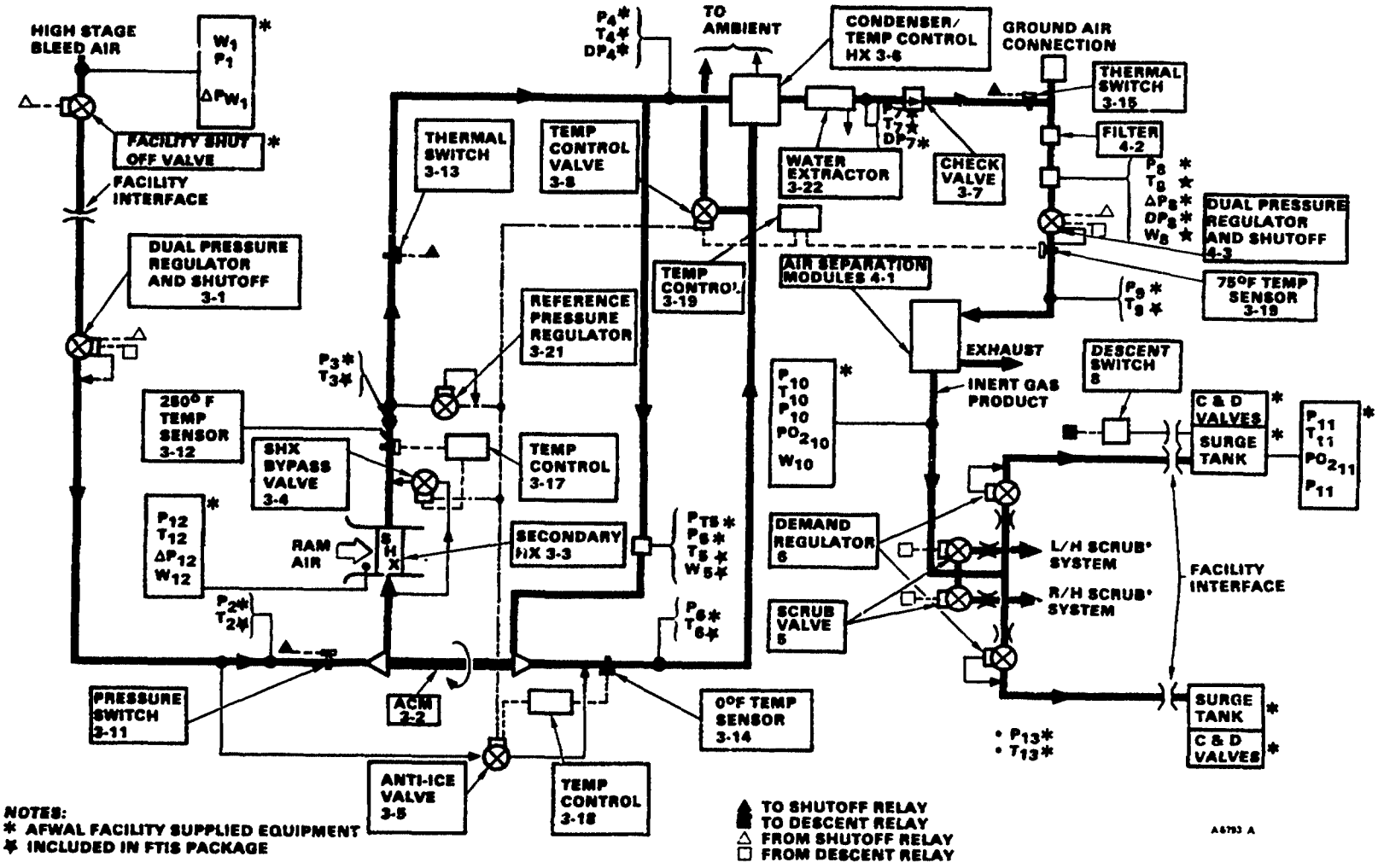

Figure 6-8. FTIS Schematic Showing Test Instrumentation

TABLE 6-4

FTIS INSTRUMENTATION DESCRIPTION

		PARAMETERS									
					Temperature T				Gas Flow W		
	Description	Static P*	Differential P*	Total P_T*	Included in FTIS	AFAPL Supplied *	Dew Point DP*	Percent Oxygen PO_2*	In FTIS	AFAPL Supplied*
1	Facility reg, inlet	1	1			1				1
2	Compressor, inlet	2			2					
3	Sec Hx out, mixed	3			3					
4	Cond/Hx, inlet	4			4		4			
5	Turbine, inlet[1]	5		5	5				5	
6	Turbine, outlet	6			6					
7	Water extractor, outlet	7			7		7			
8	Dual reg (4-3) inlet[2]	8	8		8		8		8	
9	ASMA, inlet	9			9					
10	ASMA, outlet	10	10			10	10		10	
11	Surge tank	11	11		11		11			
12	Sec Hx ram air	12	12			12			12	
13	Ambient	13				13				

NOTES:

Instrumentation included in FTIS package

1 Calibrated (lb/min) duct P_T-P included in FTIS package

2 Calibrated (lb/min) laminar flow element included in FTIS package

3 AFAPL Facility supplied instrumentation

* .o All pressure transducers
o All other flow measurement devices

SECTION 7

HARDWARE FABRICATION AND TESTING

GENERAL

Hardware fabrication progressed through January, 1981, on schedule, until the stop work order was received. Fabrication was scheduled to continue through February and March with most components being delivered by mid-February. Due to program redirection, further fabrication of bleed air conditioning subsystem hardware was stopped.

Inert gas generator component hardware deliveries made during February, 1981, consisted of a dual pressure regulator, Item 4-3; two scrub solenoid valves, Item 5; and two demand pressure regulators, Item 6. In addition to these complete components, hardware details consisting of head assemblies, shell and miscellaneous detail hardware for the first two air separation modules were completed and delivered to Dow Chemical. Detail hardware for the descent switch, Item 8, was received in February, 1981.

AIR SEPARATION MODULES

Large Diameter Internally Pressurized Modules

1. Construction and Fabrication Characteristics

Fabrication of the original large diameter, inside-to-out configuration air separation modules, designated by Dow as BMF-1 through BMF-7, was completed in August, 1981. Photographs of a typical BMF module are shown on Figures 7-1 and 7-2. The construction and fabrication characteristics of these modules are listed in Table 7-1. As indicated in the table, modules BMF-6 and BMF-7 had slightly more fiber area and slightly lower packing factors than the previous three units. The lower packing factors were desired to reduce the shell-side pressure drop. Module BMF-7 was the most uniform module, having no significant sections of high fiber density. This module also had the minimum amount of internal wrappings used to provide bundle integrity. In all instances, module weights were in the 61-64 lb range, well below the design weight of 69 lb.

Table 7-2 shows shell flow-ΔP data at 1-5 psid for all BMF units. With the design shell flow-ΔP needing to be at least 5.2 cfm/psid to achieve proper average shell-side pressure, only one of the modules met this criterion. This module, BMF-3, satisfied the shell-ΔP constraint only because of its sparsity of fibers. Module BMF-7, which had the prerequisite number of fibers and good bundle uniformity, was significantly below the shell design ΔP value. Thus, extrapolations of design data formulated for smaller modules during the development phase were not necessarily valid for the large size BMF units.

2. Performance Test Results

With fabrication completed, the modules were assembled into their pressure housings, pressure tested at 100 psig, and then subjected to air separation

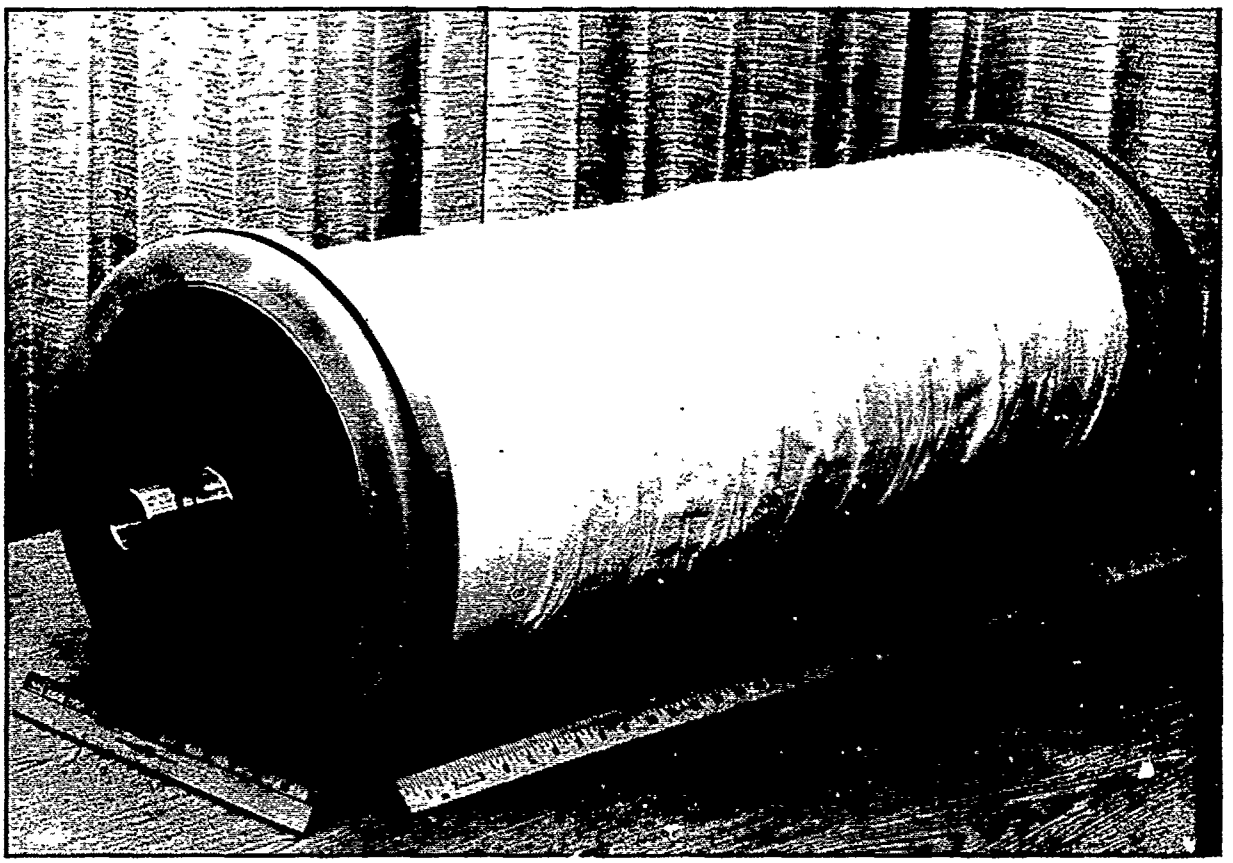

F-36459

Figure 7-1. Hollow Fiber Membrane Bundle

F-36458

Figure 7-2. Air Separation Module

TABLE 7-1

BMF-1 THROUGH BMF-7 MODULE FABRICATION CHARACTERISTICS

Module No.	Fiber Size (μ)	No. of Fibers (N)			Bundle O.D. (in)	Active Length (in)	Packing Factor	Surface Area (ft^2)	Fabrication Eff. (%)	Module Wt. (lb
		Weight	Wraps	Avg.						
BMF-1	29.8 x 42.5	34.00	34.27	34.13	12.97	36.5	.582	38280	98.3	73.0
BMF-2	30.0 x 42.2	34.33	34.23	34.28	12.76	35.3	.596	37160	98.0	60.0
BMF-3	29.1 x 41.3	31.89	31.50	31.75	13.33	34.3	.483	32590	98.3	61.8
BMF-4	29.1 x 41.3	33.84	33.21	33.52	13.35	34.8	.509	34910	98.2	61.5
BMF-5	29.3 x 40.9	34.32	34.01	34.16	13.06	35.0	.532	35720	97.4	61.2
BMF-6	29.5 x 41.5	34.25	34.52	34.39	13.45	35.0	.519	36350	99.2	62.9
BMF-7	29.8 x 41.7	34.41	34.47	34.44	13.50	35.3	.521	36960	99.1	63.5
DESIGN	30.0 x 42.0	33.73	33.73	33.73	13.65	36.0	.506	37190	—	69

TABLE 7-2

SHELL FLOW-ΔP VALUES FOR BMF-1 THROUGH BMF-7 (CFM/PSID)

Module No.	Shell Pressure Drop (PSID)					Avg.
	1	2	3	4	5	
BMF-1	2.26	2.04	1.89	1.82	1.77	1.96 ± .20
BMF-2	1.08	1.07	1.07	1.03	1.04	1.06 ± .02
BMF-3	6.45	5.74	5.37	5.17	5.01	5.55 ± .57
BMF-4	2.89	2.95	2.97	2.93	2.90	2.93 ± .03
BMF-5	1.85	1.92	2.03	2.11	2.15	2.01 ± .13
BMF-6	1.54	1.84	1.89	1.88	1.87	1.80 ± .15
BMF-7	3.94	3.55	3.23	3.06	2.94	3.34 ± .40
DESIGN						5.2

performance testing. In performance testing, three operating modes were examined: (1) design feed pressure with atmospheric permeant exhaust through both shell and core, (2) design feed pressure with core closed to gather shell pressure drop and, (3) design feed pressure with shell and core operating at a back pressure of 0.8 psig. The latter condition was the design test point. As well as testing the modules in the above three modes, they were fed at each end to check performance symmetry.

Table 7-3 summarizes the results. For the last five modules, performance was below the 1.79 lb/min minimum inert flow and 4.17 lb/min maximum feed flow listed for the design conditions in Table 7-4. Furthermore, the data showed significant performance asymmetry indicating a possible chronic problem. Initial concerns that the shell- P might account for the substandard behavior proved spurious. Table 7-5 lists the module computer simulation as a function of average shell pressure. Using Table 7-3, which gives shell-ΔP values of 6-7 psid for modules BMF-3 through BMF-7, the average shell pressure computes to be only 18-19 psia. This higher shell pressure may explain the lower inert flow readings, but predicted substantially higher inert recoveries (40-41 percent) than the 27-32 percent actually seen. The asymmetry, by the same token, cannot be accounted for by shell effects. Examination of the data indicated that the following causes may have contributed to module inadequacy:

(a) Broken tubesheet or core--Breaks such as these would manifest themselves in low inert and flow and low inert and recovery. Performance asymmetry would be anticipated.

(b) Poor fiber initial separation--This would be seen in lower inert flows and inert recoveries. Performance would likely be symmetric, however.

(c) Good initial fiber, poor strength--Performance would be initially satisfactory. Inert flow and recovery would decline during testing as fibers ruptured at the test pressure. A slight asymmetry might be seen because of pressure differences at each end of the module.

(d) Module seal leakage--Seal leakage would be seen in low inert flow and recovery. Asymmetry would result.

3. Analysis of Results

Of the four possibilities listed, fiber quality was deemed most crucial since the other problem areas lent themselves to possible repair. Because land-based modules had shown good performance containing fiber spun around the time of the BMF units, the fiber quality was not considered a point of concern. Nevertheless, eight beaker units from two spin runs that went into the BMF units were analyzed. Eight beaker units from each run were made and separation factors tabulated (Table 7-6). Because of the fragile nature of the fibers, the beaker unit acceptance ratio was typically 50-80 percent, depending upon the smoothness of the fiber spool. To sort out initial performance and fiber strength, the units were tested at 50 psig external pressure to avoid pressure rupture. Table 7-6 shows separation factors above 4.1 in at least 50 percent of the units in both sets. The high factors are indicative of good fibers, since past experience with poor fibers has shown poor separation factors in

TABLE 7-3

AIR SEPARATION PERFORMANCE OF MODULES BMF-1 THROUGH -7

Module No.		Case 1 Inert (lb/min)	Case 1 Feed (lb/min)	Case 1 Rec. (%)	Case 2 Inert (lb/min)	Case 2 Feed (lb/min)	Case 2 Rec. (%)	Case 2 Δ P (PSID)	Case 3 Inert (lb/min)	Case 3 Feed (lb/min)	Case 3 Rec. (%)
BMF-1	F	1.781	4.01	44.4	1.679	3.88	43.3	6.94			
	R										
BMF-2	F				1.47	4.02	36.6	12.02	1.54	4.12	37.4
	R										
BMF-3	F	1.620	5.20	31.2	1.484	5.14	28.9	2.86	1.442	4.93	29.2
	R	1.567	5.04	31.1	1.445	5.06	28.6	2.71	1.448	5.06	28.6
BMF-4	F	1.537	5.15	29.8	1.495	5.10	29.3	7.01	1.406	4.99	28.2
	R	1.615	5.19	31.1	1.546	5.11	30.3	6.96	1.545	5.10	30.2
BMF-5	F	1.740	5.29	32.9	1.578	5.24	30.1	6.73	1.585	5.24	30.2
	R	1.447	4.93	29.4	1.286	4.74	27.1	6.61	1.375	4.83	28.5
BMF-6	F	1.350	5.04	26.7							
	R	1.417	5.22	27.1							
BMF-7	F	1.702	5.18	32.9	1.577	5.05	31.2	6.20			
	R	1.522	5.01	30.4	1.396	4.83	27.9	6.30			

Case 1: 85.8 psig feed, atmospheric shell and core
Case 2: 85.8 psig feed, atmospheric shell, core closed with shell Δ P tap
Case 3: 85.8 psig feed, shell and core 0.8 psig
Polycarbonate Core: Modules BMF-2-7

TABLE 7-4

DESIGN CONDITIONS FOR BMF MODULES

PHYSICAL CHARACTERISTICS

FIBER SIZE:	30 x 42μ
FIBER ACTIVE LENGTH:	36"
OVERALL:	40"
NUMBER OF FIBERS:	33.73×10^6
PACKING FACTOR:	50.6%
MANDREL (CORE) DIAMETER:	2.00"
BUNDLE DIAMETER (MAX.):	13.65"
OPEN FIBER PERCENTAGE (MIN.):	85
WEIGHT (MAX.):	69 LBS.

SHOP TEST PERFORMANCE

MINIMUM O_2/N_2 SEPARATION:	4.05
MINIMUM INERT FLOW:	1.79 LB/MIN.
MAXIMUM FEED FLOW:	4.17 LB/MIN.
MAXIMUM SHELL Δ P:	3.08 PSID
MAXIMUM AVERAGE SHELL PRESSURE:	17.04 PSIA
MINIMUM SHELL FLOW/ Δ P:	5.2 CFM/PSID

END-OF-LIFE PERFORMANCE

MINIMUM O_2/N_2 SEPARATION:	3.95
MINIMUM INERT FLOW:	1.77 LB/MIN.
MAXIMUM FEED FLOW:	4.20 LB/MIN.

TESTING AT 100.5 PSIA INLET, 15.5 PSIA SHELL, 75°F

TABLE 7-5

DESIGN MODULE PERFORMANCE AS A FUNCTION OF AVERAGE SHELL PRESSURE (COMPUTER ISOLATION)

Avg. Shell Pressure	Feed Flow (lb./min.)	Inert Flow (lb./min.)	Inert Recovery (wt. %)
17.04	1.753	4.182	41.9
18	1.678	4.075	41.2
19	1.588	3.952	40.2
20	1.509	3.845	39.3
21	1.430	3.729	38.4

Testing at 9.0% O_2, 100.5 psia feed, 23.9°C (75°F).

TABLE 7-6

FIBER GAS SEPARATION AND HOOP STRENGTH STUDY

Unit Number	Separation Test (50 psig, Ext.) O_2 (SCCM)	N_2 (SCCM)	α	Pressure Test (85 psig, Int.) Start	Pass	Failure Mode
R202-119-1	14.70	3.71	3.96	Y	N	Fiber
-2	14.48	3.47	4.17	Y	Y	—
-3	15.32	3.73	4.11	Y	Y	—
-4	14.68	3.71	3.96	Y	N	Tubesheet
-5	15.23	3.71	4.11	Y	Y	—
-6	15.12	3.85	3.92	Y	N	Tubesheet
-7	14.32	3.48	4.11	Y	Y	—
-8	14.34	3.42	4.19	Y	Y	—
R208-147-1	12.45	2.96	4.21	Y	Y	—
-2	14.20	3.84	3.70	N	—	—
-3	13.57	3.92	3.46	N	—	—
-4	15.31	4.92	3.11	N	—	—
-5	13.93	3.27	4.26	Y	Y	—
-6	17.84	8.38	2.13	N	—	—
-7	13.45	3.19	4.22	Y	Y	—
-8	13.65	3.26	4.18	Y	Y	—

R202 fibers into BMF-3
R208 fibers into BMF-6
Y = Yes
N = No

virtually every beaker unit tested. To further substantiate fiber quality, five random samples from each package were axially scanned for stress marks. No such marks were seen.

To check fiber pressure stability, several of the beaker units were tested at 85 psig internal pressure at 25°C for a minimum of 12 hours. Considering that the maximum time that the fibers were exposed to pressure during testing was 20-30 minutes, the 12-hour test seemed reasonably conservative. Again, the fibers exhibited satisfactory strength to rule out this factor as the source of module problems.

To discern whether the case seals may be faulty, a hydrostatic proof test was run to carefully observe module motion under pressure. The test was done on BMF-6, the poorest performer, by pressurizing both heads and the fiber bundle interior with 90 psig water. During testing, considerable leakage was seen on the shell side of the bundle. Movement of the outer wrap to allow viewing the fibers revealed no gross fiber breakage. This absence of fiber breakage suggested a pronounced leak in the tubesheet region. To positively define the nature of the leak, a shroud was procured to permit a slow permeating gas to be pressurized on the shell side. This gas provided a bubble source for leaks to be seen on the water-covered tubesheet.

BMF module testing in the shroud produced the following results. BMF-6, the poorest of the large diameter modules, was installed in the shroud to determine the origin of the leakage seen when the unit was hydrotested. Prior to its installation in the shroud, visual examination of BMF-6 revealed a circumferential crack on each tubesheet at a radius of 4-1/2 inches from the center of the bundle. One significant radial crack also was evident. A possible indicator that the crack caused poor module performance was a discovery of residue inside the crack that was deposited by water leakage during 90 psig hydrotesting.

After installation in the shroud, the shell was pressurized to 1-2 psig with N_2, and the exposed tubesheet face was covered with water. Bubbling was seen throughout the face due to permeation of the nitrogen. However, no particularly gross flow increase was seen at the crack interface. This suggested that the crack may be oriented so that leakage occurs when tube pressure is higher, but does not occur when shell pressure is higher.

After the N_2 shell pressurization, a vacuum test was employed to test the crack orientation theory. The shell was evacuated to 20 in. Hg and water was placed on the tube sheet face. As expected, water was drawn into the fibers to replace permeated gas. Unfortunately, the water flow also did not appear to be significantly greater at the crack. This again suggested that the crack "opened up" at high pressure (85 psig), but was relatively "tight" at lower pressure (10 psig).

The conclusion reached was that the use of a polycarbonate core, combined with large diameter headers, was the determining factor in producing the cracks. It was found that the cracks appeared in the headers at the joints forming when each module was wrapped on successive days. Because of the poor heat transfer characteristics inherent with the polycarbonate core, which led to premature curing, more than one day was needed to complete the wrapping operation. Repair

of the cracked headers was not totally successful, and left the headers in a condition that could lead to premature failures.

Small Diameter Externally Pressurized Modules

1. Design and Construction Characteristics

A comparison of characteristics for the internally and externally pressurized module designs are presented in Table 7-7. Advantages of the externally pressurized ASM are increased fiber life and lower cost. The commercial, externally pressurized version of this design has thousands of hours of continuous operation at similar conditions in the chemical processing industry, and with very high reliability. For aircraft applications, the externally pressurized ASM incorporates a polycarbonate core material in place of aluminum alloy. The polycarbonate core provides improved life at the extreme ambient temperatures encountered in aircraft.

TABLE 7-7

AIR SEPARATION MODULE (ASM) DESIGN CHARACTERISTICS
AT 8.85 LB/MIN AND 9-PERCENT O_2 DESIGN POINT

	Internally Pressurized Design	Externally Pressurized Design
Module diamter, in.	14.7	9.1
Fiber size, microns	30 x 42	30 x 41
Feed pressure, psig	85.5 internal	85.5 external
Temperature, °F	75	75
Fiber lifetime, hr	5600	28,000
Inert flow, lb/min	1.77	0.8
Feed flow, lb/min	4.2	1.9
Ratio, inert/feed	0.42	0.42
Weight of ASM, lb		
Fiber bundle	64	28
End caps	17	1
Pressure case	16	13
Total	97	42
Required ASM per IGG	5	10
Total IGG, system weight, lb	485	420

The externally pressurized air separation module is constructed in a similar manner to the internally pressurized module. In both cases, it is constructed analogously to a conventional tube and shell heat exchanger, as shown in Figure 7-4, with the tubes being tiny polymethyl pentene hollow fibers (nominally of 30 microns I.D. and 41 microns O.D.). The fibers are wrapped around a mandrel and are contained on the ends of epoxy tube sheets. In operation, the pressurized feed air flows through the core and into the fiber bundle. The air flows outside-in through the fiber wall, with the gas product (inertant) becoming depleted of oxygen during its passage through the fiber bundle. Depending upon the flow, pressure, temperature, and membrane surface area, this inert gas product will typically contain a low oxygen content, usually less than 9 percent. The inertant flow rate as a function of oxygen content is presented in Figure 7-5 for feed air pressures of 90, 75, and 60 psig.

2. Fiber Life

Extensive testing of polymeric fibers to obtain fiber life data has demonstrated that the principal failure mode for internally pressurized membrane design is leakage resulting from axial creep and hoop stress. This creep behavior, which is a function of the combination of differential pressure across the fiber and the temperature of the fiber, determines the fiber life. The failure modes for the externally pressurized membrane design are collapsed fibers and compression creep. The fiber life is approximately five times as long as that of the internally pressurized design. Figure 7-6 shows the relationship between fiber life, differential pressure, and fiber temperature for the externally pressurized membrane design. It should be noted that the fiber life shown by the curves in Figure 7-6 is the accumulated time for continuous operation at specific conditions.

Since the IGG is designed for operation at a constant temperature (75°F), the selection of the design pressure is a tradeoff between weight and life. The original internally pressurized ASM operated with a dual pressure regulator for optimum performance at minimum weight. Using this regulator with low and high pressure settings of 70 and 85 psig, respectively, establishes the fiber life. Continuous operation at 75°F and 70 psig will yield a fiber life of 42,704 hours for the externally pressurized design and only 8,540 hours for the internally pressurized design.

In contrast, continuous operation at 75°F and 85 psig will yield a fiber life of 12,400 hours and 2,480 hours for the external and internal ASM designs, respectively. Since operation at 85 psig will only occur during aircraft descents, it is only applicable part of the operating life.

Utilizing a "damage fraction" concept, the reduced useful life (L_U) due to part-time operation at the high pressure condition would be:

$$L_U = L_{LP}\left[1 - \frac{L_{HP} \times \%HP}{L_{HP}}\right]$$

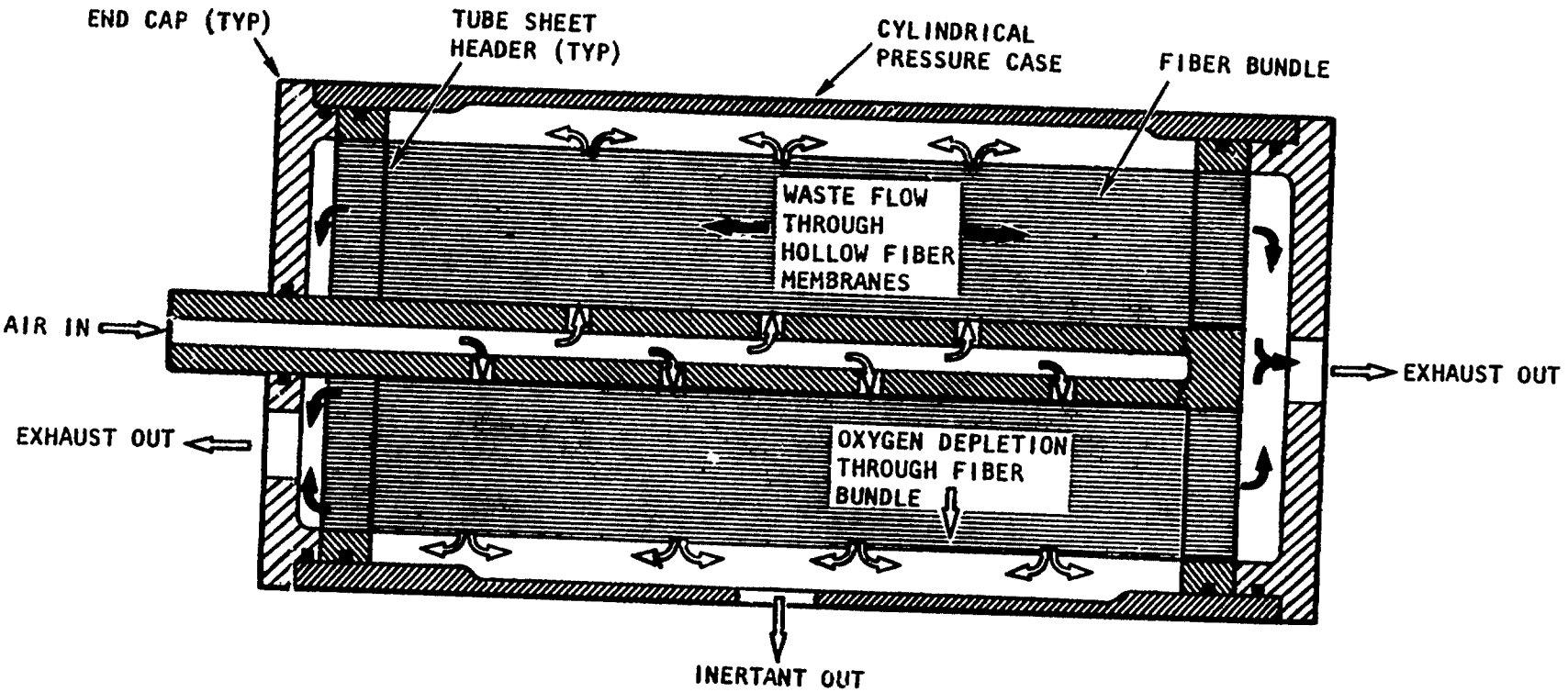

Figure 7-3. Cross-Sectional View of ASM With Externally Pressurized Membranes

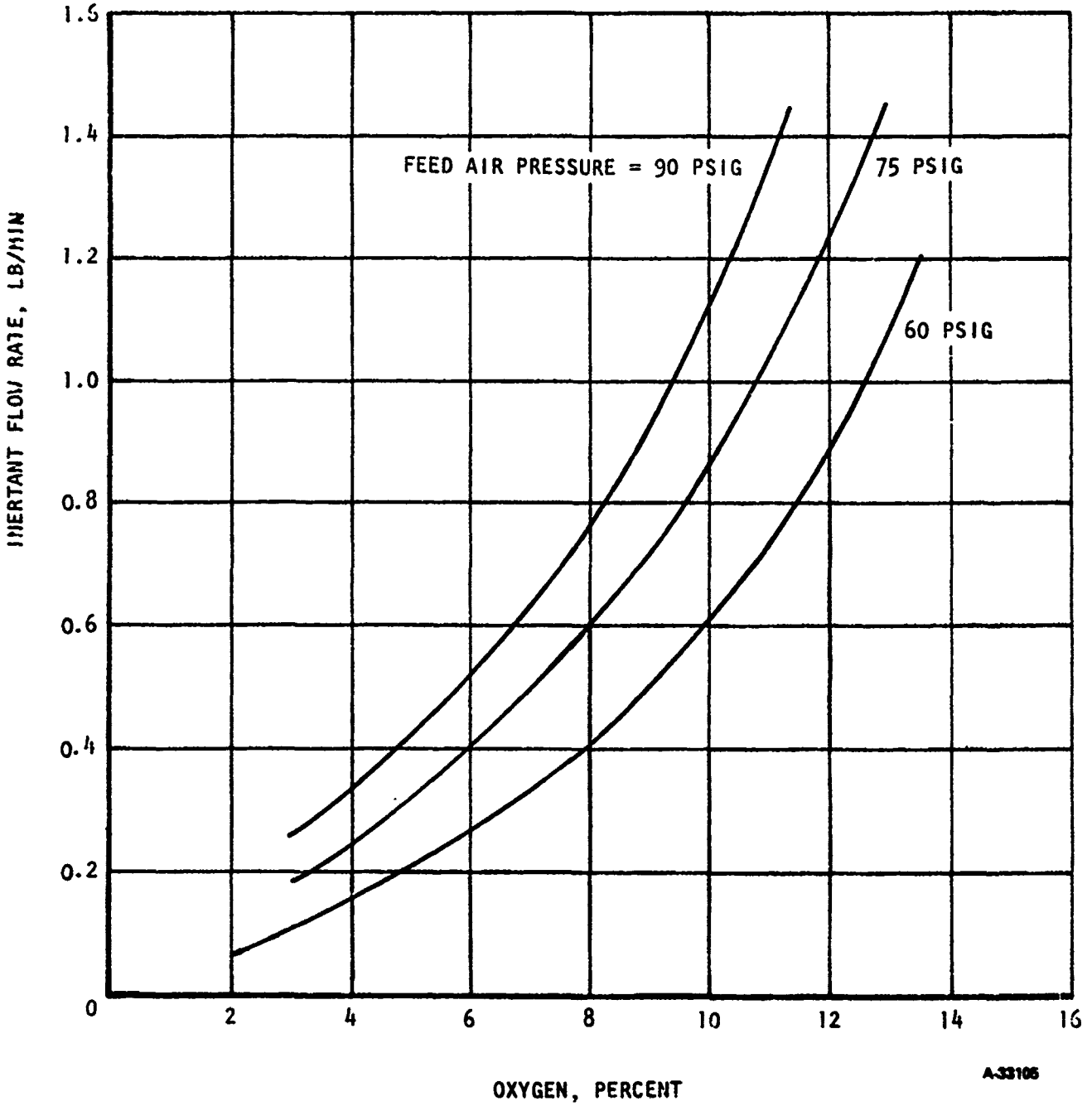

Figure 7-4. Inertant Flow as a Function of Oxygen Content and Feed Air Pressure

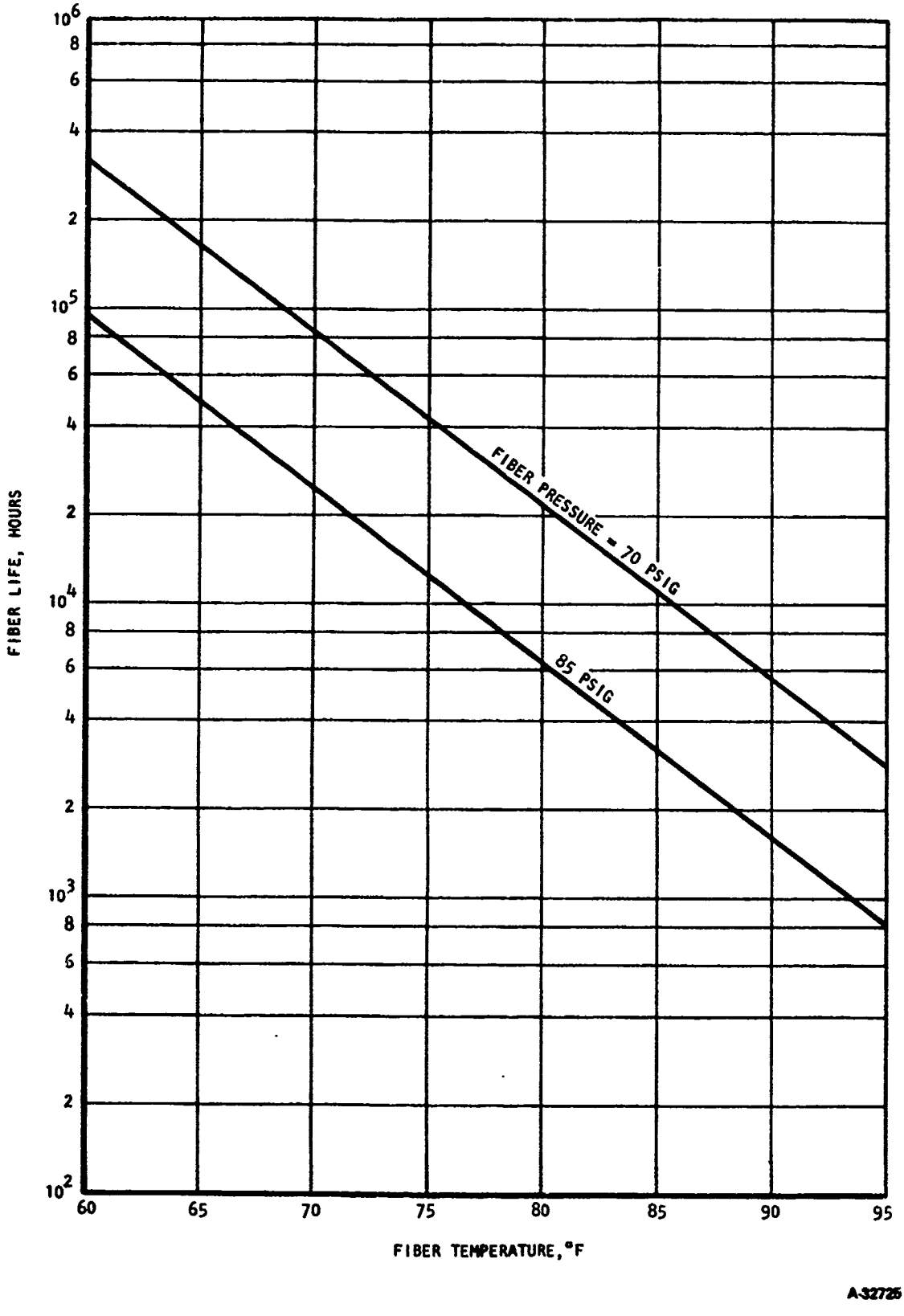

Figure 7-5. Fiber Life of Externally Pressurized Membrane ASM as a Function of Fiber Pressure and Temperature

where:

L_{LP} = Life at low pressure

L_{HP} = Life at high pressure

%OS = Percent of time at high pressure

Assuming that ten percent of the time will be at the high pressure condition for worldwide operations during aircraft descents, the predicted useful life would be as follows:

Externally Pressurized Design

$$L_U = 42{,}704 \left[1 - \frac{42{,}704 \times 0.10}{12{,}400}\right]$$

$$= 28{,}000 \text{ hours}$$

Internally Pressurized Design

$$L_U = 8540 \left[1 - \frac{8540 \times 0.1}{2480}\right]$$

$$= 5600 \text{ hours}$$

With a 28,000-hr predicted useful life (five times that of the internally pressurized ASM design), the externally pressurized design will have a useful life greater than that of the aircraft.

3. Fabrication Characteristics and Test Results

Detail evaluation of the five externally pressurized modules indicated excellent correlation with the design targets. Table 7-5 presents the detailed fabrication characteristics for each module. In all cases, fiber efficiency exceeded the target value, while module weight was below the target value.

Each module was performance tested at Dow prior to shipment to AiResearch. The inert flow and percent recovery exceeded the design targets in all cases. Table 7-9 presents the test results.

IGG Assembly and Test

The original IGG frame design was modified to incorporate adapters for the smaller 9.1-in. dia modules. These adapters were located at both ends of each ASM in the IGG as shown in Figure 7-6. In addition to this mounting modification, the feed, exhaust, and inert gas manifolds were completely redesigned to accommodate the externally pressurized modules shown in Figures 7-6, 7-7, and 7-8. Instrumentation ports were incorporated in the feed air and exhaust manifolds, as shown in Figure 7-6. Prior to final assembly and test of the IGG, the

TABLE 7-8

LMF-1 THROUGH LMF-5 MODULE FABRICATION CHARACTERISTICS

Module No.	LMF-1	LMF-2	LMF-3	LMF-4	LMF-5	Design Target
Fiber Size (μ)	30.5 x 4.13	30.4 x 40.5	30.3 x 40.7	30.3 x 40.9	29.3 x 40.4	30 x 41
Number of Fibers ($\bar{M}$)	13.73	13.79	13.61	13.65	13.77	13.50 min.
Packing Factor (%)	54.5	55.5	52.6	52.0	54.4	55.0
Fiber Eff. (%)	96.2	96.7	95.5	95.7	96.5	95.0
Active Length (in.)	37.0	37.5	37.0	37.5	38.0	37.0
Avg. Bundle Dia (in.)	8.29	8.14	8.34	8.40	8.25	8.50 max.
Module Wt. (lb)	27.70	27.74	27.50	26.86	27.16	28 max.

TABLE 7-9

AIR SEPARATION PERFORMANCE OF MODULES LMF-1 THROUGH LMF-5

Module No.	LMF-1	LMF-2	LMF-3	LMF-4	LMF-5	Design Target
Feed Pressure (psig)	85.8	85.8	85.8	85.8	85.8	85.8 set
Shell ΔP (psi)	3.82	6.40	4.96	5.66	7.48	--
Feed Flow (lb/min)	1.997	1.992	2.024	2.034	2.060	2.100 max.
Inert Flow (lb/min)	0.928	0.901	0.947	0.936	0.969	0.885 min.
Inert O_2 Content (%)	9.00	9.02	9.03	9.00	9.01	9.0 max.
Permeate Flow (lb/min)	1.069	1.071	1.077	1.098	1.091	--
Permeate O_2 Content (%)	31.67	31.44	32.00	31.33	32.02	--
Temperature (°F)	75.0	75.0	75.0	75.0	75.0	75.0 set
Inert Recovery (%)	46.5	45.7	46.8	46.0	47.0	41.2 min.

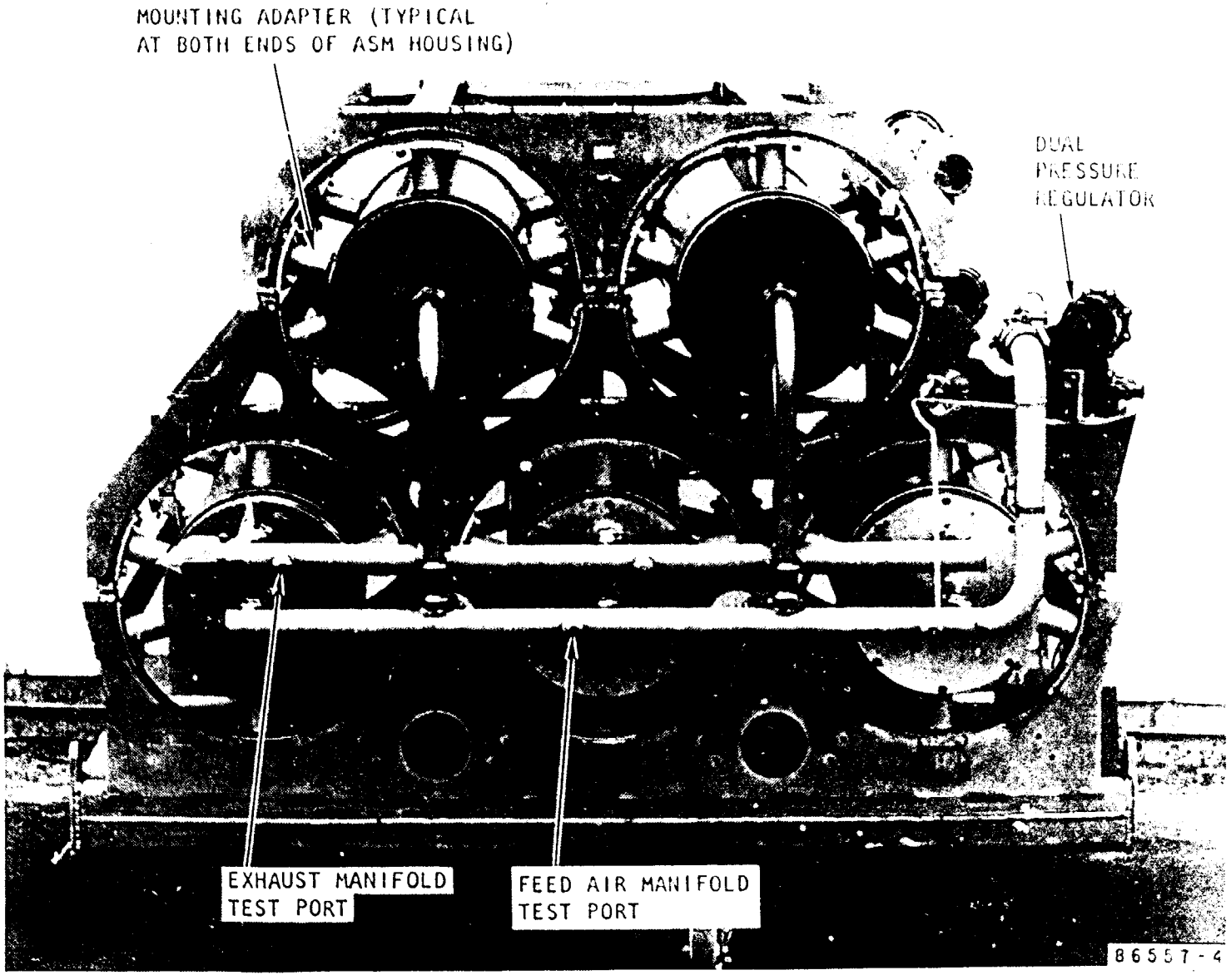

Figure 7-6. Side View of IGG Showing Instrumentation Test Ports

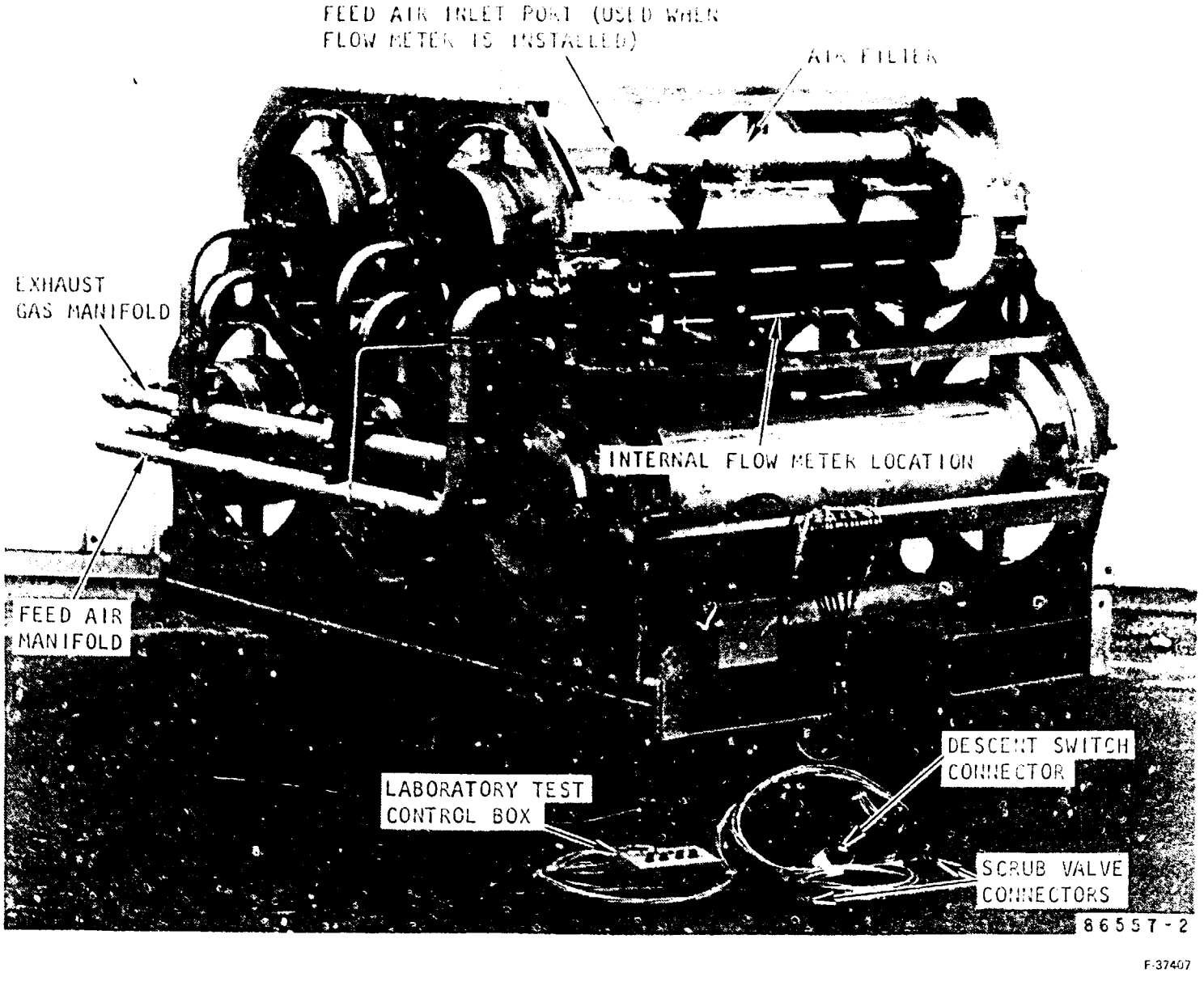

Figure 7-7. View of IGG Showing Control Box and Auxiliary Hardware Connector

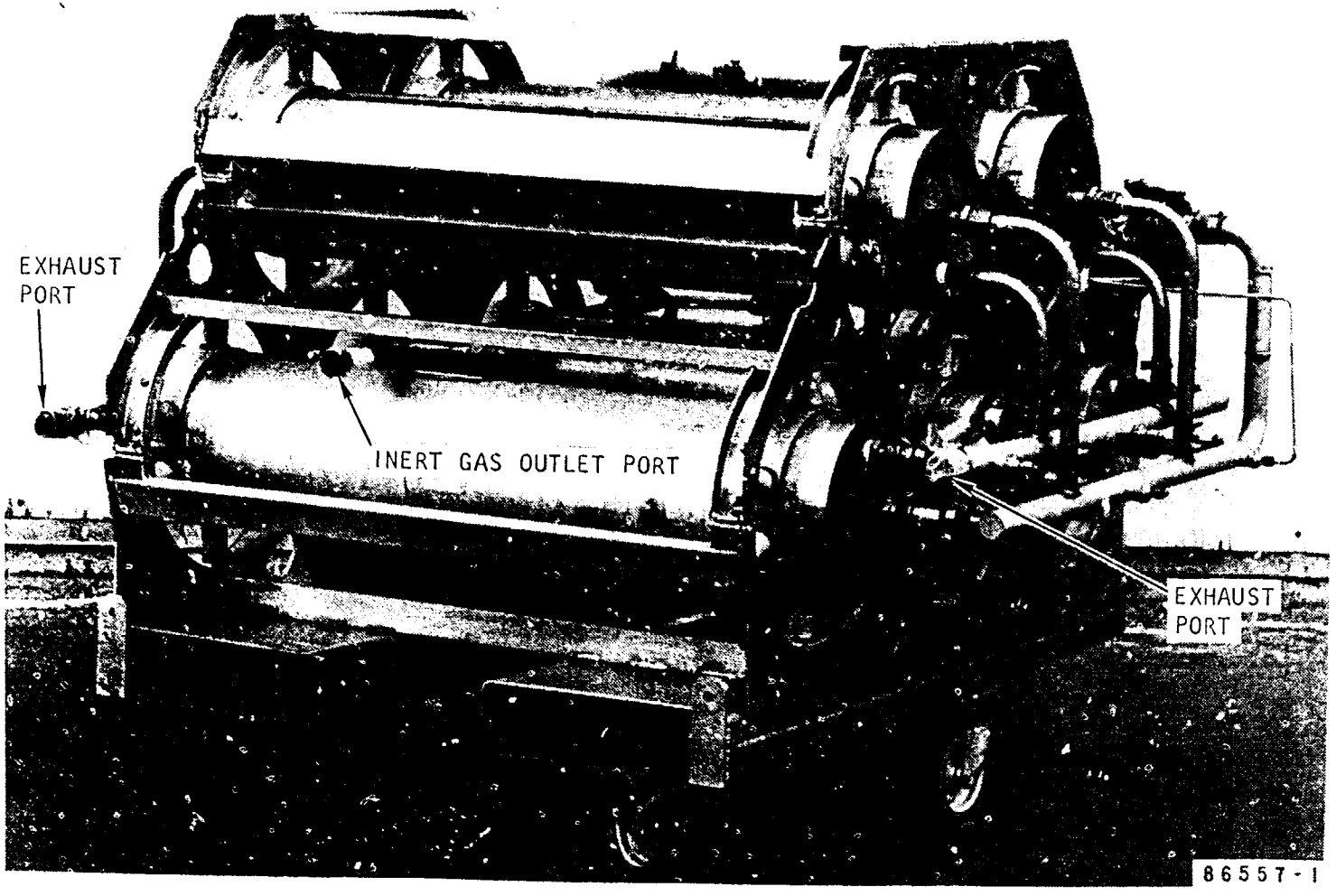

F-37406

Figure 7-8. View of IGG Showing Exhaust Ports and Inert Gas Outlet Port

internal flow meter was shipped to the Air Force. Figure 7-7 shows the intended location for the flow meter. Since this flow meter was not available, a laboratory flow meter was used to measure feed flow as shown in Figure 7-9. Note: The feed air filter was not utilized during the IGG system test.

Prior to IGG system testing, each ASM was flow tested to improve the combined performance. A 0.312-in. dia orifice was placed in the inert gas outlet of LMF-1, LMF-3, and LMF-4. This fine tuning was accomplished to offset the shell side ΔP differences (see Table 7-9). With these orifices, the shell side ΔP of all modules was within +0.54 psid. Photos of the IGG system test setup are shown in Figures 7-9 and 7-10. The pneumatic test setup schematic is presented in Figure 7-11, and the electrical interconnections are shown in schematic drawing 51682. Testing was accomplished to verify the IGG system performance. The dual regulator was calibrated to establish 85.0 $\pm$0.5 psig in the high mode and 70.0 $\pm$0.5 psig in the low mode. Testing was accomplished by adjusting the inert gas flow control valve in each of these modes. Test results, listed in Table 7-10, showed that the design target of 4 lb/min of inert gas in the high mode with a maximum oxygen concentration of 9.0 percent was met.

Other Hardware

In addition to the Item 4 IGG (Part No. 2202752-1), the following hardware was shipped to the Air Force for laboratory testing at WPAFB. A photograph showing Items 5, 6, and 8 is presented in Figure 7-12. The pneumatic interconnection of the scrub valves and demand regulators to other components of the IGG laboratory test system is shown schematically in Figure 7-13.

Item No.	Name	Part No.	No. Req.
5	Scrub Valve	2202573-1	2
6	Demand Regulator	3214352-1	2
8	Descent Switch	2202564-1	1
3-22	Water Extractor	194476-1	1

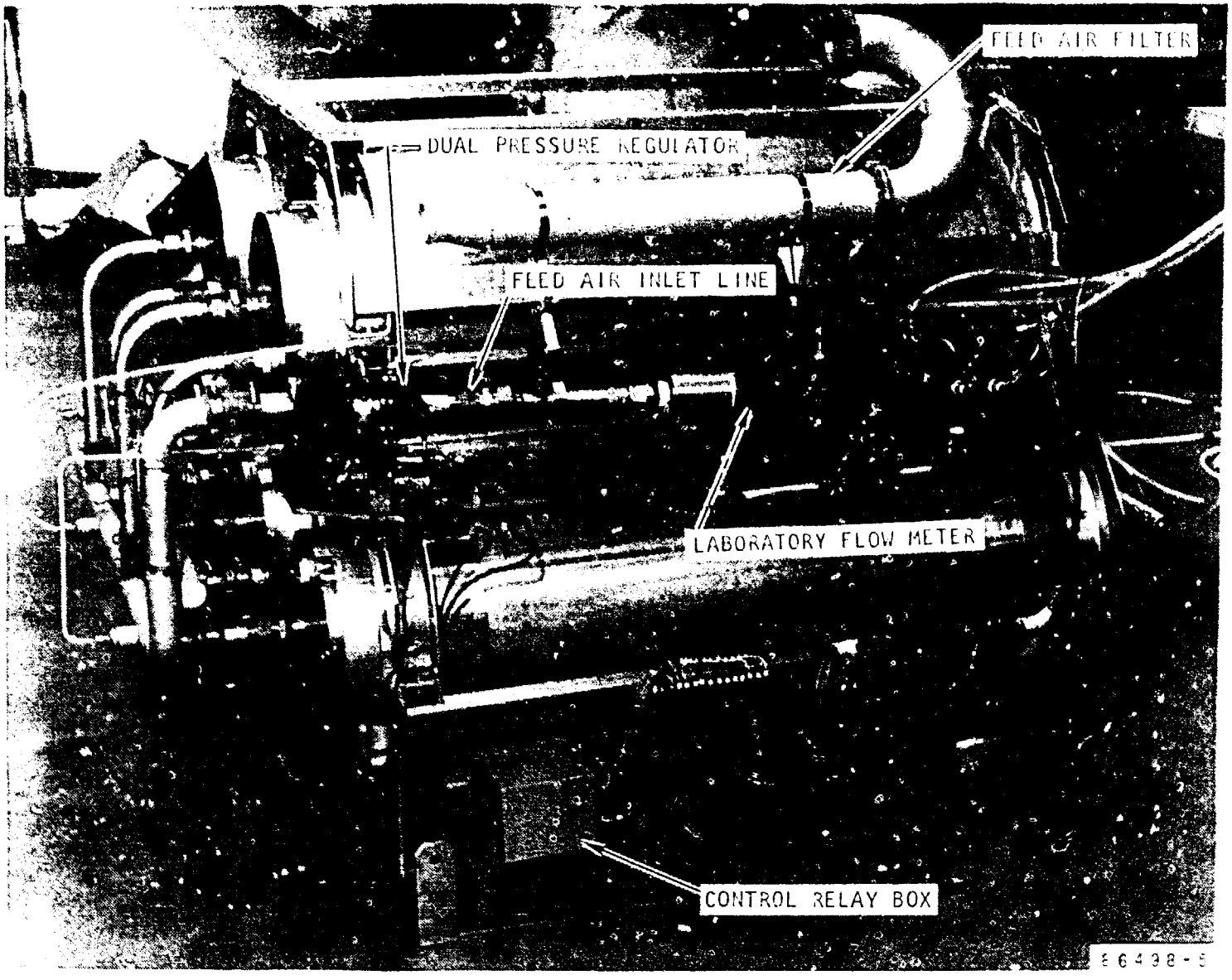

F-37411

Figure 7-9. View of IGG System Test Setup

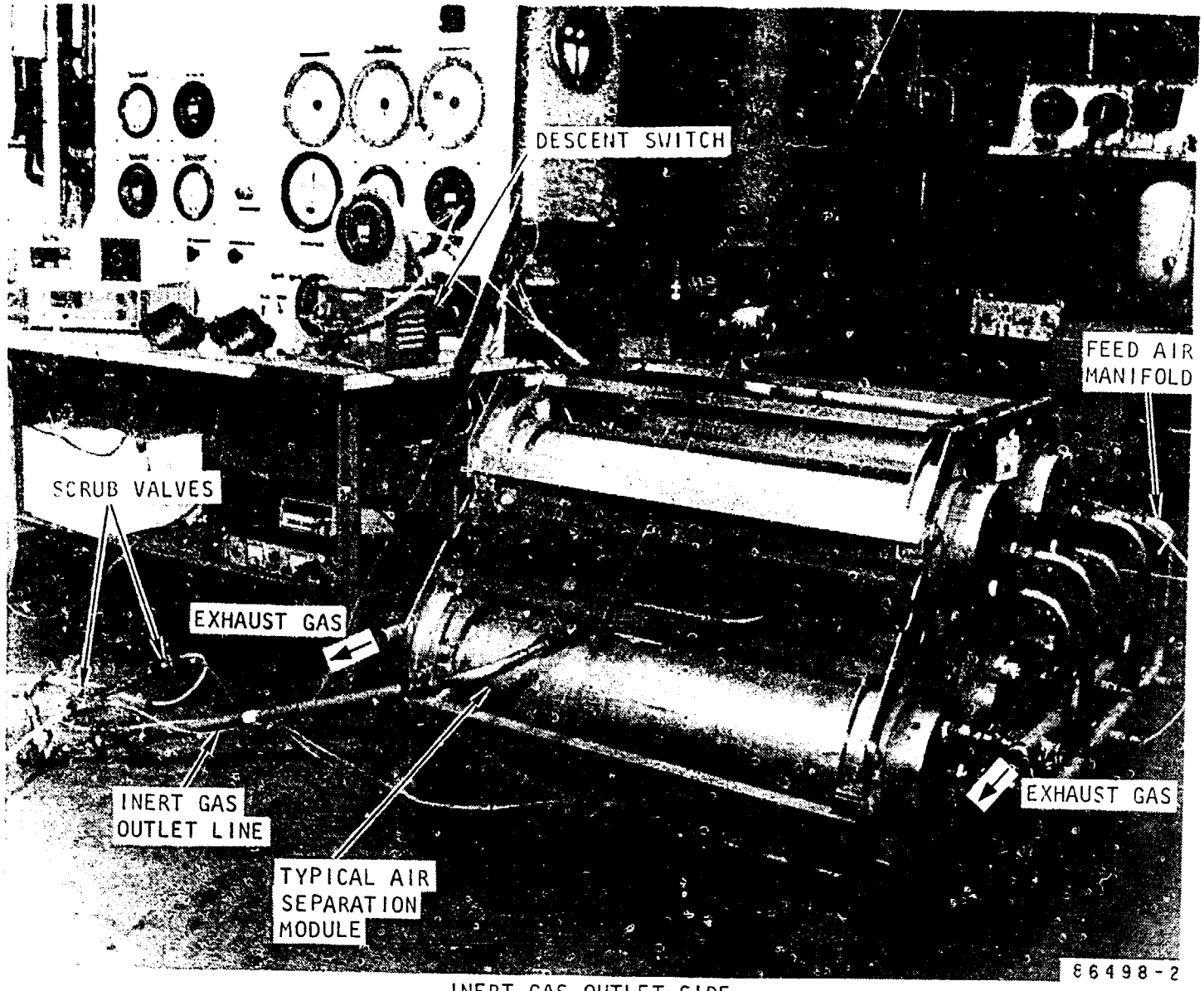

Figure 7-10. View of IGG Test Setup and Control Panel

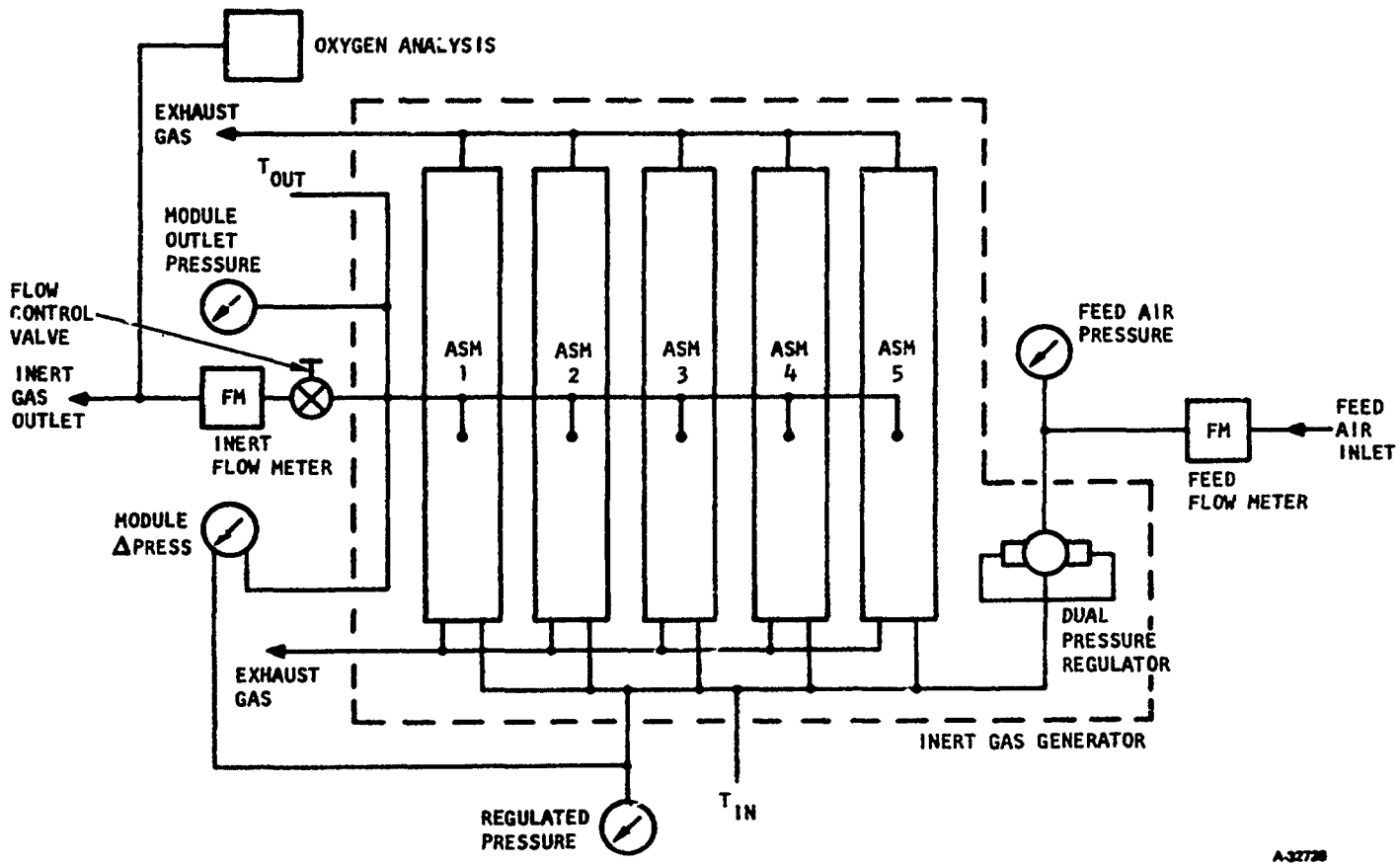

Figure 7-11. IGG System Test Setup Schematic

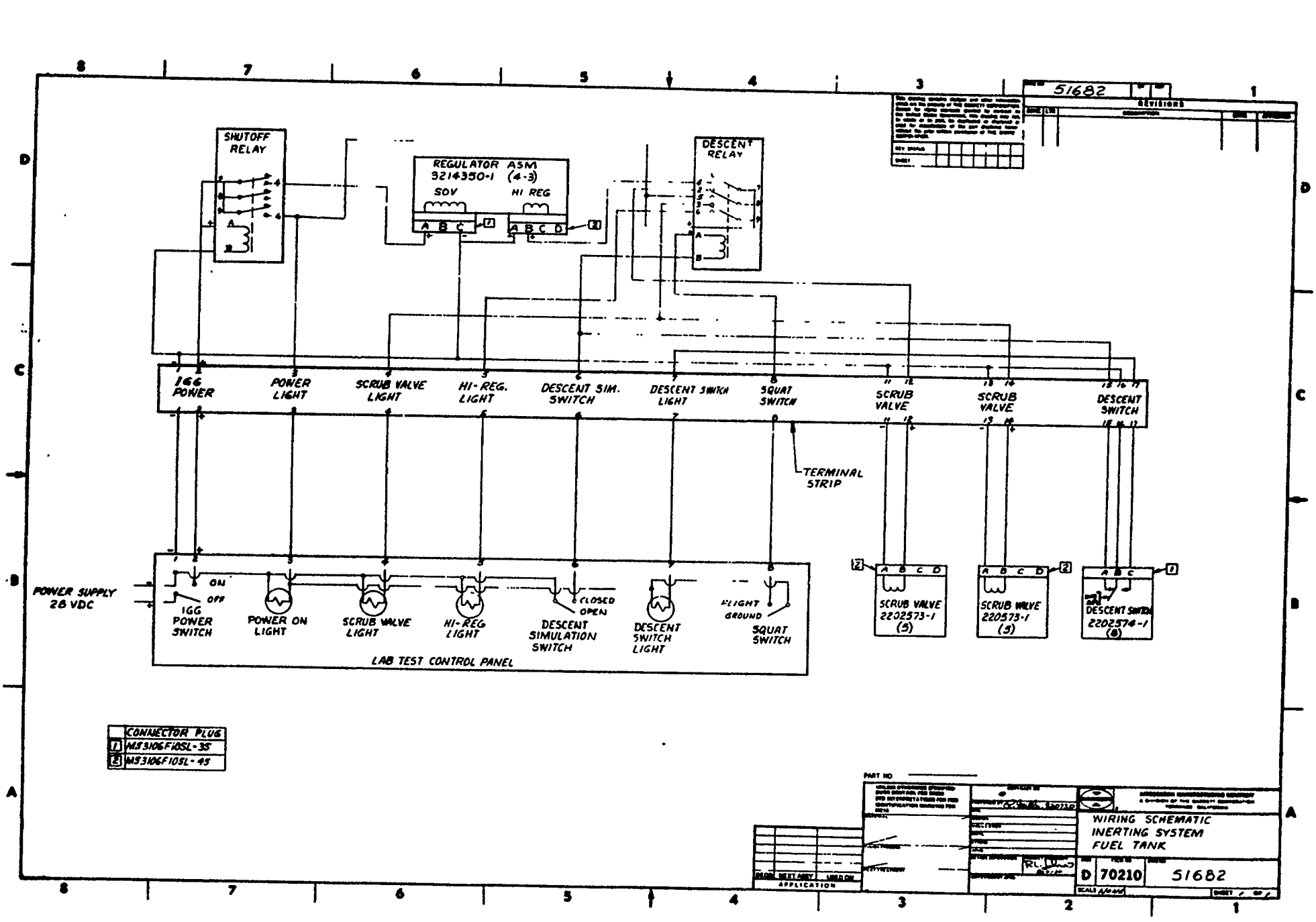
SHUTOFF RELAY
REGULATOR ASM 3214350-1 (4-3)
SOV
HI REG
DESCENT RELAY
IGG POWER
POWER LIGHT
SCRUB VALVE LIGHT
HI-REG. LIGHT
DESCENT SIM. SWITCH
DESCENT SWITCH LIGHT
SQUAT SWITCH
SCRUB VALVE
SCRUB VALVE
DESCENT SWITCH
TERMINAL STRIP
POWER SUPPLY 28 VDC
ON
OFF
IGG POWER SWITCH
POWER ON LIGHT
SCRUB VALVE LIGHT
HI-REG LIGHT
CLOSED
OPEN
DESCENT SIMULATION SWITCH
DESCENT SWITCH LIGHT
FLIGHT
GROUND
SQUAT SWITCH
LAB TEST CONTROL PANEL
SCRUB VALVE 2202573-1 (5)
SCRUB VALVE 220573-1 (5)
DESCENT SWITCH 2202574-1 (6)
CONNECTOR PLUG
1 MS3106F10SL-3S
2 MS3106F10SL-4S
51682
REVISIONS
PART NO
WIRING SCHEMATIC
INERTING SYSTEM
FUEL TANK
D 70210 51682

TABLE 7-10

IGG PERFORMANCE

System Test Results*

Inlet Pressure, psig	Inlet Flow, lb/min	Dual Regulator Reg. Press, psig	Reg. Mode	Inert Flow, lb/min	Inert O_2 Content, percent	Recovery, percent
100.0	9.91	85.5	High	4.38	9.0	4
99.5	9.68	85.0	High	4.50	9.0	46.5
100.4	8.05	71.25	Low	3.53	9.0	43.9
100	7.85	71.25	Low	3.40	9.0	43.3

Component Test Results

S/N	Inlet Pressure, psig	Inlet Flow, lb/min	Inert Temperature, °F	Inert Flow, lb/min	Inert O_2 Content, percent	Recovery, percent
LMF1	85.75	1.786	68.4	0.846	9.0	47.53
LMF2	86.25	1.788	68.5	0.820	9.0	45.55
LMF3	86.0	1.776	68.9	0.861	9.0	48.37
LMF4	86.0	1.815	68.0	0.832	9.0	46.22
LMF5	85.75	1.867	69.2	0.886	9.0	47.89

*NOTE: System data are corrected to 75°F.

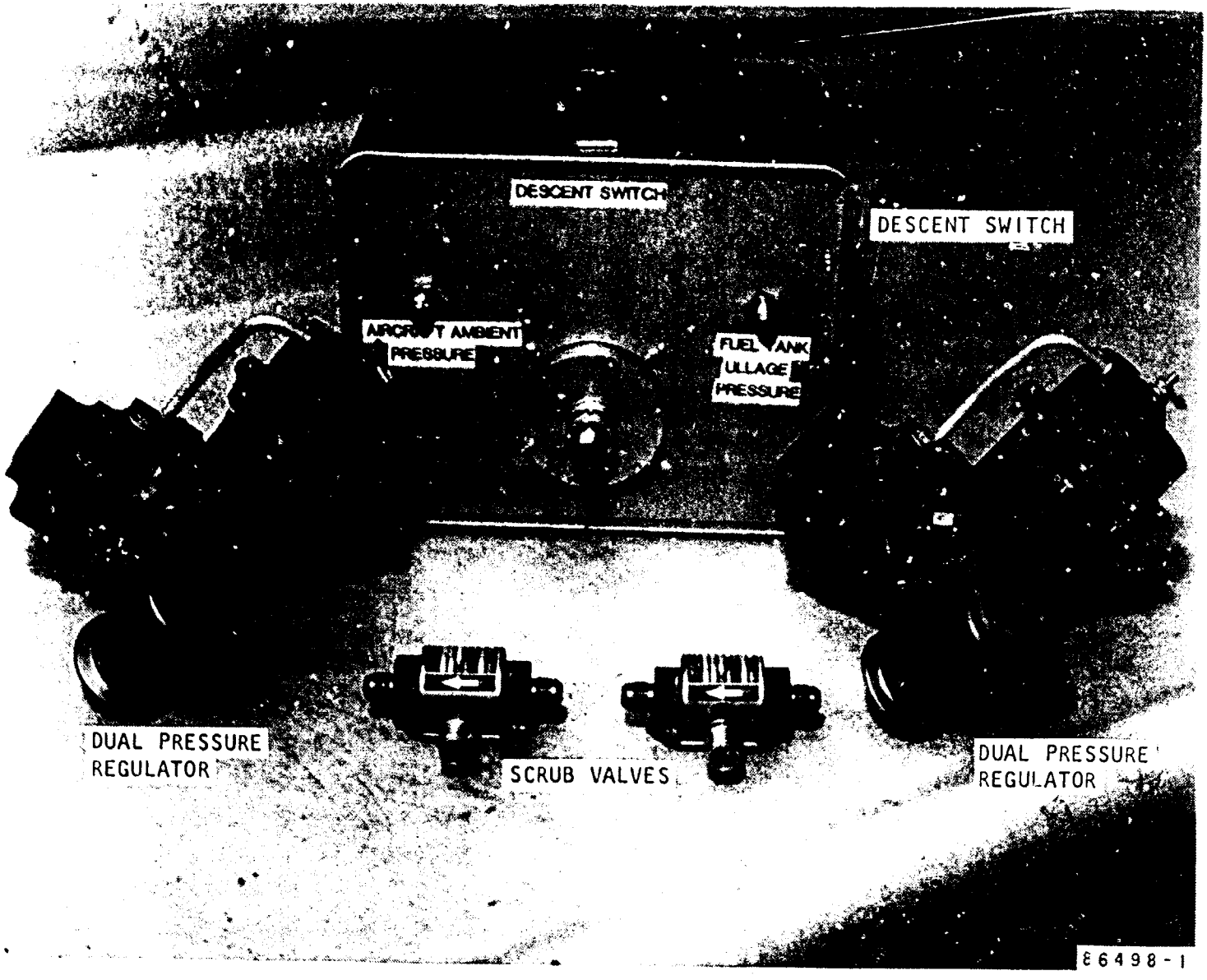

Figure 7-12. View of IGG Auxilary Hardware

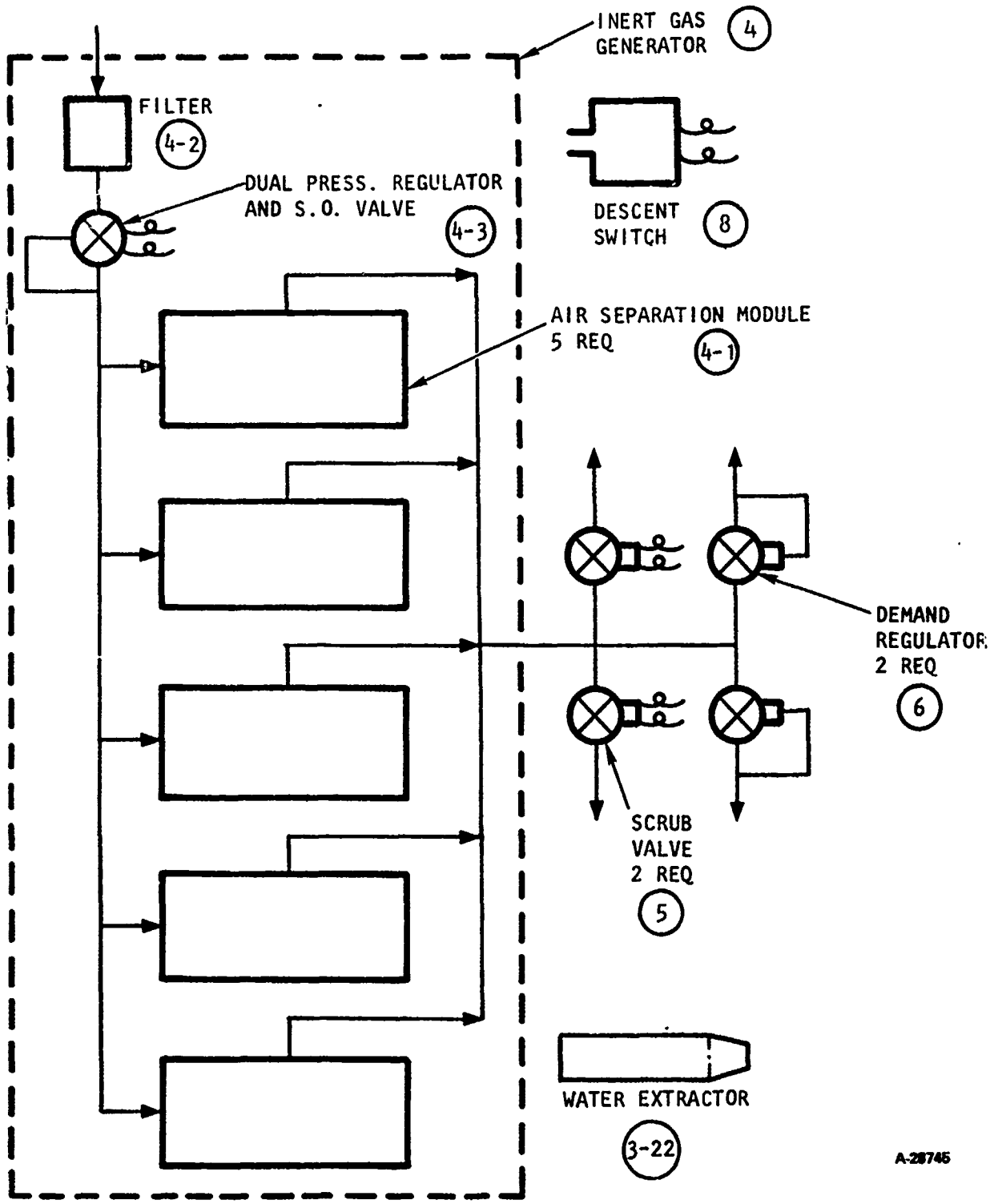

Figure 7-13. Schematic of Hardware Provided for IGG Laboratory Testing at WPAFB

SECTION 8

AIR SEPARATION MODULE SUPPLEMENTAL DEVELOPMENT

PHASE 1 EFFORTS

In Phase 1, Dow Chemical performed supplemental development work to acquire additional information necessary for the design of the hollow fiber membrane air separation modules to be used for inerting the KC-135A fuel tanks. During this program, a number of areas were explored and evaluated, among them being fiber size optimization, fiber crosslinking to increase mechanical strength, module performance simulation, and characterization of actual module operating performance. Module fabrication techniques were also explored in the fabrication of 6-inch diameter units. From data gathered on these units, design equations were obtained for use in predicting performance of the 14.5-inch diameter modules designed for use in the KC-135A inerting system.

Dow Phase 1 supplemental development report, entitled "Hollow Fiber Membrane Module Fuel Tank Inerting System for Aircraft", covers the Phase 1 efforts. A copy of the Dow report is presented in Appendix A of this report.

PHASE 2 EFFORTS

In Phase 2, Dow Chemical evaluated various methods of crosslinking the hollow fiber membranes for the purpose of upgrading its physical properties and increasing its service temperature. Dow then studied the effect of changes in orientation and crystallinity on the oxygen and nitrogen permeability of the fibers by annealing. Results of the Dow efforts are summarized in a Dow Report, entitled "Development of Improved Polymethylpentene Hollow Fibers and Air Separation Modules for Inerting the Fuel Tanks of Aircraft". A copy of the Dow report is presented in Appendix B of this report.

SECTION 9

CONCLUSIONS AND RECOMMENDATIONS

This program has provided valuable experience in assessing the military aircraft application of systems for inert gas generation by membrane permeation. The program also has provided an insight into the general requirements for an onboard inert gas generator system (OBIGGS) for fuel tank inerting. Based upon the results of the efforts summarized in this report, recommendations for future activity have been set forth for U.S. Air Force consideration. These recommendations are presented following a discussion of the conclusions.

CONCLUSIONS

The following conclusions are presented:

- Laboratory test data on inert gas generation by membrane permeation corroborate the performance prediction capability of the mathematical models developed for analysis of system performance, enabling their use for system design with a high degree of confidence.

- The use of a production aircraft membrane inerting system, which will of necessity be integrated with the aircraft environmental control system, will not impose additional demands upon the ECS to provide very dry air to the air separation module. Permeable membranes are unaffected by water vapor in providing the proper inertant concentrations.

- Except for the membrane modules, the system designed and fabricated for this program comprises state-of-the-art aircraft environmental control system hardware. No new controls and/or other hardware developments are required. The noncyclic, steady flow process of the membrane system will not require frequent replacement of high cycle life hardware, which normally is the main contributor to reduced system reliability. The membrane modules have been involved in a maturation process in parallel with this program. Dow Chemical has had a chemical process plant system in continual operation for over one year, supplying very low oxygen content inertant. Additional installations have been in operation for shorter periods, providing additional data demonstrating the efficacy of the membrane process.

RECOMMENDATIONS

As a result of the experience gained during this program, it is recommended that the U.S. Air Force consider a design, development and flight test program for a permeable membrane, nitrogen inert gas generation system. This program is necessary to evaluate system performance characteristics during aircraft operation. The system should be completely integrated with the other aircraft systems so that its interface with the total aircraft can be meaningfully demonstrated.

APPENDIX A

THE DOW CHEMICAL COMPANY

HOLLOW FIBER MEMBRANE MODULE FUEL TANK INERTING SYSTEM FOR AIRCRAFT

PHASE I - SUPPLEMENTAL DEVELOPMENT REPORT

Prepared for

AIRESEARCH MANUFACTURING COMPANY
OF CALIFORNIA, P. O. 424-85817-8

Author

T. T. Revak

March, 1979

SUMMARY

This report describes work performed by The Dow Chemical Company for the Phase I, Supplemental Development portion of a program to produce a membrane based aircraft fuel tank inerting system. The objective of Phase I was to acquire additional information necessary for the design of TPX hollow fiber membrane devices capable of inerting a KC 135 aircraft. During this program, a number of areas have been explored and evaluated, among them: fiber size optimization, fiber lifetimes variation with stress and temperature, fiber crosslinking to increase mechanical strength, module performance simulation, and characterization of actual module operating performance. Module fabrication techniques were also explored in the fabrication of fourteen 6" diameter units. From data gathered on these 6" diameter devices, design equations were obtained that can be used for prediction of performance in larger diameter devices. As a result of the Phase I program, a tentative module design for the KC 135 system was obtained. This module, composed of 30 x 42μ TPX fibers, is to be about 14.5" in diameter and 42" long and is to operate at a maximum feed pressure of 100.5 psia at 75°F. The expected in-flight lifetime of such a device is in excess of 1000 hours at the design point of peak inert demand. Successful completion of the Phase I development has enabled Dow to enter into the Design and Testing Phase, Phase II, of the Subcontract with confidence in the design and performance data.

TABLE OF CONTENTS

	Page
INTRODUCTION	136
HOLLOW FIBER OPTIMIZATION	136
Background	136
Computer Simulation	137
Fiber Spinning Research	137
Permeability Variation with Temperature and Pressure	138
Fiber Lifetime Testing	138
Thirty Hole Spinnerette	139
Fiber Optimization Summary	139
CROSSLINKING INVESTIGATION	140
Background	140
Crosslinking Summary	141
MODULE DEVELOPMENT	142
Background	142
Computer Simulation Modifications	142
Vacuum Operation	143
Flow Pressure Relationships	143
Module Washing	143
External Pressurization	144
Module Development Summary	144
FUTURE WORK	145
ACKNOWLEDGEMENTS	146

INTRODUCTION

Garrett AiResearch has been involved in the development of systems for the inerting of fuel tanks for several years. Presently the accepted techniques for aircraft fuel tank combustion control include reticulated foam and on-board liquid nitrogen storage for the supply of inert gas. Recently, the possibility of inert gas from membrane sources has been investigated. Early in 1973, AiResearch and Dow conducted preliminary studies demonstrating the plausibility of the membrane concept. This preliminary effort resulted in AiResearch receiving a contract from the FAA (DOT-FAWA-3658) to provide ground test inert gas generators compatible with the inerting requirememts for a DC-9 aircraft. AiResearch, in turn, subcontracted to Dow a development program that focused upon utilizing TPX (poly-4-methylpentene) as a membrane material. Efforts were conducted to spin hollow fibers, to determine time-temperature-pressure failure envelopes for the fibers, to develop module device manufacturing techniques, and to determine module performances. These efforts culminated in three devices approximately 11" in diameter and 42" long that were successfully used in ground test simulation. From that contract a great deal of developmental work was accomplished (Figure 1), but some unforeseen results also occurred (Figure 2).

As a result of the accomplishments achieved under previous contracts, sufficient confidence existed for Garrett and Dow to enter into the present contract to design, develop, and flight test a fuel tank inerting system for a KC-135 aircraft. The inert gas is to be provided by an inert gas generator using hollow fiber membranes. As the contract is structured, the program is divided into two phases: a supplemental development program (Phase I) and a test hardware program (Phase II). The supplemental development phase has been ordered to supplement and clarify design data to improve performance and reduce hardware risk in Phase II. The development work in Phase I has focused upon three areas: optimization of TPX hollow fiber performance by fiber size variation; crosslinking of TPX to improve its mechanical properties; and fabrication of modules for manufacturing and performance improvements. Phase II will concern itself with the manufacture and testing of in-flight devices. It is the purpose of this report to summarize the activities performed during the Phase I supplemental development program at Dow.

HOLLOW FIBER OPTIMIZATION

Background

During the previous contract, attention was focused upon the manufacturing and testing of two hollow fiber sizes: 50 x 64μ and 50 x 70μ. These

fiber sizes were chosen as the smallest attainable with the spinning technology existing at the beginning of the previous contract. From that choice of fiber sizes, permeability and fiber lifetime information indicated an acceptable and predictable performance for the system. However, the long term potential of these fibers seemed in question. Since test data showed the permeabilities of hollow fibers to be lower than anticipated from available literature data, the need existed to optimize the fiber size for maximum volumetric output.

Computer Simulation

To do this optimization, Dow wrote a computer simulation of module performance based upon a cross-flow model initiated by AiResearch. With this model, two families of curves were generated based upon the previous fiber sizes. Utilizing OD-ID ratios of 1.40 and 1.28, stresses were kept at approximately the same level as the 50μ I.D. fibers. At the same operating pressures, performance of various fiber sizes are tabulated in Table I. Table I shows a dramatic increase in performance with decreasing fiber size until a plateau is reached at about 30μ inside diameter. In both OD/ID ratios a virtual two-fold improvement was predicted in a device made with 30 micron fibers over a similar sized device made with the 50μ fibers. This modeling was successful in outlining the fiber research program that enabled realization of this predicted performance increase.

Fiber Spinning Research

Based upon the computer studies, it appeared that an optimum fiber size could be reached in the 20-30 micron range. Considering factors such as fabrication ease and economics, 30 microns I.D. was chosen as an ideal diameter for the air separation modules. As a result, a research effort was conducted to determine whether fibers of sizes smaller than 50μ I.D. could be spun and whether permeabilities and lifetime failure envelopes were comparable to the 50μ fibers. A series of spin runs were made at both the 3X and 2X spin rates investigated during the previous AiResearch subcontract. Fibers were spun in the nominal 30, 40 and 50μ inside diameters in both the 1.40 and 1.28 diameter ratios at the 2X and 3X spin rates. The size distribution information is shown in Table II. Size analysis of the spin runs indicate the following:

1. Faster spin rates seem to give less size variation in both inside and outside diameters.

2. Diameter size variations seem to increase with decreasing fiber size.

3. Variations in the wall thickness (diameter ratio) appear to increase with decreasing fiber size.

4. Beaker units made from all of the fibers have shown oxygen permeability coefficients greater than 20×10^{-10} s.u.* Oxygen-nitrogen separation factors were found to be $4.26 \pm .15$ at 25°C, and they do not seem to significantly vary with fiber size.

From this study, smaller fibers (i.e. 30μ vs. 50μ I.D.) seem to have slightly poorer size stability characteristics than larger fibers. However, these smaller fibers have the permeation and separation characteristics similar to the 50 micron fibers. Combination of these permeability properties with reduced wall thickness and increased surface area per unit volume will favor a smaller 30μ fiber size.

Permeability Variation with Temperature and Pressure

In the fiber size investigations, permeabilities of beaker units were found to be about 20×10^{-10} s.u. for oxygen. During previous work, the design permeabilities were established as 18.62×10^{-10} s.u. for oxygen and 4.34×10^{-10} s.u. for nitrogen at 25°C. Extensive permeability studies were conducted on 30μ beaker units to determine the effect of temperature upon permeation. Experimentation was done to obtain a multitude of permeation data points between 12°C and 40°C. These permeability rates were successfully fit to an Arrhenius plot. Regression correlation coefficients were in excess of 98% and equations were fit (Table III) to match the previous design oxygen permeability at 25°C. Permeability coefficients of both gases were found to be virtually independent of pressure from 0 to 100 psid.

Fiber Lifetime Testing

After determining that the 30μ fibers had permeation and separation characteristics similar to 50μ fibers, additional test data was required to define the fiber lifetime. Since data previously generated by AiResearch indicated 1000-3000 hour in-flight life at the proposed 75 psid design pressure for the 50μ fibers, it was deemed necessary to define the pressure-temperature-lifetime envelope for the fibers. During previous work, polymer creep was found to limit operating parameters since elevated pressures and temperatures caused the fibers to creep, yield, and eventually rupture. From the earlier data gathered on 50 x 64μ and 50 x 70μ fibers, it appeared that the thicker-walled fibers would be more compatible with system operation specified by Garrett. Assuming the OD/ID ratio to be constant, the stress at a given pressure should be similar for both the 30 x 42μ fibers and the 50 x 70μ fibers. Therefore, the stress lifetime curve of the 30 x 42μ fibers were expected to match the 50 x 70μ fiber lifetimes which are presented in a generalized plot from earlier data as shown in Figure 3.

$$*\text{s.u.} = \frac{(\text{cm}^3/\text{sec @ std})(\text{cm})}{(\text{cm}^2)(\text{cm Hg})}$$

Because an extensive lifetime testing program would take a long period of time and a very large testing system, some preliminary testing at elevated pressures was done to determine whether 30 x 42μ fiber beaker units would last an acceptable amount of time at 75-100 psid. This testing was conducted at 150, 175, 200 psid on both 30 x 42μ and 50 x 70μ fibers at both the 3X and 2X spin rates. Extrapolation of the data to 75-100 psid suggested that the 30 x 42μ fibers would be compatible with the Garrett lifetime expectations. Therefore, 30 x 42μ fibers at the 3X spin rate were chosen to be the fibers utilized in longer-term lifetime testing.

To do this long-term testing, four beaker units each having 800 fibers, 30 centimeters long were put into appropriate baths and run at desired temperatures and pressures. Separation factors were taken at least twice a week and single gas flows were monitored by both digital printer and multi-point recorder. A summary of the data current to February 9 is presented in Table IV. It should be noted that no fiber failures have occurred in units pressurized as high as 85 psid at times below 1000 hours. Units that have failed are summarized in Table V. Obviously the data is punctuated by statistics, but it appears that 85 psid is a conservative design point to achieve 1000 hour lifetime at 25°C. Since there are sizeable statistical considerations in this type of testing, a larger fiber sample (i.e. a module) would provide better data relative to the actual lifetimes. Dow plans to do additional tests prior to the start of the Phase II program to further increase confidence in the Phase I test data. However, based upon the Phase I data, 85 psid is recommended as the design pressure for the KC-135 system.

Thirty-Hole Spinnerette

Throughout the development work conducted during previous subcontracts and the first part of the present contract, spinning was done with a sixteen-hole spinnerette. Recently a thirty-hole spinnerette has been utilized in some preliminary runs. The advantage of the 30-hole spinnerette, is a potential increase in production rate and an improvement in fiber handling during fabrications. A summary of these two spin runs are shown in Table VI. The fiber size distribution of these runs is comparable with data obtained from 16-hole spinnerettes. Before this large spinnerette is adapted for use during the Phase II program, additional development work will be required to perfect the fiber fabrication technique. Fiber lifetime test data will also be required. The value of this information is critical because the 30-hole spinnerette is envisioned as the tool for production of the KC-135 modules.

Fiber Optimization Summary

Based upon the development of TPX fibers during Phase I, the following conclusions can be drawn:

1. Computer simulations predict that smaller fibers are volumetrically more effective than the previous 50μ fibers. When incorporating all considerations, 30 x 42μ fibers are the optimum dimension for utilization in the KC-135 system.

2. Fibers down to 30μ I.D. can be readily spun at the 3X spin rate. Permeability coefficients for these fibers are comparable to the 50μ fibers.

3. Lifetime testing of 30 x 42μ fibers has shown that 85 psid at 25°C should be sufficient for the 1000 hour lifetime compatible with Garret 's objectives.

4. Fiber permeabilities vary with temperature in a manner correlating extremely well with an Arrhenius-type plot. Roughly, nitrogen permeation increases about 3.4% per degree C while oxygen permeation increases at 2.4% per degree C. The oxygen-nitrogen separation factor at 25°C (77°F) is 4.26.

5. A 30-hole spinnerette has been implemented and fiber size distributions appear to be comparable with those obtained with the 16-hole spinnerette. The advantage of the anticipated increased fiber tow strength in manufacturing has been realized.

CROSSLINKING INVESTIGATION

Background

Because of the limitations in operating parameters caused by polymer creep, an obvious solution was to improve the mechanical strength of the TPX material. Typically, polymer mechanical strength can be upgraded by crosslinking (Figure 4).

TPX belongs to a family of polymers known as poly-α-olefins. By the very nature of their α-substitution these polymers are generally more difficult to crosslink than the unsubstituted polyolefin, polyethylene. Polyethylene has been successfully crosslinked by radiation and peroxide techniques to improve creep resistance. Crosslinking techniques found satisfactory for polyethylene do not seem compatible with TPX since TPX would probably degrade under the rigors of these treatments. This degradation would more than likely cause a loss in the separation and permeation characteristics of the TPX. Recently, the Dow-Corning Corporation has developed a novel means of crosslinking polyethylene. This technique utilizes an alkoxy-silane which grafts onto the polyolefin chain (Figure 5) after which the grafted material is crosslinked by moisture to give

siloxane (Si-O-Si) linkages between polymer backbones. This crosslinking is in contrast with the carbon-carbon crosslinking seen by radiation and peroxide techniques. It appeared that this technology had some potential to be transferred from polyethylene to TPX. As a result, a research effort was subcontracted with Dow-Corning to explore this possibility.

In their efforts, Dow-Corning investigated a variety of silanes and reaction conditions that resulted in some grafted TPX along with a recipe to graft the TPX. Initial mechanical testing showed that the grafted material when exposed to water gave some change in mechanical properties (Table VII). At this juncture two possible approaches for utilizing this crosslinking scheme could be used: (1) the grafted material could be extruded and the resulting fibers treated with moisture; (2) the fibers could be spun and after which the grafting agent and water could be added to the formed fibers. The first technique (Figure 6) did not look optimistic in that all extrusion runs were punctuated by foaming and poor fiber quality. No evidence of any crosslinking was observed. It was presumed that the silane grafting agent decomposed at the elevated temperatures necessary for extrusion. Since this first technique did not appear promising, efforts were directed toward post-grafting the spun TPX fibers using a swelling agent (Figure 7). Initial experimentation (Table VIII) showed that of the solvents studied, dichloromethane acted as the most effective swelling agent for yielding higher gel contents, even higher than the grafting agents by themselves. Unfortunately, after this treatment the fibers were too brittle to assemble into beaker units so that permeability or lifetime testing could not be conducted. Further post-treating experimentation was done by varying application times and solvent ratios, but these experiments gave mixed results. The prognosis for this post-treating technique is not necessarily promising in the short term but does show some long-range potential.

Crosslinking Summary

The experimentation to achieve crosslinking of TPX can be summarized as follows:

1. Crosslinking of TPX by the Dow-Corning method has been obtained by blending TPX, silane, and a peroxide catalyst and reacting the grafted material with water.

2. Extrusion of the grafted TPX was not successful under a variety of conditions. Degradation of the silane graft was seen as a limitation.

3. A small amount of crosslinking was accomplished when spun fibers were treated with the grafting reagents and an organic swelling agent. All of the treated fibers were too brittle to withstand handling for beaker unit fabrication. This approach has some possibility of success but has little short term promise.

4. It is recommended that any future work concern itself with exploring the post-grafting of extruded TPX fibers and reducing the brittleness of the crosslinked product.

MODULE DEVELOPMENT

Background

The culmination of efforts in previous AiResearch subcontracts resulted in nominal 11" diameter units for the DC-9 ground test. Prior to fabricating these large units, some intermediately sized six-inch diameter units were made for evaluation purposes. Because of their relative ease of fabrication and their size, the smaller units had sufficient fibers that a reasonably large statistical sample of membrane was available to determine whether the modules would perform on air testing at a level expected from the beaker unit work. During Phase I, fourteen of these six-inch modules (TJ series) were made, and their performances are summarized in Table IX.

Examining Table IX we see that in all cases, the oxygen-nitrogen separation is below the 4.26 $\pm$ .15 value obtained from ideal beaker unit testing. This discrepancy is found to be caused by breaks and clogs of some fraction of the many million fibers in the device. Tubesheet imperfections also were responsible for much of the deviation. However, from this fabrication work, considerable improvement in manufacturing techniques was realized. Smaller fibers did present a great deal of fabrication problems, but these problems were alleviated to a great degree in later modules. Preliminary indications are that the thirty fiber tows have aided the fabrication of modules. Of equal importance to the insights into module fabrication has been the operating data gathered to aid in final system design.

Computer Simulation Modifications

From the module testing data, the computer simulation was determined to be close to actual performance but some deviations were found to exist. These deviations were attributed to module non-idealities such as broken fibers, clogged fibers, or tubesheet imperfections. Accordingly, the Dow computer simulation was modified utilizing a model, more closely

describing the effect of leaks and clogged fibers upon the module. Table X compares the modified simulation, the ideal simulation, and actual module performance. By and large, the modified simulation matches the actual performance much more closely. This agreement is especially true for the inert recovery ratio. The model is presently being incorporated into the AiResearch simulation and is being employed in all design work done under this program.

Vacuum Operation

One of the features derived from the mathematics of membrane systems is the importance of the transmembrane pressure ratio. Computer simulations have shown that the inert flow will increase with decreasing shell-side pressure even though the transmembrane pressure is held constant (Table XI). Actual experimentation on a number of modules (Table XII) has borne out the theory and even suggest that the performance with evacuated shell-side is better than predicted. This increase may be partially realized and should be evaluated by trading the weight/cost and power of a vacuum pump against the decrease in required surface area to achieve a desired flow rate.

Flow Pressure Relationships

One of the major benefits of the small TJ series modules is the capability of obtaining flow-pressure relations that can be applicable to large devices. Of particular interest are the pressure drop inside the fiber bore and the pressure drop on the shell-side of the bundle. The pressure drop down the bore has been treated as incompressible flow following Poisseuille's law. This has given very good agreement with actual flow-ΔP measurements. On the other hand, the shell-side ΔP is a bit more complex. Utilizing packed bed theory, the flow-pressure relationship is found to be a complex function (termed "geometry factor") of bundle size, fiber size, and packing factor. Extensive data on the six inch modules has resulted in a linear (Figure 8) plot of flow/ΔP vs. geometry factor. With both pressure drop calculations incorporated into the computer program, computed values are quite close to the actual module test values in most cases (Table X). This correlation seems satisfactory at present, and additional data will be gathered to refine it further.

Module Washing

One of the operating modes explored by AiResearch in the previous contract was module "washing" or "sweeping". In this technique, feed air is swept across the shell-side to reduce the oxygen concentration of the shell-side mixture. As more air flow sweep is introduced, the shell-side oxygen concentration decreases and performance increases. This improvement occurs until a point is reached where increasing shell-side pressure drop decreases the pressure ratio significantly, and the performance actually decreases with further increase in sweep flow. A plot of

inert flow vs. sweep flow is very broad (Table XIII), and the washing appears to effect about a 20% increase. The effectiveness of this technique will decrease with larger bundle diameters. The value of increased module flow by this technique has to be weighed against the increased capacity of conditioned air required.

External Pressurization

Throughout the development program the internally pressurized mode has been used almost exclusively. This was because tests conducted during the previous contract on external pressurization of small devices (3" dia. x 9" long) showed only 30% of the inert productivity of the same device internally pressurized. This flow ratio was inopportune because some data indicated that the operating pressure at a given lifetime could be approximately doubled when pressurizing externally. This poor external performance was attributed to poor flow distribution caused by "end effects" from the low L/D ratio of the device.

Because the operating pressure range could be substantially increased, albeit at a penalty for a pressurized case, reinvestigation of external pressurization was undertaken. Seven of the modules were run in three modes: Mode 1 - internal pressurization; Mode 2 - external pressurization with permeate removal from one tubesheet; and Mode 3 - external pressurization with permeate removal from both tubesheets. Table XIV summarizes the data obtained from these runs. In general it appears that external pressurization does appear promising since the inert flow production of the device operating in Mode 3 averages about 95% of that of Mode 1. Modules of higher packing factor made the better showing probably because of the lesser amount of fiber bypassing. This avenue needs further exploration and, when compounded with fiber failure data, could open a new long-term design approach.

Module Development Summary

The module development effort can be summarized as follows:

1. Fourteen six inch diameter modules have been made in a variety of fiber sizes. All fiber sizes can be fabricated into modules, although the smaller fiber sizes are more difficult to work with. Single gas separation factors in some cases have been higher than 4.0, and module performance on air has been as predicted by the computer model.

2. Pressure drop-flow relationships have been characterized for both tubeside and shell-side flows. These design equations have been incorporated into the computer simulation.

3. Performance of modules with sub-atmospheric shell-side pressure showed substantial increases in performance. These improvements appear to be a bit higher than were predicted by the computer program.

4. Module washing has realized a 10-20% increase in module performance. The inert flow vs. sweep flow curves have the same broad shape as would be expected from theory and AiResearch's previous efforts. These effects can be expected to diminish in larger diameter modules.

5. External pressurization of modules looks more promising than earlier thought. However, before external pressurization can be evaluated, fiber failure envelopes must be obtained to aid in the system design.

FUTURE WORK

Although a great deal of information has been gathered during Phase I, Dow desires to obtain additional data to perhaps improve and further substantiate the tentative design. Some of the areas to be explored by Dow prior to the beginning of Phase II are:

1. More beaker unit testing will be done to determine whether 85 psid is the highest feed pressure to be operated in the system. The 30-hole spinnerette fibers will also be tested. To allow for some system upset, beaker unit testing will also be done at 30, 35, and 40°C at 85 psid.

2. Because of the statistics in beaker unit lifetime testing, a module testing system will be built to give more lifetime data.

3. Preliminary observations with external pressurization have shown it has substantial promise. Beaker unit testing will be conducted on 30 x 42μ fibers at 100 and 125 psid at 25°C.

4. Although progress has been made in module fabrication, packing factor control is still not achievable with sufficient reproducibility. This area requires additional effort.

5. In the tentative design, a two inch thick tubesheet has been specified. Calculations and experimentation will be done to determine if a thinner tubesheet can be used.

6. A large diameter module will be made. A 10-12" unit is proposed although a prototype KC-135 module (∿14" diameter) may be made.

7. A case utilizing only end plates will be fabricated to investigate the concept's use in large module design.

ACKNOWLEDGEMENTS

The authors would like to thank Earl Wagener and Tom Davis for their guidance throughout the program. Appreciation is extended to Scott Manatt and Joe Gillermann of Garrett AiResearch for their expert assistance in focusing the specific directions that the developmental efforts have taken. Special thanks to Howard Young and Steve Styer, whose assistance in the early stages of the program was invaluable. Similar thanks to Jeff Schletz, whose recent contributions to module fabrication have greatly increased the understanding of this process. The greatest thanks of all goes to Gloria Spinelli whose patience during the countless retyping of last-minute monthly reports has been nothing short of phenomenal.

FIGURE 1

MAJOR ACCOMPLISHMENTS FROM PREVIOUS CONTRACT WORK

- SUCCESSFUL SPINNING OF TPX IN 50 X 64μ AND 50 X 70μ FIBER SIZE
- MANUFACTURE OF MODULES UP TO 11" IN DIAMETER
- PRELIMINARY FIBER FAILURE ENVELOPE
- MODULE AIR PERFORMANCE AS PREDICTED FROM INDIVIDUAL FIBER DATA

FIGURE 2

SOME UNFORESEEN RESULTS DURING PREVIOUS CONTRACT WORK

- PERMEABILITIES OF HOLLOW FIBERS 30% LOWER THAN LITERATURE AND FLAT MEMBRANE DATA

- HOOP STRENGTH LESS THAN ANTICIPATED (POLYMER CREEP)

  INTERNAL PRESSURIZATION LIMITED TO <100 PSID, 30°C
  EXTERNAL PRESSURIZATION NOT AS EFFICIENT (~30%) AS INTERNAL PRESSURIZATION, BUT 2:1 PRESSURE ADVANTAGE

- TUBESHEET PROBLEMS; CANNOT BOND MODULE TO CASE

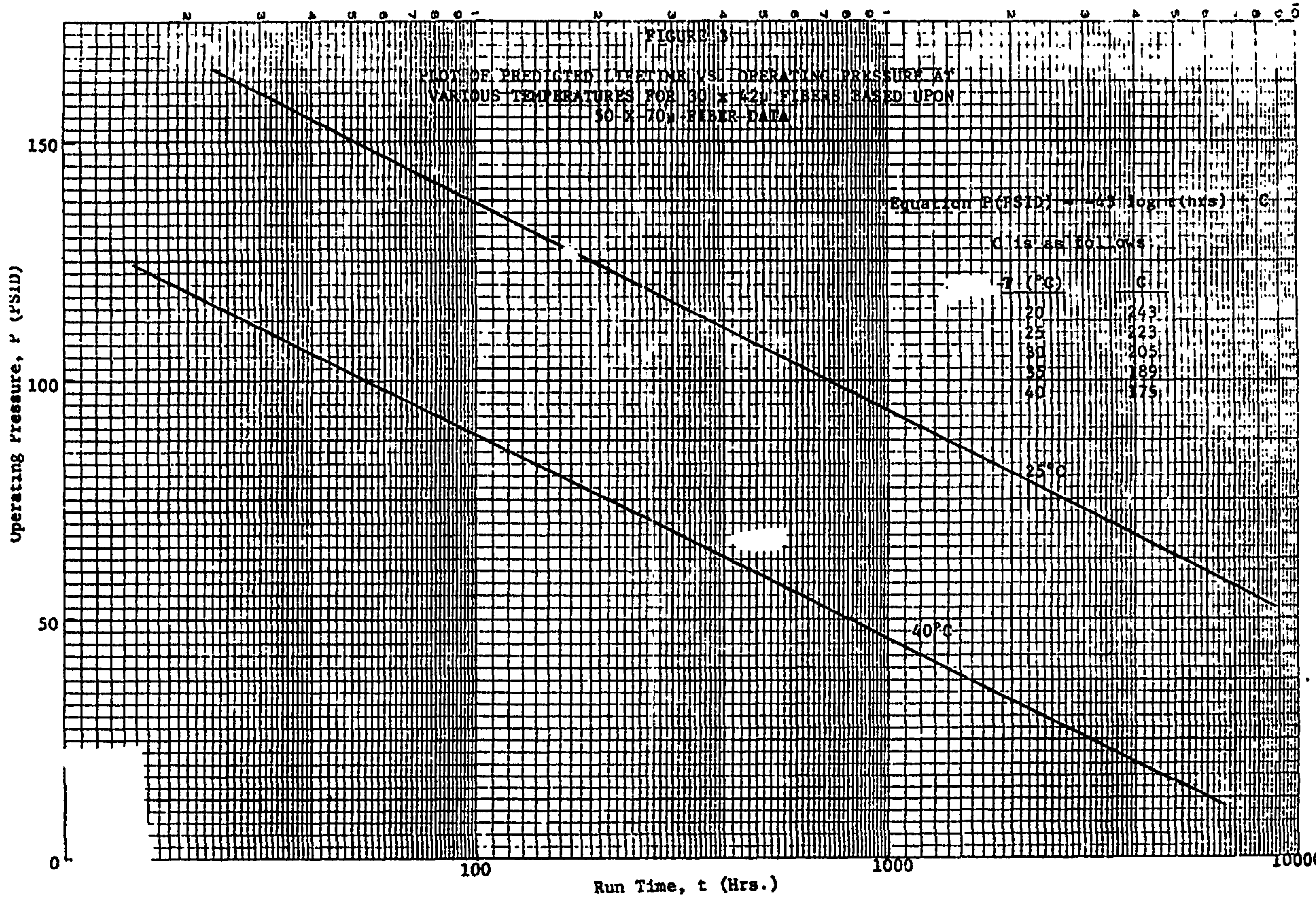

16

FIGURE 4

EFFECT OF CROSSLINKING UPON
FAILURE FROM HOOP STRESS
POLYETHYLENE TUBING

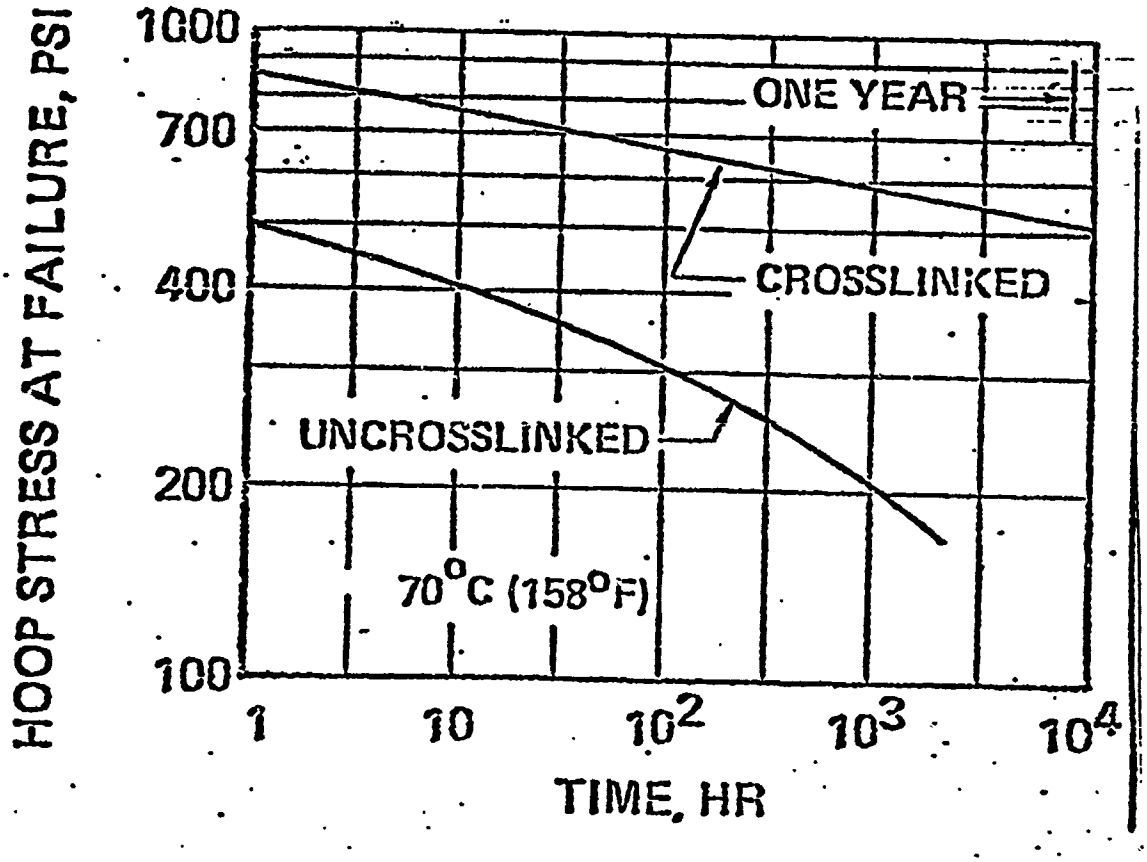

SCOTT, H. G., HUMPHRIES, J. F., MODERN PLASTICS 50, (1973)

FIGURE 5

CROSSLINKING OF TPX
GRAFTING VINYL SILANE TO TPX

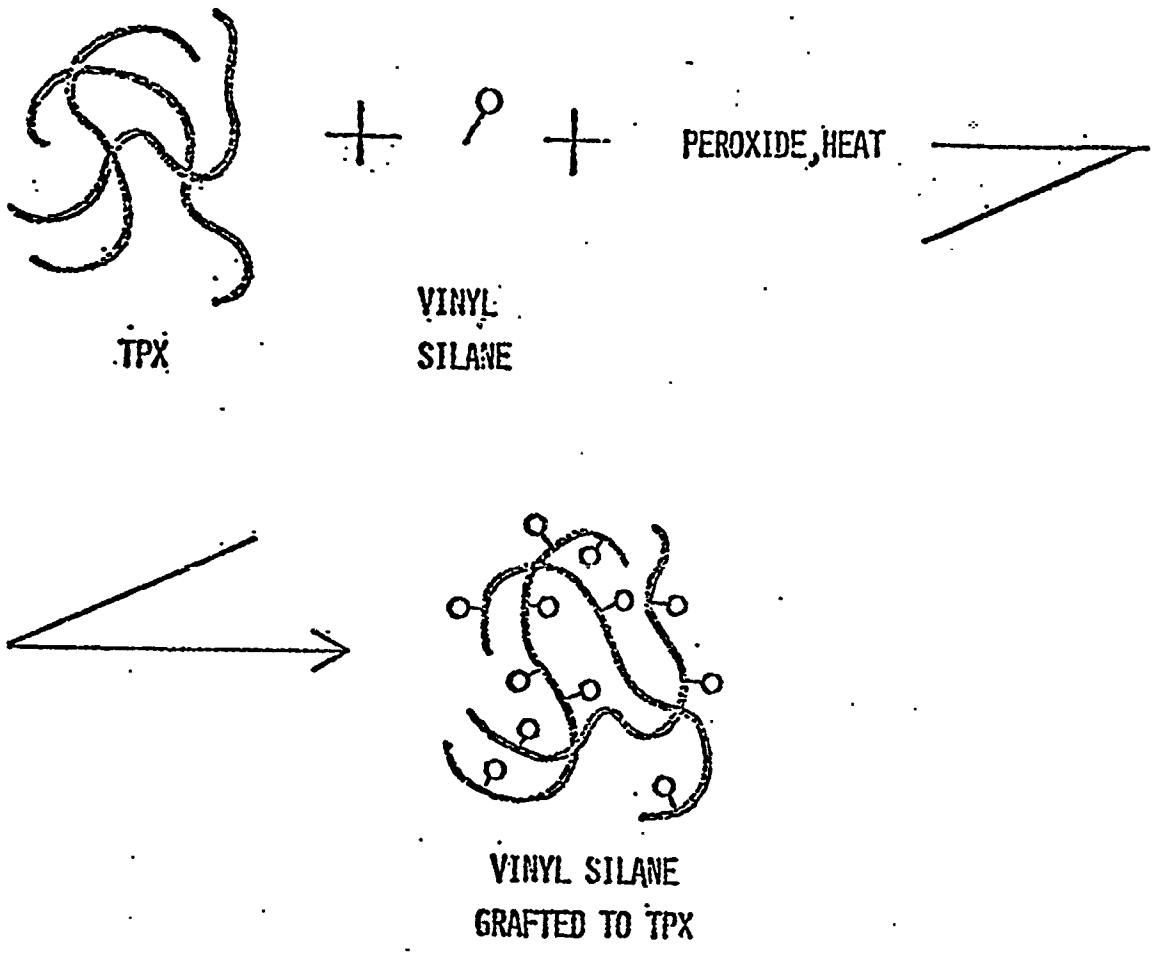

FIGURE 6

SUMMARY OF EXPERIMENTATION WITH
EXTRUSION IF SILANE-GRAFTED TPX

TPX + REACTANTS —EXTRUDE→ SILANE GRAFTED TPX FIBERS

	TEST	RESULTS
1.	TWIN SCREW EXTRUDER (DOW CORNING) LONG RESIDENCE TIME; LOW SHEAR	FOAMING, ROUGH STRAND, NO CROSSLINKING
2.	SINGLE SCREW EXTRUDER SHORT RESIDENCE TIME; HIGH SHEAR	FOAMING
3.	SINGLE SCREW EXTRUDER RE-EXTRUSION OF EXTRUDATE IN 2	SLIGHT FOAMING; POOR QUALITY FIBER; GELS AND RAPID PACK PRESSURE INCREASE; NO CROSSLINKING
4.	VENTED TWIN SCREW EXTRUDER VERY POOR TEMPERATURE CONTROL	ROUGH STRAND, NO CROSSLINKING

FIGURE 7

SUMMARY OF EXPERIMENTATION INVESTIGATING THE
POST EXTRUSION CROSSLINKING OF TPX FIBERS

TPX FIBERS + REACTANTS $\xrightarrow{\text{HEAT}}$ GRAFTED TPX FIBERS

GRAFTED TPX FIBER + H_2O $\longrightarrow$ CROSSLINKED FIBER

EXPANDED VARIABLES

SOLVENT CARRIER FOR REACTANTS (DICHLOROMETHANE BEST)

EXPOSURE TIME TO REACTANTS

REFLUX TIME IN GEL ANALYSIS

REACTANT RATIO (SILANE/PEROXIDE)

- RESULTS CLOUDED BUT SOME CROSSLINKING OBTAINED
- FIBERS BRITTLE AFTER TREATMENT
- NO PERMEATION OR LIFETIME DATA OBTAINED BECAUSE OF BRITTLENESS

FIGURE 8

PLOT OF SHELL-SIDE FLOW VS. GEOMETRY FACTOR
FOR 6" DIAMETER MODULES

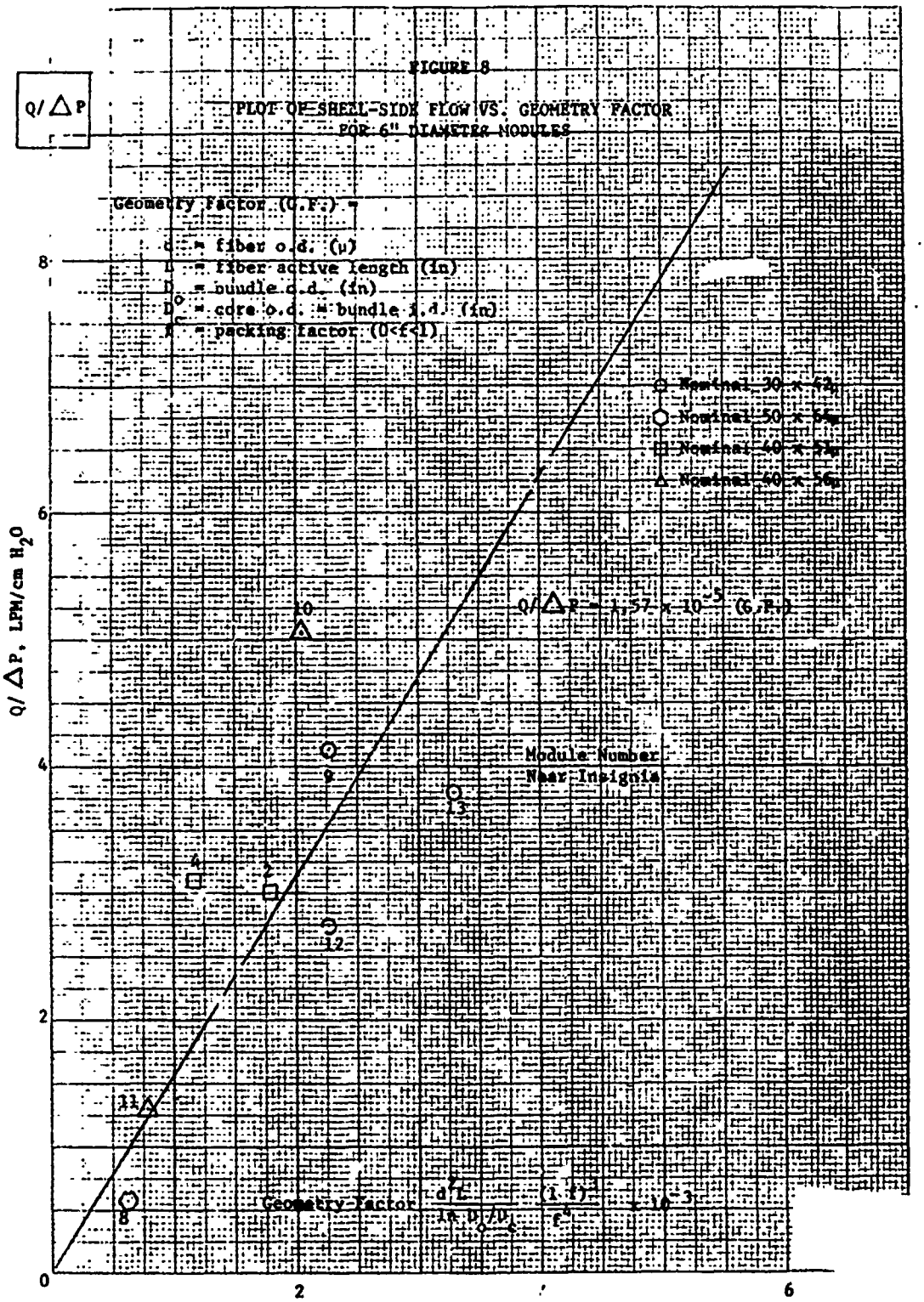

TABLE I

COMPUTER SIMULATION SHOWING DEVICE PRODUCTIVITY
AS A FUNCTION OF FIBER SIZE

Basis: 6" diameter module, 36" active length, 42" overall length; 50% packing factor, flow normalized to 50 x 64μ fiber performance, 9% O_2 inert stream, 64.7 psia feed pressure, 14.7 psia shell pressure.

OD/ID = 1.28 "Family"			OD/ID = 1.40 "Family"		
Fiber Size (Microns)	Inert Flow (Normalized)	Inert Recovery (Percent)	Fiber Size (Microns)	Inert Flow (Normalized)	Inert Recovery (Percent)
50 x 64	1.00	48.9	50 x 70	.62	49.0
45 x 57.6	1.20	48.6	45 x 63	.74	48.9
40 x 51.2	1.47	48.3	40 x 56	.94	48.6
35 x 44.8	1.81	47.9	35 x 49	1.15	48.1
30 x 38.4	2.14	46.5	30 x 42	1.41	47.2
25 x 32	2.32	43.5	25 x 35	1.63	44.5

TABLE II

FIBER SIZE SUMMARY SHEET

Run Number	Target Size	Operator	$\overline{ID}$	σ_{ID}	$\frac{\sigma_{ID}}{ID}$ (%)	$\overline{OD}$	σ_{OD}	$\frac{\sigma_{OD}}{OD}$ (%)	$\frac{OD}{ID}$
R67A (3X spin rate)	30 x 42	B	28.75	1.58	5.5	42.17	1.91	4.5	1.467 ± .076
		S	28.78	1.32	4.6	40.98	1.91	4.7	1.424 ± .043
		T	29.82	1.84	6.2	42.16	2.38	5.6	1.415 ± .032
		Avg.	29.12	1.58	5.4	41.77	2.07	4.9	1.435 ± .050
R67B	40 x 56	B	38.04	2.61	6.9	55.23	3.94	7.1	1.454 ± .092
		S	40.36	3.06	7.6	56.18	3.57	6.4	1.393 ± .031
		T	40.99	2.72	6.6	57.14	3.37	5.9	1.400 ± .036
		Avg.	39.80	2.80	7.0	56.18	3.63	6.5	1.416 ± .053
R67C	50 x 70	B	50.05	2.71	5.4	71.22	3.55	5.0	1.424 ± .050
		S	49.05	3.00	6.1	68.38	4.55	6.8	1.395 ± .028
		T	47.66	3.57	7.5	67.27	4.55	6.8	1.406 ± .031
		Avg.	48.92	3.09	6.3	68.96	3.99	5.8	1.408 ± .036
R67D	30 x 38.4	B	31.16	2.05	6.6	40.55	2.53	6.2	1.302 ± .039
		S	29.78	3.33	11.2	37.04	3.05	8.2	1.246 ± .025
		T	30.74	3.11	10.1	38.59	3.42	8.9	1.257 ± .038
		Avg.	30.56	2.83	9.3	38.73	3.00	7.8	1.268 ± .034
R67E	40 x 51.2	B	38.22	3.75	9.8	51.38	4.23	8.2	1.347 ± .049
		S	39.61	2.83	7.1	50.39	4.19	8.3	1.272 ± .067
		T	38.76	2.84	7.3	50.10	3.44	6.9	1.293 ± .030
		Avg.	38.86	3.14	8.1	50.62	3.95	7.8	1.304 ± .049
R67F	50 x 64	B	48.71	3.13	6.4	62.30	3.28	5.3	1.280 ± .030
		S	50.24	4.04	8.0	62.89	3.98	6.3	1.252 ± .030
		T	51.43	4.54	8.8	64.07	5.45	8.5	1.246 ± .025
		Avg.	50.13	3.90	7.7	63.09	4.24	6.7	1.259 ± .028

N.B. - Fiber dimensions are paired OD-ID points.

Continued

TABLE II (CONTINUED)

FIBER SIZE SUMMARY SHEET

Run Number	Target Size	Operator	$\overline{ID}$	σ_{ID}	$\frac{\sigma_{ID}}{ID}$ (%)	$\overline{OD}$	σ_{OD}	$\frac{\sigma_{OD}}{OD}$ (%)	$\frac{OD}{ID}$
R68A (2X spin rate)	30 x 42	B	30.34	2.66	8.8	40.48	3.09	7.6	1.336 ± .044
		S	30.84	2.34	7.6	40.19	3.01	7.5	1.303 ± .042
		T	30.30	3.35	11.0	40.27	3.89	9.6	1.332 ± .054
		Avg.	30.50	2.78	9.1	40.31	3.33	8.2	1.324 ± .047
R68B	40 x 56	B	40.33	2.38	5.9	56.87	3.41	6.0	1.405 ± .039
		S	43.71	3.30	7.5	57.31	3.75	6.5	1.313 ± .039
		T	41.89	2.88	6.9	55.47	3.33	6.0	1.325 ± .026
		Avg.	41.98	2.85	6.8	56.55	3.49	6.2	1.348 ± .035
R68C	50 x 70	B	50.66	3.24	6.4	69.54	4.34	6.2	1.373 ± .042
		S	51.44	4.59	8.9	66.90	4.87	7.3	1.303 ± .044
		T	53.12	3.49	6.6	69.55	4.78	7.1	1.309 ± .018
		Avg.	51.74	3.77	7.3	68.66	4.66	6.9	1.328 ± .035
R68D	30 x 38.4	B	29.06	3.02	10.4	38.19	3.16	8.3	1.318 ± .054
		S	31.04	3.79	12.2	39.12	4.47	11.4	1.262 ± .040
		T	30.72	3.50	11.4	38.44	3.77	9.8	1.253 ± .032
		Avg.	30.27	3.44	11.3	38.58	3.80	9.8	1.278 ± .042
R68E	40 x 51.2	B	39.63	2.63	6.3	52.53	3.23	6.1	1.326 ± .028
		S	40.77	3.58	8.8	51.19	4.13	8.1	1.257 ± .026
		T	40.13	3.05	7.6	50.76	3.69	7.3	1.264 ± .024
		Avg.	40.18	3.09	7.7	51.49	3.68	7.2	1.282 ± .026
R68F	50 x 64	B	49.38	3.15	6.4	64.83	4.05	6.2	1.313 ± .037
		S	52.19	4.32	8.3	64.53	5.13	8.0	1.237 ± .025
		T	53.82	5.96	11.1	66.75	6.46	9.7	1.242 ± .034
		Avg.	51.80	4.48	8.6	65.37	5.21	8.0	1.264 ± .032

N.B. - Fiber dimensions are paired OD-ID points

TABLE III

SUMMARY OF PERMEABILITY
VARIATION WITH TEMPERATURE
FOR NITROGEN AND OXYGEN

Gas	Nitrogen		Oxygen	
Beaker Unit	A106-Run 1	A106-Run 2	A106	A111
Temp. Range °C	13.7-40.0	12.8-40.4	13.4-40.0	13.4-40.1
Arrhenius Slope	-3044	-2885	-2130	-2013
Regression Correlation Coefficient	.998	.999	.997	.996
Actual SCCM @ 25°C	3.68	3.61	16.16	16.45
Predicted SCCM @ 25°C from Arrhenius Plot	3.747	3.672	15.97	16.19
Average Arrhenius Slope	-2964		-2072	
Design Equation Permeability Coefficient	9.122×10^{-6} Exp. (-2964/T) s.u.		1.948×10^{-6} Exp. (-2072/T) s.u.	
Permeability Coefficient at 25°C	4.37×10^{-10} s.u.		18.62×10^{-10} s.u.	
$\frac{Gas}{N_2}$ @ 25°C	1.00		4.26	

*s.u. = $\frac{(cm^3/sec\ @\ stp)(cm)}{(cm^2)(cm\ Hg)}$

TABLE IV

SUMMARY OF LIFETIME TESTING FOR 30 x 42u
FIBERS AT 3X SPIN RATE (AS OF FEBRUARY 9, 1979)

Temp. (°C)	Pressure (PSID)	Number Started	Fiber Failure	Other Failures	Still Running	Successful Units Run Time (Hr.)	Failed Units Run Time (Hr.)
25	60	4	0	0	0	1012, 1012, 1012, 1012	--
30	60	4	0	0	0	1104, 1104, 1104, 1104	--
25	75	4	0	0	0	1056, 1056, 1056, 1056	--
25	80	5	1	1	0	1704+, 1704+, 408+	1341, 1538
25	85	4	1	0	0	1704+, 1704+, 1056+	1658
25	90	7	2	1	4	1632+, 432+, 1776+, 744+	547, 43, 1344
25	95	5	1	0	4	1152+, 1152+, 432+, 936	424
25	100	8	6	0	4	532, 358	809, 956, 184, 420, 868, 768

Failure Criterion: $\alpha < 3.95$

TABLE V

SUMMARY OF FAILED BEAKER UNITS

Station Number	Pressure (PSID)	Total Run Time	Final α (25°C)	Failure Cause
1	80	1341	4.28	Damaged Permeate Outlet
2	80	1538	2.90	Single Fiber
5	85	1658	3.88	Single Fiber
10	90	1344	3.49	Single Fiber
12	90	547	3.88	Single Fiber
12	90	43	4.36	Leaky Tubesheet
15	95	424	3.13	Single Fiber
17	100	809	3.66	Single Fiber
18	100	184	3.44	Single Fiber
18	100	868	3.73	Single Fiber
19	100	956	3.58	Single Fiber
20	100	420	3.91	Single Fiber
20	100	768	3.79	Single Fiber

TABLE VI

SUMMARY OF 30 HOLE SPINNERETTE RUN
NOMINAL 30 X 42μ FIBERS SPIN RUN R78-W

	Operator	ID	σ ID	$\frac{\sigma \text{ ID}}{\text{ID}}$ (%)	OD	σ OD	$\frac{\sigma \text{ OD}}{\text{OD}}$ (%)	$\frac{\text{OD}}{\text{ID}}$
				RUN 1				
(30 FIBER SAMPLES)	R	30.98	3.26	10.5	42.25	3.94	9.3	1.365 ± .028
	J	30.90	2.48	8.0	41.43	3.21	7.7	1.341 ± .025
	T	31.69	3.19	10.1	43.06	4.10	9.5	1.360 ± .030
	B	31.23	3.27	10.5	43.88	4.38	10.0	1.406 ± .033
	Avg.	31.20	3.05	9.8	42.65	3.91	9.2	1.368 ± .029
				RUN 2				
(120 FIBER SAMPLES)	R	30.65	2.25	7.3	42.05	2.59	6.2	1.372 ± .026
	B	30.91	2.47	8.0	42.96	3.01	7.0	1.390 ± .041
	Avg.	30.78	2.36	7.7	42.51	2.80	6.6	1.381 ± .034

TABLE VII

SUMMARY OF INSTRON TESTING OF
GRAFTED AND CROSSLINKED TPX

Sample Number	Polymer Tested	Tensile Yield Stress (PSI)	Tensile Yield Strain (%)	Ultimate Elongation (%)	Module x 10^5 psi	Sample Treatment
1	TPX	1410-2822	1.60 - 5.87	37.3	1.06	Control - No 100°C H_2O soak
2	TPX	1974-3572	1.60 - 6.93	38.7	1.10	100°C H_2O - 16 hrs.
3	TPX	1881-3290	1.87 - 6.13	32.0	1.01	100°C H_2O - 16 hrs.
4	Grafted TPX	1693-2258	1.87 - 3.73	39.0	0.82	Control - No 100°C H_2O soak
5	Grafted TPX	1429-2700	2.07 - 3.20	5.3	1.09	100°C H_2O - 16 hrs.
6	Grafted TPX	1954-2736	2.13 - 4.27	9.3	1.05	100°C H_2O - 16 hrs.

Membrane Preparation: TPX - 225°C, 20 sec., no pressure
255°C, 15 sec., 20,000 PSIG
Water quench (room temp.)
100°C soak for 16 hours.

Grafted TPX - 220°C, 80 sec., no pressure
220°C, 15 sec., 10,000 PSIG
Air cooled in press.
100°C soak for 16 hours to crosslink.

TABLE VIII

SUMMARY OF SWELLING AGENT
EFFECTS ON TPX CROSSLINKING

	Dichloromethane Peroxide & Silane	Decalin Peroxide & Silane	Tetralin Peroxide & Silane	No Solvent Peroxide & Silane	No Solvent No Peroxide & Silane
1. Initial Fiber Weight (gms)	0.36910	0.40025	0.36245	0.39000	0.27685
2. Weight After Solvent Treatment and 90°C Reaction (gms)	0.45400	0.50082	0.40154	0.43108	---
3. Weight of Diffused Material (gms)	0.08490	0.10057	0.03909	0.04108	---
4. Weight After Overnight High Humidity Exposure (gms)	0.45390	0.50123	0.40150	0.43145	---
5. Gel Content AFter 10 Hour Reflux in Decalin and 48 Hr. 58°C Drying (gms)	0.07137	0.04297	0.03169	0.02891	0.00072
6. Gel Percentage Based Upon Initial Weight (%)	19.3	10.7	8.7	7.4	0.3

TABLE IX

SIX INCH DIAMETER MODULE TESTING SUMMARY

Module Number	Nominal Fiber Size	Actual Fiber Size	Packing Factor	Surface Area (Ft^2)	Number of Fibers ($\bar{M}$) Weight	Wraps	Flow-ΔP	Single Gas Testing O_2 Flow (accm/psi)	α	Leak (%)
TJ-1	50 x 64	50.3 x 64.0	.49	2630	1.54	--	1.23	2320	3.17	52
TJ-2	40 x 51	39.4 x 51.3	.493	2760	2.10	2.19	2.01	2670	3.93	12
TJ-3	50 x 64	51.2 x 63.8	.593	3440	2.03	2.25	EPOXY DID NOT CURE			
TJ-4	40 x 51	37.5 x 49.1	.517	4160	3.13	--	3.11	3700	3.80	18
TJ-5	40 x 56	39.4 x 54.1	.536	3580	2.53	2.69	1.45	2120	4.00	10
TJ-6	40 x 56	38.4 x 54.1	.528	3330	2.35	2.63	1.96	2160	3.82	17
TJ-7	50 x 64	48.8 x 64.8	.469	2840	1.63	1.94	1.39	2030	3.75	20
TJ-8	50 x 64	49.9 x 64.2	.602	3340	1.96	2.14	1.47	2440	4.07	7
TJ-9	30 x 42	29.3 x 42.2	.446	4410	4.00	3.97	3.45	3290	3.37	39
TJ-10	40 x 56	39.8 x 55.5	.494	3810	2.54	2.47	2.20	2330	4.00	10
TJ-11	40 x 56	41.6 x 56.9	.569	3450	2.29	--	1.48	2120	4.07	7
TJ-12	30 x 42	29.3 x 41.9	.447	3810	3.50	3.82	3.84	3410	3.75	20
TJ-13	30 x 42	29.3 x 41.9	.428	3290	3.02	3.07	3.20	2320	3.80	18
TJ-14	30 x 38	29.3 x 38.4	.382	1210	1.17	--	1.07	1725	2.79	84

TABLE IX (CONTINUED)

SIX INCH DIAMETER MODULE TESTING SUMMARY
AIR TESTING

Air Testing (50 PSIG Feed, 0 PSIG Shell, 9% O_2)

Module Number	Int. Press. Flow (SLM)	Int. Press. Recovery (%)	Ext. Press. - 1 T.S. Flow (SLM)	Ext. Press. - 1 T.S. Recovery (%)	Ext. Press. - 2 T.S. Flow (SLM)	Ext. Press. - 2 T.S. Recovery (%)
TJ-1	11.4	22	9.4	22	--	--
TJ-2	34.0	45	17.5	32	31.3	42
TJ-3	--	--	--	--	--	--
TJ-4	44.2	38	33.3	38	41.6	41
TJ-5	16.7	34	10.8	26	--	--
TJ-6	21.3	38	16.0	33	25.2	41
TJ-7	--	--	--	--	--	--
TJ-8	24.6	39	23.1	37	26.0	39
TJ-9	33.8	42	16.7	30	29.4	39
TJ-10	26.7	41	20.6	35	--	--
TJ-11	20.7	36	--	--	--	--
TJ-12	40.5	43	13.2	22	36.7	40
TJ-13	28.9	41	6.7	17	22.0	35
TJ-14	12.7	25	--	--	--	--

TABLE X

COMPARISON OF ACTUAL PERFORMANCE AND
COMPUTER MODEL FOR 6" DIA. MODULES

Module Number	Leak Pct.	Pct. Open Fibers	Inert Flow (SLM)			Inert Rec. (%)			Tube ΔP			Shell ΔP		
			ACT	MOD1	MOD2	ACT	MOD1	MOD2	ACT	MOD1	MOD2	ACT	MOD1	MOD2
TJ-2	12	95	34.0	34.9	31.1	45	49.3	43.6	4.8	5.0	4.9	.13	----	.11
TJ-4	18	99	44.2	53.6	48.2	38	49.1	43.2	5.1	6.5	6.4	.21	----	.26
TJ-5	10	58	16.7	20.5	13.6	34	49.6	25.0	3.6	4.8	4.6	---	----	.21
TJ-6	17	83	21.3	27.8	22.7	38	49.6	37.5	3.9	4.8	4.7	.63	----	.14
TJ-8	7	75	24.6	28.3	23.2	39	49.7	35.6	2.1	2.4	2.3	.68	----	.78
TJ-9	18	86	33.8	39.4	33.2	42	48.2	37.3	10.1	12.5	12.3	.08	----	.12
TJ-10	10	88	26.7	32.9	28.8	41	49.5	41.3	3.9	4.5	4.4	.05	----	.09
TJ-11	7	65	20.7	23.2	16.0	36	49.6	29.3	4.0	3.8	3.7	.20	----	.24
TJ-12	20	100	40.5	43.3	40.8	43	49.6	42.5	10.3	11.4	12.3	.13	----	.12
TJ-13	18	100	28.9	36.1	34.3	41	49.6	43.1	10.9	11.4	12.3	.09	----	.07

ACT = Actual Performance
MOD1 = Old Dow Model
MOD2 = New Dow Model (Leaks Accounted For)

TABLE XI

COMPUTER SIMULATION SHOWING DEVICE PRODUCTIVITY
AS A FUNCTION OF SHELL SIDE PRESSURE

Basis: 6" diameter module, 36" active length, 42" overall length, 50% packing factor, 40 x 51.2 fibers, 9% O_2 inert stream, 50 psid across membrane inlet, no shell side ΔP effects, flows normalized to 14.7 psia shell, leaks not included.

Shell Pressure (PSIA)	Inert Flow (Normalized)	Inert Recovery (Percent)
14.7	1.00	48.2
10.0	1.23	53.1
8.0	1.35	55.2
5.0	1.55	58.3
2.0	1.84	62.0

TABLE XII

SHELL-SIDE VACUUM TESTING SUMMARY
(50 PSID TRANSMEMBRANE PRESSURE, 9% O_2 INERT)

Module Number	Fiber Size	Packing Factor	Shell Outlet Pressure (PSIA)	Inert Flow (SLM)	Inert Recovery (PCT)	Shell Side ΔP (PSID)
TJ-2	39.4 x 51.3 (40 x 51)	.493	14.8	30.4 (1.00)	41.6	0.2
			10.1	40.8 (1.34)	48.6	0.25
			8.1	44.0 (1.45)	51.0	0.3
			5.2	51.7 (1.70)	54.9	0.4
TJ-4	37.5 x 49.1 (40 x 51)	.517	14.9	38.5 (1.00)	38.8	0.3
			10.0	49.2 (1.28)	44.8	0.45
			8.0	[illegible].2 (1.56)	48.5	0.45
			4.9	67.6 (1.76)	52.5	0.65
TJ-8	49.4 x 64.2 (50 x 64)	.553	14.8	22.3 (1.00)	36.8	0.80
			9.8	29.6 (1.33)	43.1	1.25
			8.0	33.4 (1.50)	45.6	1.45
			5.1	38.1 (1.71)	48.6	2.10
TJ-10	39.8 x 55.3 (40 x 56)	.502	14.9	26.7 (1.00)	40.8	0.2
			9.0	37.9 (1.42)	49.1	---
			5.1	47.5 (1.78)	53.7	---
			2.3	55.5 (2.08)	57.5	---
TJ-12	29.7 x 43.1 (30 x 42)	.406	14.9	39.5 (1.00)	43.2	0.2
			10.0	49.8 (1.26)	48.9	0.35
			7.9	55.1 (1.39)	51.4	0.40
			5.0	63.4 (1.61)	56.0	0.55

TABLE XIII

SWEEP EXPERIMENTATION SUMMARY

Feed Press. (PSIG)	Tube ΔP (PSID)	Inert Flow (SLM)	Sweep Flow (SLM)	Shell ΔP (PSID)	Overall Recovery (%)	Shell O_2 Conc. (%)
			TJ-8			
50	1.9	23.5	0	1.3	37	28.1
50	2.1	26.7	10.0	1.65	35	27.5
50	2.2	28.5	17.4	1.90	33	26.9
50	2.2	28.8	21.5	2.15	32	26.7
50	2.0	27.0	55.8	3.40	22	24.3
50	1.9	24.6	83.8	4.60	17	23.4
			TJ-13			
50	10.8	31.9	0	0.25	43	30.0
50	10.9	33.3	11.8	0.34	38	28.4
50	11.1	34.5	30.4	0.465	32	26.8
50	11.2	34.8	46.1	0.585	28	25.7
50	11.1	34.4	71.2	1.25	23	24.6
50	10.8	33.6	94.2	1.75	20	24.0

TABLE XIV

SUMMARY OF INTERNAL AND EXTERNAL PRESSURIZATION RUNS (2% O_2 INERT)

Module Number	Packing Factor	Internal Flow					External Flow - 1 S.S. Open						External Flow - 2 S.S. Open					
		H.P. (PSIA)	L.P. (PSIA)	P.R.	ΔP (PSID)	Exp. N.F.	H.P. (PSIA)	L.P. (PSIA)	P.R.	ΔP (PSID)	Exp. N.F.	Act N.F.	H.P. (PSIA)	L.P. (PSIA)	P.R.	ΔP (PSID)	Exp. N.F.	Act N.F.
TJ-2	.493	62.4	15.0	4.16	47.4	1.00	64.7	17.9	3.61	46.2	0.80	0.51	64.6	15.8	4.10	48.8	1.01	0.92
TJ-4	.517	62.1	15.2	4.07	46.8	1.00	64.6	18.4	3.51	46.2	0.80	0.75	64.6	15.9	4.06	48.7	1.04	0.94
TJ-6	.528	62.8	15.6	4.04	47.2	1.00	64.6	17.6	3.66	47.0	0.87	0.75	64.5	15.6	4.13	48.9	1.07	1.18
TJ-8	.602	63.7	15.3	4.16	48.4	1.00	64.6	16.6	3.88	48.0	0.90	0.94	64.5	15.4	4.21	49.1	1.03	1.06
TJ-9	.446	59.8	15.0	3.99	45.8	1.00	64.7	20.2	3.20	44.5	0.70	0.44	64.7	16.4	3.95	48.3	1.04	0.87
TJ-12	.447	59.5	15.1	3.94	44.4	1.00	64.7	20.5	3.15	44.2	0.71	0.33	64.6	16.6	3.88	48.0	1.06	0.91
TJ-13	.428	59.2	15.1	3.92	44.1	1.00	64.6	20.8	3.10	43.8	0.69	0.23	64.7	16.4	3.93	48.3	1.10	0.76

H.P. = AVERAGE PRESSURE ON FEED SIDE
L.P. = AVERAGE PRESSURE ON PERMEATE SIDE
P.R. = PRESSURE RATIO
ΔP = NET DRIVING PRESSURE = H.P. - L.P.
EXP. N.F. = EXPECTED NORMALIZED INERT FLOW (INTERNAL = 1.00) FROM PRESSURES
ACT. N.F. = ACTUAL EXPERIMENTAL INERT FLOW

APPENDIX B

The Dow Chemical Company

"DEVELOPMENT OF IMPROVED POLYMETHYLPENTENE HOLLOW FIBERS AND AIR SEPARATION MODULES FOR INERTING THE FUEL TANKS OF AIRCRAFT"

SUBCONTRACT #424-95065-0

Summary Report

Prepared for

AIRESEARCH MANUFACTURING COMPANY OF CALIFORNIA
2525 West 190th Street
Torrance, CA 90509

Author

Gunther E. Molau

June 8, 1981

SUMMARY

Various methods of crosslinking poly(4-methyl-1-pentene) (PMP) have been evaluated with the purpose of upgrading its properties and increasing its service temperature. While none of the studied methods have produced a crosslinkable polymer, our experiments and theoretical considerations suggest that PMP responds to generation of radicals along its backbone with main chain scission rather than crosslinking. Also, our literature studies revealed that PMP is so sensitive to disruption of its crystallinity that introduction of 3% comonomer units, which is about the percentage of required crosslinks, causes a drop in heat distortion temperature from 58°C to 30°C. Thus, we conclude that crosslinking is not the right approach to upgrading the service properties of PMP.

We then studied the effect of changes in orientation and crystallinity on the oxygen and nitrogen permeability of PMP. Hollow fibers of PMP were annealed in air at 153°C and 174°C and in vacuum at 136, 154, 176, and 195°C. While the initial annealing experiments in air had indicated a slight possibility that annealing may increase gas permeability, the later vacuum annealing experiments did not corroborate this indication. It appears that two opposing effects cancel each other out: Annealing can reduce orientation, which would increase permeability, and increase crystallinity, which would decrease permeability.

Thus, neither chemical nor physical modification of PMP led to an improvement in its application in hollow fiber gas separation modules. However, PMP is definitely useable in this application in its present form. If improvement of the gas separation modules above and beyond their present performance is desired, a search for a material replacing PMP is indicated, rather than an improvement of PMP itself by modification.

TABLE OF CONTENTS

	Page
INTRODUCTION	176
BACKGROUND OF THE CHEMICAL MODIFICATION STUDY	177
STUDY OF CROSSLINKING VARIABLES	177
CHLORINATION	178
TABLE 1 - CHLORINATION OF PMP	179
SULFOCHLORINATION	180
REACTIONS OF CHLORINATED OR SULFOCHLORINATED PMP	181
TABLE 2 - REACTION OF CHLORINATION OR SULFOCHLORINATED PMP WITH DOW-CORNING SILANE Z-6020	183
THERMAL STABILITY OF RELATED POLYMERS	184
PMP WITH DOUBLE-BONDS	185
SOLVENTS FOR PMP	186
GRAFTING WITH VINYL ALKOXY SILANES	187
Hydrolysis	188
Crosslinking	189
TABLE 3 - HALF-LIFE DATA OF SELECTED COMMERCIAL PEROXIDES	195
TABLE 4 - HALF-LIFE TIMES AT 270°C CALCULATED FROM FIGURE 1 WITH EQUATION 1	196
FIGURE 1 - HALF-LIFE DATA OF SELECTED COMMERCIAL PEROXIDES	197
TABLE 5 - PMP/SILANE Z-6030 GRAFTING EXPERIMENTS AT VARIOUS PEROXIDE LEVELS	199
IRRADIATION OF PMP	200
FIGURE 2 - DEGRADATION OF POLYOLEFINS UNDER GAMMA-RADIATION	202
EFFECT OF PEROXIDES ON PMP	203
SIDE REACTIONS CAUSING POLYMER DEGRADATION	204
EXPERIMENTAL EVIDENCE FOR DEGRADATION OF PMP	207

TABLE OF CONTENTS CONTINUED

Page

TABLE 6 - MOLECULAR WEIGHT OF PUMP VERSUS PEROXIDE NOT USED 207

FIGURE 3 - WITCO USP-130 PEROXIDE 208

FIGURE 4 - 2,5-DIMETHYLHEXANE-2,5-DIHYDROPEROXIDE 208

FIGURE 5 - MOLECULAR WEIGHT AS A FUNCTION OF ELUTION VOLUME 209

A CROSSLINKABLE TERPOLYMER 210

BACKGROUND FOR THE PHYSICAL MODIFICATION STUDY 210

LITERATURE STUDY 212

TABLE 7 - HEAT DISTORTION DATA FOR VARIOUS POLYMERS 213

TABLE 8 - EFFECT OF ANNEALING ON HEAT DISTORTION TEMPERATURE OF PMP 213

TABLE 9 - EFFECT OF ANNEALING ON CRYSTALLINITY AND GLASS TRANSITION TEMPERATURE OF PMP 214

COMPARISON OF HOLLOW FIBER AND FLAT SHEET PMP MEMBRANES BY X-RAY DIFFRACTION 216

TABLE 10 216

ANNEALING OF PMP HOLLOW FIBERS AND TESTING OF GAS PERMEABILITY 217

UNITS FOR EXPRESSING GAS PERMEABILITY 220

GAS PERMEABILITY OF PMP HOLLOW FIBERS ANNEALED IN AIR . . . 220

TABLE 11 - SUMMARY OF PERMEATION RATE DATA 221

TABLE 12 - AVERAGED CORRECTED PERMEATION RATES 222

TABLE 13 - ANNEALING IN AIR 223

TABLE 14 - ANNEALING IN AIR 224

GAS PERMEABILITY OF PMP HOLLOW FIBERS ANNEALED IN VACUUM . . 225

TABLE 15 - ANNEALING IN VACUO FOR 6 HOURS 226

TABLE 16 - ANNEALING IN VACUO FOR 6 HOURS 227

TABLE OF CONTENTS CONTINUED

Page

TABLE 17 - ANNEALING IN VACUO FOR 6 HOURS 228

TABLE 18 - ANNEALING IN VACUO FOR 6 HOURS 229

TABLE 19 - GAS PERMEABILITY OF UNANNEALED PMP HOLLOW FIBERS 230

GAS PERMEABILITY OF PMP FLAT SHEET MEMBRANES 230

TABLE 20 - GAS PERMEABILITY OF PMP FLAT SHEETS 231

TABLE 21 - COEFFICIENTS IN EQ 1 FOR PMP 232

ACKNOWLEDGEMENT 232

REFERENCES 233

INTRODUCTION

Poly(4-methyl-1-pentene) is being used as a gas separation material in a nitrogen generation system which is being developed by Garrett AiResearch and Dow for the U. S. Air Force. This report summarizes an investigation into possibilities of modifying poly(4-methyl-1-pentene) so as to improve its performance in this application.

In a report to the Federal Aviation Administration, S. A. Manatt (1) of AiResearch Manufacturing Company of California, in collaboration with the Western Division of The Dow Chemical Company, had established that inertion of aircraft fuel tanks with nitrogen is an effective means of providing aircraft explosion prevention by reducing the concentration of oxygen in fuel tanks to levels below the threshold for vapor ignition. Among various possibilities considered, he showed that hollow fiber membranes from Dow made from poly(4-methyl-1-pentene) had the necessary balance of properties to be used as gas separation membranes in gas modules which would generate nitrogen aboard aircraft.

Early in ths work, Dow had cooperated with Garrett AiResearch on this project, and in September 1973, sufficient quantities of hollow fibers with repeatable geometry had been manufactured, and the decision to fabricate small-scale test units had been made (1).

Initially, Dow had worked as a subcontractor to Garrett AiResearch on a contract with the Federal Aviation Administration (DOT FA75WA-3658). At present, Dow is working as a subcontractor to AiResearch on their contract with the U. S. Air Force, Wright-Patterson Air Force Base, Ohio (Contract F-33615-77-C-2023). The objective of the current project is the development of a hollow fiber membrane-based inert gas generating system designed to meet the U. S. Air Force fuel tank inerting requirements.

Poly(4-methyl-1-pentene), the membrane material, is a polyolefin polymer. It is usually abbreviated PMP in the literature, but it is known also under the trade name TPX, under which it is sold commercially by Mitsui Petrochemical Company in Japan. Originally, TPX was a trade name of ICI (Imperial Chemical Industries) in England, which had introduced this new polymer commercially in 1965. Later, ICI had sold the technology and the trade name to Mitsui.

Although the properties of PMP are such as to make this material suitable for use in gas separation modules now, there is room for improvement. Particularly any improvement in gas separation performance which would allow a reduction in the weight of the gas module would be attractive in aircraft applications. Thus, the present investigation of various chemical and physical means of modifying PMP was undertaken and the effect of such modification on gas separation performance was studied.

BACKGROUND OF THE CHEMICAL MODIFICATION STUDY

Being a polyolefin, PMP is a polymer of relatively low creep resistance and of low chemical reactivity. Its low creep resistance limits the range of pressure and temperature under which it can be used in a gas separation module; its low chemical reactivity makes any attempts at chemical modification a challenge.

Polymer creep behavior is cold-flow under stress, whereby "cold" refers to approximately room temperature or to temperatures that are low compared to molding temperatures. On a molecular level, creep is a gliding of polymer chains past each other, thus slowly relieving internal stresses in the material. Creep is possible because the only restraining force is the mutual attraction of polymer chains to each other. More restraint is added to a polymer system, if the gliding of polymer chains is reduced or prevented by a positive locking action, eg. by crosslinks. A crosslinked polymer is a three-dimensional network, somewhat like a three-dimensional fishnet, in which all polymer chains are tied to all other chains by chemical bonds.

The classical example of a crosslinked polymer is vulcanized rubber, vulcanization being a name for a certain type of crosslinking. Unvulcanized synthetic rubber, such as polybutadiene, cold-flows, not unlike honey. It has some bouncing, elastic properties, but not nearly the elastic behavior for which rubber is known. The elastic behavior is introduced into this polymer by vulcanization, ie. by crosslinking. Crosslinking eliminates the cold-flow behavior of the unvulcanized polymer.

There are numerous examples in the literature where the effect of crosslinking on creep behavior has been demonstrated. In particular, creep in polyethylene, another polyolefin, can be reduced by crosslinking; thus, it seems reasonable to assume that the creep resistance of PMP also can be increased by crosslinking. However, while it is relatively straightforward to predict that crosslinking should increase the creep resistance of PMP, it is not as straightforward to actually introduce crosslinks into PMP, because not much prior knowledge on the chemical behavior of this polymer exists, and the chemical structure of PMP is significantly different from that of polyethylene for which crosslinking has been studied in great detail.

STUDY OF CROSSLINKING VARIABLES

Since PMP has no functional groups to which crosslinks could be attached, the immediate necessity was to study reactions which could be used to introduce functional groups into this polymer. These functional

groups could either serve directly as sites for crosslinking, or they could be used as centers for further reactions by which crosslinkable functions could be attached.

The following types of reactions have been considered:

Chlorination
Sulfochlorination
Grafting with Vinyl Alkoxy Silanes
Introduction of Double-bonds
Treatment with High Energy Radiation

In the selections of reactions to be evacuated, the goal was to develop a two-step process for crosslinking such that crosslinking sites would be introduced into PMP before spinning, and crosslinking would be induced after spinning of the fibers.

CHLORINATION

Chlorination of a polymer is carried out by exposing the polymer to chlorine gas and illuminating with a UV-light source. A simple sun lamp can be used for this purpose, but mercury lamps would be employed in larger-scale operations. The UV-light activates the chlorine by splitting chlorine gas molecules into radicals. The radicals abstract hydrogen atoms from the polymer (P), thus generating radicals along the polymer backbone which then react with chlorine to form chlorinated polymer and new chlorine radicals:

$$Cl_2 \xrightarrow{h\nu} 2\,Cl\cdot$$

$$P - H + Cl\cdot \longrightarrow P\cdot + HCl$$

$$P\cdot + Cl_2 \longrightarrow P - Cl + Cl\cdot$$

$$P\cdot + Cl\cdot \longrightarrow P - Cl$$

In order to achieve uniform chlorination, it is necessary to expose all portions of the polymer equally well to the chlorine gas. The best way to accomplish this is to dissolve the polymer in a solvent and then to sparge chlorine gas into the solution. If a polymer is not soluble, a slurry of the polymer in a liquid can be made. The polymer should be finely divided, eg. in the form of a powder. Since chlorination will start at the surface of the particles and gradually proceed inwards, the chlorination will not be uniform. A small particle size is advantageous in this process.

Chlorination in a slurry can be carried out in water or in an organic solvent. In water, the integrity of the polymer particles will remain, and the polymer will not become soluble at any point. In an organic solvent, typically in a chlorinated hydrocarbon such as carbon tetrachloride, the polymer will swell with the solvent, thus facilitating attack by the chlorine. The swelling increases as the chlorination proceeds leading eventually to complete dissolution of the polymer.

Polyolefins are partially crystalline polymers. The chlorination occurs at the amorphous regions and may not touch the crystalline regions at all or very little, unless the swelling effect of the solvent eventually disrupts the crystalline centers.

Chlorination of PMP was carried out in water and in carbon tetrachloride; it worked very well in both cases. The chlorinations were carried out in regular laboratory glass equipment using a 275 W Sylvania sunlamp as a light source. The results are shown in Table 1.

TABLE 1

CHLORINATION OF PMP

Ref.	Solvent	Chlorine Content %	Chlorine Capacity meq/g
T300	Carbon Tetrachloride	2.2	0.6
T322	Water	14.2	4.0
T301	Water	42.5	12.0

The variation in chlorine content was achieved by varying the time and speed of chlorine input.

These experiments demonstrate that chlorination of PMP poceeds with great ease. The chlorination can be expected to go to either one (or both) of the tertiary C-atoms in each monomer unit (see arrows):

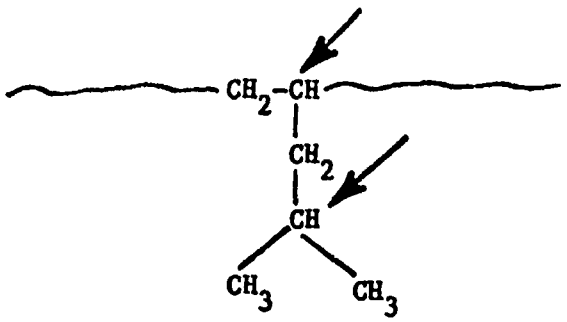

At 29.9% chlorine content (8.4 meq/g chlorine capacity), each monomer unit has, in the average, one chlorine atom, which is way above the needed amount. The objective is to chlorinate just enough to introduce a sufficient number of reactive sites without altering the properties of the polymer too much. If one assumes that chlorination of 2% of the monomer units is sufficient to give enough crosslinking sites, the desired chlorine content of the polymer would be 0.8%.

Chlorination at this very low level presents the problem of uniformity of the product because the chlorination is done in a heterogeneous system. Bromination was tried also, because bromination is usually slower and more selective than chlorination, but PMP brominates as easily as it chlorinates and the chlorination was not pursued further because it offered no real advantage.

Rather than fine-tuning the chlorination to achieve low chlorine content and uniformity of the product at this time, the decision was made to go on to the next planned experiments and to carry out reactions on the chlorinated PMP with the materials described in Table 1 above.

SULFOCHLORINATION

Sulfochlorination of paraffins (R-H) and cycloparaffins with sulfur dioxide and chlorine under illumination with UV light is known as the Reed reaction.

$$R\text{-}H + SO_2 + Cl_2 \xrightarrow{h\nu} R\text{-}SO_2Cl + HCl$$

This is a convenient reaction for introducing reactive groups into paraffins and thus activate these quite inert materials for further reactions.

In the polymer area, sulfochlorination has been used in order to introduce crosslinking sites into polyethylene. DuPont offers a commercial product under the trade name HYPALON, which is sulfochlorinated polyethylene. This material is a rubber and is chlorinated above the amount of chlorine needed in the $-SO_2Cl$ groups. In general, chlorinatin proceeds along with sulfochlorination, and the two reactions compare with each other.

Using the same standard glass laboratory equipment as with the chlorination experiments, PMP was sulfochlorinated by sparging sulfur dioxide (SO_2) and chlorine (Cl_2) into a dispersion of PMP in carbon tetrachloride using a 275 W Sylvania sun lamp as a light source. These are the same conditions as used in the sulfochlorination of polyethylene.

The resulting polymer contained 25.3% chlorine and 9.0% sulfur, i.e., a considerable amount of chlorination had occurred in addition to the sulfochlorination. If every monomer unit had one $-SO_2Cl$, and if no separate chlorination had occurred, the polymer would contain 19.4% chlorine and 17.6% sulfur and have a capacity of 5.5 meq/g of $-SO_2Cl$ groups. A sulfur content of 9% corresponds to a capacity of 2.8 meq/g of $-SO_2Cl$ groups.

If a goal is set such that 2% of the monomer units in the polymer chains have a functional group for crosslinking, a sulfur content of 0.75% and a chlorine content of 0.82% would be required.

This goal is realistic, because in commercial sulfochlorinated polyethylene 1% to 2.2% of the monomer units have a $-SO_2Cl$ group which corresponds to a sulfur content of 0.9-1.7% in that polymer.

(Sulfochlorinated polyethylene also contains typically 25-35% chlorine, which means that 25-42 of the monomer units have one chlorine atom attached and that the polymer is a rubber.)

Considerable fine-tuning of the sulfochlorination of PMP would be necessary in order to make a product which has the intended low levels of sulfur and chlorine and is still uniform. As with the chlorination, such fine-tuning work was postponed until further reactions of the sulfochlorinated PMP had been studied and, especially, until information on the thermal stability of this polymer had been obtained. The reactions described in the next section were carried out with the material (ref. T302) which contained 25.3% and 9.0% sulfur.

REACTIONS OF CHLORINATED OR SULFOCHLORINATED PMP

Chlorinated PMP and sulfochlorinated PMP can undergo essentially the same reactions with functional groups, such as amino groups, but the sulfochlorinated product would be more reactive than the chlorinated product. Typical reactions that can be done with these materials are as follows:

$$PMP\text{-}Cl + H_2N\text{-}R \longrightarrow PMP\text{-}NH\text{-}R + HCl$$

$$PMP\text{-}SO_2Cl + H_2N\text{-}R \longrightarrow PMP\text{-}SO_2NH\text{-}R + HCl$$

With a difunctional reagent such as diamine, the chlorine groups or sulfochloro groups could be used directly for crosslinking.

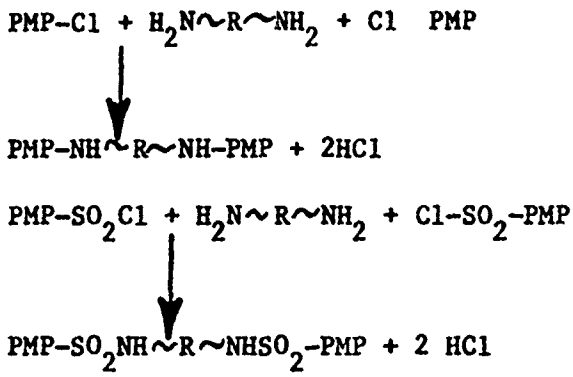

Reactions of this type have been carried out with HYPALON sulfonated polyethylene and are described in the literature. The resulting links are sulfonamide groups, which are very stable. Most aliphatic diamines react at room temperature in a few minutes or in a few hours, depending on their chemical structure. Aromatic diamines require curing at higher temperatures. Stable crosslinked networks are obtained in all cases.

If a spun fiber had chloro or sulfochloro groups, crosslinking could be achieved very easily by immersing the entire module into a solution containing a diamine and allowing this diamine to diffuse into the fibers to react and to cause crosslinking to occur.

Another alternative is to react a chlorinated or sulfochlorinated PMP with an amino compound which contains another functional group such that the amino group is only the link to the polymer while the newly introduced functional group is the actual precursors of the future crosslink.

Compounds useful for this purpose can be found among the so-called "coupling agents" offered by Dow-Corning and other companies. These coupling agents are silanes which have alkoxy silane groups together with a variety of other functional groups in the same molecule. They are used for treatment of glass surfaces, eg. in glass-reinforced polymers, in order to make glass more compatible with polymers. A Dow-Corning coupling agent, designated at Z-6020, which is of interest for the present project, is shown below:

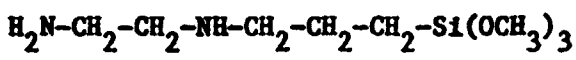

Z-6020

This compound can be used to introduce silane functionality into PMP by reaction with the chloro and/or sulfochloro groups as follows:

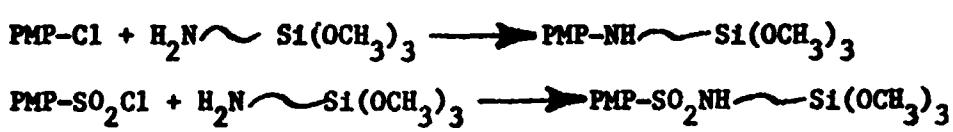

The silanated PMP could then be melt-spun in the usual way, if it were thermally stable, and the hollow fibers would crosslink spontaneously on exposure to water via silanol and siloxane chemistry:

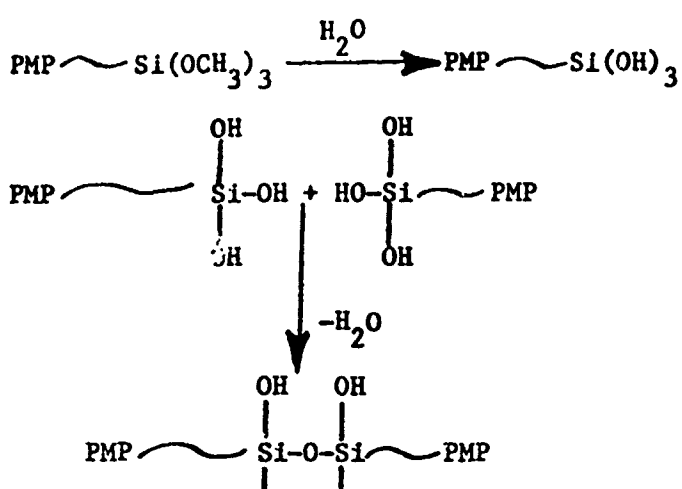

(The SiOH groups shown above will react further with each other to produce crosslinks.)

The chlorinated PMP samples listed in Table 1 and the sulfochlorinated PMP listed in the preceding section have been reacted with Dow-Corning Z-6020 silane and the resulting polymers have been analyzed for silicon as a criterion as to whether reaction had occurred. The results are listed in Table 2.

TABLE 2

REACTION OF CHLORINATION OR SULFOCHLORINATED PMP WITH DOW-CORNING SILANE Z-6020

Sample Ref.	Type	Polymer Ref.	Capacity meq/g	Z-6020 Input *) %	Silicon Analysis % Si
T305	PMP-Cl	T300	0.6	150	0.6
T306	PMP-Cl	T301	12.0	7.5	1.2
T309	PMP-SO_2Cl	T302	2.8	16	1.3

*) meq amino groups as % of meq -Cl or -SO_2Cl in the polymer.

The reactions were run in methanol under reflux (b.p. 65°C) for one hour. The column in Table 2 marked Z-6020 input shows the amounts of Z-6020 silane used as percent of the reactive groups available in the polymer. Thus, in run T305, a 50% molar excess of silane was used while in run T306 only enough silane was used to cover 7.5% of the chloro groups available in the polymer. These amounts were chosen, because the polymer used in run T305 had a low chlorine capacity which makes it

reasonable to react all of the chloro groups with the silane. However, in run T306, the polymer had a very high chlorine capacity and only some of the chloro groups would be needed for reaction with the silane. The same reasoning was applied in run T309 with a sulfochlorinated polymer. The reason for the variation of initial polymer capacity and amount of silane was to test how easily the silane would react with the polymer under the conditions used.

The results indicate that reaction did occur, and that the amount of silicon picked up by the polymer should be sufficient to ensure crosslinking via siloxane bonds when exposed to water. However, the uniformity of the distribution of the alkoxy silane groups over the polymer matrix is open to questions, because methanol is a non-solvent for the polymer. Thus, silanation may have occurred primarily on the surface of the polymer particles while the interior may still be full of unreacted -Cl or $-SO_2Cl$ groups.

Based on the chemistry of reacting an amino group with a chloro or sulfochloro group, the choice of methanol as a solvent is conventional, ie. methanol would be a good reaction medium if only low molecular weight organic compounds were involved. However, if a polymer is one of the reaction partners, the choice of solvent is dictated also by the solubility of the polymers. Solvents which dissolve PMP are not necessarily good reaction media for the reaction of an amino group with a -Cl or $-SO_2Cl$ group. Nevertheless, we tried to run this reaction in decalin which is the best solvent for PMP which we found so far. (Decalin is the standard solvent used in our crosslinking tests.) In order to get PMP to dissolve in decalin, or in any solvent, the polymer/solvent mixture must be heated, usually above 150°C. In decalin, we usually reflux (b.p. 192°C) when dissolving PMP or its derivatives.

Attempting to dissolve chlorinated or sulfochlorinated PMP in hot decalin led to decomposition of the polymer as evidenced by formation of dark-brown to black color. In this test, aminosilane-functionalized PMP was insoluble and, because of degradation, one could not decide whether the sample was crosslinked before being heated in decalin or whether crosslinking (and thus insolubilization) occurred as a result of degradation reactions.

THERMAL STABILITY OF RELATED POLYMERS

In order to obtain a feel for the temperature stability of a chlorinated or sulfochlorinated polyolefin, such as PMP, it helps to review the thermal behavior of related polymers, such as polyvinylchloride, chlorinated polyethylene, and sulfochlorinated polyethylene.

Unplasticized polyvinylchloride (PVC) is extruded customarily at temperatures at the die as high as 185-195°C. Chlorinated polyethylene is said to be more temperature-stable than PVC, particularly at lower levels of chlorination. Based on this information, one might expect chlorinated PMP to be at least somewhat stable in boiling decalin (b.p. 192°C), but it is not. The fact that decomposition of chlorinated PMP starts immediately after heating has commenced seems to idicate that chlorinated PMP is considerably less thermally stable than either chlorinated polyethylene or PVC. While this finding could not necessarily be anticipated, it can be rationalized, after the fact, on the basis of the chemical structure of PMP and its chlorinated derivatives.

A sulfochlorinated polymer, on the other hand, is expected to have a low temperature stability because organic sulfochlorides are known to decompose on heating. Sulfochlorinated polyethylene can be processed on standard equipment using ordinary procedures, but at lower temperatures. Thus, a "cool" extruder must be maintained with a barrel temperature of about 50-60°C and a head temperature of about 70-80°C. This is possible, because sulfochlorinated polyethylene is an unvulcanized rubber. It is known that sulfochlorinated polyethylene starts losing SO_2 and some HCl at 150°C and that all $-SO_2Cl$ groups are removed by heating in tetralin solution at 175°C for two hours. Thus, sulfochlorinated PMP was not expected to survive boiling in decalin at 192°C for any length of time.

PMP WITH DOUBLE-BONDS

When a chlorinated hydrocarbon is reacted with any base, including an amine, a dehydrochlorination can occur as well as substitution. Thus, for chlorinated PMP the following reaction pathways are possible.

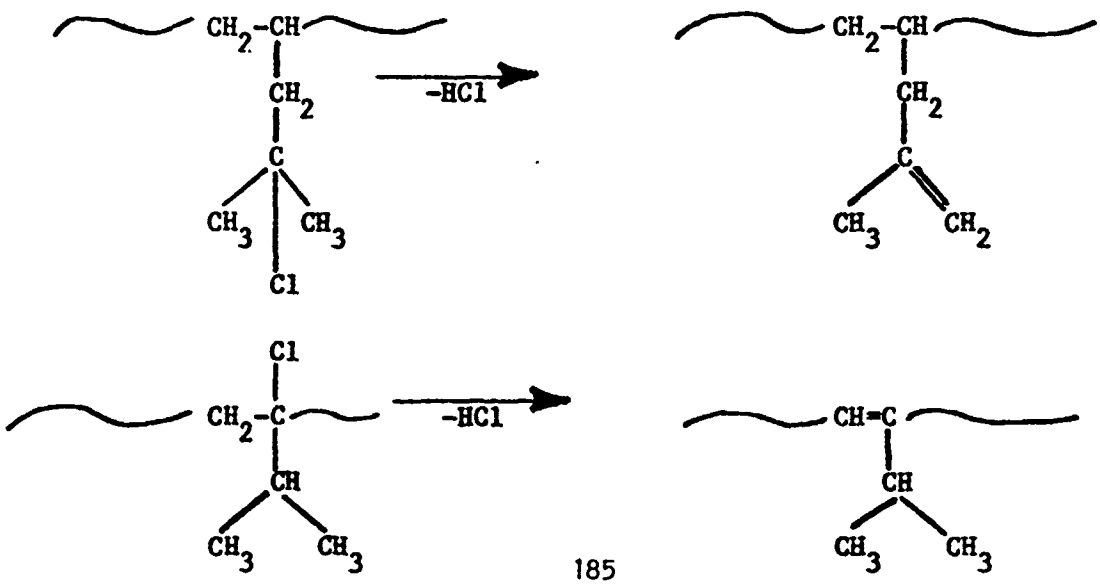

These reactions can occur either parallel to the reactions shown previously for an aminosilane functioning as a base, or they can occur mainly or even exclusively. Exclusive dehydrochlorination can be expected when a tertiary amine is used as a base.

This possibility suggests a method of making PMP which contains some double-bonds. In analogy to ethylene-propylene rubbers and Butyl rubbers which contain 3% double-bonds as sites for vulcanization (crosslinking), a PMP with 3% double-bonds could be made and could then be crosslinked using methods already established for ethylene-propylene and Butyl rubbers. (However, this approach would not permit a two-step process of the type where the final crosslinking is induced after extrusion.)

Dehydrochlorination of chlorinated PMP was tried using either pyridine of collidine as a base; both compounds are tertiary amines. Refluxing of a chlorinated PMP (14.2% clorine) in pyridine (b.p. 115°C) for 75 minutes produced a white polymer with a reduced chlorine content of 3.8% and an IR-spectrum which indicated the presence of double bonds. The dehydrochlorination was not complete, possibly because the polymer was not soluble in pyridine. This polymer was then dehydrochlorinated again, but this time by heating to 100-120°C in a mixture of decalin and collidine, in which it was soluble. The resulting polymer was white and the chlorine content had been reduced further to 2.7% chlorine. It appears that the dehydrochlorination becomes more difficult as the reaction proceeds towards completion. The white color of the polymer in both treatments is very encouraging because it suggests that degradation may not have taken place, or at least not to a detrimental degree.

This approach of producing a PMP with double bonds by a sequence of two reactions, namely chlorination followed by dehydrochlorination, could be useful for making smaller amounts of partially unsaturated PMP for experimental purposes. If large amounts of partially unsaturated PMP are needed, a better approach would be to make the polymer in house by copolymerization of its monomer, 4-methyl-1-pentene, with a comonomer that introduces double-bonds. As an example, Butyl rubber is made by cationic copolymerization of isobutylene with 3% isoprene. The copolymerization of 4-methyl-1-pentene would have to be carried out by Ziegler catalysis. The technology is available but it would require start-up time and setting up special equipment, and some experimentation would be necessary to establish the right comonomer to be used. Thus, if such work is to be done, the usefulness of the product should be established beforehand.

SOLVENTS FOR PMP

As pointed out earlier in this report, only very low levels of chlorination or sulfochlorination are required for introduction of

crosslinking sites into PMP, and it is difficult to achieve such low levels of reaction and still obtain a uniform distribution of the functional groups over the polymer. This problem exists because the chlorination and the sulfochlorination were carried out in a heterogeneous system, where the polymer is suspended but not dissolved in the liquid medium. Thus, chlorine can attack only on the surface of the polymer particles. In order to expose all points in all polymer chains to the chlorine, the polymer should be dissolved in a suitable solvent. The problem is that not too many solvents are suitable for PMP and for chlorination at the same time.

PMP, being a polyolefin, ie. a high molecular weight paraffin, dissolves best in another paraffin. Thus, decalin (decahydronaphthalin, a cycloparaffin) is an excellent solvent for PMP, but the polymer must be heated to above 150°C, better refluxed at 192°C, in order to dissolve. High heating is necessary in order to disrupt the crystallinity of PMP. Once dissolved in decalin, the solution can be cooled down to 30°C and still remain clear. At this point, the solution can be diluted with carbon tetrachloride or with methylenechloride without any problem. A 10% solution of PMP in decalin can be made easily.

Decalin is not a solvent normally used for chlorination, because it would itself be chlorinated. Typical solvents for chlorination are chlorinated solvents such as carbon tetrachloride or perchloroethylene, but these solvents do not dissolve PMP at room temperature.

We tried a number of solvents that could be used as media for chlorinating PMP. Perchloroethylene (b.p. 121°C) dissolved some PMP but reprecipitated it on cooling. Hexachlorobutadiene (b.p. 210-220°C) behaved in a similar manner, but it turned dark brown. o-Dichlorobenzene (b.p. 180°C) again showed similar behavior. 1,2,4-Trichlorobenzene (b.p. 214°C) was an excellent solvent for PMP; it dissolved a considerable amount of polymer and remained colorless, but the polymer precipitated from solution on cooling to room temperature. Hexachlorobenzene was also tried, even though this compound is a solid and is not normally considered a solvent. We thought that it may dissolve PMP in the melt. However, the mixture turned black and gassed. Thus, it was totally useless.

The best solvents for PMP found so far were decalin and 1,2,4-trichlorobenzene. Both dissolve PMP when hot, but only decalin retains the polymer in solution on cooling to room temperature.

GRAFTING WITH VINYL ALKOXY SILANES

Polyethylene (PE), the oldest of the polyolefin polymers, has been crosslinked traditionally with peroxides or high-energy radiation. More recently, a two-stage crosslinking process has been developed by Dow-Corning (through Midland Silicones) (2) for crosslinking of

polyethylene in wire-coating operations. Similar processes have been developed also in Germany, Japan, and France (3-5). All of these processes work apparently very well, because they are being used in large-scale extrusion operations. However, they have been used commercially only for polyethylene.

The chemistry involved in this two-step process comes from two independent areas of polymer science, namely from the area of "graft copolymers" and the area of "silicone rubbers". These operations are carried out in sequence on molecules whose molecular architecture is such that one end of the molecule can "graft" while the other end can crosslink, forming bonds which are encountered also in silicone rubbers. The molecules making this approach possible are the "vinylalkoxysilanes", shown schematically below:

The waved line represents any molecular structure that connects the two essential groups, i.e.,the vinyl group, CH_2=CH-, and the alkoxysilane group, -Si(OR)$_3$. In addition to plain vinyl groups, methacrylato groups are used also, but these are variations of vinyl groups for all practical purposes.

"Grafting" is a term used in polymer science for an operation involving the attachment of one polymer chain to another, analogous to the grafting of a branch of an apricot tree to the trunk of a peach tree. In this analogy, the trunk is the polyethylene, and the grafted branch is the vinyl silane. The point of attachment is the vinyl group, i.e., the CH_2=CH- group. In order for the grafting to work, the trunk polymer must be activated, i.e.,reactive centers must be created along the polymer chain. The activation is more difficult with polyolefins than with most other polymers, because polyolefins are high molecular weight paraffins, and the word "paraffin" means "little affinity", i.e., denoting a relatively unreactive material.

While the vinyl group, CH_2=CH-, is the active group in vinyl polymerizations, the alkoxysilane group, -Si(OR)$_3$, is one of the basic groups in the chemistry of silicone rubbers. This group is most often a trimethoxysilane group, -Si(OCH$_3$)$_3$, but triethoxysilanes, -Si(OC$_2$H$_5$)$_3$, are employed as well. These groups hydrolyze spontaneously upon exposure to water under formation of silanol groups, -Si(OH)$_3$. The silanol groups condense with each other under elimination of water, thus forming a three-dimensional crosslinked network. Curing catalysts are often used to speed up the crosslinking process. The chemistry works as follows:

Hydrolysis:

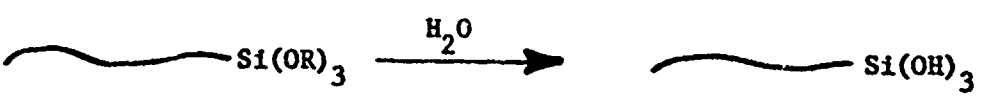

Crosslinking:

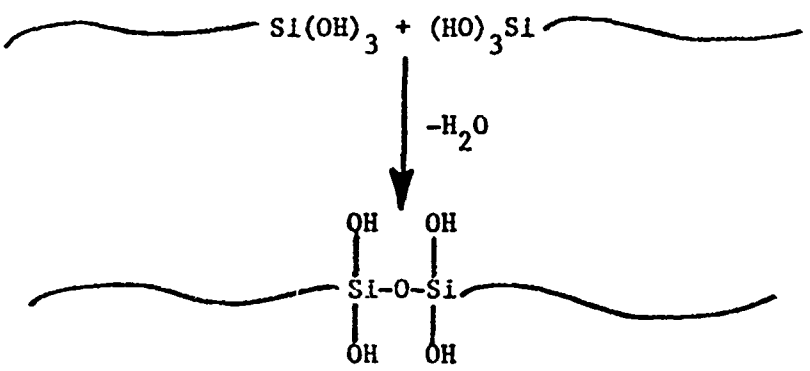

As the condensation process goes on, more and more siloxane (Si-O-Si) bonds are formed, and a three-dimensional network is built up. This network is not shown in the reaction scheme because it is too elaborate to be drawn.

The silicone chemistry of this process is well known. A popular example of a practical application is the silicone rubber caulking compound used around bathtubs; this is a good illustration of the gradual build-up of the three-dimensional crosslinked polymer network during the curing process.

The silicone chemistry portion of the vinylsilane crosslinking process should be no problem when applied to PMP. However, problems may be encountered with PMP in the grafting portion of the process because in the grafting step the difference in chemical structure between PMP and PE becomes apparent.

PMP is significantly different from PE not only in its chemical structure and thus in its chemical behavior, but also in its physical properties. Particularly the crystalline melting point of PMP (about 240°C) is much higher than that of PE (109-125°C for low density PE and 130-135°C for high density PE). This difference in melt temperature requires the use of peroxides of higher thermal stability for PMP as compared with PE.

Grafting affects the degree of crystallinity in crystalline polymers, such as PE and PMP. This effect may be more important in the application of PMP in a gas separation membrane than in the application of PE in the wire and cable industry because it may influence the gas permeation properties and the separation factor.

Thus, we were looking for answers to two questions:

1. Can PMP be grafted with a vinyl alkoxy silane?

2. If it can, will the grafting affect the properties of PMP in a way that may be detrimental in its application as a gas separation membrane?

The first question had been addressed earlier to Dow-Corning who made a $10,000 research effort in 1976 and came to the tentative conclusion that the silane grafting/crosslinking process is applicable to PMP. At that time, Dow received from Dow-Corning a very brief report stating that one formulation of PMP, a vinylsilane, and a peroxide had produced a crosslinkable material on a very small scale (40 g of polymer). This formulation was the only one which was claimed to work, and the process could not be scaled up at Dow-Corning because of excessive foaming of the polymer as it left the extruder die. Other formulations had been studied also by Dow-Corning but were not disclosed in the report to Dow because of a clause in the agreement between Dow and Dow-Corning which prevented this disclosure.

The silane crosslinking process, as practiced with polyethylene, is carried out in an extruder. Typical temperatures in the extruder barrel are 177-184°C, according to the main Dow-Corning patent. The hollow fiber spinning process used at Dow for making PMP hollow fibers also is an extrusion process, but the temperatures required are much higher because of the higher crystalline melting point of PMP.

The boiling point of the silane used by Dow-Corning (Z-6030) is 190°C. It seemed advisable to keep the silane under pressure, eg. in the inside of an extruder, in order to prevent it from boiling off. Thus, our initial plans called for grafting in an extruder. Since polymer pellets and liquids are difficult to extrude together, we decided to employ the PMP in the form of a powder rather than pellets and thus ensure better extrusion and more uniform distribution of the silane and the peroxide throughout the polymer. However, PMP turned out to be unavailable in powder form, although polyolefin polymers are normally obtained as powders in the polymerization process. Therefore, the work presented in this report was being done using PMP pellets but employing a Brabender mixer rather than an extruder.

The small-scale work done at Dow-Corning had been carried out in a Brabender mixer. This mixer is a small stainless steel unit, electrically heated, and having two curved blades rotating in a mixing chamber. The mixing chamber is open at the top which means that evaporation of liquids is possible; thus, it is possible to lose some of the vinylsilane by evaporation. Since this mixer, particularly because of its small size, is a convenient tool for small-scale screening operations such as trying out various silanes and peroxides, we carried out a number of preliminary experiments, particularly in order to evaluate how much of a problem a loss of silane by evaporation would be at the high blending temperatures that had to be used. These preliminary experiments convinced us that the potential evaporation loss

was not as severe a problem as we had feared. Evaporation of silane is minimized in this mixer because the blending action is so efficient and the heat transfer is so rapid that the silane is blended into the polymer so fast that it dissolves in the molten polymer before it has a chance to evaporate. Once dissolved, its vapor pressure decreases because it forms a one-phase mixture with the molten polymer.

The formulation described by Dow-Corning as successful in their preliminary experiments became the point of departure for our experiments. In our first experiment, we used the Dow-Corning formulation with exactly the same materials, quantities, equipment, and conditions described by Dow-Corning.

The PMP was used in the form of pellets (Mitsui TPX, grade DX-810). The silane was a Dow-Corning material, designated as Z-6030. The structure of this material is shown below:

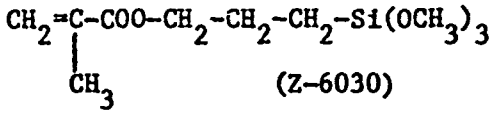

(Z-6030)

The generic name of this compound is γ-methacryloxypropyl trimethoxysilane.

The peroxide was a cyclic peroxyketal, manufactured by Witco Chemical Company, U.S. Peroxygen Division, and designated as USP-130. The chemical structure of this material is shown below:

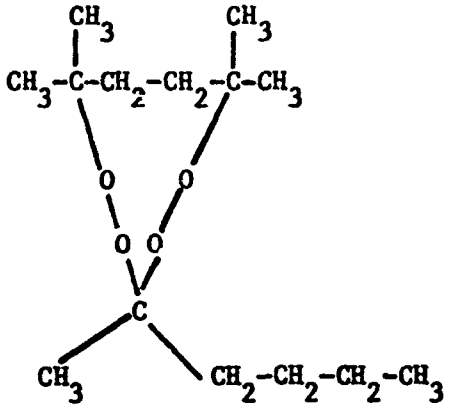

(USP-130)

The material had been designated as USP-130D in the past, when it was still in the developmental ("D") stage.

The formulation was as follows:

40.0 g	PMP pellets	=	100%
1.2 g	DOW-Corning Z-6030 silane	=	3%
0.16 g	USP-130 Peroxide	=	0.4%

All components were mixed in a glass bottle with screw-cap and allowed to stand for 24 hours to allow for as much equilibration as possible and to permit at least some of the silane liquid to penetrate into the polymer.

The Brabender mixer was preheated to 270°C, and half of the mixture was added and mixed until the polymer just melted. Then, the remaining half was added, and the entire mass was melt-blended for six minutes at 270°C. After this time, the polymer was removed from the mixture and was allowed to cool to room temperature.

The polymer was now ready for the crosslinking test. As described above, we had tested the solubility of PMP in a number of solvents and had come to the conclusion that decalin, which boils at about 192°C, is the best solvent for this polymer and for the intended purpose. Thus, we dissolved the Brabendered polymer in decalin under reflux: it was completely soluble, indicating that no premature crosslinking had taken place.

For crosslinking to occur, the polymer has to be exposed to water, preferentially at elevated temperature in order to speed up the curing process. We prepared films from the silane-treated polymers and boiled these films in water, usually for about 24 hours. In most experiments, a small amount of hydrochloric acid was added as a condensation catalyst. The polymers were made into a film in order to ensure maximum surface exposure to water and also to decalin in the subsequent re-dissolving test.

Films were prepared from the Brabendered PMP by pouring the solution of the polymer in decalin onto a glass plate and immersing the plate in absolute ethanol. The ethanol precipitates the polymer and extracts the decalin, thus leaving a porous film with a large surface area.

The film was boiled in water and was then dried and boiled in decalin again to check whether the polymer had become crosslinked and thus had become insoluble. The result was that the polymer dissolved completely in the decalin, indicating that it was not crosslinked at all.

Another test was performed which was designed to determine whether the silane was chemically attached to the polymer or whether it had not reacted at all. For this test, the solution of the Brabendered polymer in decalin was diluted, either with n-hexane or with methylene chloride, and the polymer was precipitated as a fine, white, stringy material by pouring the solution slowly into absolute ethanol under stirring. The polymer was collected, dried in vacuo, and submitted for silicon analysis. Any unreacted silane would remain in the solvents and would thus be removed from the polymer. If the reprecipitated polymer contained any silicon, it would have to be in a polymeric form, since it had survived the reprecipitation. Thus, the silane could either have formed a graft copolymer with the PMP, or it could have formed a homopolymer.

Two silicon analyses were obtained for this first polymer one from a sample diluted with methylene chloride and one diluted with n-hexane. The results were 0.2% Si and 0.3% Si, respectively. The difference is within the range of experimental error of the analysis.

These analytical results indicate that most of the silane had survived the reprecipitation and was thus in the form of a polymer; calculation

of % Si for the combination of 1.2 g silane and 40 g PMP gives 0.33% Si for the total mixture. However, the silane was incorporated into the polymer, or polymer mixture, in a form that did not lead to crosslinking.

Two questions arise: In which way is the silicon incorporated into the polymer? and: What is the reason for the disagreement between our results and those of Dow-Corning?

Our immediate suspicion was that the "gel" measured at Dow-Corning may not have been crosslinked polymer, but simply undissolved polymer, i.e., that the crosslinking test used at Dow-Corning may not have been rigorous enough. How this "gel test" had been performed was not described in the letter to Dow, and this information is no longer available.

We turned to the main Dow-Corning patent, U.S. Pat. 3,646,155 (February 29, 1972), on the silane crosslinking process for a clue. This patent describes crosslinking of polyethylene (PE) by the silane method, but does not mention PMP. The patent discloses that the proportion of insoluble gel was measured by refluxing a sample in xylene for 20 hours; the proportions of polymer and xylene were not given.

Since we had established by our solubility experiments that PMP is soluble in hot decalin at a concentration of 10%, we tried to dissolve PMP and PE in xylene at 10% concentration. (The boiling point of xylene is about 140°C, while the boiling point of decalin is about 192°C. The exact boiling points depend on the mixture of isomers.) It turned out that PE dissolved easily in xylene at 10% polymer concentratin, but PMP was only incompletely soluble, leaving a gel-like portion of undissolved polymer behind. Thus, xylene seems to be a much better solvent for PE than for PMP. However, in a very dilute solution, PMP does dissolve completely in xylene without leaving a residue.

A possible explanation of the discrepancy between our results and the results obtained at Dow-Corning in 1976 is that our crosslinking test was much more rigorous and severe than the test used at Dow-Corning. However, if a polymer is truly crosslinked, it should be insoluble in all solvents at all temperatures. It may swell to different extents in various solvents and at various temperatures, but it should not dissolve. On the other hand, a non-crosslinked polymer that is swollen with a solvent and is incompletely dissolved or is in the process of dissolving can appear as a swollen, crosslinked polymer, if it is not treated with solvent rigorously enough.

In order to check our technique, we grafted polyethylene with a silane and crosslinked by exposure to water, following Example I of the Dow-Corning patent cited above but using a Brabender mixer instead of an extruder, and accordingly, a smaller scale. Thus, 40 g of PE were mixed with 1.2 g of vinyltriethoxysilane and 0.05 g of dicumylperoxide (Luperox 500), and the mixture was blended for 5 minutes at 180°C in the Brabender mixer as described above for one experiment with PMP. The

resulting polymer was boiled in water and tested for insolubility in xylene. The result was that PE was completely crosslinked. Thus, the problem appears to be with the polymer rather than with the technique.

Vinyltriethoxysilane was used in the experiment with polyethylene, because this is the silane specified in the Dow-Corning patent. This silane has a boiling point of about 160°C, which is acceptable with PE in the open Brabender mixer inspite of the mixing temperature of 180°C, because the blending is so rapid that the silane dissolves in the polymer before it has much of a chance to evaporate. For PMP, at a blending temperature of 260-270°C, the low boiling point of 160°C may present a problem. On the other hand, to use a vinylsilane rather than a methacryloxy silane is attractive, because the vinyl group has different chemical properties. It is known that a vinyl group attached directly to a silicon atom does not polymerize, but it does graft, as the Dow-Corning patent demonstrates. Thus, a vinylsilane may graft to the polyolefin, attaching only single silane groups, and not form any homopolymer.

In order to raise the boiling point and still employ a vinylsilane, we evaluated vinyltris(methoxyethoxy)silane, which is sold by Dow-Corning under the designation Z-6082. The chemical structure of this compound is shown below:

$$CH_2=CH-Si(OCH_2-CH_2-O-CH_3)_3 \qquad \text{(Z-6082)}$$

Thus, the structure of this compound is very similar to vinyltriethoxy silane, but its boiling point is about 125°C higher, namely 284-286°C.

The evaluation of a high-boiling silane was done in the Brabender mixer, using the same procedure as described above. Thus, 40 g of PMP pellets (TPX, DX-810) were mixed with 1.2 g of Dow-Corning silane Z-6082 and 0.16 g of Witco USP-130 peroxide, and the mixture was melt-blended at 270°C for five minutes. The resulting polymer was reprecipitated by dissolving in hot decalin and precipitating with absolute ethanol in order to remove all unreacted silane. Analysis of the dried polymer gave 0.2% Si. The calculated amount of silicon, for the case that all of the silane had reacted, would be 0.25% Si. Thus, most of the silane had become part of the polymer. However, the polymer could not be crosslinked: after boiling a film in water, the film was still soluble in hot decalin.

The relatively high processing temperature necessary for PMP may create a problem with respect to the peroxide. If the peroxide decomposes too fast, it may be exhausted in the initial few seconds, or even fractions of a second, of the grafting reaction and may have disappeared before it had a chance to initiate grafting. Thus, literature data on the temperature stability of a peroxide is usually expressed by its "half-life", i.e.,the time after which half of the initial amount of peroxide is still undecomposed at a certain temperature. The half-life is expressed either as a half-life time at a certain temperature or as a half-life temperature at a certain time interval. Data are available for half-life temperatures of various peroxides after time intervals of 1 min., 1 h, 10 h, and 100 hours. However, the available data do not

extend to the high processing temperatures, 260-270°C, required for PMP because such high processing temperatures are unusual for polyolefins. The so-called "high-temperature" peroxides were developed mainly for crosslinking polyethylene, which is processed at temperatures of about 180-185°C or less. Available data can be extrapolated to higher temperatures on the basis of the following equation:

$$\ln t_{1/2} = \frac{E}{RT} + B \qquad (1)$$

which related the half-life time, t_{12}, to the temperature T; E, R, and B are constants, where R is the gas constant, E is an activation energy, and B is a constant of the particular system.

Table 3 gives a list of some commercially available peroxides which are of interest for the present project. These peroxides were selected from the considerable number of available peroxides on the basis of their chemical structure and half-life data. The chemical structure should be such that the radicals formed upon decomposition have a high probability of abstracting hydrogen atoms from polymers, thus initiating grafting; the half-life temperatures are simply the highest that can be found with commercially available peroxides.

TABLE 3

HALF-LIFE DATA OF SELECTED COMMERCIAL PEROXIDES

Peroxide	Half-Life Temperature, °C		
	1 Min.	10 h	100 h
2,5-dimethylhexane-2,5-dihydroperoxide	257	154	126
Cumenehydroperoxide	255	158	132
Witco USP-130(1)	201	130	-
di-tert. butylperoxide	193	126	106
di-tert. butylhydroperoxide(2)	179	121	104
dicumylperoxide	171	117	101
Witco-333P(3)	169	111	-
tert. butylperbenzoate	166	105	87
benzoylperoxide	133	72	54

(1) 17.3 h at 125°C; 1 h at 154°C.
(2) contains about 20% di-tert. butylperoxide.
(3) forms tert. butoxy radicals.

The data in Table 3 were plotted on semi-logarithmic paper, shown in Figure 1, in order to determine the constants E and B in equation 1. Based on these constants, half-life times at 270°C were calculated. These calculated data are listed in Table 4.

TABLE 4

HALF-LIFE TIMES AT 270°C CALCULATED FROM FIGURE 1 WITH EQUATION 1

Peroxide	t_{12}, sec
2,5-dimethylhexane-2,5-dihydroperoxide	24
Cumenehydroperoxide	24
Benzoylperoxide(1)	(4)
Witco USP-130	2.9
di-tert. butylperoxide	2.5
Witco USP-333P	0.7
dicumylperoxide	0.6

(1) This figure, 4 sec., was obtained from the slope in Figure 1. However, it is difficult to believe that this slope is real, because there is no apparent reason for this slope to be different from those of the other peroxides. Thus, the input data on benzoylperoxide may not be correct.

The Dow-Corning patent on silane grafting/crosslinking of PE lists dicumylperoxide as the preferred grafting catalyst and an operating temperature of 182-184°C. Table 3 lists a half-life of one minute for a temperature of 171°C; thus, at the preferred processing temperature, the half-life is somewhat less than one minute. The patent teaches that the half-life of the peroxide used in the process should be less than 6 minutes and preferably less than one minute; a lower limit is not given, but common sense would suggest that very low half-lifes, such as a few seconds or fractions of a second would be unsuitable.

According to Table 4, dicumylperoxide has a half-life of only 0.6 seconds at 270°C, i.e., at the processing temperature of PMP. Thus, half of all the catalyst has decomposed within the first second of the grafting reaction. The fast disappearance of the catalyst very probably makes this peroxide unsuitable for use with PMP. However, the fact that it does work with PE shows that the radicals formed from dicumylperoxide are suitable for attacking the PE chain.

FIGURE 1

HALF-LIFE DATA OF SELECTED COMMERCIAL PEROXIDES

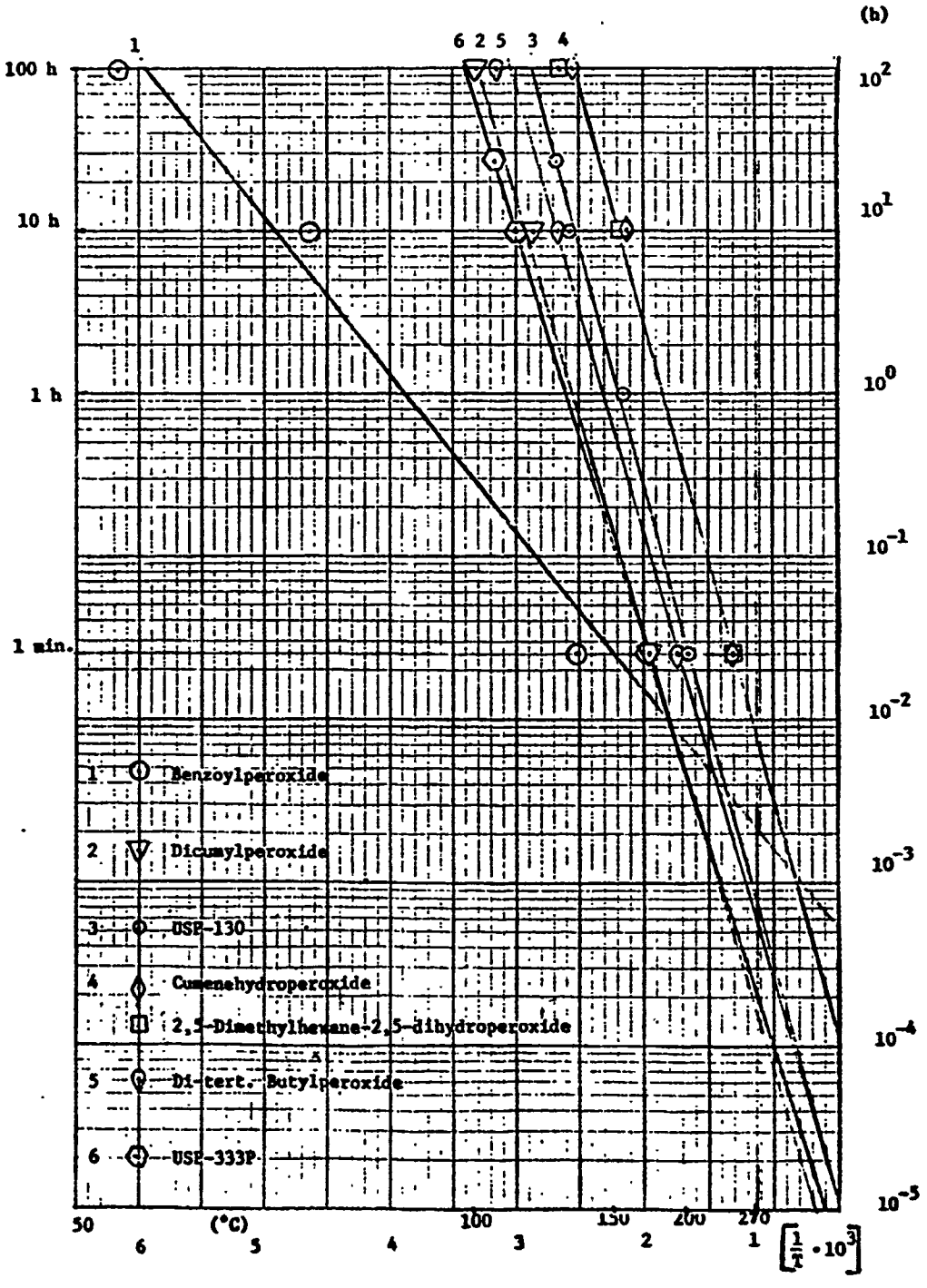

The same radicals, together with hydroxyl radicals, are formed from cumenehydroperoxide, but with a half-life of 24 seconds at 270°C (Table 4). Thus, cumenehydroperoxide might be suitable for grafting PMP on the basis of half-life temperature and chemical structure. 2,5-dimethylhexane-2,5-dihydroperoxide (Table 4) has the same half-life temperature, i.e.,24 seconds at 270°C, but it forms rather bulky radicals which may be subject to sterical hindrance. However, it also forms hydroxyl radicals which are small and aggressive and could initiate grafting. Thus, both of these two high-temperature peroxides were evaluated in this project for grafting of PMP with silanes.

Using the recipe described above, cumenehydroperoxide (CHP) and 2,5-dimethylhexane-2,5-dihydroperoxide (2,5-D) were evaluated with the two Dow-Corning silanes, Z-6030 and Z-6082. Thus, 40 g PMP pellets (TPX, DX-810) and 1.2 g silane (3%) were mixed with 0.16 g peroxide (0.4%) and melt-blended in a Brabender mixer at 270°C for ten minutes. The melt-blending time was increased to ten minutes, as compared to runs with lower-temperature peroxides, because the peroxides are available longer and the polymer would have a longer useful grafting exposure.

The work-up and crosslinking test were the same as in previous experiments, i.e., reprecipitation from decalin/abs. ethanol, boiling in water, and trying to dissolve again in hot decalin. In all of these experiments, the polymers dissolved in decalin after boiling in water. Thus, they were not crosslinked.

Our next step was considering the effect of the antioxidant.

PMP is quite sensitive to oxidation and must be stabilized by incorporation of an antioxidant. The function of an antioxidant is to intercept the radical chain reactions occurring during oxidation. Unfortunately, since an antioxidant is a radical chain stopper, it also interferes with the grafting reaction.

There are essentially three ways around this problem:

1. to buy unstabilized PMP and use it immediately, i.e.,before it has a chance to oxidize much.

2. to overpower the antioxidant with peroxide.

3. to remove the antioxidant from the commercial-grade polymer.

Regardless of what method is to be used, the polymer must be stabilized by addition of new antioxidant after the grafting reaction. This could be done during the extrusion spinning of the hollow fibers.

The first approach turned out to be unfeasible, because Mitsui refuses to sell any unstabilized MP, giving as a reason that it deteriorates very fast. The second approach is common in the polymerization of inhibited monomers. Commercial monomers are shipped with a polymerization inhibitor. The inhibitor is overpowered, in the initial phase of the polymerization, with the radicals which form either by decomposition of a catalyst, such as a peroxide, or thermally. The

third approach would be a last resort becausc it requires tedious work and would make the process quite expensive.

Three series of experiments were done with increasing peroxide concentrations under otherwise the same conditions which were described above, except that the melt-blending temperature was lowered to 260°C because experience had shown that sufficient blending could be obtained at this somewhat lower temperature. The charge to the Brabender mixer was again 40 g PMP-pellets (Mitsui TPX DX-810), and the silane was Dow-Corning Z-6030 (1.2 g = 3%) for all experiments. The peroxide concentration ranged from 0.4 to 3%, based on the amount of PMP. Three peroxides were employed, namely USP-130, CHP, and 2,5-D. (The abbreviations were explained in the text above.) These experiments are summarized in Table 5.

TABLE 5

PMP/SILANE Z-6030 GRAFTING EXPERIMENTS
AT VARIOUS PEROXIDE LEVELS

Run No.	Peroxide %	Peroxide Type	Observations	Crosslinked after H_2O
T324	0.4	USP-130	smoothly running	no
T341	1.0	USP-130	smoothly running	no
T330	0.4	2,5-D	smoothly running	no
T346	1.0	2,5-D	smoothly running	no
T348	2.0	2,5-D	more viscous	no
T350	3.0	2,5-D	very viscous	no
T345	1.0	CHP	smoothly running	no
T347	2.0	CHP	more viscous	no
T349	3.0	CHP	very viscous	no

A definite effect, judged visually, of the peroxide level was observed during Brabender mixing. At the low peroxide levels the melt blended smoothly, but as the peroxide level increased the molten polymer became more and more viscous. This behavior suggested, as an immediate explanation, that the peroxide itself started to crosslink the polymer. However, the polymer remained soluble and no molecular weight build-up occurred. (The effect of the peroxides on molecular weight will be discussed in a subsequent report.)

For the crosslinking test, the Brabendered polymer was compression-molded into sheets at 260°C. The sheets were boiled in water for 24 hours and then exposed to hot decalin. The polymer was completely soluble. Thus, crosslinking had not occurred either on exposure to water or under the influence of the peroxides.

For the third possible approach, the removal of antioxidant from the commercial polymer, PMP (Mitsui TPX, DX-810) was dissolved in hot decalin and precipitated with absolute ethanol. The reprecipitated polymer was dried in vacuo. The antioxidant should be removed completely from the polymer by this procedure; it remains dissolved in the solvents when the polymer precipitates.

The reprecipitated polymer was melt-blended with Z-6030 silane and USP-130 peroxide (0.4%) in the Brabender mixer at 260°C for five minutes. Compression-molded sheets were prepared as described above and boiled in water for 24 hours. The sheets were still soluble in hot decalin, thus, no crosslinkig had occurred, inspite of the absence of antioxidant. These experiments show that interference of the antioxidant with the silane grafting reaction is not the only cause for the failure to crosslink.

The behavior of PMP at high levels of peroxide is distinctly different from that of polyethylene. According to the Dow-Corning patent cited above, peroxide levels higher than 0.75% are undesirable with PE, because PE begins to crosslink prematurely, i.e.,in the extruder, under the influence of the peroxide alone, thus defeating the purpose of the silane crosslinking method. In contrast to this behavior, PMP does not crosslink even at 3% peroxide.

Under all the conditions studied, polyethylene either would have given a crosslinkable polymer after grafting with the vinyl alkoxy silane or would have crosslinked directly. In contrast, PMP did not crosslink under any of these conditions. Thus, the experiments described above led to the conclusion that PMP cannot be crosslinked by the vinyl alkoxy silane process. Reasons for the apparent difference in behavior of PE and PMP will be discussed later in this report.

IRRADIATION OF PMP

Crosslinking of polymers can be affected by high-energy radiation. The common radiation sources are the Van De Graaff generator, which produces beta-radiation (accelerated electrons), and the Cobalt-60 source, which produces gamma-radiation (electromagnetic waves). Both types of radiation have the same effect of polymers: they abstract hydrogen atoms by splitting C-H bonds, thus leaving C-radicals behind. Unfortunately, C-C bonds are split as well, thus leading to chain scission, i.e., polymer degradation. Chain scission can be induced also by secondary reactions of the C-radicals, which will be discussed later.

In the polyolefin series, two main types of response to radiation have been observed (1): crosslinking and degradation. Both types of response can occur simultaneously within the same polymer but if the crosslinking reactions exceed the chain scission reactions, the end effect will be a crosslinked polymer.

PE responds to radiation by crosslinking, while poly(i[illegible]tylene) responds by degradation. Other polymers, such as polypropylene, are between these two extremes. Chapiro (6) and Lenz (10) pointed out that the difference in behavior is related to the number of substituents along the polymer chain. PE has no substituents, ergo: it crosslinks. Poly(isobutylene) has two methyl groups on every second C-atom, ergo: it degrades. Polypropylene has one methyl group on every second C-atom, ergo: it shows intermediate behavior. PMP is not mentioned in either Chapiro's or Lenz's book.

The dose required for crosslinking PE generally lies in the range 3-10 Mrad dependent primarily upon the initial molecular weight of the polymer (29).

A search of the literature led to two papers dealing with the effect of gamma-radiation on PMP. Pinkerton and Whelan (7) irradiated PMP at room temperature with a dose of 10 Mrad from a Co-60 source either in vacuo or in the presence of oxygen. They reported that oxygen inhibits crosslinking, but that crosslinking can be obtained in vacuo. They also irradiated at low temperatures (77°K) in vacuo and found a radical of structure I. This radical was unstable and converted rapidly to the radical of structure II as the sample warmed up. The conversion was irreversible.

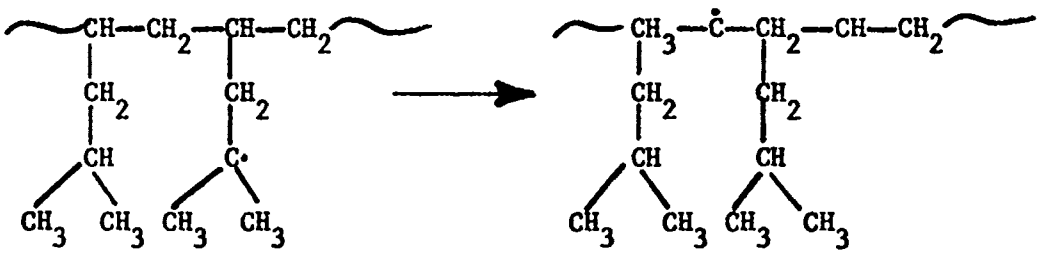

I II

Irradiation of PMP in vacuo at room temperature yielded hydrogen, methane, propane, n-butane, and isobutane, indicating degradation of the polymer. Evidence of crosslinking was not presented as mechanical property data were not included (the paper was only a short communication).

Cianetti and Vinciguerra (8) irradiated various polyolefins with doses ranging from 5 to 50 Mrad from a Co-60 source and characterized the samples by differential thermal analysis. They defined a so-called "significant temperature", T_s, whose decrease is indicative of polymer degradation. Their results are shown in Figure 2. As the data show, significant degradation of PMP occurs above 10 Mrad, while the other polyolefin polymers are relatively stable. Some degradation occurs also below 10 Mrad, which is in agreement with the data of Pinkerton and Whelan (7). The effect of the irradiation on crosslinking was not reported.

Figure 2

Degradation of Polyolefins under Gamma-Radiation

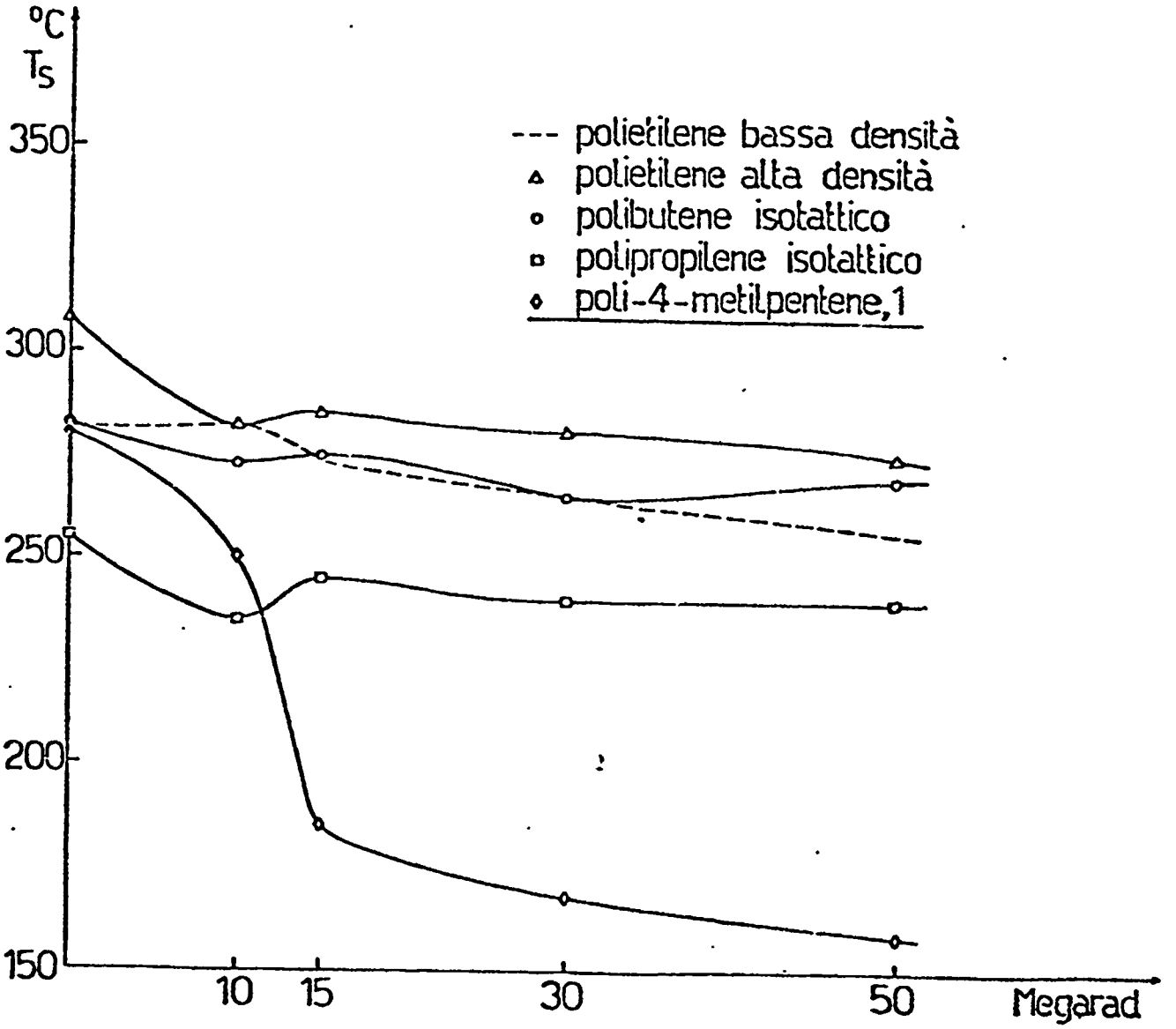

From: E. Cianetti and N. L. Vinciguerra, Rassegna Chimica, 24, 300 (1972).

T_S = "significant temperature", a temperature related to polymer weight loss.

A decrease in T_S indicates polymer degradation.

Even though PMP obviously degrades, the literature data do not exclude the possibility that crosslinking also occurs, particularly in view of Pinkerton and Whelan's mentioning of crosslinking upon irradiation under vacuum. For practical applications, irradiation under vacuum is not easy to do, but irradiation under nitrogen is feasible. Thus, we irradiated samples of commercial PMP (TPX, DX-810) under nitrogen with a Van De Graaff generator. The difference between this apparatus and a Co-60 source lies not so much in the effect produced on the polymer, but in the dose rate and the depth of penetration. A Van De Graaff generator delivers a high dose fast, but the radiation does not penetrate deeper than a few millimeters, while the Co-60 source delivers deeply penetrating radiation at a slow dose rate.

Thin sheets (0.2-0.24 mm) of PMP were prepared by compression molding. These sheets were irradiated with doses of 5, 10, and 15 Mrad under nitrogen at room temperature with a Van De Graaff generator. The samples did not change their visual appearance. The irradiated samples were boiled in decalin (192°C) to check for insolubility resulting from crosslinking. All samples were completely soluble, indicating that crosslinking had not taken place.

EFFECT OF PEROXIDES ON PMP

The primary reaction of peroxides is homolytic cleavage, caused by heat, which produces two free radicals per molecule:

$$ROOR \longrightarrow 2\ RO\bullet$$

The exact structure of the formed radicals depends on the type of peroxide. Different radicals have different reactivities; particularly their power to abstract hydrogen from polymer chains depends very much on their structure.

In the presence of a polymer, P-H, peroxide radicals can abstract hydrogen and thus create radical centers on the polymer:

$$RO\bullet + P\text{-}H \longrightarrow P\bullet + R\text{-}H$$

The polymer radicals can react with each other, forming crosslinks:

$$P\bullet + P\bullet \longrightarrow P\text{-}P$$

Treatment with peroxides or with radiation were the conventional methods of crosslinking polyethylene before the silane grafting method (discussed in the preceding report) was introduced. The main Dow-Corning patent (2a) on the silane grafting method of crosslinking PE teaches that the peroxide concentration should be not higher than 0.75% in order to avoid free radical crosslinking becoming the predominant mechanism.

The patent recommends 0.05-0.2% peroxide, based upon the weight of the polymer.

Our work on the application of the silane grafting/crosslinking method to PMP discussed above has produced data which permit drawing conclusions also about the effect of peroxides on MP. In line with the recommendations of the Dow-Corning patent (2a), most of this work had been done with peroxide concentrations below 0.75%, but a set of experiments had been performed where the peroxide concentration had been varied up to 3%. If the polymer had been PE, it would have crosslinked by the peroxide alone, regardless of the presence or absence of the vinylsilane. However, with PMP no crosslinking at all was observed. Thus, PMP is totally different from PE in its response to peroxide treatment and can, apparently, not be crosslinked by the peroxide method.

The reason for this difference between the two polymers is the difference in chemical structure and the occurrence of side reactions which can become dominant in one polymer but not in another.

SIDE REACTIONS CAUSING POLYMER DEGRADATION

A radical is a very reactive species. It must undergo reactions which result in the formation of structures of lower energy and thus higher stability. Crosslinking is only one of the possible pathways along which polymer radicals can stabilize. Other pathways are oxidation and chain scission. Which of these reactions is predominant depends on polymer structure and on the presence or absence of other reactive species.

All of these potential pathways of radical reactions are independent of the method by which the radicals have been formed. Thus, what is said here applies to the treatment of PMP with either radiation or peroxides as well as to the grafting/crosslinking with vinylalkoxysilanes discussed in the preceding report.

In the presence of oxygen, polymer radicals may form hydroperoxides which will decompose thermally, leading to polymer degradation:

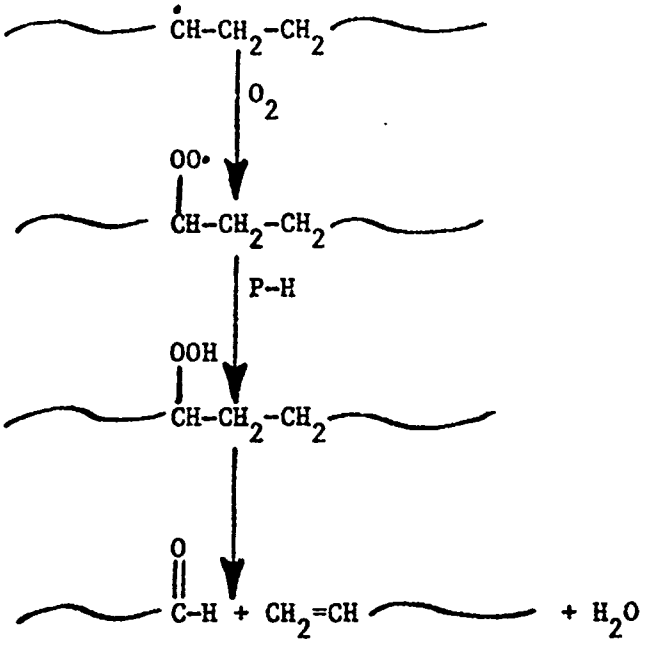

This chain scission reaction can occur with PE as well as with PMP. However, in PE new bonds are formed by the crosslinking reaction at a faster rate than are lost through chain scission. Thus, crosslinking predominates. This is apparently not the case in PMP.

PMP has two tertiary C-atoms per monomer unit, while PE has none. Tertiary carbon radicals can undergo a beta chain scission reaction which leads to polymer degradation:

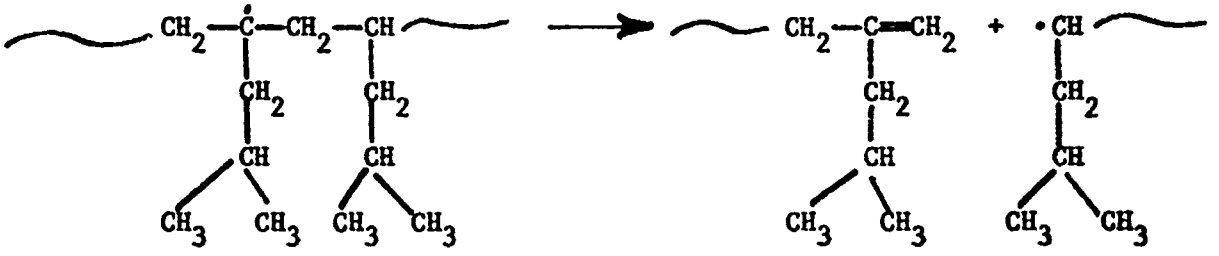

On a formal basis, the same reaction mechanism would not lead to main chain scission, if the radical is located at the other tertiary carbon atom:

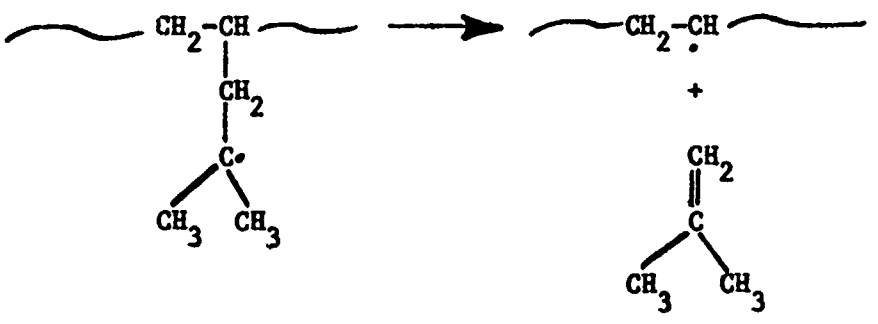

However, in view of the results of Pinkerton and Whelan (7), discussed above, this reaction may not occur in practice because the radical shown above can rearrange and then also can undergo main chain scission:

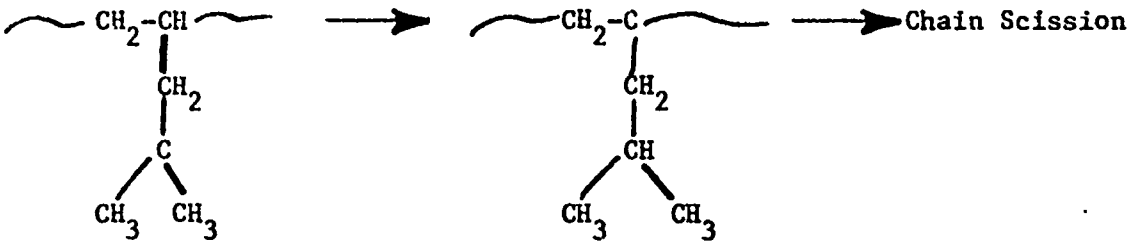

Thus, PMP appears to have so many chances to degrade that degradation reactions take place in preference to crosslinking reactions. This does not say, however, that no crosslinking reactions take place at all. Both types of reactions can occur simultaneously in both PE and PMP. In PE, crosslinking is favored over degradation as the experimental evidence shows. In PMP, degradation is apparently favored, partly because of the tertiary C-atoms and partly also because of sterical reasons. The side chain substituents in PMP are so large and bulky that they may have the same effect, favoring degradation over crosslinking, as the two substituents per C-atom in polymers such as poly(isobutylene). (See the discussion of the effects of radiation in this report.)

While PMP itself is too new a polymer to be discussed in standard textbooks and review articles, the principles of polymer degradation reactions are covered in detail in the literature (9, 10).

The degradation reactions outlined above can be expected to occur also in preference to the silane grafting reaction covered in the preceding report. After chain scission has occurred, loose ends of polymer chains could pick up vinylsilane:

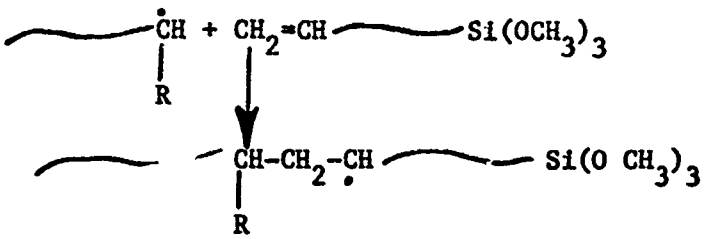

This would explain why Si is found in the polymer.

However, the attachment of silane groups at the ends of individual polymer chains is unlikely to result in the formation of a three-dimensional crosslinked network upon hydrolysis.

EXPERIMENTAL EVIDENCE FOR DEGRADATION OF PMP

In the studies on the grafting of PMP with vinylsilanes discussed above, three series of experiments were listed in Table V where the peroxide concentration was increased from 0.4% to 3%. If degradation occurs as a result of radical formation, the molecular weight should decrease with increasing peroxide concentration. We have shown that this is, indeed, the case.

Samples from two of the polymer series were sent to the Texas Division of the Dow Chemical Company for high-temperature gel permeation chromatography (GPC). GPC is the most modern method for obtaining molecular weight distributions of polymers. For polyolefins, a special GPC has been developed that can operate at the higher temperatures necessary to keep polyolefins in solution. The results are listed in Table 6. Computer plots of the GPC data are shown in Figures 3 and 4.

TABLE 6

MOLECULAR WEIGHT OF PMP VERSUS PEROXIDE CONCENTRATION

Ref.	%	Type	M_n	M_w	$\frac{M_w}{M_n}$	M_Z
PMP	0.0	—	35890	155960	4.35	383920
T325	0.4	USP-130	21770	92520	4.34	387570
T341	1.0	USP-130	16000	92520	5.78	561070
PMP	0.0	2,5-D	35890	155960	4.35	383920
T330	0.4	2,5-D	16110	91640	5.69	198610
T346	1.0	2,5-D	22240	112050	5.04	255170
T348	2.0	2,5-D	20340	110490	5.43	284800
T350	3.0	2,5-D	18980	96210	5.07	223410

The listed weights are relative values because the calibration was based on polyethylene molecular weight data. However, for the present purpose, this does not matter and the listed values are probably quite close to the actual molecular weights. Figures 3 and 4 give the raw GPC data, i.e., the optical response of the detector versus the elution volume. The originate translates into the number of molecules of each molecular weight species, while the abscissa, i.e., the elution volume, translates into molecular weight. The correlation of molecular weight to elution volume, prepared by plotting data from Table 6 is shown in Figure 5.

FIGURE 3: WITCO USP-130 PEROXIDE

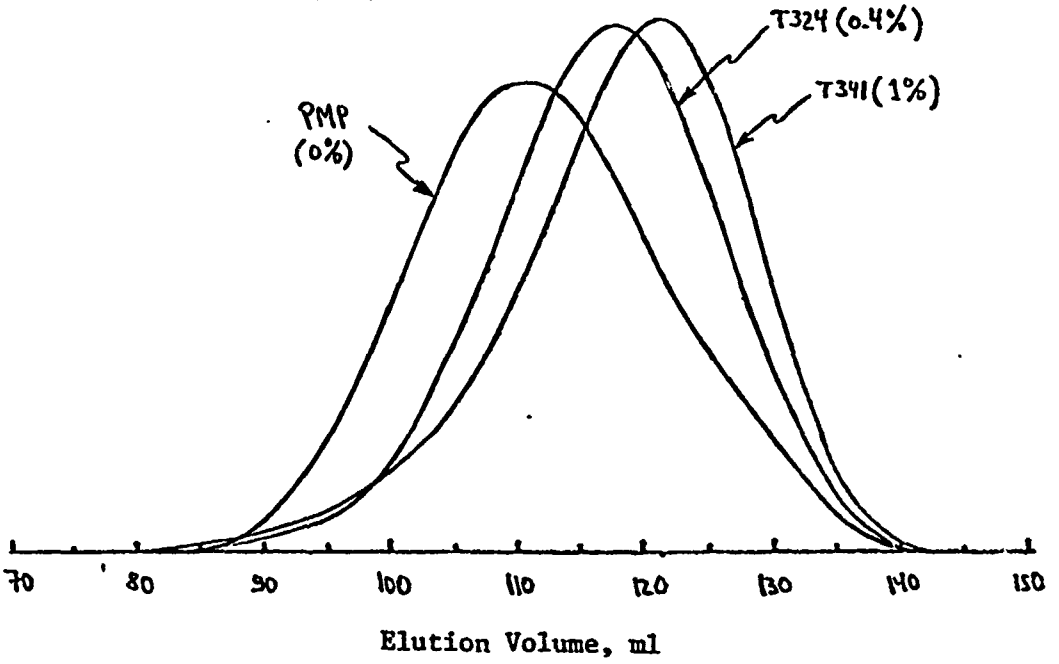

FIGURE 4: 2,5-DIMETHYLHEXANE-2,5-DIHYDROPEROXIDE

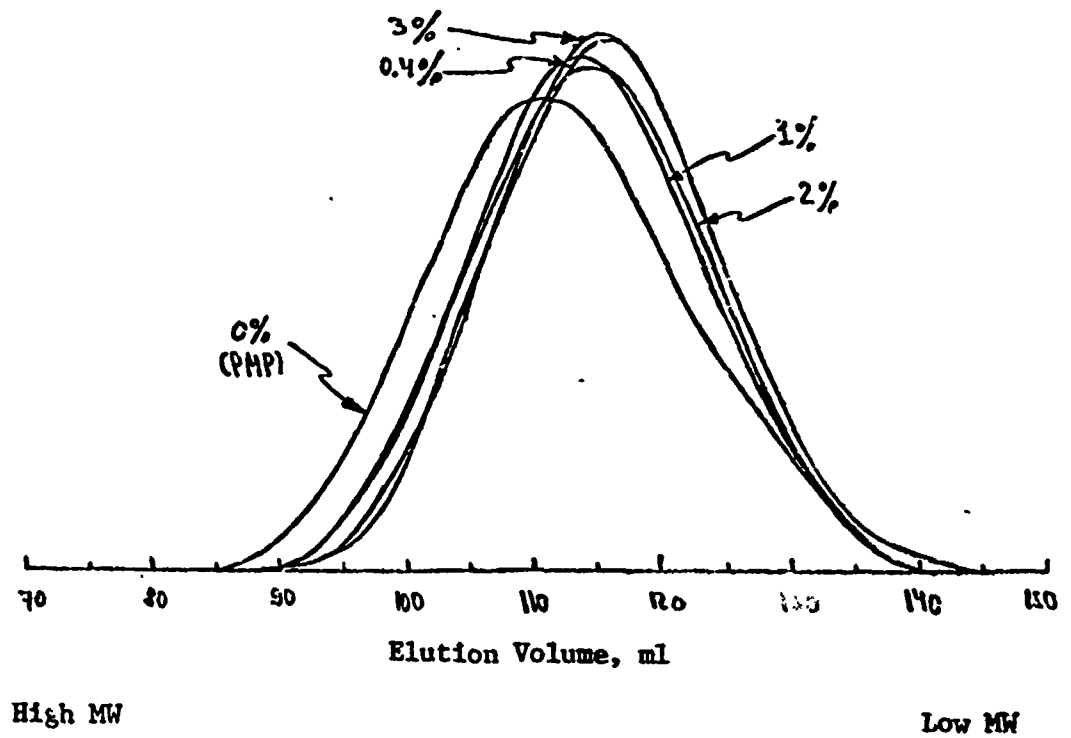

FIGURE 5

MOLECULAR WEIGHT AS A FUNCTION OF ELUTION VOLUME

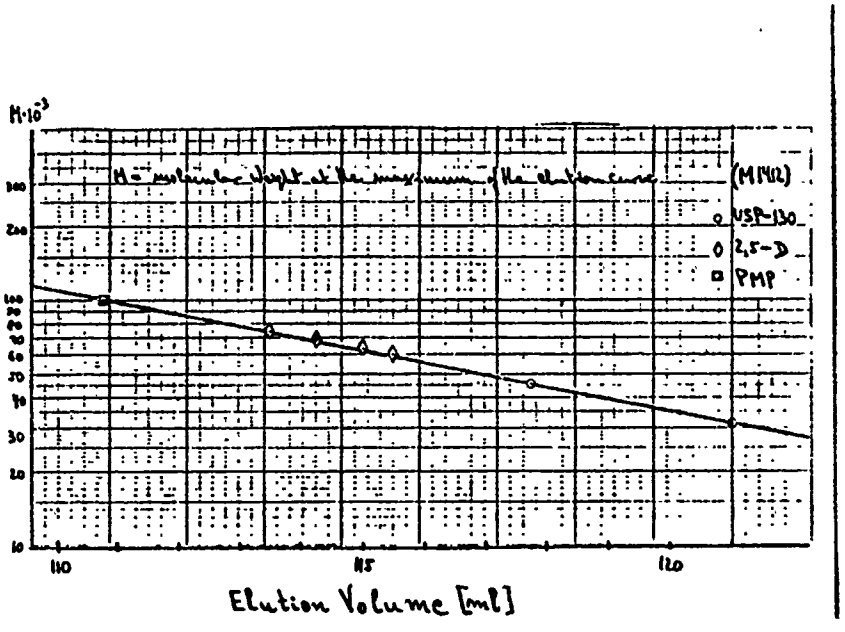

The data show that degradation of PMP occurs upon exposure to the peroxide. The decrease of molecular weight with increasing peroxide concentration is most easy to see in Table 4 and Figure 3; Figure 4 is somewhat more difficult to read but it shows the same effect.

For WITCO USP-130 peroxide, the number and weight average molecular weights decrease uniformly with increasing peroxide concentration. For 2,5-dimethylhexane-2,5-dihydroperoxide, an initial decrease in molecular weight is followed by a slight increase which is then followed by a decrease (see Table 6). A similar pattern is seen in the $\bar{M}_z$-column, Table 6, for USP-130 peroxide. These patterns can be taken as an indication that some formation of new bonds (crosslinking) does occur in competition with splitting of bonds (degradation). This means that decrease and increase of molecular weight take place simultaneously and in competition with each other. This is seen also visually, as reported in the preceding report on silane grafting of PMP, because an increase in viscosity at the higher peroxide levels was observed in the Brabender experiments as judged by visual appearance. However, even though formation of new bonds very probably occurs, it is overpowered by the breakdown of other bonds so that, in the end result, a three-dimensionally crosslinked network is never formed.

A CROSSLINKABLE TERPOLYMER

Campbell (11) prepared a number of soluble copolymers of 4-methyl-1-pentene and other hydrocarbon monomers for use in solution-spinning. The most satisfactory comonomer, to him, was 1-hexane. He also prepared a crosslinkable terpolymer by copolymerization of 40 ml of 4-methyl-1-pentene, 10 ml of 1-hexane, and 10 ml of divinylbenzene. This terpolymer was completely soluble in cyclohexane and could be cast into a film which was rapidly (in less than 15 minutes) insolubilized on heating at 225°C.

At first glance, it would appear attractive to prepare a crosslinkable copolymer of 4-methyl-1-pentene and divinylbenzene, following Campbell's procedure. However, he used 16.7 vol-% divinylbenzene in his composition, and it may be that such a high quantity of crosslinkable comonomer is necessary for achieving the spontaneous thermal crosslinkability obtained by him. Considering the results of Isaacson et al. (12), which will be discussed later, one has to expect that such a high amount of comonomer will cause a sharp drop in heat distortion temperature, thus very probably cancelling out any gains achieved by crosslinking.

BACKGROUND FOR THE PHYSICAL MODIFICATION STUDY

The conceptual approach to the problem of improving the gas permeability of PMP hollow fiber membranes by physical modifications was developed using an observation made by Tom Davis of this laboratory as a point of departure. Tom Davis noticed in 1976 that the oxygen permeability of PMP hollow fibers is lower than the value given for flat sheets by Mitsui in their manufacturer's bulletins. Later, in 1977, Dana Overman, also of this laboratory, measured the permeability of compression-molded flat sheets of PMP to oxygen and nitrogen and obtained data consistent with the Mitsui data.

If we accepted that the observed differences in gas permeability between flat sheets and hollow fibers of PMP were real, we could possibly improve the performance of the hollow fiber modules by eliminating these differences and bringing the gas permeability of the hollow fibers up to the level of flat sheet membranes.

In the literature on gas separation by membranes, a paper by Antonson et al. (13) on the mathematical analysis of gas separation by hollow fiber membranes states as a matter of fact that the advantages of hollow fibers are partially compensated by their generally lower permeabilities. Without offering an explanation for this phenomenon,

the authors refer to Lynch et al. (14) and Probstein (15) who had made the same observation with flat sheet and hollow fiber desalination devices. In the reverse osmosis area, these reports are corroborated by the experience of our own RO researchers who were aware for quite some time that hollow fibers have lower permeabilities than flat sheet membranes in RO applications.

Antonson et al. (13) point out that, in addition to the lower permeability which hollow fibers have per se, the pressure drop along the fiber bore is not negligible, thus reducing the driving force available for permeation and further contributing to a lower gas flow rate in hollow fiber devices.

It appears that:

a) the observed difference between the permeability of hollow fibers and flat sheet membranes is real and has been observed in many laboratories throughout the industry, and

b) the decrease in permeability of the hollow fibers has two components, one of which, namely the pressure drop along the fiber bore, is inherent in the geometry of the system and thus cannot be changed by methods of polymer technology; the other component, however, should respond to changes induced in the internal structure and morphology of the polymer.

Flat sheets, used for measuring gas permeability of polymers, are made usually either by compression molding or by solution casting. In either case, internal stresses have time to relax before the film solidifies; thus, flat sheets made by compression-molding or solution casting have a minimum of internal orientation of the polymer molecules. If a film is made by extrusion, there will be frozen-in internal stresses, i.e., molecular orientation, because the film cools before flow can occur to an extent sufficient for total stress relaxation. This is even more true for the extrusion of hollow fibers because, in the spinning process, very high built-in stresses can be expected because of the very high shear occurring in the thin annuli of the spinnerette. Thus, the degree of molecular orientation should increase from compression-molded films to extruded films to melt-spun hollow fibers.

While it is conceivable that internal stresses in hollow fibers may be minimized by manipulating the spinning variables, it appears unlikely that this approach alone can be sufficient to reduce molecular orientation to a level even near that of compression-molded flat sheets. This assumption is based simply on the small dimensions of the fibers themselves; the tiny orifices necessary to produce thin fibers will necessarily also produce high shear forces.

A more feasible approach would be to relax internal stresses, and thus reduce molecular orientation, <u>after</u> the fibers have been made. This has been the approach taken in the present project.

The standard method of reducing internal stresses is annealing. However, in a semicrystalline polymer, such as PMP, the effect of annealing on polymer properties is not predictable in a straightforward way, because annealing will also alter structural variables other than orientation, such as the degree of crystallinity and the general crystalline morphology of the sample. All of these variables together will affect gas permeability and other physical properties of the hollow fiber membranes. Thus, understanding the interrelationship of all of these variables is extremely important. For this reason, a literature study has been made as part of the present project in order to accumulate pertinent literature not only on PMP but also on related semicrystalline polyolefins.

LITERATURE STUDY

Most pertinent references are discussed in the text as part of the discussion of our data. Some literature sources are summarized here.

Since PMP is the newest of the polyolefin polymers, the number of papers dealing specifically with PMP is not very large compared to the vast literature on polyethylene (PE) and polypropylene (PP).

Of particular importance to the present work is the paper by Isaacson, Kirshenbaum, and Feist (12). These authors point out that PMP is, in many respects, a very unique polyolefin. It has a high melting point of 240°C and a low density and, surprisingly, the density of this amorphous material exceeds that of the crystalline material below 50°C. Although crystalline, PMP, unlike polyethylene and polypropylene, is transparent, and its transparency is probably due to limited spherulitic growth.

PMP is characterized by a relatively high tensile strength, stiffness, and surface hardness, as compared to polyethylene (PE) and polypropylene (PP), but it has an abnormally low heat distortion temperature and, at all temperatures, a lower dimensional stability than PP. It loses its strength faster with increasing temperature and its initial rate of creep is much greater than is found with PP. Isaacson et al. (12) interpret these observations on the basis of polymer crystallinity. They feel that the sensitivity of the strength and creep properties of PMP to temperature may be due to crystalline phase changes and spherulitic growth phenomena, and they provide some evidence that operating on variables which affect crystallinity and spherulitic growth can produce significant changes in the heat distortion temperature and other properties of PMP.

The heat distortion temperature is not a material constant as for instance the crystalline melting point of a polymer. Its definition is arbitrary, and it is measured according to an ASTM standard, D-648. Table 7, taken from the paper of Isaacson et al. (12), lists some heat distortion temperatures of some high-melting polymers.

TABLE 7

HEAT DISTORTION DATA FOR VARIOUS POLYMERS

Polymer	Heat Distortion Temp., °C	Melting Point, °C
Poly-4-MP	58	240
Polypropylene	110	170
Nylon 66	185	260
Polycarbonate	143	263
Poly-3-methyl-1-butene	155	310

Isaacson and coworkers (12) demonstrated experimentally that increasing crystallinity and spherulitic growth in PMP can raise the heat distortion temperature, while decreasing crystallinity can result in a sharp drop in heat distortion temperature. They showed that annealing compression-molded sheets of PMP at various temperatures can raise the heat distortion temperature by as much as 35–40°C. Their data are shown in Table 8.

TABLE 8

EFFECT OF ANNEALING ON HEAT DISTORTION TEMPERATURE OF PMP (ISAACSON, KIRSHENBAUM, AND FEIST, REF. 12)

Sample Treatment	Heat Distortion Temperature °C
unannealed PMP (control)	58
PMP annealed for 6 hrs. at 155°C	71
PMP annealed for 6 hrs. at 195°C	95

It is interesting to note that Isaacson et al. (12) also annealed a sample of PMP for 12 hours at 200°C and found through electron microscopy that there was no spherulite growth. They gave a crystalline melting point of 238°C, as evidenced by loss of birefringence, for their PMP samples.

Morphological studies, by the same authors, showed that, although PMP is comparatively highly crystalline polymer, very little spherulitic growth occurs in this material under normal fabrication conditions. Indeed, the

high clarity of molded plaques of PMP is indicative of small crystallites which are not associated into larger spherulitic aggregates.

While no literature data on the effect of annealing on orientation in PMP exist, Griffith and Ranby (17) have shown that annealing raised the crystallinity of PMP samples by 10-20% and, at the same time, lowered the glass transition temperatures (T_g) by 5-10°C. Some of their data are shown in Table 9.

TABLE 9

EFFECT OF ANNEALING ON CRYSTALLINITY AND GLASS TRANSITION TEMPERATURE OF PMP (GRIFFITH AND RANBY, REF. 17)

Sample	Crystallinity %	Tg °C
A) amorphous PMP	0	29
B) unannealed	37	25
B) annealed	46	22
C) unannealed	50	19
C) annealed	70	19

The samples were annealed in dilatometers (under mercury) at temperatures of 5-10°C below the crystalline melting point, which Griffith and Ranby give at 247-250°C. The annealing time was 8 hours. The PMP was not commercial polymer; it was prepared in house by Ziegler catalysis, which is normal for this polymer but can give molecular weights considerably different from those of commercial materials, depending on preparation conditions.

None of the above-cited authors reported on the effect of annealing on mechanical properties of PMP; it appears that there are no data to this effect in the open literature. The cited papers, to our knowledge, cover all of the published literature on annealing of PMP.

Crystallinity of a polymer sample is greatly affected by the chemical structure of the polymer. It is well known that the crystallinity of most crystalline polymers can be disrupted greatly by incorporation of only very small amounts of comonomers. Incorporation of a second monomer introduces points of irregularity into a polymer chain, and irregularity disrupts crystallinity. As an example, completely linear polyethylene has a degree of crystallinity of 80-90%. The incorporation of only 2 mol-% vinylacetate monomer decreases the crystallinity to about 60%, and more than 10 mol-% vinylacetate destroy the crystallinity completely (16). In the case of PMP, Isaacson et al. (12) showed that disturbing the crystallinity of the polymer by incorporation of only

3.4% propylene as comonomer reduces the heat distortion temperature of PMP from 58°C (see Table 8) to 30°C and decreases the crystalline melting point from 238°C to 226°C.

The crystalline morphology of a polymer sample has a very pronounced effect on gas transport properties. Generally, the crystalline phase is essentially impervious to gases and most liquids, and transport occurs only in the amorphous phase. The crystallites act as giant crosslinks and reduce the mobility of the polymer chain segments in the amorphous phase. Both effects combine to reduce the permeability of gases as the degree of crystallinity increase. Usually, parallel to a decrease in permeability occurs an increase in the separation factor, and vice versa.

The effect of orientation on permeability is not as clear-cut. Existing data can be interpreted such that the effect of orientation on permeability is opposite in crystalline and amorphous polymers. Even though no data on hollow fibers exist, the interpretation of data on flat-sheet membranes can be translated for hollow fibers into the following, simplified statements:

In crystalline polymers, orientation aligns the crystallites such that permeability through the fiber wall perpendicular to the fibers axis will be reduced. Thus, annealing should lead to an increase in permeability of hollow fibers made from semicrystalline polymers.

In amorphous polymers, orientation affects only the polymer chains, and no crystallites are involved. In this case, orientation seems to increase permeability of hollow fibers, because diffusion of gas molecules seems to be easier perpendicular to the stretched polymer chains than parallel to the chains.

It appears then that annealing of PMP hollow fibers may produce two overlapping effects: A reduction in orientation may increase gas permeability while a simultaneously occurring increase in the degree of crystallinity may have the opposite effect, namely decrease permeability. Which of these two possible effects will prevail must be shown by experiment.

PMP is an unusual semicrystalline polyolefin, because it is glass-clear in spite of its crystallinity. In contrast, semicrystalline polyethylene and polypropylene are translucent but not transparent because of the two-phase structure of these polymers (the crystalline and the amorphous phase). It has been speculated in the literature that the optical clarity of PMP is a consequence of an extremely small size of the crystallites and that the spherulitic structure typical for other semicrystalline polyolefins never forms in PMP under normal fabrication conditions. This different behavior may be directly related to the long side chain in the monomer unit of PMP.

One may speculate on this basis that annealing may reduce orientation more than it increases crystallinity. Thus, annealing experiments are definitely of interest.

COMPARISON OF HOLLOW FIBER AND FLAT SHEET PMP MEMBRANES BY X-RAY DIFFRACTION

While the literature study was in progress and while preparations for annealing experiments were being made, samples of hollow fibers and of flat sheets made of PMP by standard methods were submitted to specialists in our analytical laboratories in Midland, Michigan for x-ray diffraction analysis in order to check for differences in crystallinity and crystallite orientation. The following results were obtained:

Poly(4-methyl-1-pentene) crystallizes in a tetragonal unit cell with a = 18.66 Å and c = 13.80 Å (30). The polymer chain has been shown to lie parallel to the c-axis and exhibit extended chain folding, as does polyethylene, in order to accommodate the long chains in the 100 Å microcrystallites. Based upon the tetragonal cell the observed d-spacings for the membrane and hollow fibers can be indexed and their relative intensities calculated (Table 10) (I_o is the most intense observed line).

TABLE 10

d, Å	(hKl)	Flat Membrane I/I_o	Hollow Fiber I/I_o
9.21	200	100	100
6.56	220	10	11
5.41	311	43	3
5.28	312		
4.82	321	27	6
4.29	411	10	2
4.15	331, 420	14	9

The intensities most affected by loss of intensity are those with a c-axis component (non-zero). Therefore, fewer reflections with non-zero are perpendicular to the fiber axis than expected for a random oriented sample. Referring to a schematic of the crystal cell, (helix growth upwards, paralleling), the reflections with non-zero components are those that are generally perpendicular to the polymer helix (i.e., parallel to the paper).

The fiber sample has a decreased population of these planes, which means the polymer chains must be preferentially oriented <u>parallel</u> to the fiber growth axis. This is consistent with the known tendency of the extrusion process to result in highly oriented polymers. Compression molding has been shown to induce the least amount of preferred

orientation, so the flat membrane scan can be taken to represent a randomly oriented sample.

Calculation of "relative crystallinities" for the two samples is made difficult by a poorly defined amorphous halo. When this halo is approximated by a smooth curve from 14° to 31° 2θ, and the diffraction peaks and halo integrated, the following numbers result:

	Membrane	Hollow Fiber
Diffraction peak area, %	49	40
Amorphous halo area, %	51	60

These numbers are consistent with greater crystallinity in the compression molded flat membranes.

X-ray diffraction patterns were made from 2θ = 50° to 2θ = 10° with CuK_α radiation. Hollow fibers were monitored with ethyl alcohol to help keep them flat in the sample holder. Three sections of flat membranes were placed together for these scans.

"Relative crystallinities" were calculated by assuming a smooth amorphous halo between 2θ = 14° and 31° and integrating this area above a smooth baseline. Diffraction intensities were integrated above the amorphous halo. The calculated values are area ratios expressed as a percent of total area.

X-ray diffraction scans exhibit noticeable differences in relative intensities, indicating widely different degrees of crystallite orientation exists between the two samples. These differences indicate the polymer growth chain is orienting parallel to the fiber axis during the extrusion process. The relative crystallinity of the fibers appears to be lower than for the membrane.

The difference in crystallite orientation observed by x-ray diffraction in the hollow fiber and the flat-sheet membranes lead further impetus to the pursuit of the annealing experiments outlined above.

ANNEALING OF PMP HOLLOW FIBERS AND TESTING OF GAS PERMEABILITY

All experiments reported in this series of reports was performed using the same batch of PMP hollow fibers, identified as spinning batch R-147. The PMP is Mitsui TPX Grade DX-810. The fibers have the following dimensions:

Inner Diameter	32.2 µm
Outer Diameter	41.7 µm
Log-mean Diameter	36.8 µm
Fiber Wall Thickness	4.8 µm
Effective Fiber Length in Beaker Units	30 cm
Number of Fibers per Beaker Unit	810

In our initial experiments, we annealed bundles of PMP hollow fibers in an air convection oven at 153, 173, and 195°C, respectively, for periods ranging from 6 to 7.5 hours. This time-temperature schedule was based on the published data of Isaacson et al. (12) who showed (see Table 8 above) that significant changes in heat distortion temperature are caused in PMP samples by annealing under these conditions.

An immediately obvious effect of annealing was very pronounced curling of the fibers. Apparently, this curling is caused by changes in the internal stress patterns of the fibers and may, therefore, be taken as direct evidence that internal stresses had been present and were, at least partially, released. The curly fibers bear some resemblance to curly and kinky hair. This comparison is valid also at the molecular level, because the permanent wave process used on hair is based on setting up internal stresses in the hair fibers and fixing these stresses by crosslinking.

The curliness of the fibers presented a problem in the preparation of beaker test units, because the curly fibers can become entangled easily which then results in damage and fiber breakage. All initial annealing experiments had to be repeated because the fibers had become so entangled as to make fabrication into test beaker units meaningless. The same problem has to be anticipated in the manufacture of larger units, such as gas separation modules. The modules would probably have to be annealed after fabrication, if annealing proved to be fruitful, because the annealed fibers are too curly to be fabricated into gas modules.

With the initial experiments, no problems with temperature stability were encountered at the 153°C and 173°C annealing temperatures. However, the fibers annealed at 195°C in the air oven showed signs of degradation, particularly at the fiber ends. Some of the fibers had melted completely, forming a yellow honey-like liquid. This degradation was puzzlig at first, because Isaacson et al. (12) had annealed PMP at 195°C and had reported no problems. Their annealing conditions are not described in their paper to any great detail. Thus, it is not apparent, whether the annealing was done in air or under exclusion of air. Griffith and Ranby (17) had annealed their PMP in dilatometers, i.e., the samples were covered with mercury.

Zollner (18) has studied the specific volume of PMP as a function of temperature and pressure, using commercial PMP (TPX from Mitsui, grade RT-20). He reported that, although this material is said by the manufacturer to have a crystalline melting point of 240°C, melting of his samples started actually at 170-180°C. At 235°C, he found a distinct discontinuity in the slope of his specific volume-temperature curves, which he interpreted as the crystallie melting point. However, he points out that this is actually the end of a wide melting range,

extending from about 175°C to 235°C. In view of these data, it was no longer surprising that our PMP samples melted at 195°C. However, the yellowing of the samples upon melting suggests oxidation, and the later samples were annealed in vacuo for this reason.

In the initial vacuum-annealing experiments, fiber bundles were taped at their ends to a metal pan. The pan was heated to the annealing temperature in a vacuum oven while sitting on a metal rack. With this rack, the pan was not in direct contact with the oven walls. Thus, local overheating may not have occurred. However, there were still degradation problems which may have been associated with poor heat transfer. Another problem was presented by the rubber gasket which sealed the door of the vacuum oven. At 195°C, this gasket exuded liquid which distributed on the glass window of the oven door, thus making it impossible to read the thermometer. The vacuum oven annealing experiments were given up soon, because too many problems were encountered.

Eventually, a vacuum-annealing technique was developed which was simple and proved to be very satisfactory. Long glass tubes of 15 mm diameter were made and testtubed on one end. The PMP hollow fiber bundles were inserted into the tubes, one fiber bundle per tube. The tubes were then evacuated and sealed under vacuum by melting off the open end with a glassblower's torch. Prior to insertion into the tubes, th fiber bundles were taped at each end with masking tape to prevent entanglement of the fibers. The glass tubes were suspended on metal racks in the middle of an air convection oven and heated to the desired annealing temperatures.

This technique allowed handling and annealing of the individual fiber bundles in vacuo with a minimum chance for fiber entanglement. Although there was a considerable amount of extra work involved in making, sealing, and breaking the glass tubes, the results were worth the effort.

After annealing, the glass tubes were broken by cutting them with a glass knife at their center and breaking the tube. Breaking the tube in the center was very important for preventing fiber entanglement as much as possible. (If a tube was cut open at one end rather than in the middle, the incoming air would collapse the fiber bundle at the other end of the tube.)

Samples were annealed in vacuo at 136, 154, 176 and 195°C for periods of six hours. All of the fibers remained completely white and showed no visible sign of degradation, including the sample annealed at 195°C. This infers that the degradation observed previously in air was caused by air oxidation.

UNITS FOR EXPRESSING GAS PERMEABILITY

There has been a lot of confusion in the literature about the units in which gas permeability is expressed, and much has been written about this topic. In recent years, the National Bureau of Standards (NBS) and the American Society for Testing Materials (ASTM) have been advocating exclusive use of SI-units. We decided to adopt the SI-units used by NBS (19) and use them exclusively. These new SI-units are related to the most commonly used older CGS-units by the following conversion equation:

$$10^{-10}\left[\frac{cm^3(STP)\cdot cm}{cm^2\cdot s\cdot cm\ Hg}\right] = 0.3347\left[\frac{fmol\cdot m}{m^2\cdot s\cdot Pa}\right]$$

(1 fmol (femto-mol) = 10^{-15} mol)

GAS PERMEABILITY OF PMP HOLLOW FIBERS ANNEALED IN AIR

The annealing method employed with these samples was the older technique which was used before the vacuum-annealing technique with glass tubes described above had been developed. Bundes of hollow fibers were taped at their ends to metal pans. The pans were covered with aluminum foil and were suspended on metal racks in the middle of an air convection oven, where they were heated for six hours at 153°C and 174°C, respectively. The annealed samples were taken out very carefully and were potted into loop beaker units for measuring gas permeability. To the two series of annealed fibers, one series of unannealed fibers from the same batch was added as a control. Each series consisted of five beaker units so that a statistically significant average permeability could be calculated.

The three series of beaker units were tested by Tim Revak of this laboratory for gas flow rates of nitrogen and oxygen, using the soap bubble method routinely employed in his group. The tests were done at a feed gas pressure of 345 kPa (50 psi) (gauge pressure). The test data are listed in Table 11.

The left columns in Table 11 list the raw data, i.e., the gas flow rates measured and the separation factors, α, calculated from the measured data. The scattering of the data is caused by broken fibers which are a result of the curliness of the annealed fibers and entanglements that occurred during potting. Broken fibers were identified by a dye test after the gas flow rates were measured.

TABLE 11

SUMMARY OF PERMEATION RATE DATA

Sample No.	Annealing Temperature	Flow Rate [cm^3(stp)/min] N_2	Flow Rate [cm^3(stp)/min] O_2	Flow Rate [cm^3(stp)/min] α	Corrected $^3N_2$ Flow [cm^3(stp)/min]	Corrected $^3O_2$ Flow [cm^3(stp)/min]
M1446A-1	Control	3.27	14.01	4.28	3.27	14.01
-2		3.40	14.31	4.21	3.35	14.26
-3		3.28	13.80	4.20	3.22	13.74
-4		3.50	14.61	4.18	3.41	14.52
-5		3.45	14.32	4.15	3.33	14.20
M1446B-1	153°C	4.62	16.07	3.48	3.51	14.96
-2		12.24	22.01	1.79	3.00	12.77
-3		3.90	15.61	4.00	3.59	15.30
-4		3.50	14.99	4.28	3.50	14.98
-5		4.05	16.23	4.00	3.73	15.91
M1446C-1	174°C	3.37	13.85	4.11	3.21	13.69
-2		13.66	23.65	1.73	3.07	13.06
-3		7.37	18.56	2.52	3.43	14.62
-4		6.89	18.73	2.72	3.63	15.48
-5		6.13	17.10	2.79	3.37	14.34

TABLE 12

AVERAGED CORRECTED PERMEATION RATES

Sample Ref.	Annealing Temperature	Annealing Time	Averaged Corrected Gas Flow Rates [cm³ (stp)/min] N_2	O_2	α
M1446 A	Control	—	3.32 ± 0.07	14.15 ± 0.29	4.26
M1446 B	153°C	6 hr.	3.58 ± 0.11	15.28 ± 0.44	4.27
M1446 C	174°C	6 hr.	3.41 ± 0.17	14.53 ± 0.74	4.26

The "corrected flow rates", shown in the right columns in Table 11, were calculated from the raw data by subtracting the leak rate from the measured "permeation rates to account for the broken fibers. From these corrected flow rates, average gas flow rates and separation factors were calculated for each test series. These final values are listed in Table 12.

The data in Table 12 indicate that the gas permeability, for both nitrogen and oxygen, increases upon annealing, but the initial increase is followed by a decrease. Thus, the 153°C-annealed samples have the highest gas permeability in this group of experiments. The 174°C-annealed samples have a higher gas permeablity than the unannealed samples, but their permeability is lower than that of the 153°C-annealed samples.

The correction of the raw data for broken fibers was done by normalization using a theoretical separation factor of 4.26. The corrected gas flow rates listed in Table 12 were recalculated into actual gas permeabilities; these recalculated data are listed in Table 13.

TABLE 13

ANNEALING IN AIR
CORRECTED GAS PERMEABILITIES AVERAGED OVER
5 SAMPLES PER SET

Reference	Annealing Temp. [°C]	Annealing Time [h]	Permeability $\left[\frac{fmol \cdot m}{m^2 \cdot s \cdot Pa}\right]$ O_2	N_2	α
M1446A-1,2,3,4,5	Control		5.16 ± 0.11	1.21 ± 0.03	4.26
M1446B-1,2,3,4,5	153	6	5.58 ± 0.16	1.31 ± 0.04	4.26
M1446C-1,2,3,4,5	174	6	5.30 ± 0.27	1.24 ± 0.06	4.27

The trend in the data listed in Tables 12 and 13 seems to indicate that the gas permeability of the samples annealed at 153°C is somewhat higher than the gas permeability of the other samples. In order to check whether this may be an artifact introduced by the normalization procedure, the raw data from Table 11 were treated in a different way, omitting the normalization procedure. Since some of the original data were more affected by broken fiber leaks than others, as indicated by very low separation factors combined with very high permeability, all data with a separation factor below 4.0 were rejected, and the remaining

flow rates were recalculated into gas permeabilities. Average gas permeabilities were then calculated from the data that were left after the weeding-out process. These average gas permeabilities are listed in Table 14.

TABLE 14

ANNEALING IN AIR

AVERAGE GAS PERMEABILITIES CALCULATED FROM SAMPLES WITH A SEPARATION FACTOR HIGHER THAN 4.0

(n = number of samples used for the average)

Reference	n	Annealing Temp. [°C]	Annealing Time [h]	Permeability $\left[\frac{fmol \cdot m}{m^2 \cdot s \cdot Pa}\right]$ O_2	N_2	α
M1446A-1,2,3,4,5	5	Control		5.18 ± 0.11	1.23 ± 0.04	4.21
M1446B-3,4,5	3	153	6	5.70 ± 0.23	1.39 ± 0.10	4.10
M1446C-1	1	174	6	5.05	1.23	4.11

With this different data treatment, the gas permeabilities of the samples annealed at 153°C are still higher than those of the other samples. Thus, these higher values are not an artifact of the normalization procedure. It appears that the data treatment leading to Table 14 makes the 153°C-annealed samples stand out even more than in Table 13. However, the uncertainty range of the 153°C-samples in Table 14 is also higher than that of the same figures in Table 13.

As pointed out above, annealing in air at 195°C was not feasible, because the polymer melted to a yellowish liquid, apparently as a result of oxidation. For this reason, all of the above-described experiments were repeated in vacuum, exercising great care in handling the samples and avoiding broken fibers as much as possible, and including one more annealing temperature.

GAS PERMEABILITY OF PMP HOLLOW FIBERS ANNEALED IN VACUUM

As described above, fiber bundles were sealed under vacuum into glass tubes and annealed for six hours by heating the glass tubes in an air convection oven at 136, 154, 176, and 195°C, respectively. No visually obvious degradation problem was encountered at any of these temperatures. The lowest temperature of 136°C was added, because the air annealed samples discussed above seemed to have a permeability maximum around 153°C. Thus, testing at a lower annealing temperature was necessary in order to establish whether this observationwas real or an artifact.

The fiber bundles were removed from the glass tubes and potted into beaker test units in the usual way. The beaker units were immersed in a 25°C uniform temperature bath for at least 30 minutes for each measurement, and gas flow rates were measured using the usual soap bubble method under a pressure differential of 350 kPa (about 50 psi) across the membrane.

The original gas flow rates are listed in Table 15 together with corrected gas flow rates which were calculated from the original data by the same normalization against a theoretical separation factor used in Table 11. (Note: the data in Table 15 are given in different dimensions than those in Table 11, because one set was determined by Tim Revak of this laboratory and the other set was measured by the author; each person followed his own convention.) As above, this method resulted in five flow rate values per gas and per annealing temperature, because no data were rejected. Averaging over these five values per set and conversion into actual gas permeabilities gave the data listed in Table 16.

Inspecting the data in Tables 15 and 16 shows that the normalization procedure works very well for data with high separation factor, i.e., when the number of broken fibers is low. However, if the number of broken fibers is higher and the separation factor is very low, as in samples M1465-3.4, 4.3, and 4.4 in Table 15, the methods over-corrects and leads to unrealistically low permeabilities (see samples M1465-3 and 4 in Table 16). For this reason samples M1465-3.3, 4.3, and 4.4 have been eliminated from the set. Also, since the extra sample M1453 in Table 15, which came from another test series, has very few broken fibers, it was averaged into set M1465-4, which was annealed at essentially the same temperature. After the new average flow rates were calculated, gas permeabilities were calculated from these somewhat weighted averages and listed in Table 17.

TABLE 15

ANNEALING IN VACUO FOR 6 HOURS

Original and Normalized Gas Flow Rates Measured at 25°C and 350 kPa Pressure Differential.

Polymer Reference	Annealing Temperature [°C] 6 h	P_2 [kPa]	$\frac{dv}{dt}\left[\frac{cm^3}{s}\right]$ observed at 25°C O_2	N_2	α observ.	$\frac{dv}{dt}\left[\frac{cm^3}{s}\right]$ corrected O_2	N_2
R147-58	Control	101.	0.266	0.0646	4.12	0.263	0.0617
85	"	5	250	0.0563	4.44	253	593
86	"	9	290	0.0813	3.57	273	640
95	"	5	267	0.0633	4.22	266	624
97	"	8	267	0.1030	2.59	214	502
98	"	7	250	0.0560	4.46	253	594
		101.7				0.254 ± 0.021	0.0595 ± 0.0049
M1465-1.1	136	101.6	0.253	0.0611	4.14	0.251	0.0588
1.2	"	5	244	578	4.22	243	570
1.3	"	6	270	727	3.71	258	604
1.4	"	6	260	690	3.77	250	586
		101.6				0.250 ± 0.006	0.0587 ± 0.0014
M1465-2.1	154	101.6	0.281	0.100	2.81	0.236	0.0554
2.2	"	"	311	0.143	2.17	219	513
2.3	"	"	255	0.0606	4.21	254	596
2.4	"	"	254	0.0615	4.13	252	590
2.5	"	102.4	204	0.0487	4.19	203	476
		101.8				0.233 ± 0.022	0.0546 ± 0.0051
M1465-3.1	176	102.4	0.281	0.1045	2.69	0.231	0.0541
3.2	"	"	365	0.189	1.93	230	538
3.3	"	"	251	0.0786	3.19	225	527
3.4	"	101.9	524	0.380	1.38	188	422
		102.3				0.219 ± 0.021	0.0512 ± 0.0047
M1465-4.1	195	101.7	0.277	0.0702	3.95	0.270	0.0634
4.2	"	"	308	0.127	2.43	0.237	556
4.3	"	"	741	0.647	1.15	0.124	297
4.4	"	"	935	0.885	1.06	0.0663	163
		101.7				0.170 ± 0.10	0.0413 ± 0.0220
M1453	192	101.1	0.276	0.0735	3.76	0.265	0.0621

TABLE 16

ANNEALING IN VACUO FOR 6 HOURS

Corrected Gas Flow Rates and Permeabilities Averaged Over 5 Samples Per Set

(Measured at 25°C and 350 kPa Pressure Differential)

Polymer Reference	Anneal Temperature [°C]	Average $\frac{dv}{dt}$ $\left[\frac{cm^3}{s}\right]$ At 25°C O_2	N_2	Permeability $\left[\frac{fmol \cdot m}{m^2 \cdot s \cdot Pa}\right]$ O_2	N_2	α
R147	Control	0.254 ± 0.021	0.0595 ± 0.0049	5.03 ± 0.42	1.18 ± 0.10	4.26
M1465-1	136	0.250 ± 0.006	0.0587 ± 0.0014	4.95 ± 0.12	1.16 ± 0.03	4.27
M1465-2	154	0.233 ± 0.022	0.0546 ± 0.0051	4.62 ± 0.44	1.08 ± 0.10	4.28
M1465-3	176	0.219 ± 0.021	0.0512 ± 0.0047	4.36 ± 0.42	1.02 ± 0.09	4.27
M1465-4	195	0.170 ± 0.10	0.0413 ± 0.022	3.37 ± 1.98	0.82 ± 0.44	4.11
M1453	192	0.265	0.0621	5.22	1.22	4.28

TABLE 17

ANNEALING IN VACUO FOR 6 HOURS

Gas permeabilities at 25°C and 350 kPa pressure differential calculated from the corrected gas flow rates in Table 3 under exclusion of samples M1465-3.4, M1465-4.3 and M1465-4.4 and combining M1465 and M1465-4.1 and 4.2 into one average.

Polymer Reference	Anneal Temperature [°C] 6 h	Gas Permeability at 25°C P $\left[\frac{\text{fmol} \cdot \text{m}}{\text{m}^2 \cdot \text{s} \cdot \text{Pa}}\right]$ O_2	N_2	α
R147	Control	5.03 ± 0.42	1.18 ± 0.10	4.26
M1465-1	136	4.95 ± 0.12	1.16 ± 0.03	4.27
M1465-2	154	4.62 ± 0.44	1.08 ± 0.10	4.28
M1465-3	176	4.57 ± 0.06	1.07 ± 0.01	4.27
M-1465-4 M1453	194	5.08 ± 0.36	1.19 ± 0.08	4.27

In order to double-check whether the normalization procedure has introduced any artifacts, as had been done with the samples annealed in air, the raw data in Table 15 were subjected to the treatment used before, namely rejection of all data with unusually low separation factor, because these samples had obviously a large number of broken fibers. The remaining data were averaged and recalculated into gas permeabilities. The data so obtained are listed in Table 18.

Inspection of the data in Tables 17 and 18 leads to the same conclusion, namely that the gas permeability is essentially independent of annealing at any of the temperatures employed in the vacuum-annealed samples. Within the range of uncertainty of the data, all gas permeabilities are essentially the same.

Looking at all the data together (Tables 13, 14, 17, 18), the somewhat higher gas permeability found with the sample-set annealed in air at 153°C (Tables 13 and 14) stands very much alone and must be interpreted as a quirk of the data rather than being given any significance.

The general conclusion drawn from all the annealing experiments together is then that the gas permeability of PMP hollow fibers cannot be improved by annealing. This does not mean at all that orientation does not play a significant role in its effect on gas permeability of hollow fibers - there is too much general evidence that it does. (As an

example that came out of the present work: the severe curling of the PMP hollow fibers and the 15% shrinkage in length observed after annealing is very much an indication that internal stresses had existed and have been released through annealing.) What it does mean is that the annealing affects the crystalline structure of the material and relaxes orientation simultaneously, and the two opposing effect apparently balance each other out.

TABLE 18

ANNEALING IN VACUO FOR 6 HOURS
(excluding data with low separation factors)
Gas Permeability at 25°C and 350 kPa Pressure Differential

Reference	Annealing Temp. 6 h	n	Permeability $\left[\frac{fmol \cdot m}{m^2 \cdot s \cdot Pa}\right]$ O_2	N_2	α
R147-58, 85,95,98	Control	4	5.11 ± 0.19	1.17 ± 0.10	4.37
M1465-1.1 to 1.4	136°C	4	5.08 ± 0.22	1.29 ± 0.14	3.94
M1465-2.3 to 2.5	154°C	3	4.72 ± 0.56	1.13 ± 0.14	4.18
M1465-3.3	176°C	1	5.01	1.57	3.19
M1465-4.1	195°C	2	5.47 ± 0.04	1.42 ± 0.04	3.85
M1453	192°C				

n = Number of samples included in the average.
P = Permeability.

Average values for the gas permeability of PMP hollow fibers of spinning batch R-147 can be calculated from the two independently measured control sets in Tables 13 and 16 of this report. Previously, Jim Williams of this laboratory had measured oxygen and nitrogen permeabilities of another batch of PMP hollow fibers, spun from the grade of PMP (Mitsui TPX, grade DX-810). Both of these data are listed in Table 19 below for comparison with the permeability values for PMP flat sheet membranes listed in Table 20 in the following paragraph.

TABLE 19

GAS PERMEABILITY OF UNANNEALED PMP HOLLOW FIBERS

Source	Batch	Permeability $\left[\frac{fmol \cdot m}{m^2 \cdot s \cdot Pa}\right]$ O_2	N_2
Table 13	R-147	5.16 ± 0.11	1.21 ± 0.03
Table 16	R-147	5.03 ± 0.42	1.18 ± 0.10
Average	R-147	5.10 ± 0.27	1.20 ± 0.07
Jim Williams (1-28-77)	R-20	6.6	1.6

GAS PERMEABILITY OF PMP FLAT SHEET MEMBRANES

In the course of this work, the literature has been searched and all the available data on gas permeability of PMP have been compiled. The combined data on oxygen and nitrogen permeability are listed in Table 20.

TABLE 20

GAS PERMEABILITY OF PMP FLAT SHEETS

Source	Ref.	Temp. [°C]	Permeability $\left[\frac{fmol \cdot m}{m^2 \cdot s \cdot Pa}\right]$ O_2	N_2	α
Yasuda et al.	20	25	10.8	2.62	4.12
Overman	21	RT	9.8	2.3	4.26
Mitsui	22	25	9.0	2.2	4.09
Ng et al.	23	25	7.26	1.44	5.04
Huldy	24	25	6.69	1.67	4.01
Kapanin et al.	25	20	—	2.42	—
Molau	26	20	7.25	1.73	4.19

The permeabilities give by Ng et al., Huldy, and Molau in Table 20 are significantly lower than those given by the other authors. It does not surprise us that our own values (7.25 and 1.73 in Table 20) are lower than those of Dana Overman (9.8 and 2.3 in Table 20), because our data were measured on compression-molded flat sheets. The fabrication conditions of the films of Ng et al. and Huldy are not known. Thus, one might suspect that these were probably obtained with extruded film, just like ours. Compared to these values, the data for PMP hollow fibers reported by Jim Williams (Table 19) do not appear as low as when compared only to the data of Mitsui and Overman.

The data of Ng, Pedley, and Tighe (23) were given over a temperature range of 20–40°C for oxygen and 20–55°C for nitrogen. Plots of the logarithms of the permeabilities over the reciprocals of the absolute temperature gave straight lines. There was a distinct break in the lines at about 26°C, the glass transition temperature of this particular PMP sample. We determined the coefficients in equation (2) from the data by linear regression, using two different equations for each gas, one below and one above Tg. The coefficients are listed in Table 21, together with the coefficients of determination (r^2).

$$P = P_o \, e^{-\frac{E_P}{RT}} \qquad (2)$$

TABLE 21

COEFFICIENTS IN EQ. 1 FOR PMP

System	$P_o \cdot 10^{-3}$ $\left[\frac{fmol \cdot m}{m^2 \cdot s \cdot Pa}\right]$	$\left[\frac{kJ}{mol}\right]$	r^2
O_2, below Tg	131	24.3	0.83
O_2, above Tg	15.5	19.0	0.78
N_2, below Tg	820000	50.1	0.98
N_2, above Tg	38.8	24.6	0.97

$R = 8.3144\ 10^{-3}$ [kJ/(mol K)]

Calculating the break in the data plots from eq. 2, using the coefficients listed in Table 20, gave Tg = 26.0°C from the oxygen data and Tg = 26.2°C from the nitrogen data, an excellent agreement indeed.

Measuring gas permeability may thus be a very sensitive method for determining the glass transition temperature of a PMP sample. Rånby et al. (27) have shown the glass transition temperature for amorphous PMP to be near 29°C and to decrease to below 20°C with increasing crystallinity. Zollner (18) found a glass transition temperature of about 20°C for his PMP samples, and Mitsui gives the glass transition temperature for TPX-brand PMP samples at 25-30°C (28).

ACKNOWLEDGEMENT

The author is pleased to acknowledge the help of Tom Duly, who did the chemical experiments, and of Tim Revak, who did part of the gas permeability measurements.

The x-ray diffraction measurements were contributed by J. W. Edmonds of the Analytical Laboratories in Midland.

REFERENCES

1. S. A. Manatt, "Feasibility Study and Demonstration of Nitrogen Generation for Fuel Tank Inerting", Report to the Federal Aviation Adminstration, Cat. No. AD-784 950, June 1974.

2. a) H. G. Scott, U.S. Pat. 3,646,155 (February 29, 1972) (to Midland Silicones Ltd., England).

   b) H. G. Scott and J. F. Humphries, Mod. Plastics, 83 (1973).

3. a) F. Glander and H. U. Voigt, U.S. Patent 4,058,583 (November 1977).

   b) H. U. Voigt, M. Völker, and H. Peter, U.S. Patent 4,117,063 (September 26, 1978).

   (Both patents to Kabel und Metallwerke Gutehoffnungshutte, West-Germany.)

4. A. Nojiro, T. Sawasaki, and T. Koreeda, Europ. Pat. Appl. 0 004 034 (March 1, 1979) (to Furukawa Electric Co., Japan).

5. C. Maillefer, Tech. Pap., Reg. Tech. Conf. Soc. Plast. Eng., June 19-20, 1979.

6. A. Chapiro, "Radiation Chemistry of Polymeric Systems", Interscience, New York, 1962.

7. D. M. Pinkerton and D. J. Whelan, Aust. H. Chem., 24, 183 (1971).

8. E. Cianetti and N. L. Vinciguerra, Rass. Chim., 24, 300 (1972).

9. Grassie, N., "Thermal Degradation", Chap. 8B in "Chemical Reactions of Polymers", ed. M. Fettes, Interscience, New York, 1964.

10. R. W. Lenz, "Organic Chemistry of High Polymers", Chap. 18, "Degradation Reactions of Polymers", Interscience, New York, 1967.

11. T. W. Campbell, J. Appl. Polymer Sci., 5, 184 (1961).

12. R. B. Isaacson, I. Kirshenbaum, and W. C. Feist, J. Appl. Polymer Sci., 8, 2789 (1964).

13. C. R. Anderson, R. J. Gardner, C. F. King, and D. Y. Ko, Ind. Eng. Chem., Proc. Des. Dev., 16, 463 (1977).

14. M. A. Lynch and M. S. Mintz, J. A. W. W. A., 64, 711 (1972).

15. R. F. Probstein, Am. Sci., 61, 280 (1973).

16. F. P. Reding ad E. R. Walter, J. Polymer Sci., 37, 555 (1959).

17. J. H. Griffith and B. G. Ranby, J. Polymer Sci., 44, 369 (1960).

18. P. Zollner, J. Appl. Polymer Sci., 21, 3129 (1977).

19. J. D. Barnes and G. D. Martin, "SRM1460 Polyester Film for Oxygen Gas Transmission Measurements", National Bureau of Standards Special Publication 260-58 (June 1979).

20. H. Yasuda and K. J. Rosengren, J. Appl. Pol. Sci., 14, 2839 (1970) (listed in Polymer Handbook III-235 by Brandrup and Immergut).

21. Dana Overman, The Dow Chemical Company, Industrial Membranes Laboratory, Walnut Creek, California, January 26, 1977.

22. Mitsui Petrochemical Industries Ltd., Manufacturer's Bulletins (these data apparently go back to ICI Ltd.).

23. C. O. Ng, D. G. Pedley, and B. J. Tighe, Brit. Pol. J., 8, 124 (1976), (calculated from their data after a least-square fit, see explanation in text).

24. H. J. Huldy, Plastica, 20, 348 (1967).

25. V. V. Kapanin and S. A. Reitlinger, Vysokomol. Soed., B, 18, 770 (1976).

26. G. E. Molau, The Dow Chemical Company, Industrial Membrane Research Laboratory, Walnut Creek, California, March 3, 1981.

27. R. G. Ranby, K. S. Chan, and H. Brumberger, J. Polymer Sci., 58, 545 (1962).

28. Mitsui Petrochemical Industries, Ltd., Technical Bulletin on TPX, May 1975.

29. A. Charlesby and P. J. Fydelor, Int. J. Radiat. Phys. Chem., 4, 107 (1972).

30. F. C. Frank, A. Keller, and A. O'Connor, Phil. Mag., 4, 200 (1959).

gs

APPENDIX C

COST-OF-OWNERSHIP COMPARISON FOR C-130 AIRCRAFT

ASSUMPTIONS

A comparative cost-of-ownership analysis was performed for the integrated, permeable membrane, inert gas generator (IGG) and the MIL-B-83054 blue foam fuel tank protection systems that were installed per TO 1C-130-1063. The analysis pertained to the wing and pylon tanks only. Included in this analysis were initial cost, maintenance cost, and operating cost. Cost assumptions for this analysis are summarized in Table C-1.

SYSTEM DESIGN CONSTRAINTS

This analysis assumed that the existing cargo-compartment, simple-cycle, environmental control system (ECS) would be replaced by a bootstrap ECS integrated with the IGG, as shown in Figure C-1. The new ECS will provide cooling for the cargo compartment and the IGG. The ECS is made up of existing design components as much as possible, with modifications to interconnecting tubes and ducts. Basic design requirements were derived from C-130 cargo compartment ECS requirements and the typical C-130 missions described on Table C-2. Comparative ECS aircraft penalty data are shown in Table C-3. The penalty differentials were used to determine the added operational costs of the bootstrap ECS. The logistic resupply mission shown in Table C-2 was used to size the IGG. For this analysis fuel tank pressures of +0.80 to -0.20 psid were used. The analysis indicated that four air separation modules (ASM's) would meet the inert gas flow requirements for the logistic resupply mission shown in Table C-2.

The system incorporates an inert gas flow control, which regulates steady-state flow at 0.10 lb/min, with inert gas at 3.5 percent oxygen; upon descent the control increases the flow to supply the fuel tank ullage with inert gas at oxygen concentrations shown in Figures C-2 and C-3. Each ASM is 10 in. in diameter and 43 in. long (2 cu ft). The remaining IGG components (air filter, temperature control valve, pressure regulator, and flow control) require 1 cu ft of volume.

System performance for the logistic resupply mission and typical training mission are presented in Figures C-2 and C-3, respectively. To determine the life-cycle costs compared to blue foam, both systems were evaluated using the training mission shown in Table C-2. During cruise mode, the ECS differential bleed flow shown in Table C-3 was much greater than ASM feed flow, and was used in lieu of the lower ASM feed flow. All other bleed flow requirements are those of ASM feed flow.

BLUE FOAM

Although the initial installation costs attributed to blue foam are modest (under $50K, see Table C-4), the installed weight penalty amounts to 2900 lb. This installed weight (as noted in Table 13-1 of TO 1C-130B-2-5) consists of 1494 lb of blue foam and 1406 lb of retained fuel. In addition to the added weight, the retained fuel reduces the available fuel capacity and aircraft range. The single most significant penalty for blue foam is the additional

TABLE C-1

COST ASSUMPTIONS

Total aircraft population	674
Average annual aircraft flight hours (FH)	564
Average mission length, FH	5
Average missions/yr	113
Analysis design life period, yr	20
Average ASM life, FH	8460
Aircraft per spare system	10
Total systems required	741
Average labor rate (depot level), $/hr	33.40
Average fuel cost, $/gal	1.0
Average fuel cost, $/lb	0.1539
System design life, years	20
Blue foam replacement period, FH	6000
Blue foam inspection period, FH	600
IGG average replacement period, FH	8500
IGG average aircraft power, w	400
IGG installed net weight increase, lb	190

Notes:

1. Inerting provided for wing and pylon tanks only.
2. Type IV blue reticulated foam installed with approximately 17-percent voiding.
3. A typical long-range logistics resupply mission is used to size the OBIGG system.
4. A typical training mission is used to evaluate OBIGGS versus blue foam in terms of aircraft weight/fuel burned.
5. Maintenance data from AFM 66-1 for the C-130.
6. T56-A-15 engine airbleed/fuel burned characteristics.
7. C-130H aircraft used for aircraft weight/fuel burned characteristics.
8. ASM = Air separation module
9. IGG = Inert gas generator

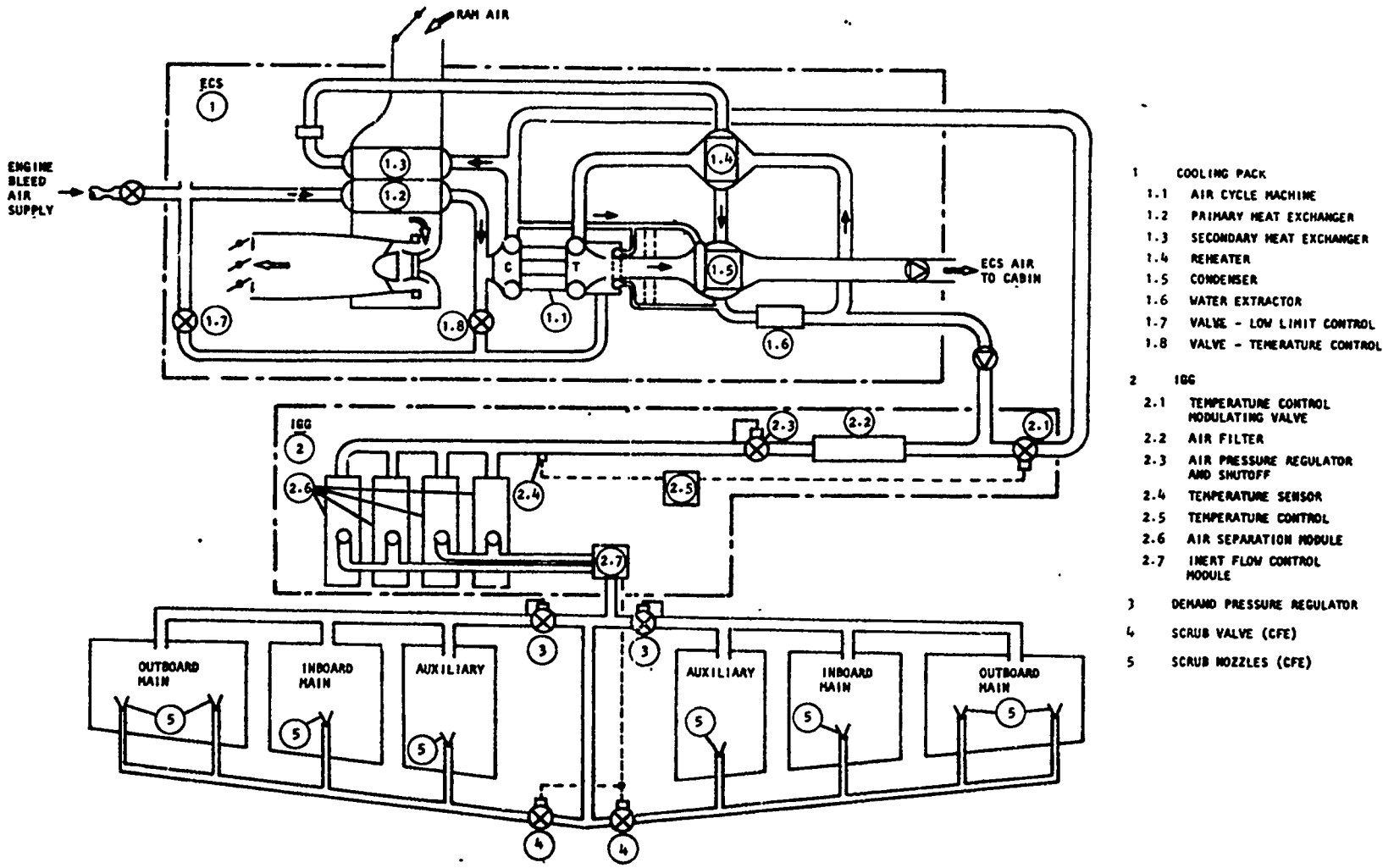

Figure C-1. Typical Schematic of Permeable Membrane, Inert Gas Generator (PMIGG)

TABLE C-2

TYPICAL C-130 MISSIONS

Logistic Resupply Mission

Mission Segment	Time Duration, hr	Flight Altitude, ft
Ground	0.25	0
Climb	0.5	0-23K
Cruise	13.5	23K-36K
Descent	0.20	35K
		30K
		20K
		15K
		10K
		5K
		0

Total time = 14.45 hr

Training Mission

Mission Segment	Time Duration, hr	Flight Altitude, ft
Ground	0.2	0
Climb	0.2	0-8K
Cruise	2.0	8K
Descent	0.2	8K-0
Climb	0.2	0-8K
Cruise	2.0	8K
Descent	0.2	8K-0

Total = 5 hr

TABLE C-3

ECS PENALTY COMPARISON

Parameter[1]	Existing C-130 ECS	New Integrated Bootstrap ECS	Differential
Weight, lb	178	185	+7
Bleed air flow, lb/min[1]	57.4	66.4[2]	+9
Ram air flow, lb/min[1]	150	254	+104

Notes:

1. Training mission cruise point estimated energy.
2. Bleed flow shown is for ECS only.

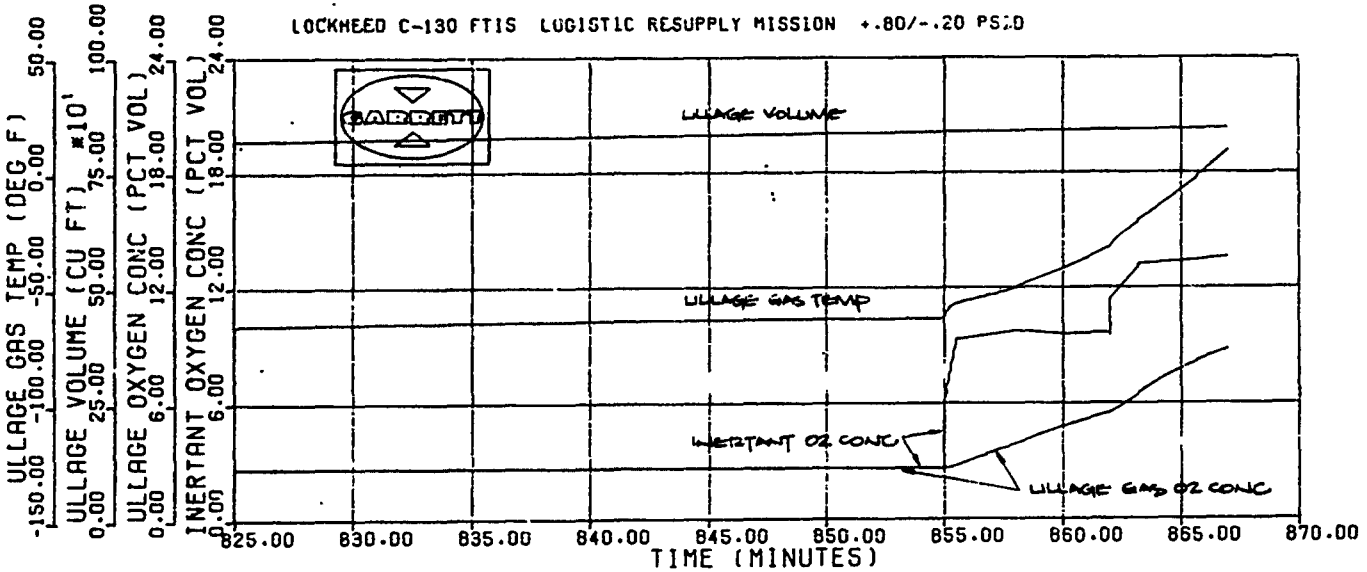

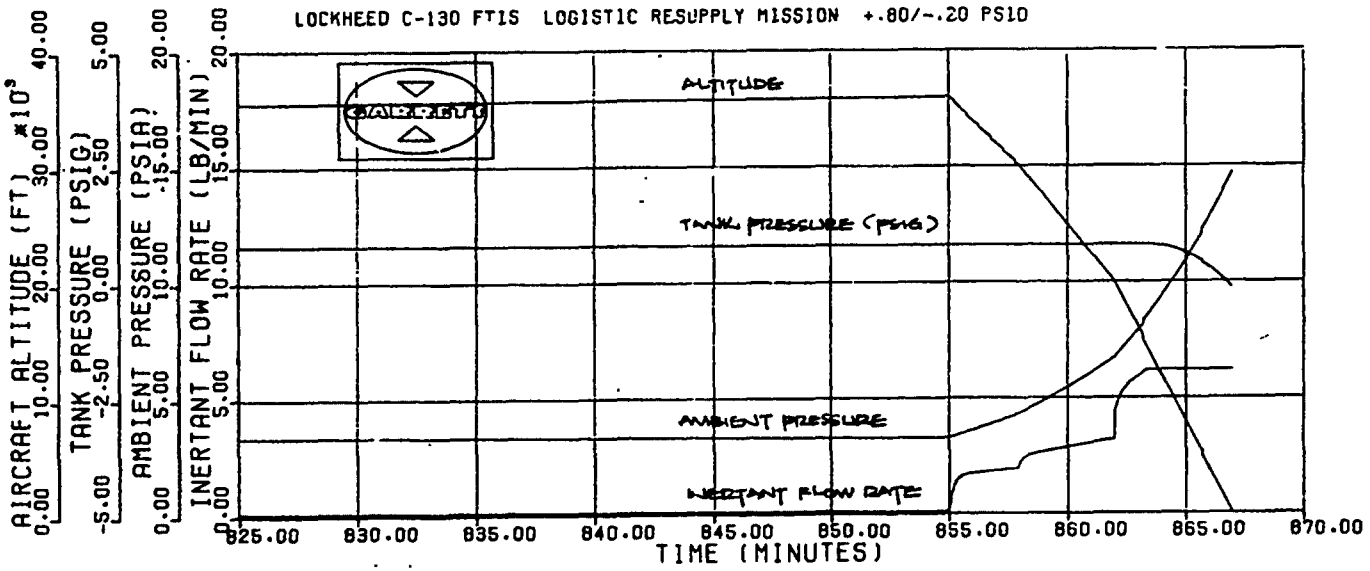

Figure C-2. PMIGG System Performance During Typical Logistic Resupply Mission

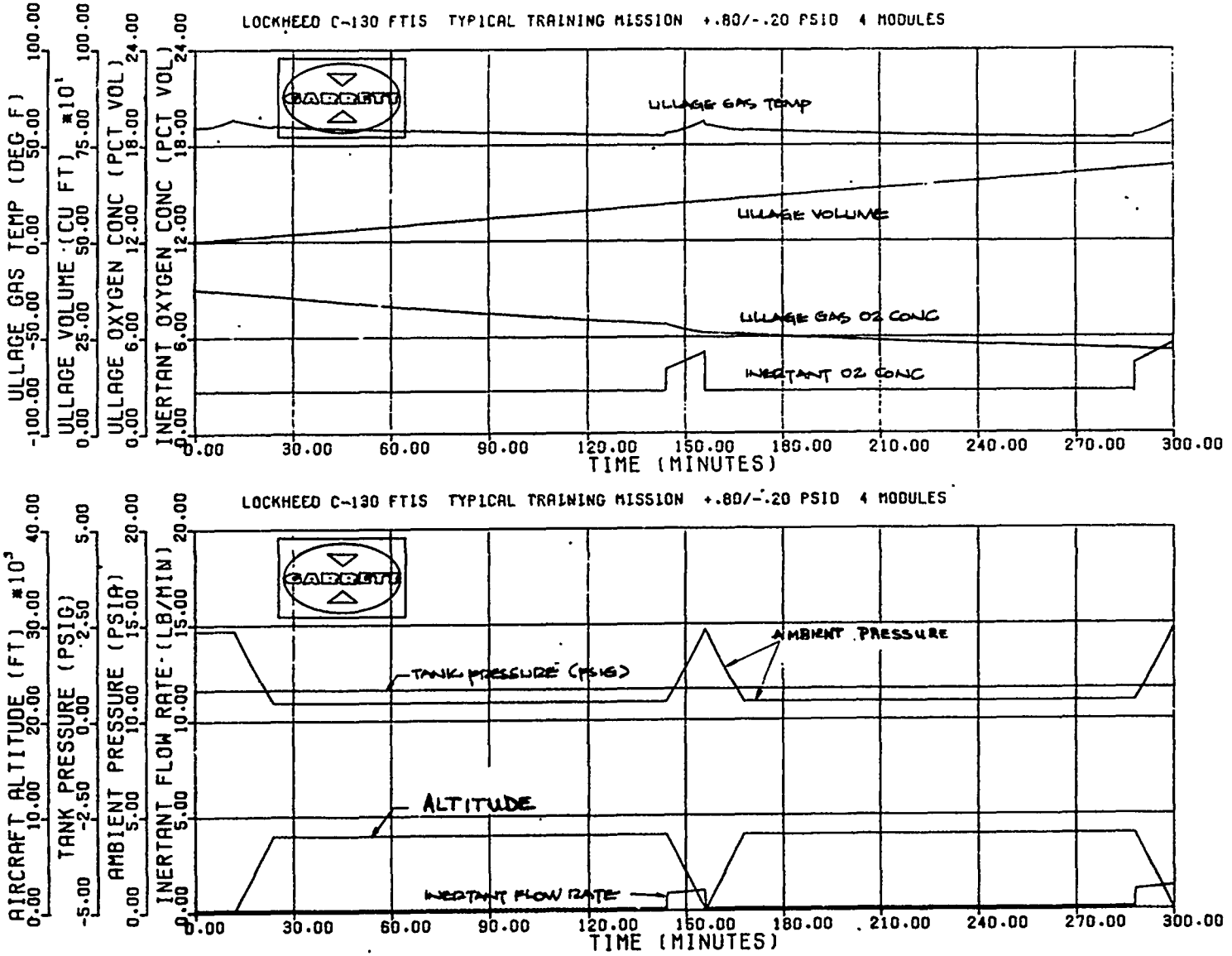

Figure C-3. PMIGG System Performance During Typical Training Mission

TABLE C-4

INITIAL INSTALLATION COSTS OF C-130/BLUE FOAM INSTALLATION

Material	Cost, $/Airplane
1100 cu ft at $30.00 cu ft.	33,000
Labor	
Install foam	
300 MMH at $33.40/MMH* = $10,020	
Purge and flush	
200 MMH at $33.40/MMH = 6,680	
Total labor	16,700
Initial installation cost per airplane	$49,700

* MMH = maintenance man-hour

maintenance labor associated with the foam handling in order to perform on-aircraft corrective maintenance. The penalty amounts to $50.10 per flight hour (see Table C-5). Most C-130 fuel system components are accessible only by entering the fuel tanks. This necessitates removal of the foam to make the corrective action. Components that require tank entry for maintenance include the tank quantity probes and wiring, the fuel level control valves, the dump pumps, vent valves, boost pumps in the pylon tanks, and the fuel scavenge or water removal system. Also, most fuel tank leaks must be corrected from inside the tank. This increment of 1.5 MMH/FH due to blue foam represents about a 25-percent increase in total aircraft maintenance manhours.

The cost of operation for blue foam amounts to $22.10 per flight hour, which is attributed to the 2900-lb weight penalty. This penalty results in an added fuel burn of 145 lb per flight hour, as shown on Table C-6.

All details pertaining to the blue foam installation, maintenance, and operation costs were supplied by Lockheed-Georgia Company.*

*Two letters from W. Arndt of Lockheed's propulsion and acoustics department, dated February 15 and March 9, 1983.

TABLE C-5

MAINTENANCE COST OF OWNERSHIP ELEMENTS FOR C-130/BLUE FOAM INSTALLATION

	MMH/FH	$/FH*
On-aircraft scheduled maintenance man-hour per flight hour (600 MMH/action, wing inspection action at PDM every 5 years, 600 FH/YR)	0.20	6.68
On-aircraft scheduled maintenance material cost per flight hour (Replace foam at $30.00/cu ft x 1100 cu ft every other PDM, 6000 FH)	-	5.50
On-aircraft corrective maintenance man-hour per flight hour increment due to blue foam	1.5	50.10
Shop repair labor cost	-	-
Shop repair material cost	-	-
Total maintenance cost for blue foam		$62.28/FH

*Estimated FY83 dollars per MMH used for calculation.

TABLE C-6

COST OF OPERATION FOR C-130/BLUE FOAM INSTALLATION *

	Lb/FH	$/FH**
Airbleed	-	-
Weight 0.05(lb/fuel/hr)/lb	145	22.10
Power	-	-
Total		$22.10/FH

*Training mission used for analysis (about 67 percent of C-130 utilization)

**Fuel cost $1.00/gal ($0.1526/lb)

IGG SYSTEM

A reliability analysis is an important consideration in system design. The reliability analysis is the starting point for estimating maintainability costs. The integrated IGG system design shown in Figure C-1 consists of a number of individual components of the type in use in aircraft pneumatic systems. The membrane air separation module is integrated into a system using components of established performance. Table C-7 presents an estimate of the MTBF for each IGG system component. The estimated MTBF values are representative of established values for generic components of the same type for similar applications. Data shown in Table C-7 is based upon analysis of data taken from field experience for components used on military and commercial aircraft. These data from military and commercial aircraft operators are summarized in the AiResearch GUARD (Garrett Unified Automated Reliability Data) System report, which is updated monthly, and in other field data sources. MTBF estimates for the membrane modules and filter consider the effect of scheduled replacement frequency.

The data of Table C-7 compare well with data for air-cycle ECS's which are in use in most military and commercial aircraft.

Cost of ownership is an important consideration in the selection of any airborne system. Not only the initial acquisition costs, but also the cost of operating and maintaining the system over its entire life cycle, must be considered. In the more sophisticated forms of financial analysis, the relationship between capital expenditure and calendar time has become increasingly important in making decisions. If system life cycle costs are evaluated in terms of absolute cost and the data relating the period of expenditure are available, more sophisticated use of the data may be feasible and applied, as appropriate, by the user. Accordingly, only absolute cost values are presented here. All estimated costs are in 1983 dollars.

The inital cost is the price of a shipset of hardware at the time of acquisition of the system. An analysis of the cost of a shipset of hardware for the applicable system was prepared (see Table C-7). The analysis was based on a preliminary design of the hardware components shown and verified by cost comparisons made against historical data for other airborne systems, with appropriate substitution in hardware content. This study was based on a lot release of 741 shipsets (674 aircraft population plus 67 spares). The initial costs included flight system hardware, and aircraft installation and was based on 1983 data.

Maintenance costs are those costs of ownership that are due to system replacement and repair needs. Numerous cost-related assumptions were required to establish maintenance cost estimates. Where background data were available, historical information was used in determining the maintenance cost assumptions.

The maintenance cost assumptions are summarized in Table C-1, and elements pertinent to the maintenance support costs are summarized in Table C-8. Cost elements attributable to performance of maintenance are comparable to those presently being demonstrated on similar pneumatic systems in military aircraft service. The estimated maintenance cost per flight hour over the life of the

TABLE C-7

ESTIMATED COST AND RELIABILITY ASSUMPTIONS

	Qty Per Aircraft	System Cost, $	MTBF Hr X1000
ECS package			
1.1 Air cycle machine	1		30
1.2 Primary heat exchanger	1		100
1.3 Secondary heat exchanger	1		100
1.4 Reheater	1		150
1.5 Condenser	1		150
1.6 Water extractor	1		200
1.7 Valve and low-limit control	1		20
1.8 Valve and temperature control	1		50
Miscellaneous hardware: controller, temperature sensors, packaging, etc.	1		150
Estimated total ECS cost		54,000	
IGG package			
2.1 Temperature control valve	1		40
2.2 Air filter	1		100
2.3 Air pressure regulator	1		40
2.4 Temperature sensor	1		40
2.5 Temperature control	1		40
2.6 Air separation module	4		200
2.7 Inert flow control	1		50
Miscellaneous hardware and packaging			100
IGG Total		40,000	
Miscellaneous hardware			
3. Demand pressure regulator/shutoff valve	2		40
4. Scrub valve	2		80
5. Climb and dive valve	2		80
Miscellaneous total		2,000	
Estimated IGG and ECS installation cost		100,000	
Total OBIGGS cost		196,000	

TABLE C-8

MAINTENANCE COST OF OWNERSHIP COMPARISON

Activity	Cost per Flight Hour: PMIGG System, $/FH	Cost per Flight Hour: Blue Foam, $/FH
• On-aircraft scheduled maintenance labor, cost per flight (MMH/FH x $33.40)	0.631427	6.68
• On-aircraft scheduled maintenance material cost per flight hour ($/FH)	3.541	5.50
• On-aircraft corrective maintenance labor cost per flight hour (MMH/FH x $33.40)	0.0138196	50.10
• Shop repair labor cost (MMH/FH x $33.40)	0.10073	-
• Shop repair material cost	0.40439	-
Total	4.1230823	62.28

system (in 1983 dollars) is the result of a preliminary quantitive maintainability analysis to evaluate scheduled on-aircraft preventive maintenance, on-aircraft corrective maintenance, and shop-level maintenance actions. The cost estimate is the result of a study in which each system component has been evaluated in terms of the task frequency (resulting from the reliability analysis of Table C-7), task definition, maintenance crew size requirements, maintenance man-hours per task, and (ultimately) maintenance man-hours per flight hour. Labor costs were then evaluated by applying the proper labor rate.

An examination of the costs in Table C-8 shows the IGG system on-aircraft scheduled maintenance costs to be of major significance. These costs are a result of the hollow fiber permeable membrane design operating life of 8500 hr. This analysis assumes a 100 percent time at stress on the ASM fibers, which results in an extremely conservative approach. By using this approach the fiber life is only 8500 hr, which amounts to a 15 year replacement period, resulting in the on-aircraft scheduled maintenance costs of $0.6314 per flight hour for labor and 3.54 $ per flight hour for material.

By using the fractional stress technique, the operating life can be extended beyond 20 yr. This analysis technique determines the fractional time at stress during a specified design mission to determine membrane fiber life.

Calculations based on the training mission profile of Table C-2 represent 0.40 hr of stress out of the 5.0-hr design mission profile. Accordingly, applying this ratio to the annual aircraft flight utilization assumption of Table C-1, the fibers can be expected to be pressurized to stress limits for only about 45 hr/yr, yielding an expected membrane useful life in excess of 20 yr.

Based on design analysis, the average aircraft energies used by the system for various flight segments can be determined for the typical training mission flight profile shown in Table C-2. Since the operation of the systems require energies that vary significantly for various flight segments, Table C-9 shows separate energy requirements for pre- and post-flight ground operation, and for the climb, cruise, and descent flight segments. These energy requirements represent relatively small increases in airflow and electrical power requirements for the baseline design aircraft, and are not expected to increase the requirement beyond aircraft capacities.

Aircraft penalties for the PMIGG installed system (energy and weight) are shown in Table C-10. These penalty factors, considered for the estimated system requirements (Table C-9), result in an estimate of the aircraft fuel consumption rate associated with the use of these energies. Application of the appropriate aircraft fuel costs then provides a measure of operating cost associated with the system use of energies, and with its installed system weight.

Aircraft fuel costs have increased substantially in recent years and are subject to further fluctuations in the future. For this study in 1983, a cost for JP-4 fuel of $1.00/gal ($0.1526/lb) was assumed. To evaluate the operating cost at a future time, a higher fuel cost assumption may be more appropriate. Fuel use and associated costs for 1983 are shown in Table C-10. As can be seen, the costs are predominantly due to bleed air, ram air, and system weight.

Summary

Cost of ownership in 1983 dollars of the two fuel tank protection systems is summarized in Table C-11. The major cost element in the OBIGGS is the initial cost of $196K per aircraft. Operation and maintenance are of minor significance ($95.3K) or about 39 percent of the total 20-yr life expectancy cost of $241K. For the blue foam, operation and maintenance is about 95 percent ($952K) of the total 20-yr cost ($1 million). Projected to the entire population of 674 aircraft, the OBIGGS operation and maintenance costs are $577 million less than the blue foam costs of $642 million. Payoff for the OBIGGS is estimated to be 3.5 years. With yearly cost savings of $28.9 million, the net savings is $471.2 million, including initial hardware cost and design development costs.

TABLE C-9

ESTIMATED AIRCRAFT ENERGIES USED DURING TYPICAL TRAINING MISSION

Mission Segment	Time Duration, hr	Flight Altitude, ft	IGG Usage		Fuel Penalty, lb/Mission Segment	
			Bleed air, lb/min	Ram air, lb/min	Bleed air 1.2 lb/fuel/hr / lb/air/min	Ram air 0.1 lb/fuel/hr / lb/air/min
Ground	0.2	0	1.05	-	0.25	-
Climb	0.2	0-8K	--		-	
Cruise	2.0	8K	9.0	104	21.6	20.8
Descent	0.2	8K-0	6.04	10	1.45	2.0
Climb	0.2	0-8K	--		-	
Cruise	2.0	8K	9.0	104	21.6	20.8
Descent	0.2 / 5.0	8K-0	6.04	10	1.45	2.0
		TOTAL FUEL PER TRAINING MISSION lb			46.35	45.6

TABLE C-10

COST OF OPERATION COMPARISON

		Expendable	IGG			Blue Foam		
		Fuel $1.00 gal ($0.1539/lb)	Penalty Element	Fuel Weight, lb/FH	Fuel Cost, $/FH	Penalty Element	Fuel Weight, lb/FH	Fuel Cost $/FH
		Bleed air						
		1.2 lb fuel/hr / lb air/min	46.35 lb/min	9.27	1.426653	-	-	-
		Ram air						
248	Penalty	0.1 lb fuel/hr / lb air/min	45.6 lb/min	9.12	1.403568	-	-	-
		Weight						
		0.05 lb fuel/hr / lb installed weight	190 lb	9.5	1.46205	2900 lb	145.0	22.10
		Power						
		0.0005 lb fuel/hr / watt	400 w	0.20	0.03078	-	-	-
		TOTAL			4.323051		145.0	22.10

TABLE C-11

COST-OF-OWNERSHIP SUMMARY

Cost Element	IGG System Cost, $	Blue Foam Cost, $
Flight system	96,000	33,000
Installation	100,000	16,700
Initial cost total, $/aircraft	196,000	49,700
Maintenance, $/FH/aircraft	4.1230823	62.28
Operation, $/FH/aircraft	4.323051	22.10
Total maintenance and operating cost, $/FH/aircraft	8.4461333	84.38
Yearly recurring cost at 564 FH/yr, $/aircraft	4,763.61918	47,590.32
20-year recurring cost, $/aircraft	95,272.38362	951,806.40
Yearly 674-aircraft cost	3,210,679.328	32,075,875.68
20-year recurring cost for 674 aircraft	64,213,586.56	641,517,513.60
Operation and maintenance savings for OBIGGS	577,303,927.00	-0-
Initial cost	132,104,000.00	33,497,800.00
Design/development costs	7,500,000.00	-0-
Net OBIGGS savings	471,197,727.00	-0-

* U.S. GOVERNMENT PRINTING OFFICE: 1984 - 759-062/841